



Document ID 1415152	Version 2.0	Status Approved	Reg no	Page 1 (193)
Author Jan Hernelind/5T Engineereing AB			Date 2014-02-13	
Reviewed by			Reviewed date	
Approved by Jan Sarnet			Approved date 2014-02-20	

Detailed models for PWR- and BWR-canisters for Earthquake induced rock shearing

Abstract

A number of analyses of earthquake induced rock shearing, based on detailed geometry descriptions of BWR and PWR inserts have been performed. The purpose was to obtain material for responses to questions posed by SSM in their review of SKB's licence application for a final repository for spent nuclear fuel at Forsmark. The shearing planes used in these analyses are located either at $\frac{3}{4}$ distances from the insert base or at the insert steel lid at the top of the insert. The obtained results show rather small differences in comparison to results from previous analyses which were based on a simplified geometry (Hernelind 2010).

Sammanfattning

Ett antal analyser av jordbävningsexiterad bergskjuvning har utförts med en detaljerad geometribeskrivning för BWR- och PWR-insatser. Avsikten var att erhålla underlag för att besvara frågor ställda av SSM i deras granskning av SKBs licensansökan för slutligt förvar av förbrukat kärnbränsle i Forsmark. Skjuvplanen som använts i dessa analyser är belägna vid $\frac{3}{4}$ -avståndet från insatsens botten eller vid insatsens stållock vid toppen av insatsen. Resultaten visar relativt små skillnader mot de tidigare analyserna som baserades på en betydligt mer förenklad geometri (Hernelind 2010).

Svensk Kärnbränslehantering AB

Swedish Nuclear Fuel and Waste Management Co
PO Box 250, SE-101 24 Stockholm
Visiting address Blekhölmstorget 30
Phone +46-8-459 84 00 Fax +46-8-579 386 10
www.skb.se
556175-2014 Seat Stockholm

Contents

1	Introduction and simulation strategy	4
1.1	Introduction	4
1.2	Simulation strategy	5
2	Meshes	7
3	Geometry of parts	9
3.1	Deposition hole	9
3.2	Buffer (Ca-bentonite, density 2,050 kg/m ³)	9
3.3	Copper shell	10
3.4	Insert (nodular cast iron)	10
3.5	BWR-insert	10
3.6	Steel channel tubes (BWR)	13
3.7	PWR-insert	14
3.8	Steel channel tubes (PWR)	16
3.9	Insert lid	17
3.10	Washer	18
3.11	Screw	18
4	Material models	19
4.1	Nodular cast iron (used by the insert)	19
4.2	Steel (used by the channel tubes in the insert)	20
4.3	Steel (used by the insert lid, support plates, bottom plates and screws)	21
4.4	Bentonite model (used for the buffer)	22
4.5	Copper material model (used by copper shell and washer)	25
4.5.1	Kimab material	25
5	Contact definitions	26
6	Initial conditions	27
7	Boundary conditions	28
8	Calculations	28
8.1	General	28
8.1.1	Rock shear calculation cases	29
8.1.2	Analysis approach	29
8.2	Short term analyses	29
9	Results for rock shear	29
9.1	Comparison with previous analyses for the PWR insert	29
9.1.1	Copper shell	33
9.1.2	Nodular cast iron insert	34
9.1.3	Steel channel tubes	36
9.2	Comparison with previous analyses for the BWR insert	37
9.2.1	Copper shell	40
9.2.2	Nodular cast iron insert	41
9.2.3	Steel channel tubes	43
9.3	Steel lid fixed with central screw or welded to the PWR insert	44
9.4	Eccentric positioning of the steel channel tubes for the PWR insert	48
9.5	Initial insert/copper shell positioning for the PWR insert	51
9.6	Stress concentrations for the detailed analyses for the PWR insert	54
9.7	Washer and steel lid fixing screw	57

9.8 Eccentric positioning of the steel channel tubes for the BWR insert	63
10 Uncertainties	73
11 Evaluation and conclusions	73
References	75
Appendix 1 – Plots for pwr_new3_quasi	77
Appendix 2 – Plots for pwr_eccentric3_quasi	92
Appendix 3 – Plots for pwr_new_gap_moved2_quasi	107
Appendix 4 – Plots for pwr_new_lock_quasi	122
Appendix 5 – Plots for pwr_new_lock_half_quasi	137
Appendix 6 – Plots for pwr_new2_washer3_quasi	145
Appendix 7 – Plots for bwr_new2_quasi	160
Appendix 8 – Comparison pwr_new3_quasi versus model6g_PWR_normal_quarter_2050ca3 at 5 cm shearing	175
Appendix 9 – Storage of files	183

1 Introduction and simulation strategy

1.1 Introduction

According to the design premises set out by SKB, see Table 1-1 of SKB TR-10-14, the copper corrosion barrier should remain intact after a 5 cm shear movement at a velocity of 1 m/s for buffer material properties of a 2,050 kg/m³ Ca-bentonite, for all locations and angles of the shearing fracture in the deposition hole, and for temperatures down to 0°C. The insert should maintain its pressure-bearing properties to isostatic loads.

One important function of the buffer material in a deposition hole in a KBS-3 repository for spent nuclear fuel is to reduce the impact of rock movements on the canister. A severe case of rock movement is a fast, earthquake-induced shear that takes place along a fracture intersecting a deposition hole. The consequences of such a rock shear movement have been investigated earlier, both by laboratory tests (Börgesson et al. 2004), laboratory simulations in the scale 1:10 and finite element modelling (Börgesson et al. 1995, 2004, Börgesson and Hernelind 2006). Those investigations were focussed on a base case with a horizontal shear plane and Na-bentonite as buffer material. Also the influence of the shear angle was studied with 45 and 22.5 degrees inclination between the shear plane and the canister.

A sequence of analyses has previously been performed for earthquake induced rock shear. The outcome of these analyses is described by Börgesson and Hernelind (2006). A final, deterministic sequence of analyses, were summarized in Hernelind (2010) where the buffer material properties are based on Ca-bentonite instead of Na-bentonite. In that study, also the copper shell, insert (nodular cast iron) and steel lid (steel) material properties were based on the most recent experimental results.

A horizontal shear plane at ¾-distance from the base of the insert was identified as the most severe shear plane position for the insert according to previous studies (Hernelind 2010). However, for the copper shell, as for the steel lid and the centre fixing screw, shearing at the steel lid is more severe.

Previous analyses of earthquake induced rock shearing (Hernelind 2010) were based on geometries with several simplifications such as:

- The steel lid was modelled without some of its details (valve, holes for mounting the valve and for the fixing screw).
- The steel lid was modelled without the centre fixing screw (instead the steel lid was tied to the insert at the periphery).
- The washer between the screw and steel lid was not modelled.
- The steel channel tubes were tied to the insert and modelled without support plates.
- The base plate of the insert was modelled without screws, nuts and support plates derived from the fixing during the casting process.

Previous analyses were also based on a construction with nominal measures and thus didn't study any effect of allowable tolerances. Also, the initial position of the steel channel tube was assumed to be centred in the nodular cast iron insert.

The aim with this study is to check if the above mentioned assumptions are reasonable and whether they have any significant influences on the stress/strain levels and the corresponding conclusions regarding damage tolerance analysis and mechanical integrity.

In the present work, the geometry definition for both the BWR and the PWR canister is therefore created based on CAD-drawings with as few simplifications as possible.

This report thus presents results for:

- Shearing at the $\frac{3}{4}$ -distance between canister base and top for the cases of
 - Centrally placed channel tubes
 - With washer between screw and steel lid
 - Without washer between screw and steel lid
 - Eccentrically placed channel tubes based on allowable tolerances
 - Eccentrically placed insert such that the insert and the copper shell are in initial contact
 - Steel channel tubes welded to steel plates
- Shearing at the steel lid (specifically to study the behaviour of the steel lid when this is modelled with a screw instead of welded to the top of the insert).

The obtained results based on the more detailed geometry are then compared with the corresponding results from previous analyses (Hernelind 2010).

The results will be used in responses to issues raised by SSM in their review of SKB's licence application for a final repository for spent nuclear fuel at Forsmark.

1.2 Simulation strategy

The performed simulations are based on the same geometry and meshes used in previous analyses (Hernelind 2010) for the buffer (bentonite), and the copper shell. The insert and channel tubes are defined by all details in the drawings for BWR and PWR inserts. The channel tubes are connected by support plates welded to the channel tubes. The support plates are glued to the cast iron insert which also applies to the base plates and base screws. Otherwise, the channel tubes are constrained by contact conditions. All screw heads are simplified to a cylindrical shape and a few extremely small holes are removed (these holes doesn't exist in reality and have been removed). The steel lid is fixed by a screw in the centre – previous analyses used a tied constrain between the outer face and the insert top.

The buffer material is Ca-bentonite with density $2,050 \text{ kg/m}^3$ for all analyses.

The default model is defined without considering tolerances and one model is defined by moving the steel channels (channel tubes) as much as possible in radial direction due to allowed tolerances. Also the sensitivity for initial positioning of the insert relative to the copper shell has been studied.

Table 1-1 shows job-names for all analyses described in this report. The comment “initial pre-stress” means that the screw has an initial condition and especially for cases including the washer most of the pre-stress in the screw is lost during the first equilibrium iteration. The comment “final pre-stress” means that the pre-stress in the screw is achieved after the first equilibrium iteration.

Table 1-1. Definition of simulation cases.

Case	Shear plane location	Comment
pwr_new3_quasi	75%	Without considering tolerances but with steel channel tubes welded to steel support plates.
pwr_new_gap_moved_quasi	75%	Insert moved to copper shell
pwr_new_lock_quasi	Insert lid	Screw initial pre-stress 355 MPa
pwr_new_lock_half_quasi	Insert lid	Screw initial pre-stress 177.5 MPa
pwr_new_lock2_quasi	Insert lid	Screw final pre-stress 355 MPa
pwr_new_lock2b_quasi	Insert lid	Screw final pre-stress 177.5 MPa
pwr_new2_lock_washer0_quasi	Insert lid	Screw final pre-stress 15 MPa with washer

pwr_new2_lock_washer3_quasi	Insert lid	Screw final pre-stress 67 MPa with washer
N34b_finer_1sekm_quasi_model6	Insert lid	Reference model (SKBdoc 1339902)
pwr_new2_washer_quasi	75%	Screw initial pre-stress 355 MPa with washer between steel lid and screw head
pwr_new2_washer3_quasi	75%	Screw final pre-stress 67 MPa with washer between steel lid and screw head
pwr_eccentric3_quasi	75%	The steel channels have been positioned due to tolerances
model6g_PWR_normal_quarter_2050ca3	75%	Previous PWR model - reference model (Hernelind 2010)
bwr_new2_quasi	75%	Without considering tolerances
bwr_eccentric_1	75%	The steel channels have been positioned due to tolerances
bwr_eccentric_lock	Insert lid	The steel channels have been positioned due to tolerances
model6g_normal_quarter_2050ca3	75%	Previous BWR model - reference model (Hernelind 2010)

2 Meshes

The geometry used for the earthquake induced rock shear consists of the insert (made of nodular cast iron), the insert lid (made of steel) and the copper shell surrounded by buffer material (Ca-bentonite, density 2,050 kg/m³). The geometry is based on CAD-geometries received from SKB, “Ritningsförteckning för kapselkomponenter” (SKBdoc 1203875, ver 1 for the reference model and ver 2 for the new detailed model) and should therefore correspond to the current design.

Due to symmetry only one half has been modelled. The mesh is then generated by 3-dimensional solid elements, mainly 8-noded hexahedral (most of them using full integration technique) and a few 6-noded wedge elements.

The model size is defined by about 126,000 elements and 160,000 nodes (total number of variables about 650,000).

The buffer has been partitioned at two different positions defining the rock shear perpendicular to the axis of the canister at the top of the insert lid and at $\frac{3}{4}$ -distance from the base of the insert, Fig 2-1. Fig 2-2 shows details of the mesh at the top corner, Fig 2-3 details when the washer is included and finally Fig 2-4 shows details at the base.

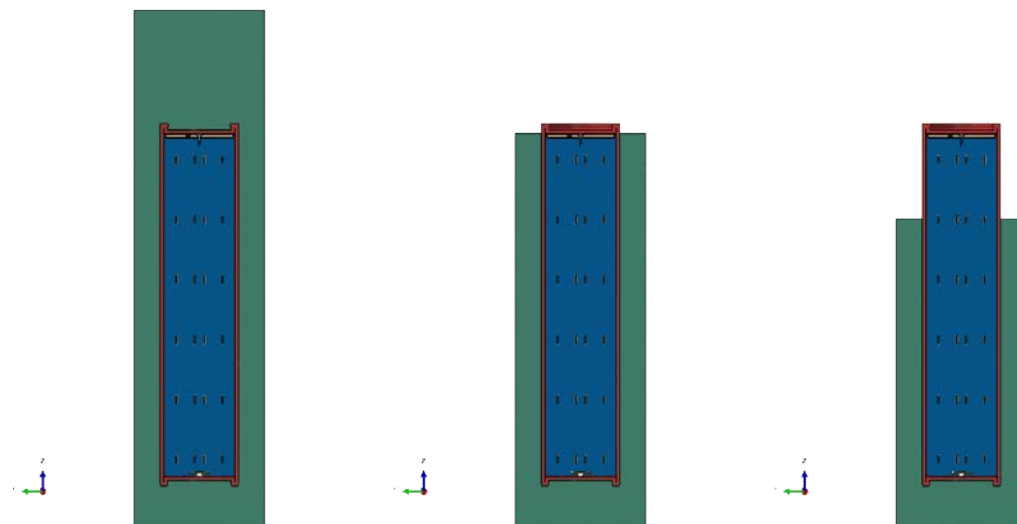


Figure 2-1. From left to right plot of geometry for rock shear perpendicular to axis of canister, shearing plane at the insert lid and shearing plane at $\frac{3}{4}$ -distance from the base of the insert.

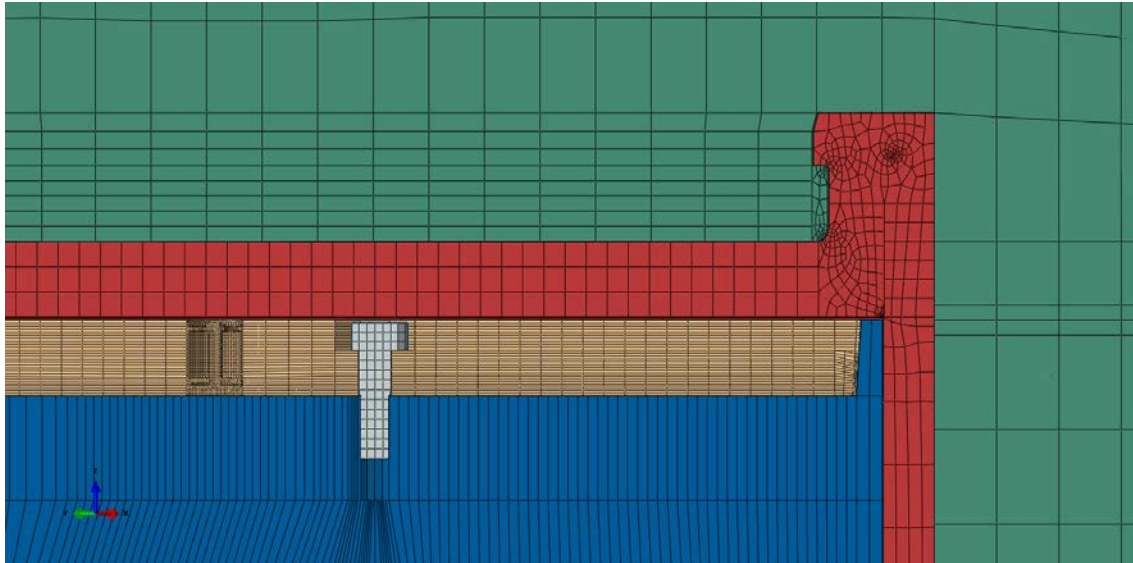


Figure 2-2. Detail of upper corner showing bentonite (green), copper shell (red), insert lid (brown), inserts (blue) and screw (white).

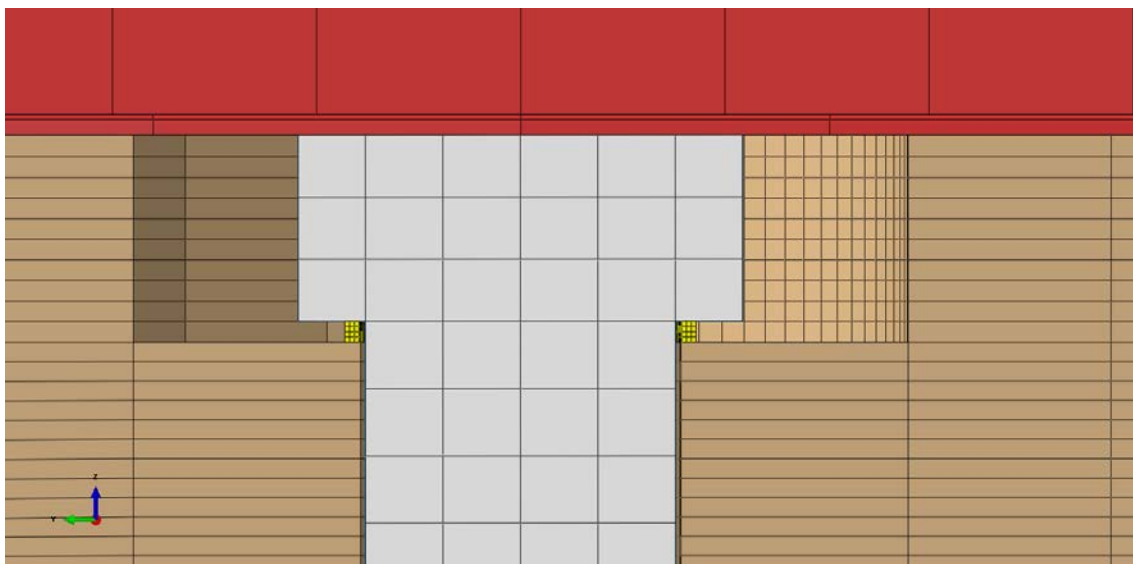


Figure 2-3. Detail of screw (white) and washer (yellow) with copper shell (red), insert lid (brown).

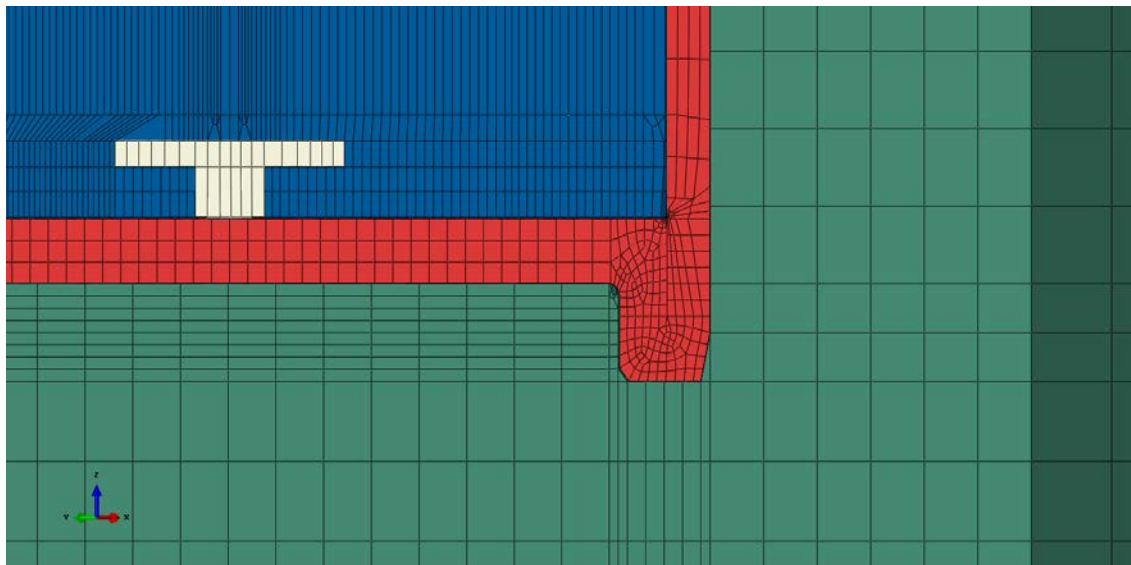


Figure 2-4. Detail of base showing bentonite (green), copper shell (red), insert (blue) and steel channel screw (white).

3 Geometry of parts

3.1 Deposition hole

The model of the deposition hole has a diameter of 1.75 m and a length of 6.9 m. The canister is placed about 0.5 m above the base and about 1.5 m below the top of the deposition hole. Buffer material (bentonite) surrounds the canister and will fill out the deposition hole. The rock shear is then simulated by prescribing boundary conditions at the buffer envelope.

3.2 Buffer (Ca-bentonite, density 2,050 kg/m³)

The buffer has same geometry and mesh as in previous analyses and is modelled with 3D solids, see Fig. 3-1.

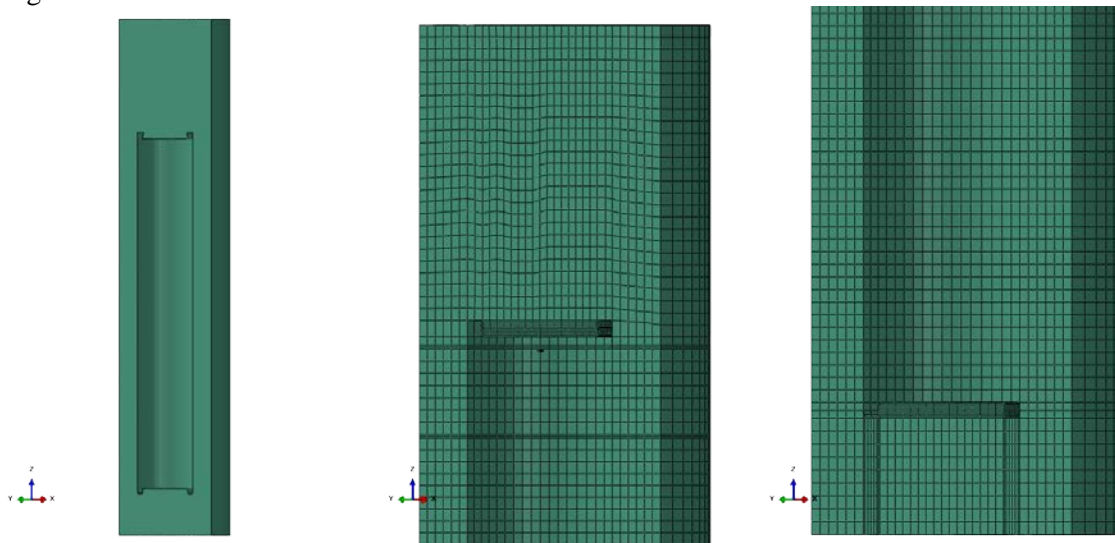


Figure 3-1. Plot of buffer. Left – geometry, middle – mesh at the top, right – mesh at the base.

3.3 Copper shell

The copper shell surrounds the insert and interacts with the buffer and the insert. The canister has been modelled rather accurately in order to catch “hot spots” where large strains are expected, e.g. the fillets at the base and top (the copper lid). The lid is welded to the flange and will act as one part, see Figure 3-2.

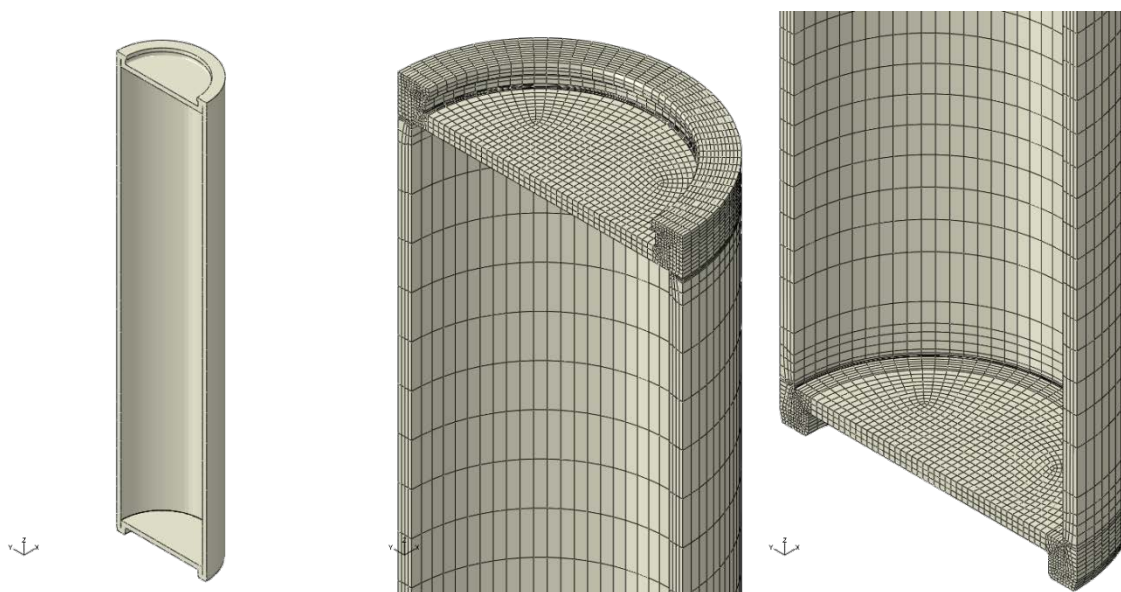


Figure 3-2. Copper shell geometry (left), mesh top (mid) and mesh base (right).

3.4 Insert (nodular cast iron)

The insert is made of nodular cast iron. The steel channel tubes with plates are placed inside the cast. One set-up is for BWR and one is for PWR and furthermore one PWR-model are defined where the tolerances have been included.

3.5 BWR-insert

The BWR-insert is modelled as a homogeneous part with 3D solids based on SKB drawings, see Figures 3-3 to 3-7. A few simplifications have been made:

- Screw head geometry is modified to a cylindrical shape.
- A few small cylindrical holes have been removed (these holes doesn't exist in reality and have been removed).
- Conical screw hole bottom modified to cylindrical shape.

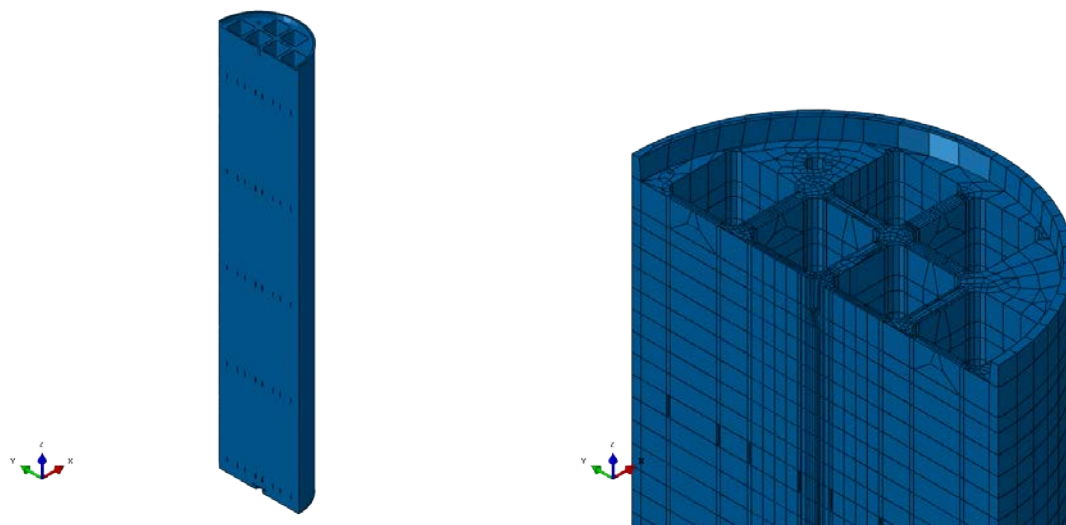


Figure 3-3. Insert BWR geometry (left), and mesh (right) – top view.

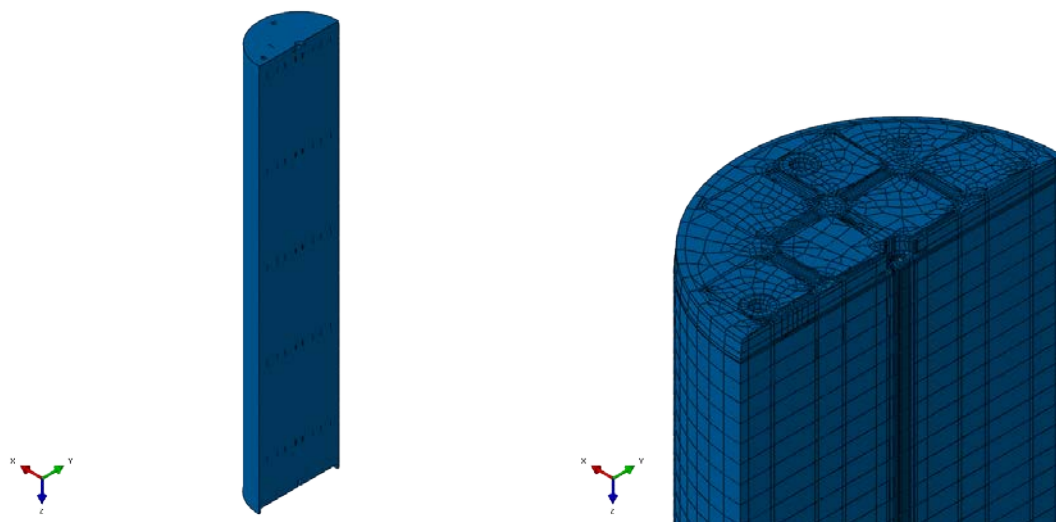


Figure 3-4. Insert BWR geometry (left), and mesh (right) – base view.

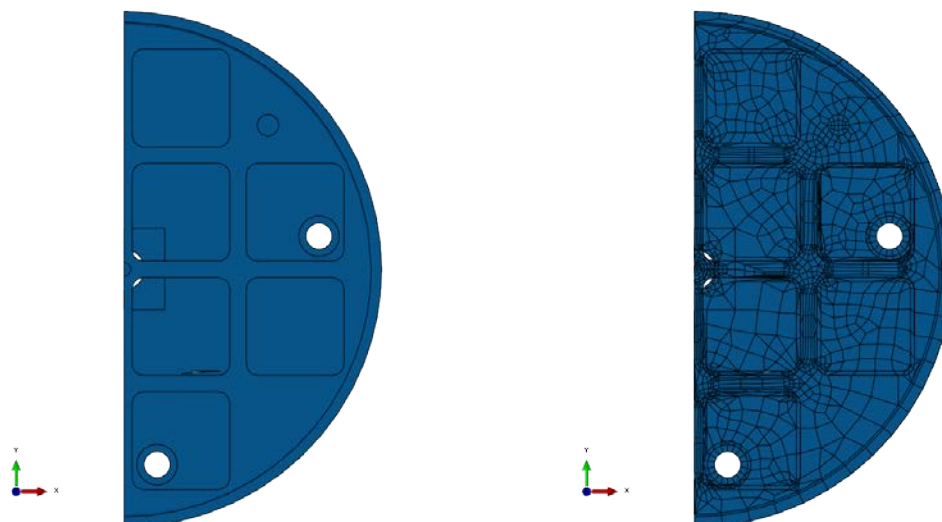


Figure 3-5. Insert BWR geometry (left), and mesh (right) – top view.

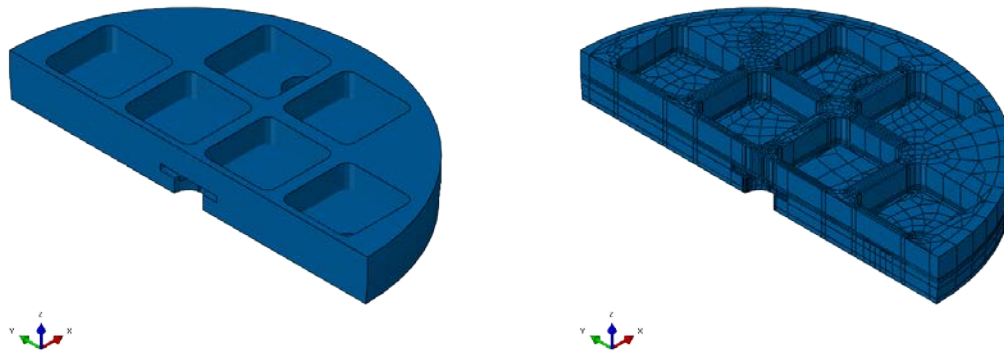


Figure 3-6. *Insert BWR geometry (left), and mesh (right) – base plate*

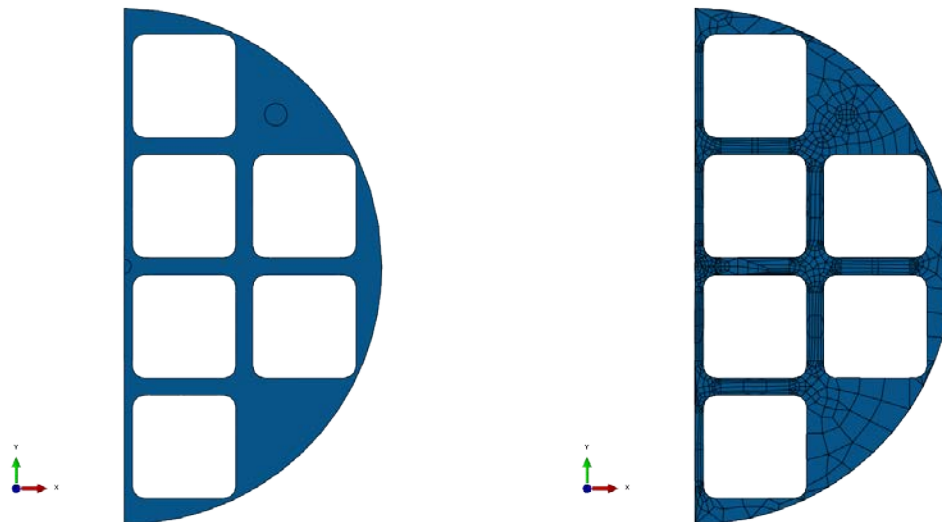


Figure 3-7. *Insert BWR geometry (left), and mesh (right) – top view showing the cross section.*

3.6 Steel channel tubes (BWR)

The BWR steel channel tubes are connected by support plates which are tied to the insert (the weld has not been modelled), see Figures 3-8 to 3-10.

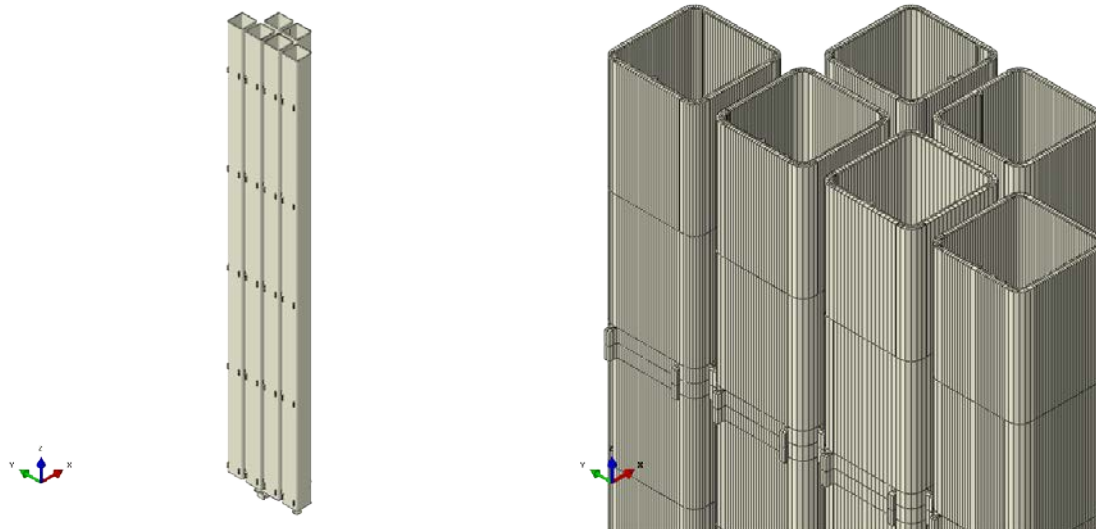


Figure 3-8. Steel channel tubes geometry (left), and mesh (right) – top view.

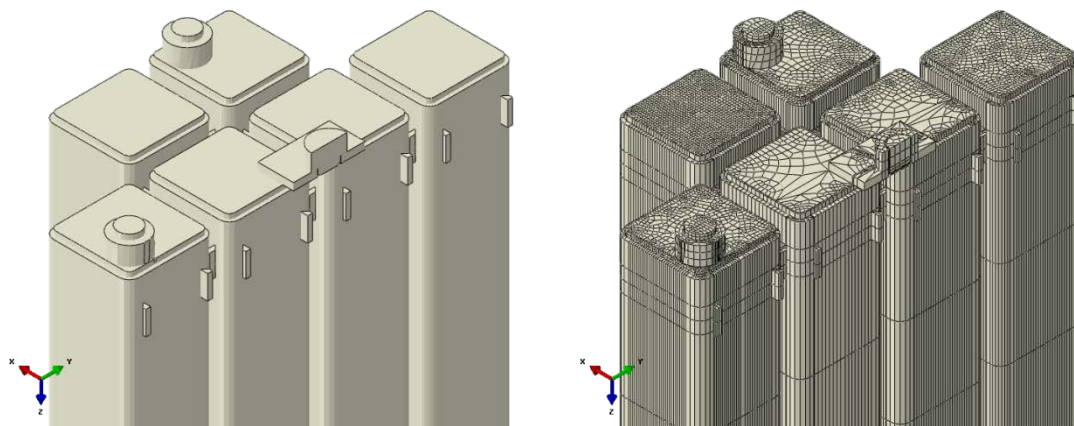


Figure 3-9. Steel channel tubes geometry (left), and mesh (right) – base view.

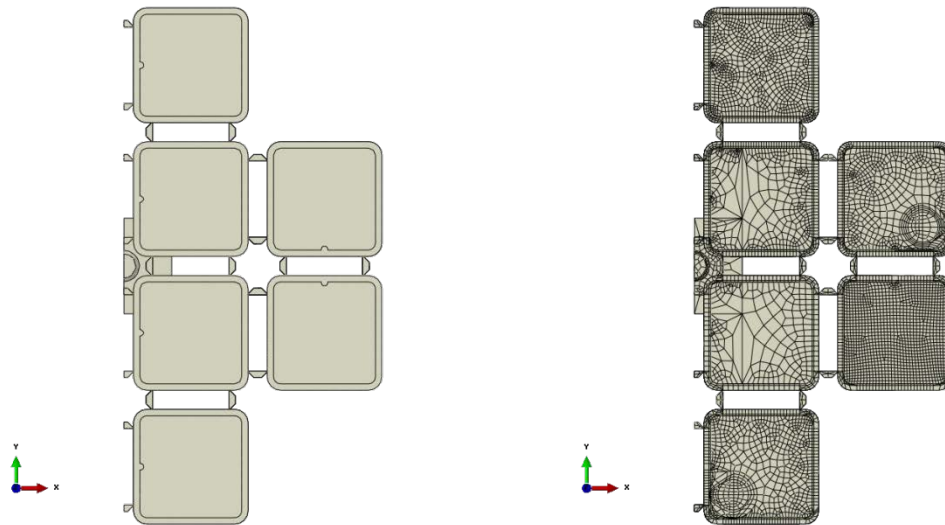


Figure 3-10. Steel channel tubes geometry (left), and mesh (right) – base view showing also the support plates.

3.7 PWR-insert

The PWR-insert is modelled as a homogeneous part with 3D solids based on SKB drawings, see Figures 3-11 to 3-14. Some modifications have been made.

- Screw heads are modified to cylindrical shape.
- Some small cylindrical screw holes have been removed (probably caused by exporting CAD-drawings to a new format).
- Screw hole conical bottom has been modified to cylindrical shape.

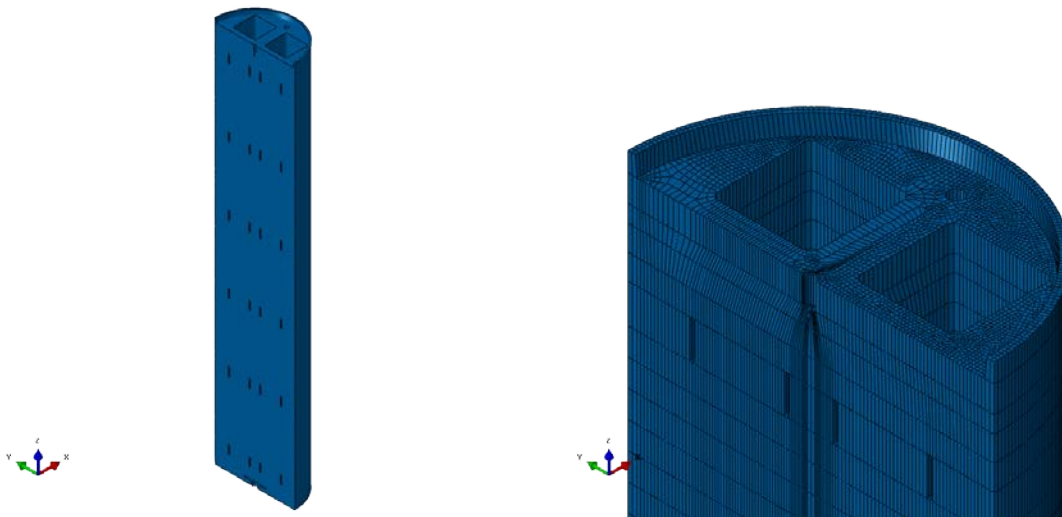


Figure 3-11. Insert PWR geometry (left), and mesh (right) – top view.

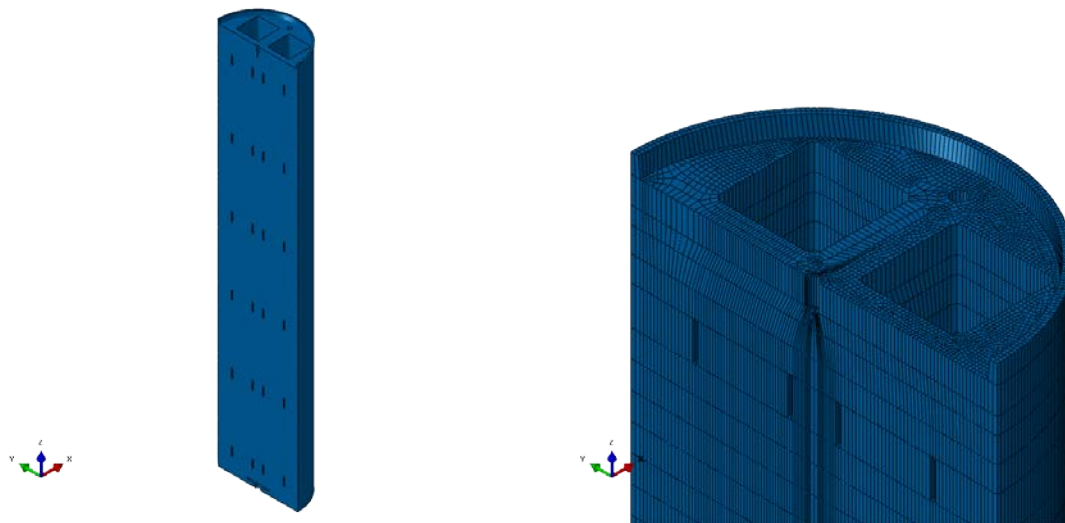


Figure 3-12. Insert PWR geometry (left), and mesh (right) – top view.

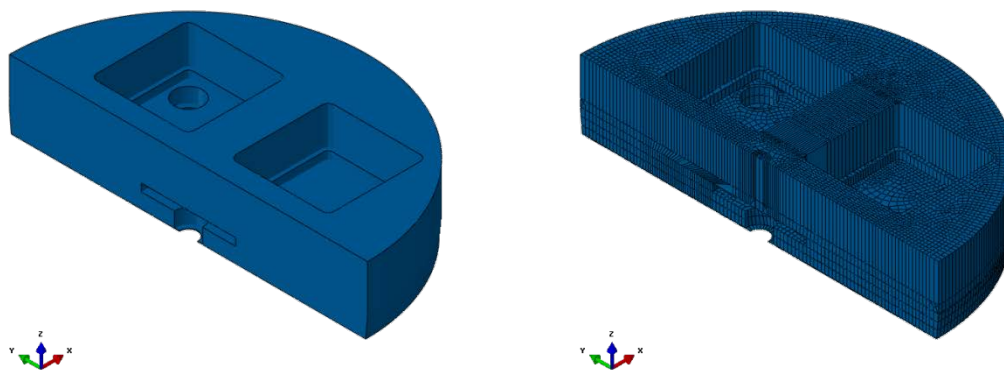


Figure 3-13. Insert PWR geometry (left), and mesh (right) – base plate.

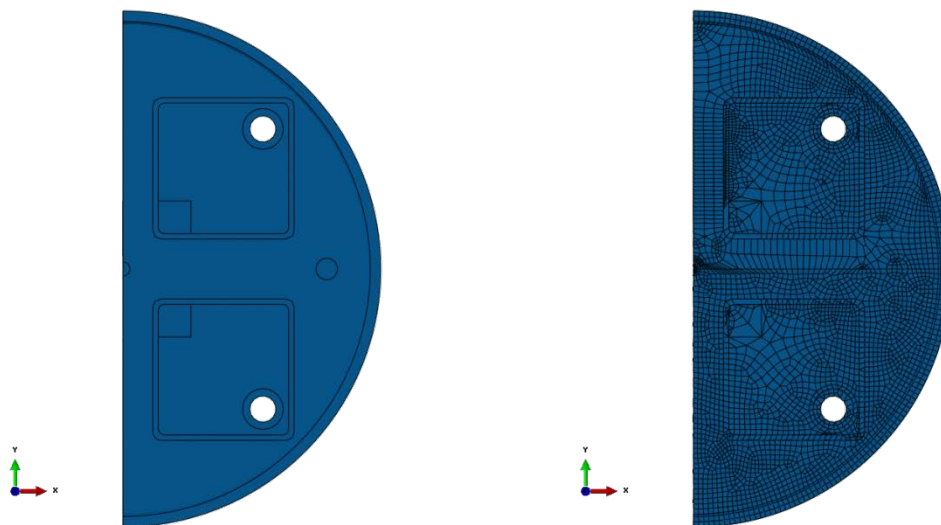


Figure 3-14. Insert PWR geometry (left), and mesh (right) – base view.

3.8 Steel channel tubes (PWR)

The PWR steel channel tubes are connected by support plates which are tied to the insert (the weld has not been modelled), see Figures 3-15 to 3-17.

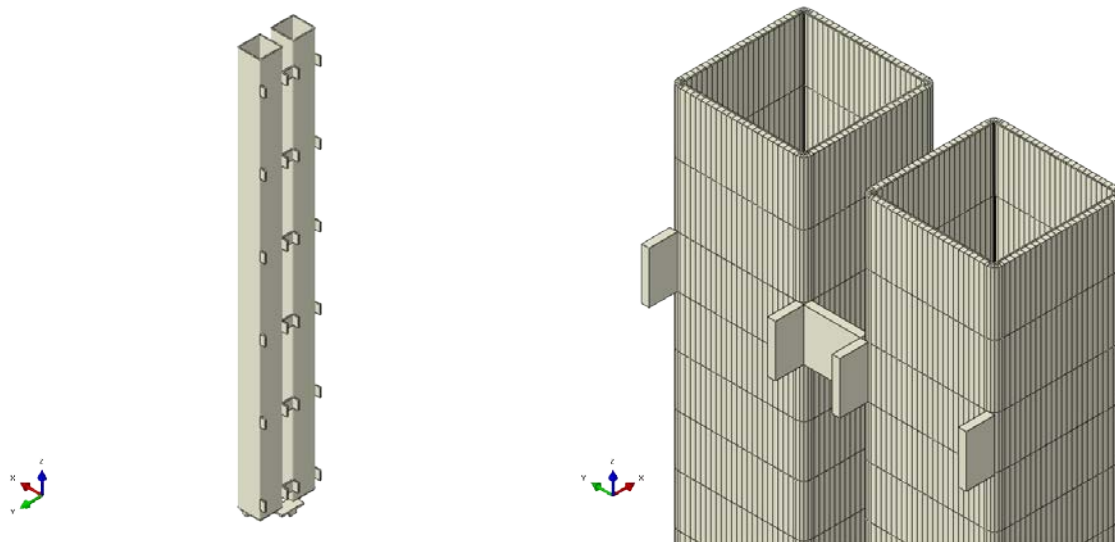


Figure 3-15. Steel channel tubes geometry (left), and mesh (right) – top view.

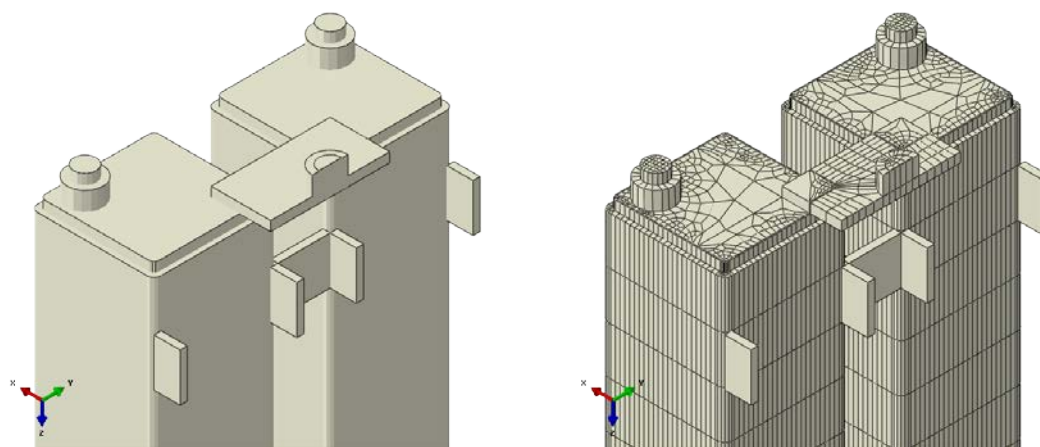


Figure 3-16. Steel channel tubes geometry (left), and mesh (right) – base view.

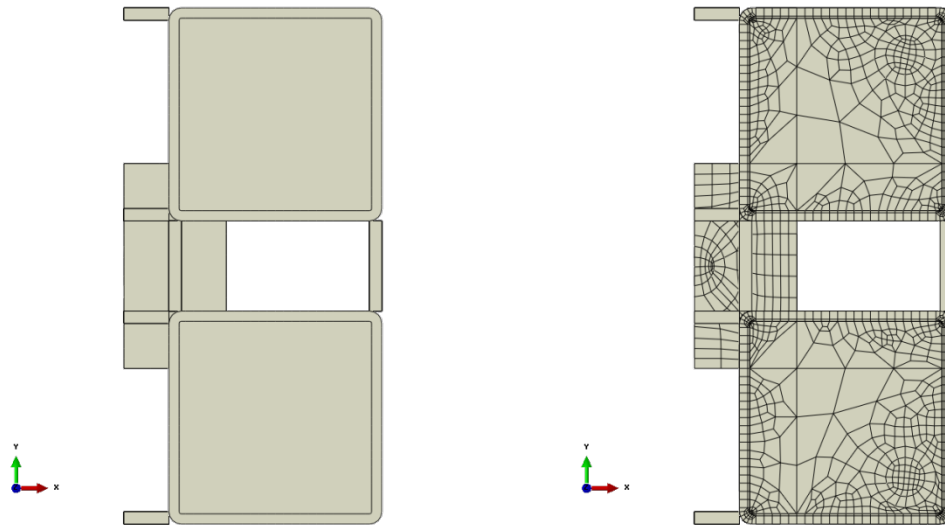


Figure 3-17. Steel channel tubes geometry (left), and mesh (right) – bottom view showing also the support plates.

3.9 Insert lid

The insert lid is made of steel and is modelled with 3D solids, see Figure 3-18. The surrounding gasket is not included which is assumed to have a minor effect on the stress distribution in the contact zone. Also a few details in the vent hole have been neglected since they hardly have any effect on the stiffness of the steel lid.

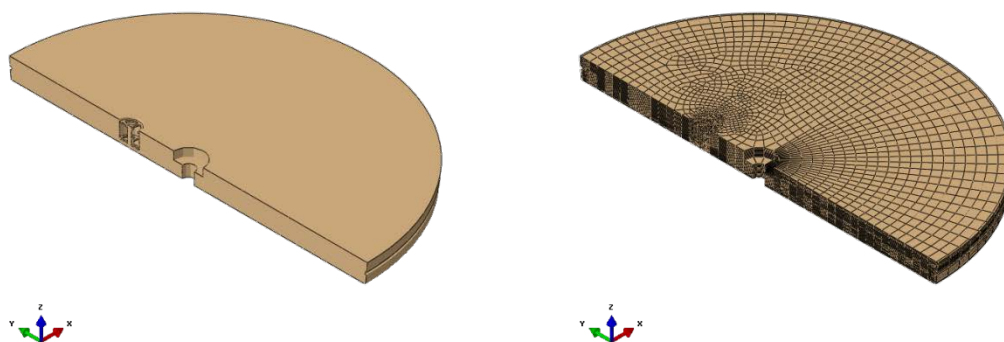


Figure 3-18. Insert lid geometry (left) and mesh (right).

3.10 Washer

The washer is modelled with 3D solids, see Figure 3-19.

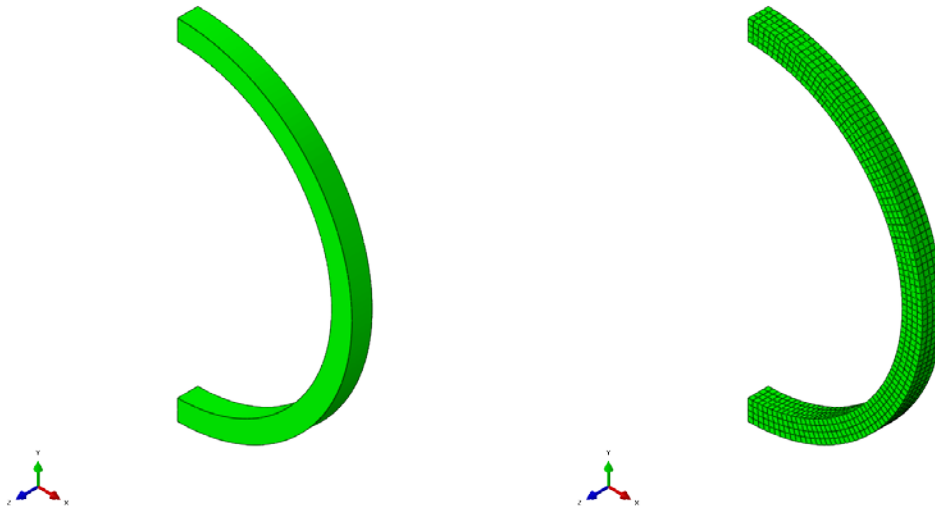


Figure 3-19. Washer geometry (left), and mesh (right) – positioned between screw head and steel lid.

3.11 Screw

The screw fixing the steel lid to the insert is modelled with 3D solids, see Figure 3-20

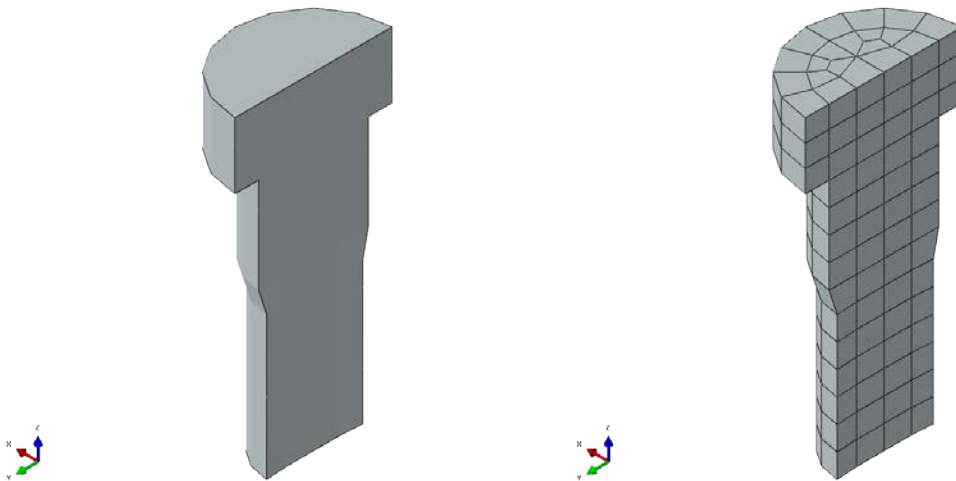


Figure 3-20. Screw geometry (left), and mesh (right) – used to fix the steel lid to the insert.

4 Material models

The finite element code ABAQUS version 6.12 (ABAQUS, Dassault Systèmes Simulia Corp.) was used for the calculations. The materials have been modelled as elastic-plastic with stress-strain properties that correspond to each material and the applied shear load induced strain rate, when applicable. The strains obtained from the simulations are below any necking and the material definitions thus cover the range of obtained results.

Note that in ABAQUS values outside the definition range will be constant with the last value defined.

4.1 Nodular cast iron (used by the insert)

The material model for the insert is based on a von Mises material model with elastic behaviour defined by Young's modulus and the Poisson's ratio and the plastic behaviour defined through yield surface (true stress) versus plastic strain (defined as logarithmic strain), see Table 4-1 and Figure 4-1 "Dragprovning av gjutjärn" (SKBdoc 1201865). The same material properties have been used for BWR and PWR inserts which will have a minor influence on the PWR-insert results.

Data is available up to 15% plastic equivalent strain which covers the range of obtained results for the performed analyses.

The experiments were performed at 0° C.

Table 4-1. True stress-true strain definition for BWR-insert.

Plastic Strain (%)	Stress (MPa)			Strain rate factor at strain rate=0.5
	Strain rate=0	Strain rate=2×10 ⁻⁴	Strain rate=0.5	
0	293	293	348	1.19
1	324	324	367	1.13
2	349	349	385	1.10
3	370	370	406	1.10
4	389	389	423	1.09
5	404	404	438	1.09
6	418	418	451	1.08
7	428	428	464	1.08
8	438	438	474	1.08
9	447	447	483	1.08
10	456	456	490	1.07
11	465	465	498	1.07
12	472	472	504	1.07
13	478	478	510	1.07
14	484	484	516	1.07
15	488	488	520	1.07

The strain rate dependency is defined by assuming that the yield surface is proportional to the strain rate factor (at the strain rate 0.5 1/s the factor 1.08 has been chosen and at strain rate 0 1/s the factor is 1.0). The instantaneous strain rate factor is then linearly interpolated between 1 and 1.08 using the instantaneous strain rate.

Furthermore, Young's modulus $E = 166$ GPa and Poisson's ratio $\nu = 0.32$ (Raiko et al. 2010).

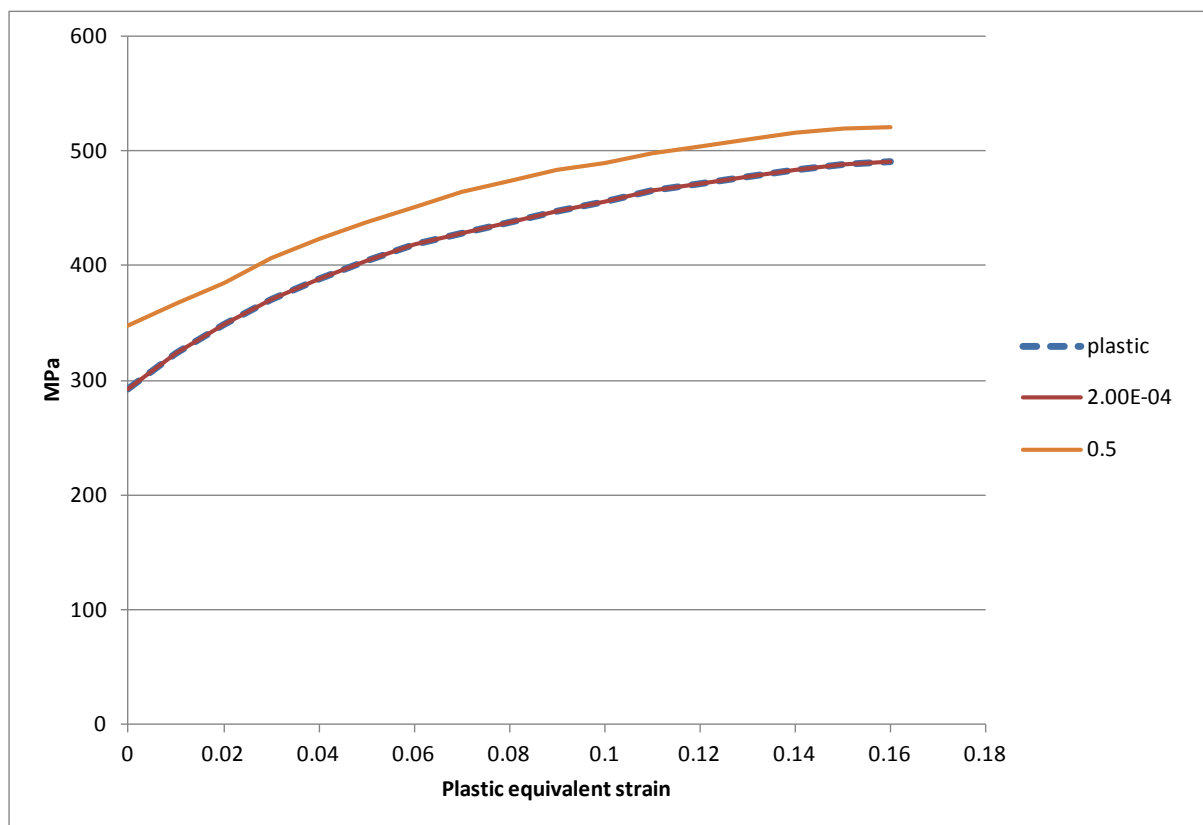


Figure 4-1. Insert yield surface (nodular cast iron), true stress, [MPa] versus logarithmic plastic equivalent strain for different plastic strain rates. Note that the base (plastic) is defined to coincide with strain rate = 2×10^{-4} [1/s].

4.2 Steel (used by the channel tubes in the insert)

The material model for the channel tubes in the insert is based on a von Mises material model with elastic behaviour defined by Young's modulus and the Poisson's ratio. The plastic behaviour is defined through yield surface (true stress) versus plastic strain (using logarithmic strain).

The steel channel tubes are manufactured by steel S355J2H, for example Domex 355 MC B. SKB has earlier supplied test data for the yield point of their material, however no stress-strain data to be used in a plastic analysis. The stress-strain curve for Domex 355 MC B (SSABDirect 2008) can be scaled using the yield stress and tensile ultimate strength measured by SKB, $R_e = 412$ MPa (yield stress) and $R_m = 511$ MPa (ultimate stress). With this procedure a simplified stress-strain curve is obtained and described by Table 4-2 and Figure 4-2.

Table 4-2. Stress-strain definition for channel tubes used in the insert.

Strain (%)	Stress (MPa)	Log Strain (%)	True Stress (MPa)	Plastic equivalent strain (%)
0	0	0	0	0
0.196	412	0.196	412	0
15	509	14.3	587	14.0
20	511	18.5	613	18.2

Furthermore, Young's modulus $E = 210$ GPa and Poisson's ratio $\nu = 0.3$ according to Raiko et al.(2010, Table 4-3).

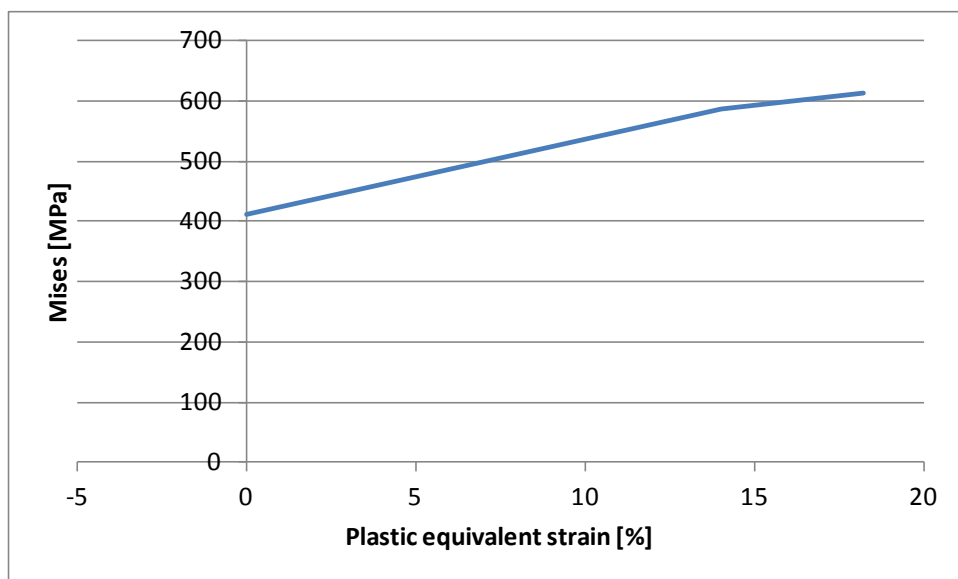


Figure 4-2. Channel tube yield surface, true stress [MPa], as a function of the logarithmic plastic equivalent strain.

The data with lowest value from the experiment has been chosen for the yield surface. However, the plasticity definition for the steel channel tubes has very minor influence on the overall results. Furthermore the obtained results from the performed analyses are within the range for available material data.

4.3 Steel (used by the insert lid, support plates, bottom plates and screws)

The material model for the insert lid is based on a von Mises material model with elastic behaviour defined by Young's modulus and the Poisson's ratio. The plastic behaviour is defined through yield surface (true stress) versus plastic strain (calculated as logarithmic strain).

Manufacturing drawings for the lid specify steel S355J2G3. Strain versus stress for steel Domex 355 MC B with $R_e = 389$ MPa (yield stress) and $R_m = 484$ MPa (ultimate stress) can be found from SSABDirekt (2008). According to SS-EN 10025-2:2004, the material S355 with nominal thickness 40-63 mm has $R_e = 335$ MPa (yield stress) and $R_m = 470$ -630 MPa (ultimate stress). Scaling stress-strain curves for Domex 355 by the minimum values given in SS-EN 10025-2:2004 implies the simplified material definition (engineering data) shown in Table 4-3 and Figure 4-3.

Table 4-3. Stress-strain definition for the insert lid.

Strain (%)	Stress (MPa)	Log Strain (%)	True Stress (MPa)	Plastic equivalent strain (%)
0	0	0	0	0
0.1595	335	0.1593	335	0
15	470	13.98	540	13.7
20	470	18.2	564	17.9

Furthermore, Young's modulus $E = 210$ GPa and Poisson's ratio $\nu = 0.3$ according to Raiko et al. (2010, Table 4-3).

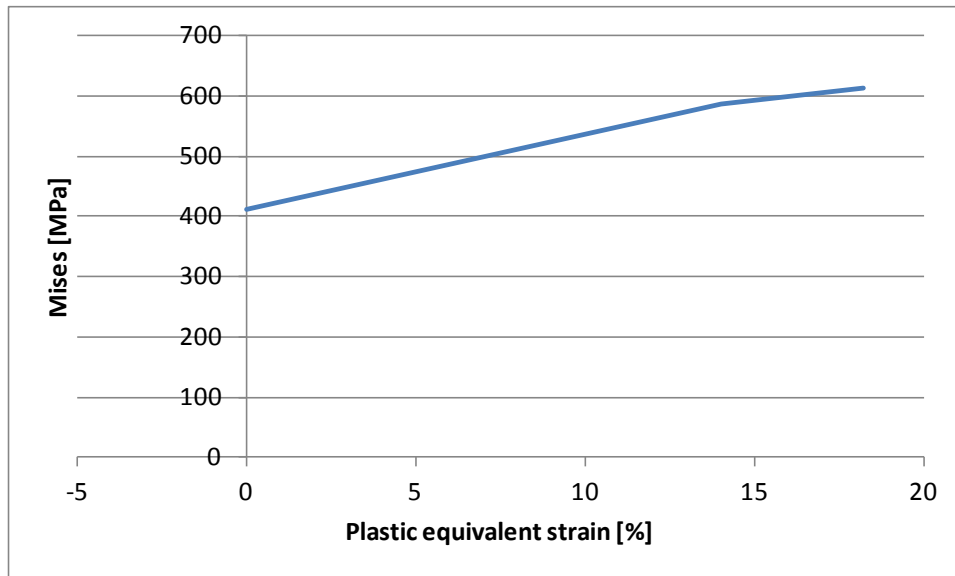


Figure 4-3. Insert lid yield surface, true stress [MPa], as a function of the logarithmic plastic equivalent strain.

The data with lowest value from the experiments (SS-EN 10025-2:2004) has been chosen for the yield surface. However, the plasticity definition for the insert lid has very minor influence on the overall results. Furthermore, the obtained results are within the range of available material data.

4.4 Bentonite model (used for the buffer)

The bentonite is modelled based on recent experiments, see Börgesson et al. (2010) and adapted to the actual density of the bentonite. The bentonite buffer is modelled using only total stresses that do not include the pore water pressure, the reason being the very fast compression and shear.

The most important properties of the bentonite for the rock shear are the stiffness and the shear strength. These properties vary with bentonite type, density and rate of strain. Ca-bentonite has higher shear strength than Na-bentonite and the shear strength increases with increasing density and strain rate. Since it cannot be excluded that the Na-bentonite MX-80 will be ion-exchanged to Ca-bentonite the properties of Ca-bentonite is used in the modelling. The acceptable density at saturation of the buffer material is 1,950 kg/m³ – 2,050 kg/m³ which is covered by the models below.

The material model is in ABAQUS expressed with the von Mises stress σ_j that describes the “shear stress” in three dimensions according to Equation 3-1.

$$\sigma_j = (((\sigma_1 - \sigma_3)^2 + (\sigma_1 - \sigma_2)^2 + (\sigma_2 - \sigma_3)^2) / 2)^{1/2} \quad (3-1)$$

where

σ_1 , σ_2 and σ_3 are the principal stress components.

The material model defines the relation between the stress and the strain and is partitioned in elastic and plastic parts. For details regarding definition of the shear strength and the influence of density, pressure and rate of shear, see Börgesson et al. (1995, 2004).

“Rate dependent elastic-plastic stress-strain relation

The elastic-plastic stress strain relations used for the three different densities are derived according to the description above in an identical way as the relations used in all previous calculations.

The bentonite is modelled as linear elastic combined with the von Mises plastic hardening - Table 4-4 shows the elastic constants. The plastic hardening curve is made a function of the strain rate of the material. The reason for the latter relation is that the shear strength of bentonite is rather sensitive to the strain rate. It increases with about 10% for every 10 times increase in strain rate. Since the rock shear at an earthquake is very fast (1 m/s) the influence is strong and the resulting shear strength will be different at different parts of the buffer. Figure 4-4 shows the material model. The stress-strain relation is plotted at different strain rates.

Table 4-4. Elastic material data for the bentonite buffer Na converted to Ca.

Density (kg/m ³)/Swelling pressure (MPa)	Elastic part	
	<i>E</i> (MPa)	<i>v</i>
Low - 1950/5.3	243	0.49
Mean - 2000/8	307	0.49
High - 2050/12.3	462	0.49

The experiments (Börgeon et al. 2010) show that also Young’s modulus *E* is dependent on strain rate but in the calculations this has been neglected and a representative stiffness has been chosen (sensitivity analyses did show minor changes of the results when varying Young’s modulus between maximum and minimum values achieved from the experiments).

From the performed analyses it’s obvious that the bentonite gets plastic strains outside the defined range for material data. However, other studies, “Earthquake induced rock shear through a deposition hole – Part 2. Additional calculations of the influence of inhomogeneous buffer on the stresses in the canister.” (SKBDoc 1407337) show that it doesn’t affect the results significantly.

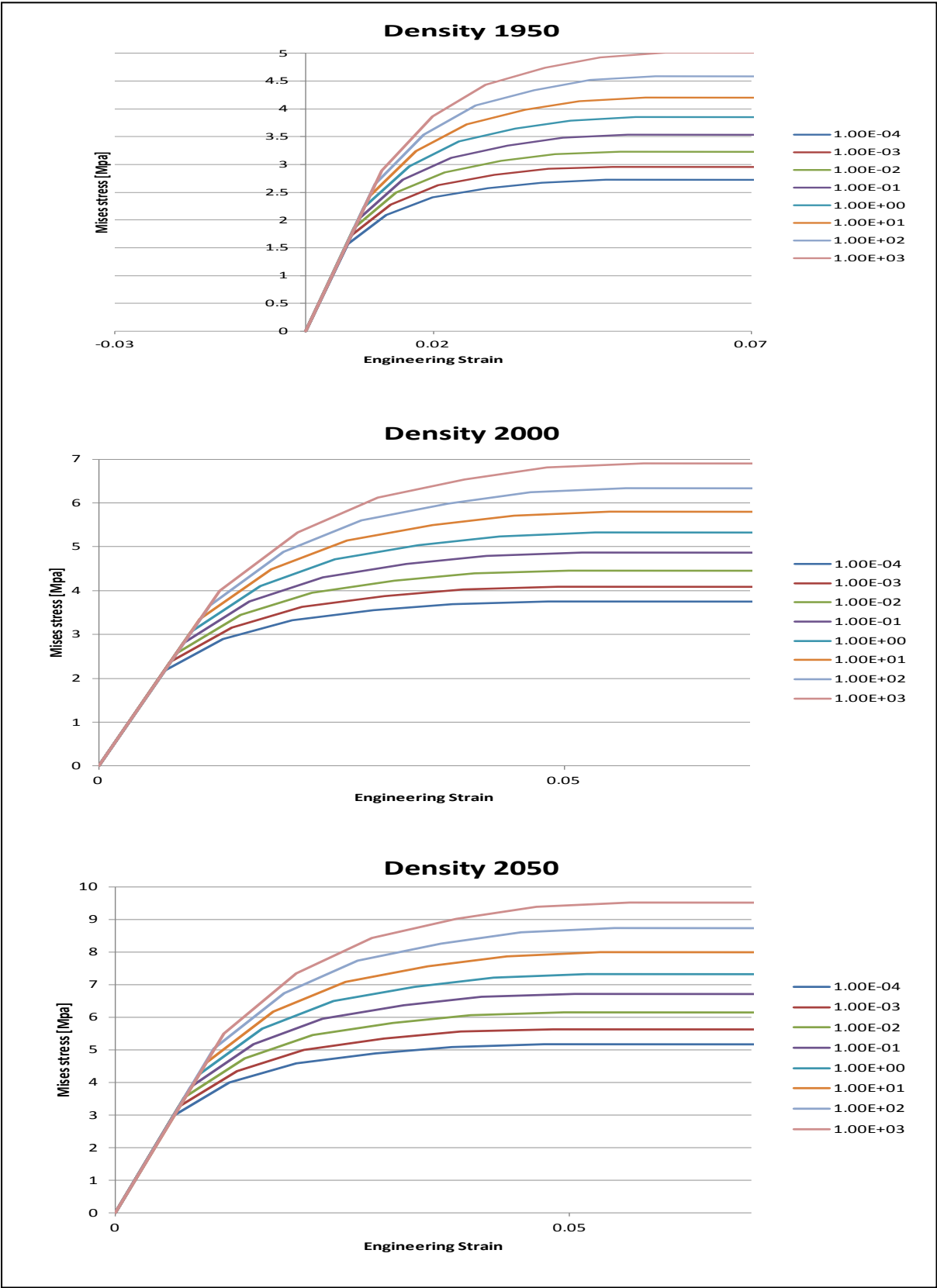


Figure 4-4. Plot of material definition for the bentonite buffer for different densities [kg/m³] and strain rates [1/s]. Mises stress [MPa] versus engineering strain.

4.5 Copper material model (used by copper shell and washer)

4.5.1 Kimab material

The material model used for copper for most of the global analyses is described below.

The stress-strain properties of the copper in the copper shell were investigated by the Corrosion and metals research institute Swerea Kimab and the results are then represented by a creep material model developed by Rolf Sandström, see Sandström and Andersson (2008), Jin and Sandström (2008) and Sandström et al. (2009).

The material model for the short duration rock shear analysis, used for all analyses in this study and also in previous studies for short duration rock shear analyses (Hernelind 2010) and “Global simulation of copper canister – final deposition” (SKBdoc 1339902), is based on a simplified elastic-plastic material model, see Table 4-5, using data from the creep model assuming a strain rate of $5 \times 10^{-3}/s$ which is considered as conservative.

The flow curve data has been calculated from Sandström et al. (2009) wherein eq.(17) has been used together with the parameter values defined in the corresponding Table 4-2, as well as $m = 3.06$, $\alpha = 0.19$, $\omega = 14.66$.

The copper model data is shown in Figure 4-5. Data is available up to 50% and covers the range of obtained results.

Table 4-5. Elastic-plastic material data for the copper at strain rate $5 \times 10^{-3}/s$.

Elastic part		Plastic part: von Mises stress σ_j (MPa) at the following plastic strains (ϵ_p)					
E (MPa)	ν	0	0.10	0.20	0.30	0.40	0.50
$1.2 \cdot 10^5$	0.308	72	178	235	269	288	300

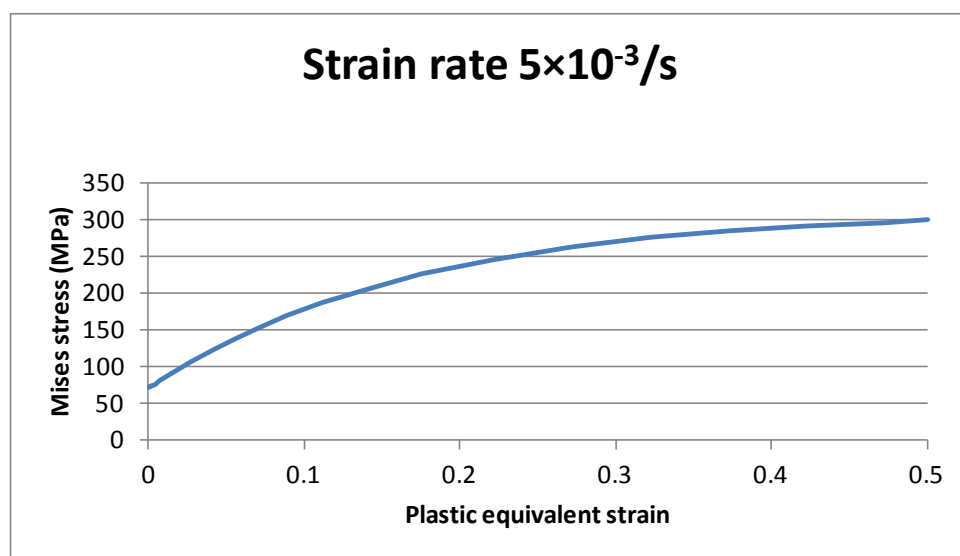


Figure 4-5. Copper shell yield surface, true stress, [MPa] as a function of the logarithmic plastic equivalent strain.

5 Contact definitions

All the boundaries of the buffer, the copper shell, the insert and the insert lid interact through contact surfaces allowing finite sliding. All contact surfaces have friction at sliding with no cohesion and the friction coefficient 0.1, i.e. the friction angle (ϕ) is 5.7° and the cohesion (c) is 0 kPa.

The contact is released when the contact pressure is lost.

A few contact pairs are tied together (tied means that the surfaces are constrained together and will not allow for opening/closing or sliding) in order to improve the numerical convergence rate. This applies at the contact pairs between the insert and insert lid and also at the base of insert and copper shell bottom.

The interaction between the buffer and the rock (not modelled) is assumed to be tied through prescribed boundary conditions and will not allow for opening/closing or sliding.

6 Initial conditions

Initial conditions are defined as:

- Temperature for all nodes in the model as 300 K (only used when the copper material is defined by a creep material model which has not been done in this study). The temperature is assumed not to change during the analysis.
- The fixing screw between the steel lid and the insert has an initial stress in the axial direction.
- Total pressure for the buffer (17.3 MPa) based on the swelling pressure (12.3 MPa for bentonite with density $2,050 \text{ kg/m}^3$) plus 500 meter water pressure (5 MPa) when using elastic-plastic material model without pore pressure. Since the canister deforms when the initial stresses are applied, the calculated magnitude of the swelling pressure will decrease. For that reason the initial condition for pressure is given as 40.2 MPa based on the obtained pressure (about 17.3 MPa) after equilibrium iterations. At the start of rock shearing simulation the pressure on the outer surface of the copper shell thus is about 17.3 MPa. Another observation is that the calculated swelling pressure will vary both in the axial and radial direction which means that it's not possible to have the correct swelling pressure without using elements with pore pressure as a degree of freedom (ABAQUS have those elements but the material model is tuned to total stresses and not effective stresses).

7 Boundary conditions

Symmetry conditions have been specified for the symmetry plane (displacements in the normal direction to the symmetry plane prescribed to zero), see Fig 7-1.

The surrounding rock has been simulated by prescribing the corresponding displacements at the outer surface of the buffer and depends also on type of simulation.

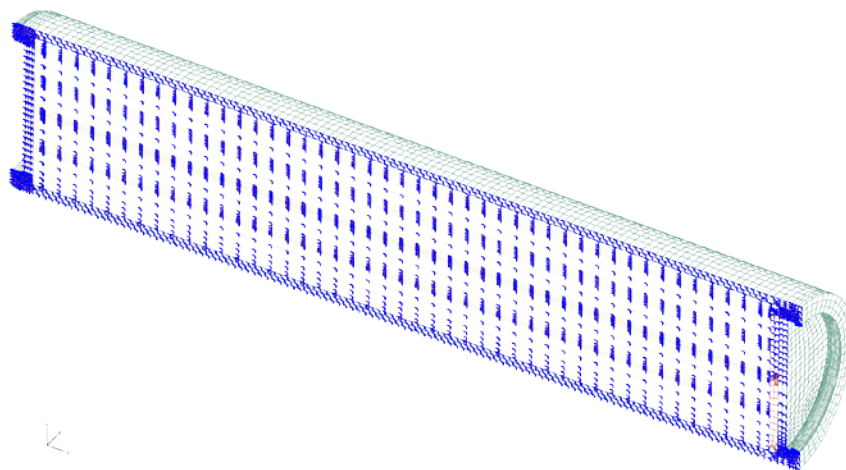


Figure 7-1. Prescribed symmetry conditions.

8 Calculations

8.1 General

Previous analyses for Earthquake induced rock shearing (Hernelind 2010) have been based on geometries having several simplifications as:

- Steel lid modelled without some details (valve, holes for mounting the valve and for the fixing screw).
- Steel lid without the centre fixing screw (instead the steel lid was tied to the insert at the periphery).
- The washer between the screw and steel lid was not modelled.
- Steel channel tubes tied to the insert and modelled without support plates.
- Base plate of the insert was modelled without screws, nuts and support plates derived from the fixing during the casting process.

Previous analyses also assumed a construction based on nominal measures and thus didn't study any effect of allowable tolerances and also the initial position of the steel channel tubes was assumed to be centred in the nodular cast iron insert.

The aim with this study is to check if the above mentioned assumptions are reasonable and not have a significant influences on the stress/strain levels and corresponding conclusions regarding damage tolerance analysis and mechanical integrity.

The geometry definition for both the BWR and the PWR canister is therefore created based on CAD-drawings with as few simplifications as possible.

The obtained results are compared with previous analyses (Hernelind 2010) when Ca-bentonite with density $2,050 \text{ kg/m}^3$ is used for the buffer. Two horizontal shear planes, one at 75% of the insert height from the base and one at the steel lid.

For the BWR insert only two cases are compared since most of the findings made for the PWR analyses also are valid for the BWR insert.

8.1.1 Rock shear calculation cases

The reference cases for BWR and PWR are based on Na-bentonite converted to Ca-bentonite with density $2,050 \text{ kg/m}^3$. Two cases of rock shear positions perpendicular to the axis of the canister have been analyzed (see also Table 1-1):

- at 75% of the height from the base of the insert
- at top of the insert lid

8.1.2 Analysis approach

The numerical calculations are performed using the FE-code ABAQUS version 6.12 (ABAQUS, Dassault Systèmes Simulia Corp.) assuming non-linear geometry and material definitions. This means that all non-linearities defined by the input will be considered such as large displacements, large deformations, non-linear interactions (contact) and non-linear materials. All non-linear contributions will be used when forming the equations to be solved for each equilibrium iteration. Short term analysis is based on quasi-static response but the results will depend on the time used for the simulation since rate-dependent material data is used. The code will choose suitable time-increments for the loading based on (in most cases) default convergence tolerances.

8.2 Short term analyses

The short term analyses (few seconds with 1 m/s as shearing velocity) consist of three steps where the shearing is prescribed by boundary conditions.

In the first step initial stresses corresponding to the swelling pressure (12.3 MPa for bentonite with density $2,050 \text{ kg/m}^3$) plus 5 MPa hydrostatic pressure (the deposition is made about 500 meters below the surface) in the bentonite is applied, see also in chapter "Initial conditions".

In the second step 5 cm is used for the shearing magnitude and finally the third step defines additional 5 cm shearing.

The results are shown in Appendix 1-6 and 8 for the PWR insert and in Appendix 7 for the BWR insert.

9 Results for rock shear

For each analysis a large amount of results are available and to have an indication only a few values are reported. When stress components are plotted S22 corresponds to normal stress in y-direction (lateral) and S33 corresponds to normal stress in z-direction (axial).

9.1 Comparison with previous analyses for the PWR insert

As reference case the horizontal shear plane at $\frac{3}{4}$ -distance from the insert base have been chosen since this case experience the highest stresses/strains for the insert. Figures 9-1 to 9-15 show the outcome at 10 cm shearing for the PWR insert. Appendix 8 contains the comparison at 5 cm shearing but since the detailed model includes the screw pre stress the comparison with the reference model shows significant differences for small shearing magnitudes and the comparison is misleading at 5 cm shearing.

Figures 9-1 to 9-6 show that the global response (stresses/strains) has small differences between the detailed modelling and the reference model for the PWR-insert. The biggest differences are found close to steel lid fixing bolt (which not exists in the reference model), Figure 9-6. Also at the steel lid connection to the insert shows an expected difference due to different approach for the contact (tied in the reference model and contact pair (simulates opening/closing) for the detailed model, Figures 9-2 and 9-3.

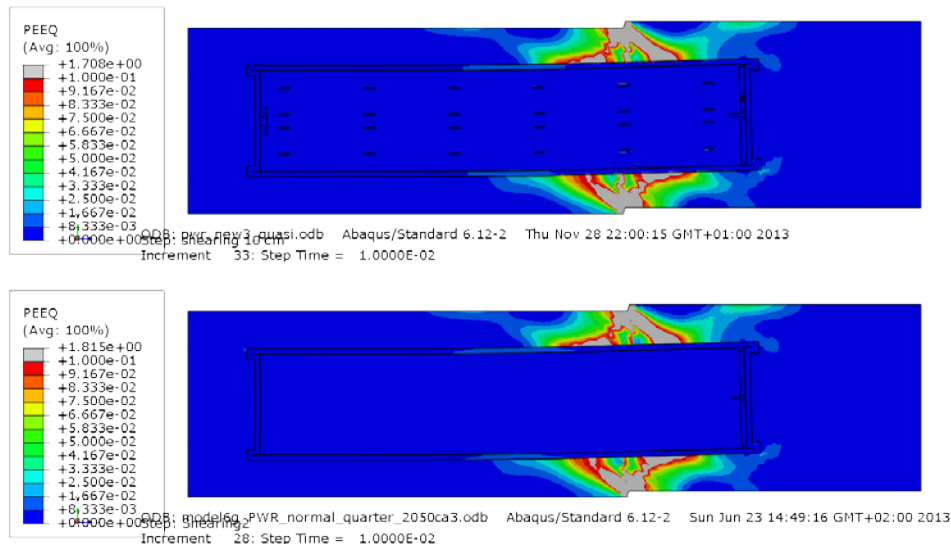


Figure 9-1 Plot showing plastic equivalent strain (PEEQ) after 10 cm shearing for detailed PWR model (top) and the reference PWR model (bottom).

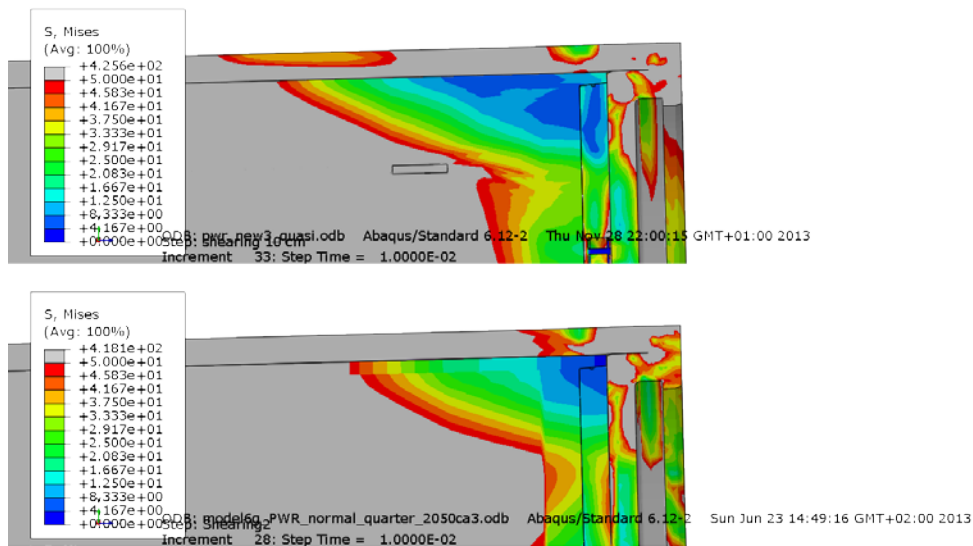


Figure 9-2 Plot showing Mises stress at the top left corner after 10 cm shearing for detailed PWR model (top) and the reference PWR model (bottom).

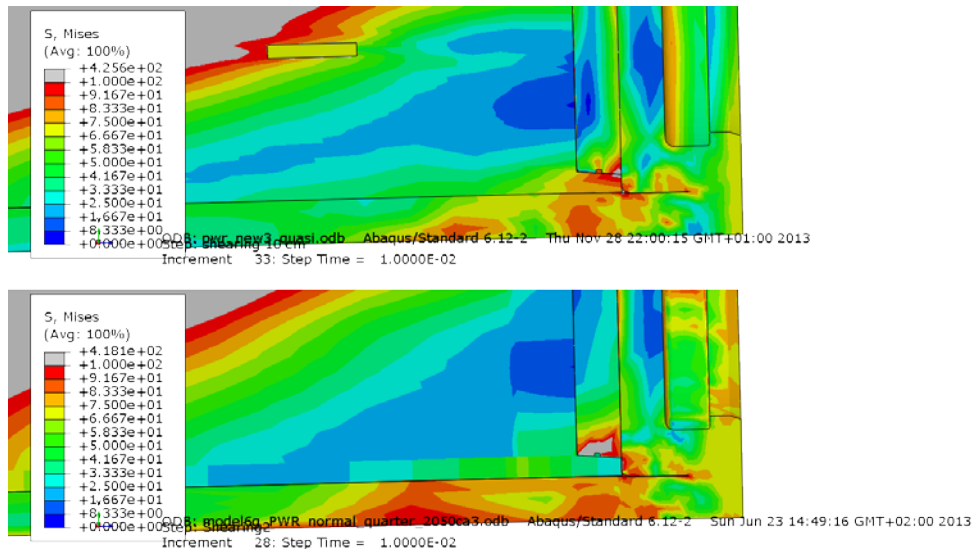


Figure 9-3 Plot showing Mises stress at the top right corner after 10 cm shearing for detailed PWR model (top) and the reference PWR model (bottom).

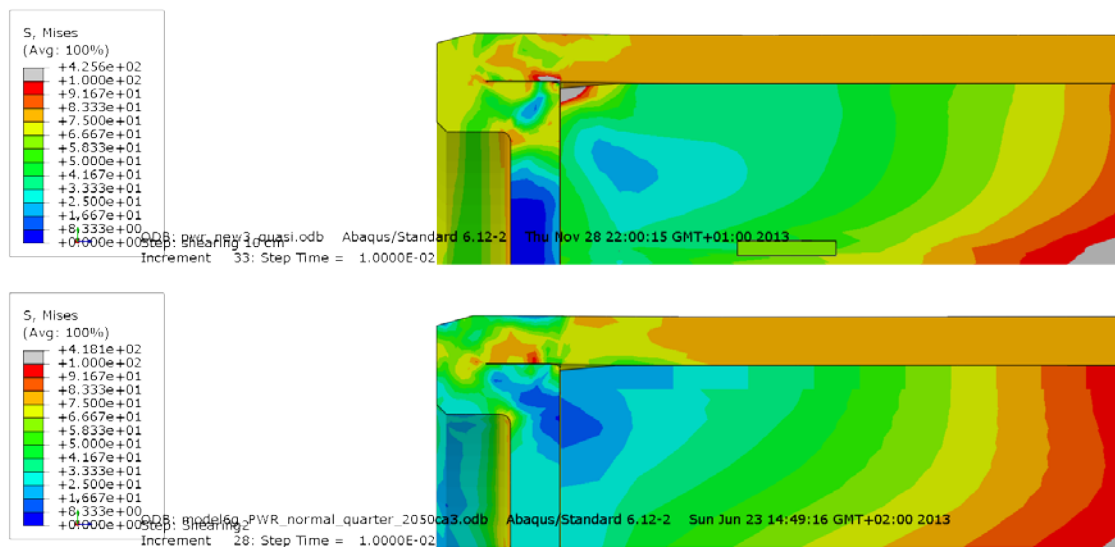


Figure 9-4 Plot showing Mises stress at the bottom left corner after 10 cm shearing for detailed PWR model (top) and the reference PWR model (bottom).

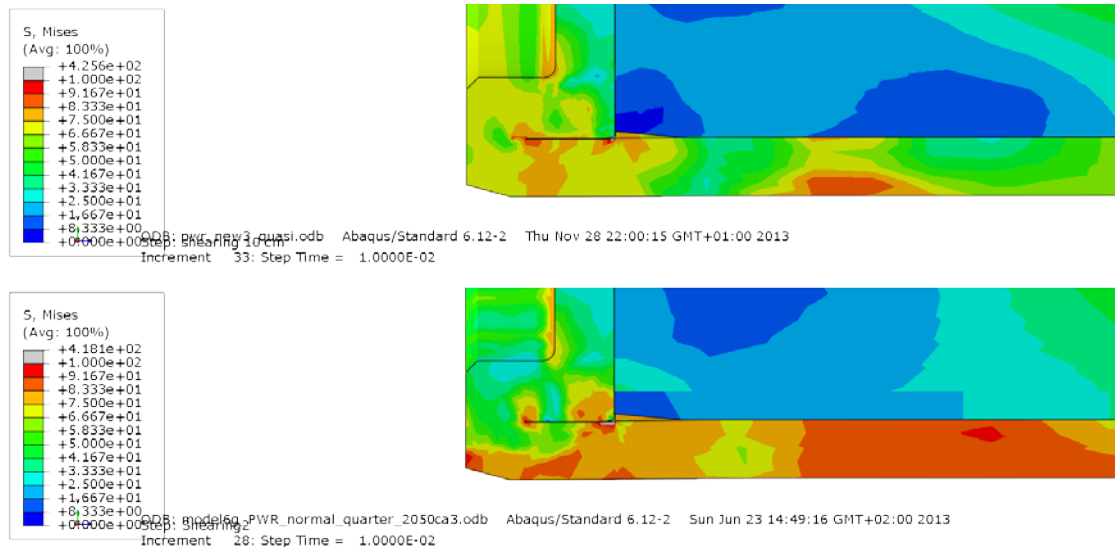


Figure 9-5 Plot showing Mises stress at the base right corner after 10 cm shearing for detailed PWR model (top) and the reference PWR model (bottom).

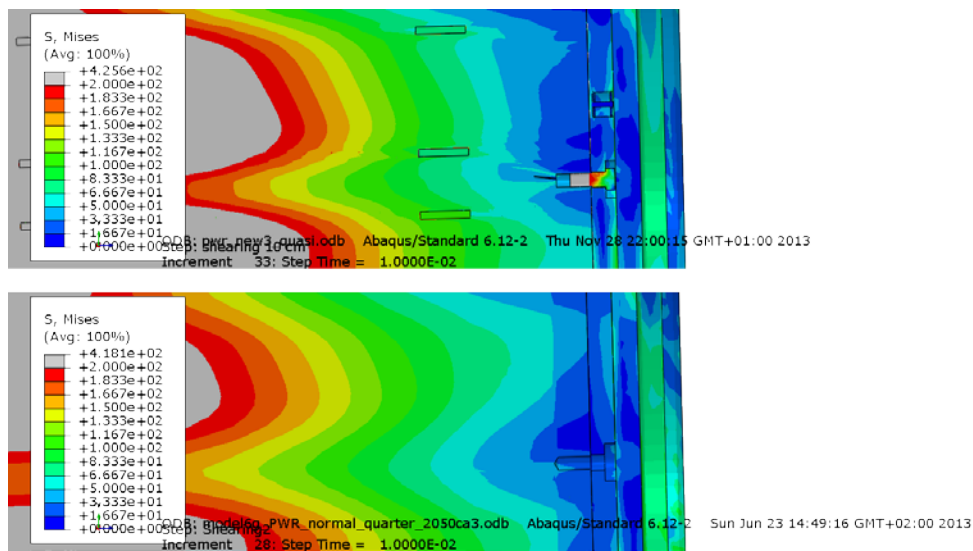


Figure 9-6 Plot showing Mises stress at the top close to the screw after 10 cm shearing for detailed PWR model (top) and the reference PWR model (bottom).

9.1.1 Copper shell

The results for the copper shell are shown in Figures 9-7 to 9-8 with almost no differences between the two models. The FE-model for the copper shell is identical for the two models and the results indicate that the stiffness for the insert including steel channels in a global sense has similar stiffness properties. The reference case has a higher peak value (occurs at a geometry discontinuity) but the magnitude is far below the level for causing severe damage.

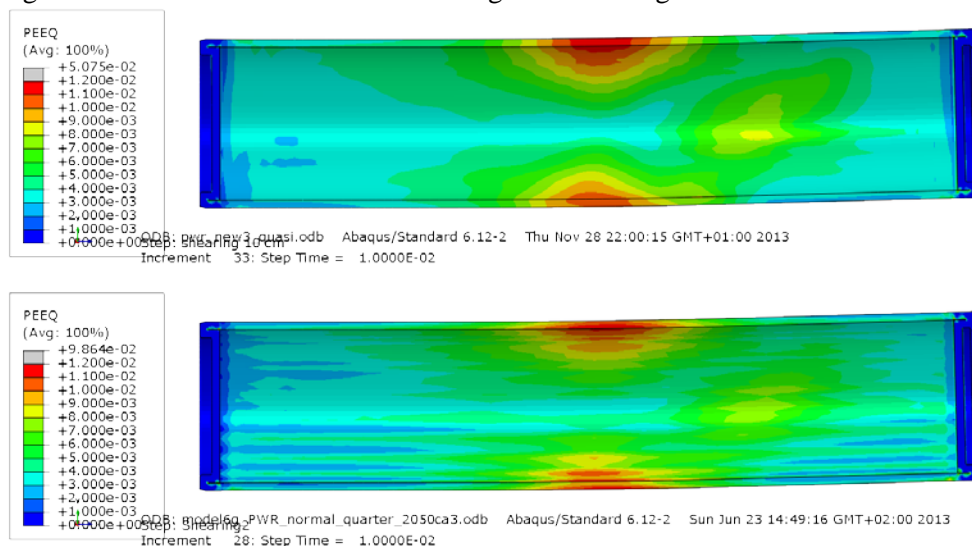


Figure 9-7 Plot showing plastic equivalent strain (PEEQ) for the copper shell after 10 cm shearing for detailed PWR model (top) and the reference PWR model (bottom).

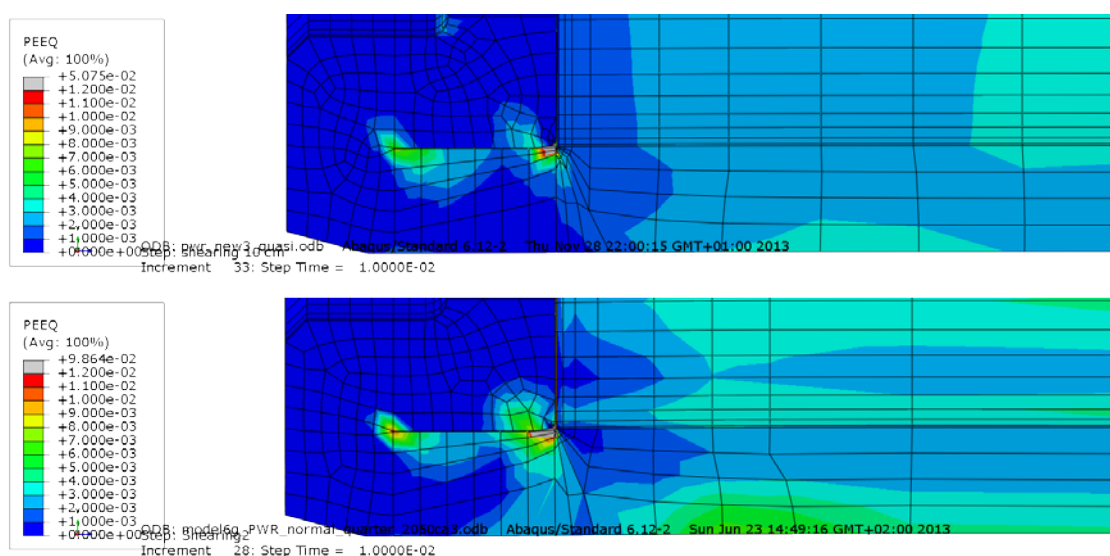


Figure 9-8 Plot showing plastic equivalent strain (PEEQ) for the copper shell after 10 cm shearing for detailed PWR model (top) and the reference PWR model (bottom).

9.1.2 Nodular cast iron insert

Figures 9-9 and 9-10 show similar results for the detailed and reference model for the equivalent plastic strain except at the corner radius for the steel channel tubes. The reason for the difference (0.91% for the detailed model and 0.80% for the reference model) is explained by different radius at the corners (15 mm radius at the corner for the detailed model and 20 mm for the reference model). The minimum allowed radius is 15 mm and the nominal value is 20 mm.

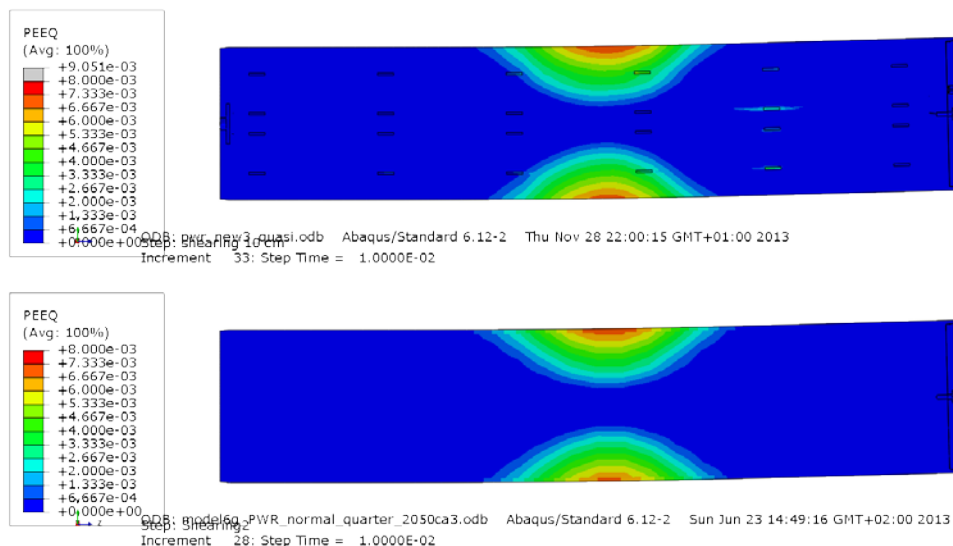


Figure 9-9 Plot showing plastic equivalent strain (PEEQ) for the insert after 10 cm shearing for detailed PWR model (top) and the reference PWR model (bottom).

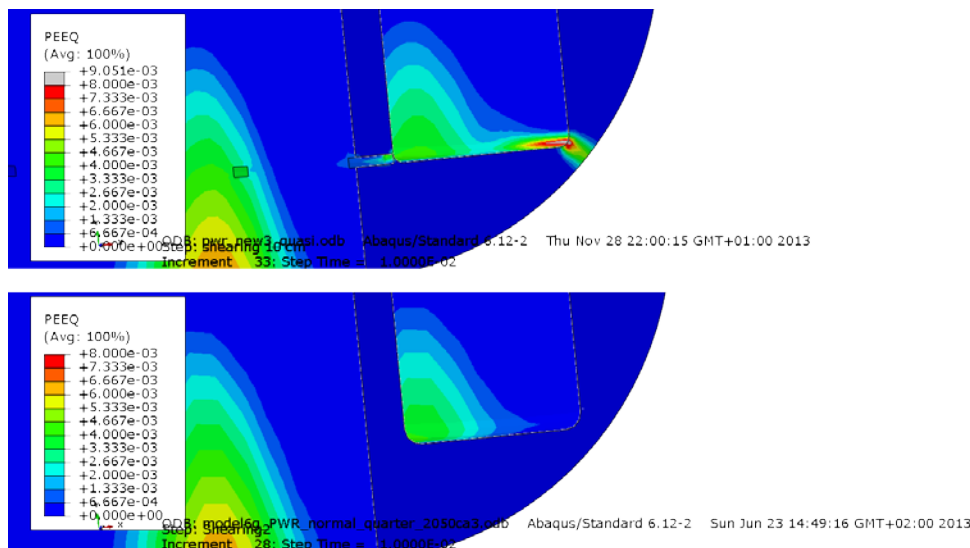


Figure 9-10 Plot showing plastic equivalent strain (PEEQ) for the insert after 10 cm shearing for detailed PWR model (top) and the reference PWR model (bottom).

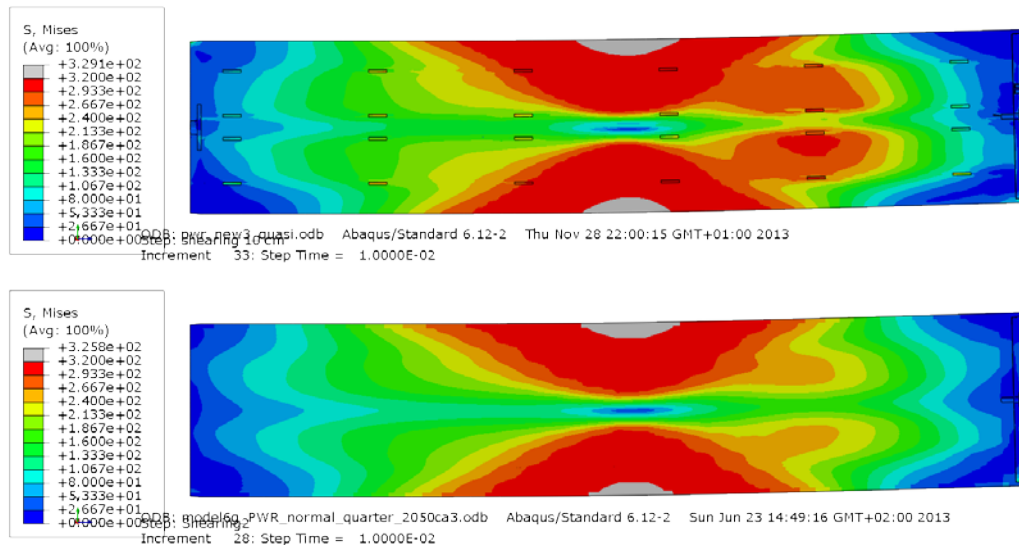


Figure 9-11 Plot showing Mises stress for the insert after 10 cm shearing for detailed PWR model (top) and the reference PWR model (bottom).

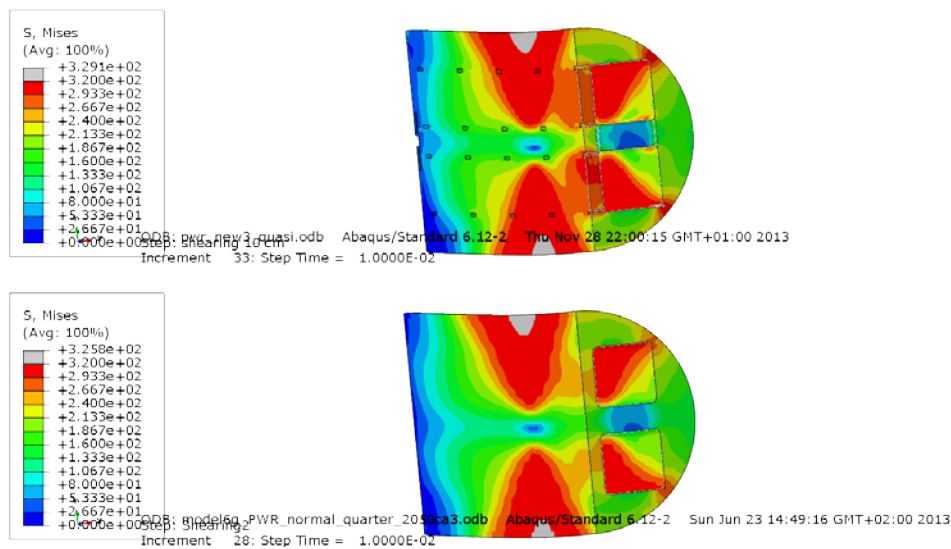


Figure 9-12 Plot showing Mises stress for the insert after 10 cm shearing for detailed PWR model (top) and the reference PWR model (bottom).

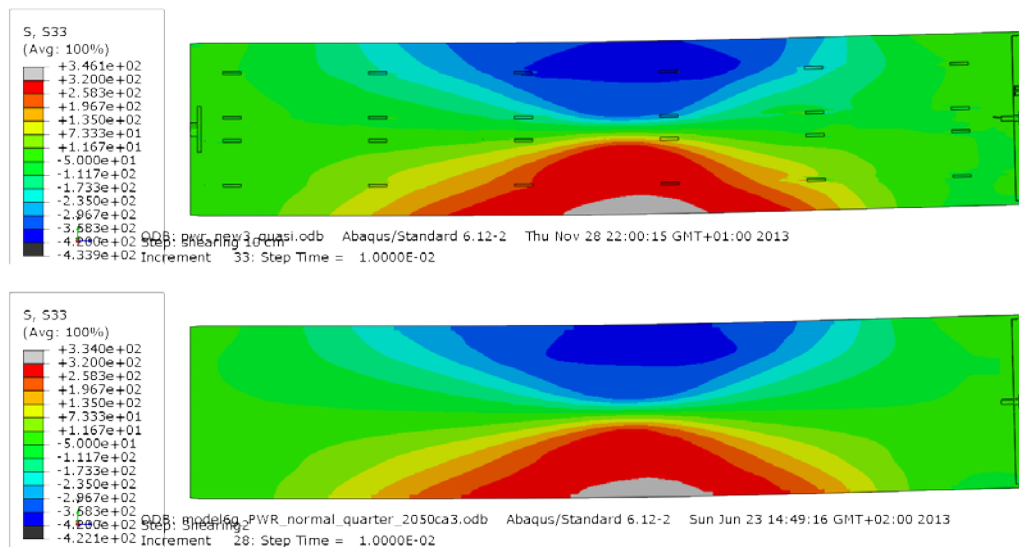


Figure 9-13 Plot showing axial stress (S_{33}) for the insert after 10 cm shearing for detailed PWR model (top) and the reference PWR model (bottom).

9.1.3 Steel channel tubes

Figures 9-14 to 9-15 show rather small differences between the detailed PWR-model and the reference model even though the reference model has the steel channel tubes tied to the cast iron insert. A small disturbance of the stress field is observed at the support plates connection to the channels tubes.

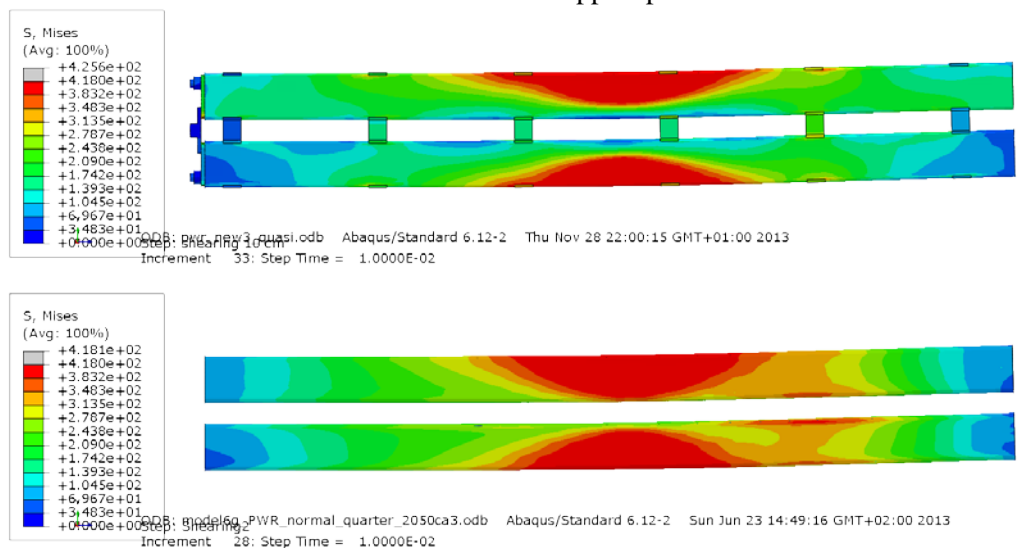


Figure 9-14 Plot showing Mises stress for the steel channel tubes after 10 cm shearing for detailed PWR model (top) and the reference PWR model (bottom).

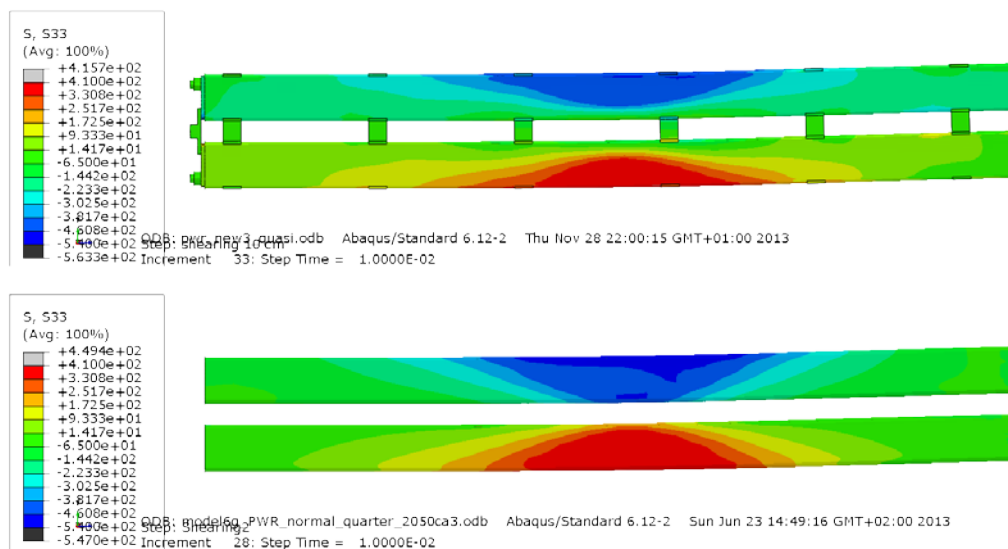


Figure 9-15 Plot showing axial stress (S_{33}) for the steel channel tubes after 10 cm shearing for detailed PWR model (top) and the reference PWR model (bottom).

9.2 Comparison with previous analyses for the BWR insert

As reference case the horizontal shear plane at $\frac{3}{4}$ -distance from the insert base have been chosen since this case experience the highest stresses/strains for the insert. Figures 9-16 to 9-28 show the outcome at 8 cm shearing (last converged result) for the BWR insert.

Figures 9-16 to 9-21 show that the global response (stresses/strains) shows similar but not identical results for the detailed modelling and the reference model for the BWR-insert.

It is a more noticeable difference for the BWR-insert compared to the PWR-insert – the main reason for this is that the BWR-insert has less material and therefore is more sensitive to local changes in the geometry modelling. Another observation is that even though the global response is similar for the two models the peak values differ more substantially. Some of this difference comes from geometry modelling difficulties due to extremely many details have been included.

Significant differences are observed for the steel lid which is expected due to different modelling of the interaction with the insert - steel lid fixing screw which only exists for the detailed model and also the peripheral connection which is a tied connection for the reference model and contact pairs (simulating opening/closing) for the detailed model.

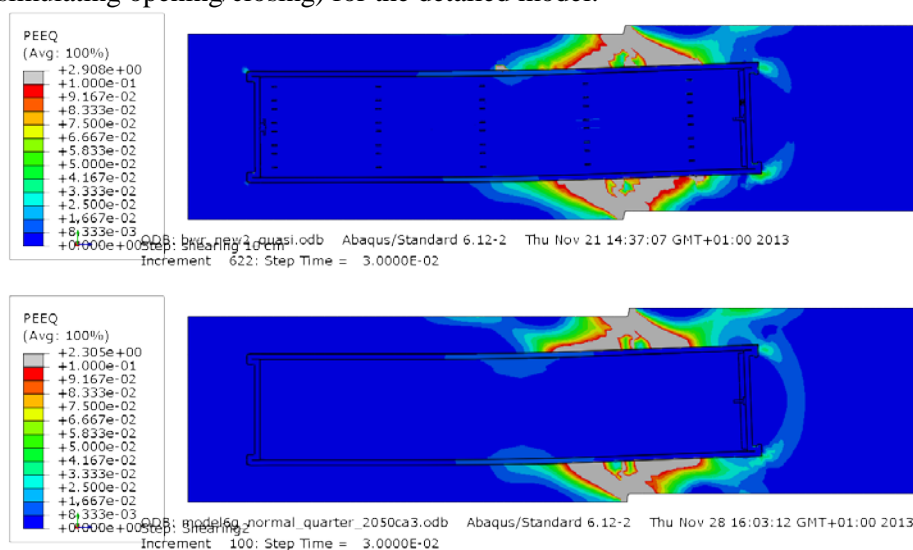


Figure 9-16 Plot showing equivalent plastic strain (PEEQ) after 8 cm shearing for detailed BWR model (top) and the reference BWR model (bottom).

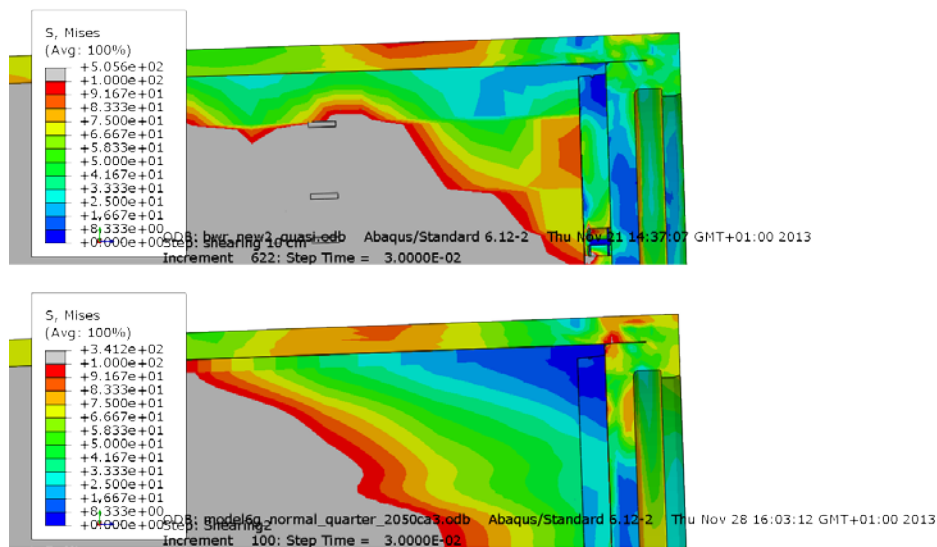


Figure 9-17 Plot showing Mises stress at the left top corner after 8 cm shearing for detailed BWR model (top) and the reference BWR model (bottom).

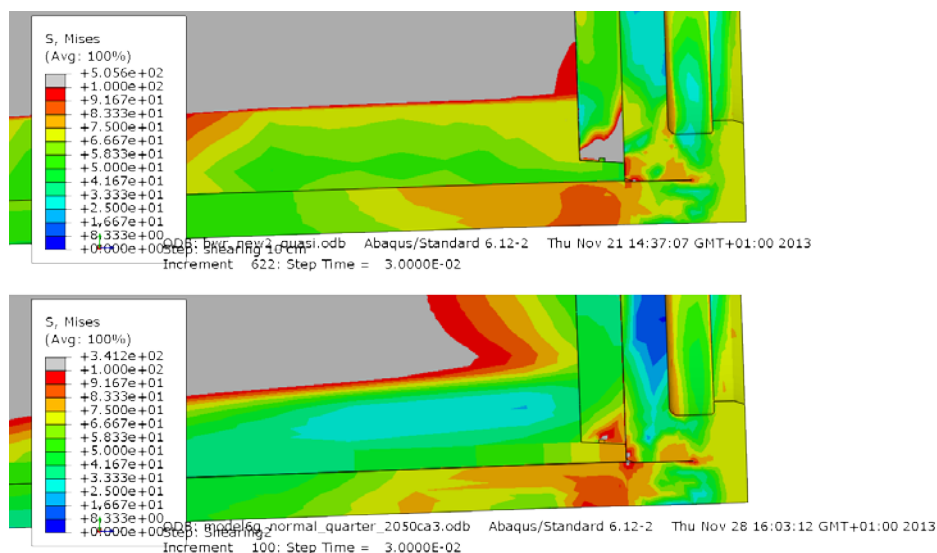


Figure 9-18 Plot showing Mises stress at the right top corner after 8 cm shearing for detailed BWR model (top) and the reference BWR model (bottom).

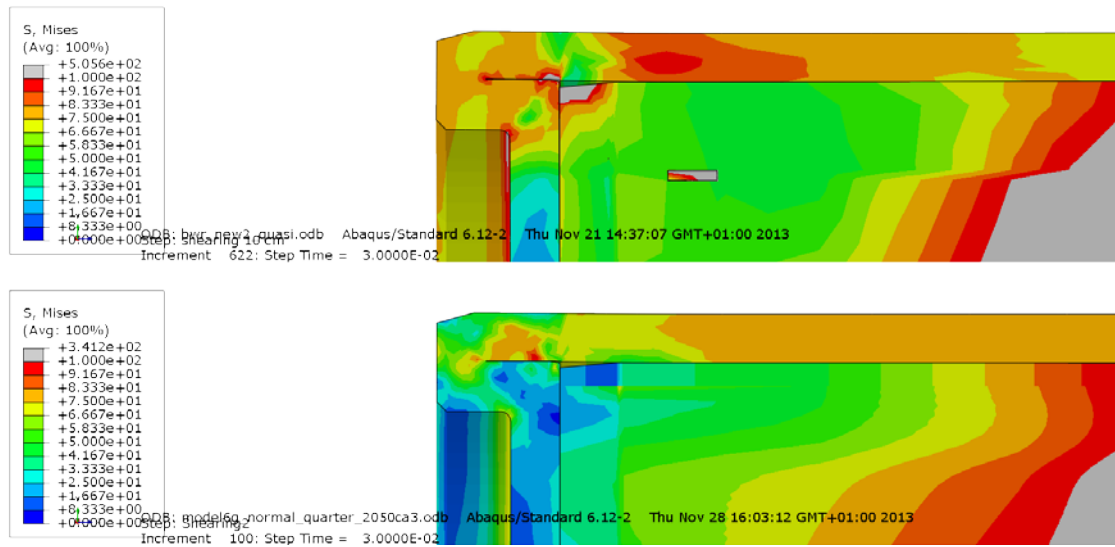


Figure 9-19 Plot showing Mises stress at the left bottom corner after 8 cm shearing for detailed BWR model (top) and the reference BWR model (bottom).

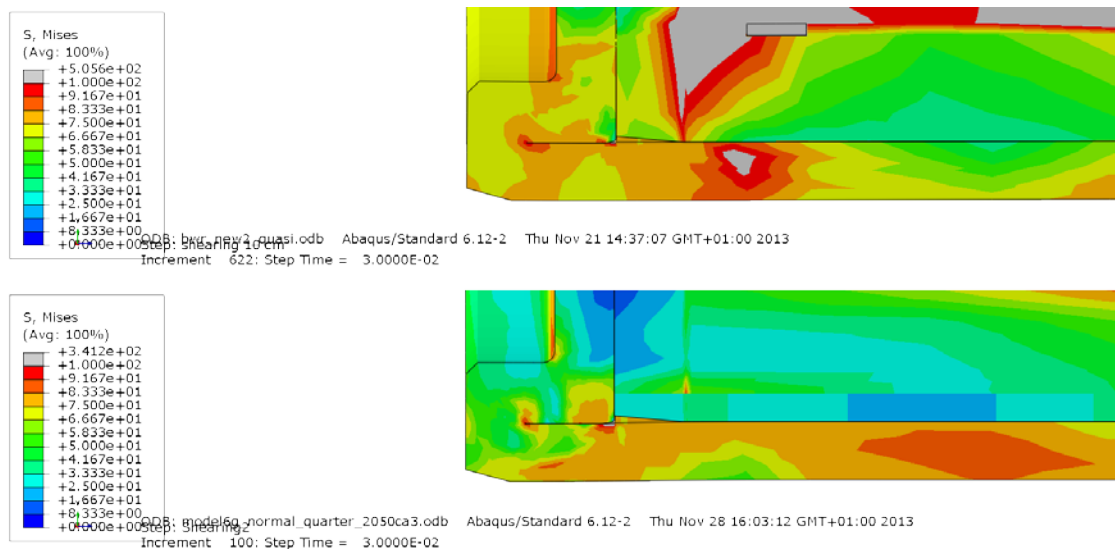


Figure 9-20 Plot showing Mises stress at the right top corner after 8 cm shearing for detailed BWR model (top) and the reference BWR model (bottom).

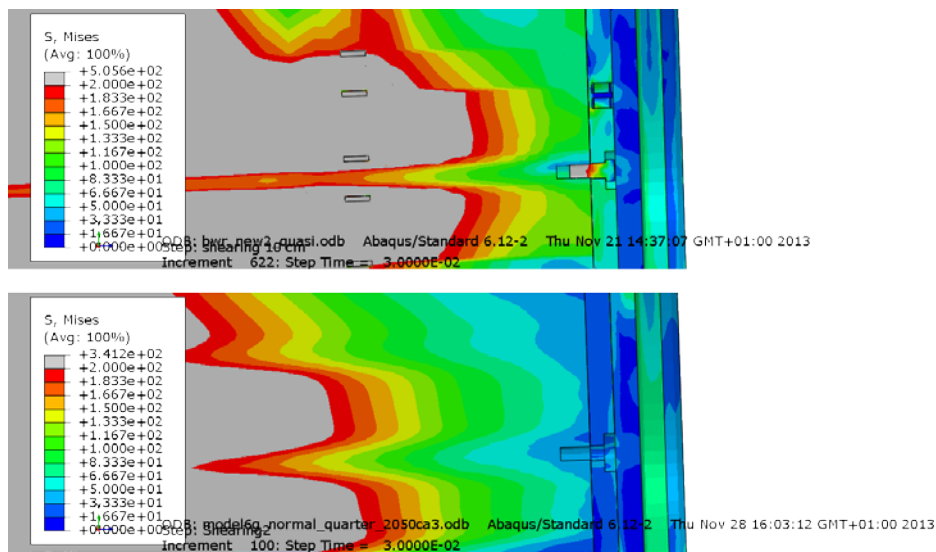


Figure 9-21 Plot showing Mises stress at the top close to the screw after 8 cm shearing for detailed BWR model (top) and the reference BWR model (bottom).

9.2.1 Copper shell

Figures 9-22 to 9-23 show rather small differences between the detailed BWR-model and the reference model for the copper shell. Highest values are for the reference model even though the global response shows higher values for the detailed BWR-model. The global values are acceptable and the local peak values occur in areas mainly in compression and where the model has discontinuities.

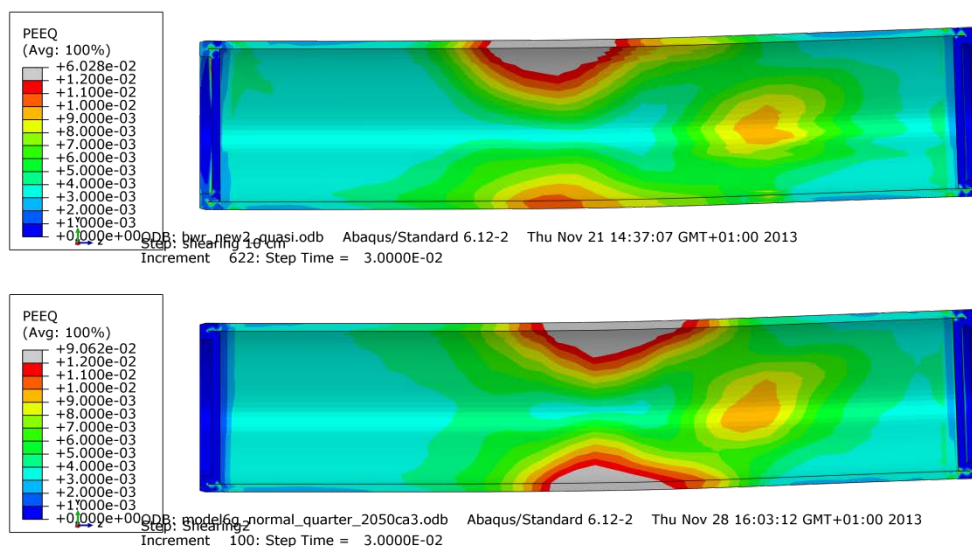


Figure 9-22 Plot showing equivalent plastic strain (PEEQ) for the copper shell after 8 cm shearing for detailed BWR model (top) and the reference BWR model (bottom).

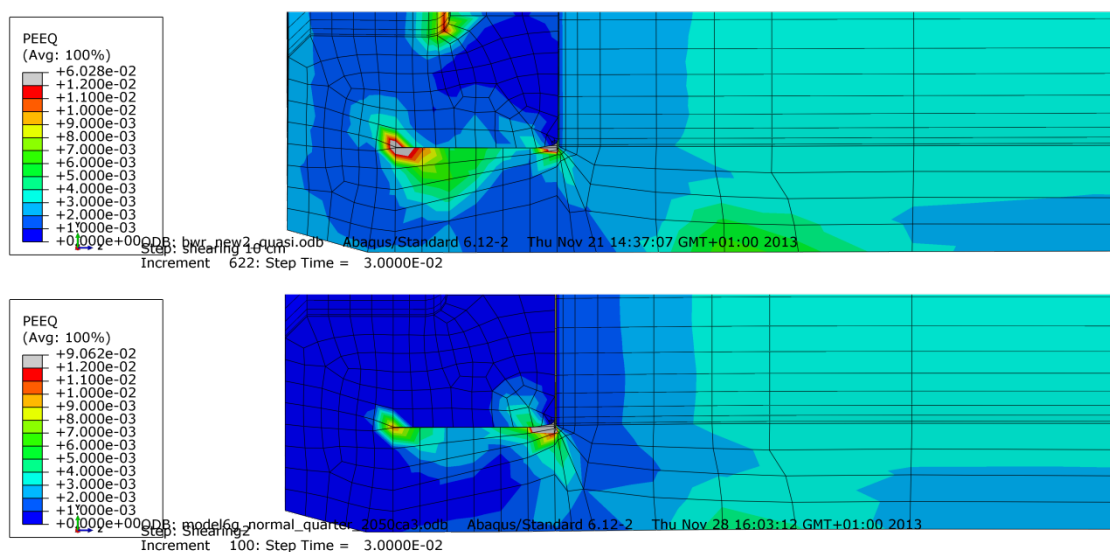


Figure 9-23 Plot showing equivalent plastic strain (PEEQ) for the copper shell after 8 cm shearing for detailed BWR model (top) and the reference BWR model (bottom).

9.2.2 Nodular cast iron insert

Figures 9-24 and 9-25 show similar results for detail modelling and the reference case for the equivalent plastic strain except at the corner radius for the steel channel tubes.

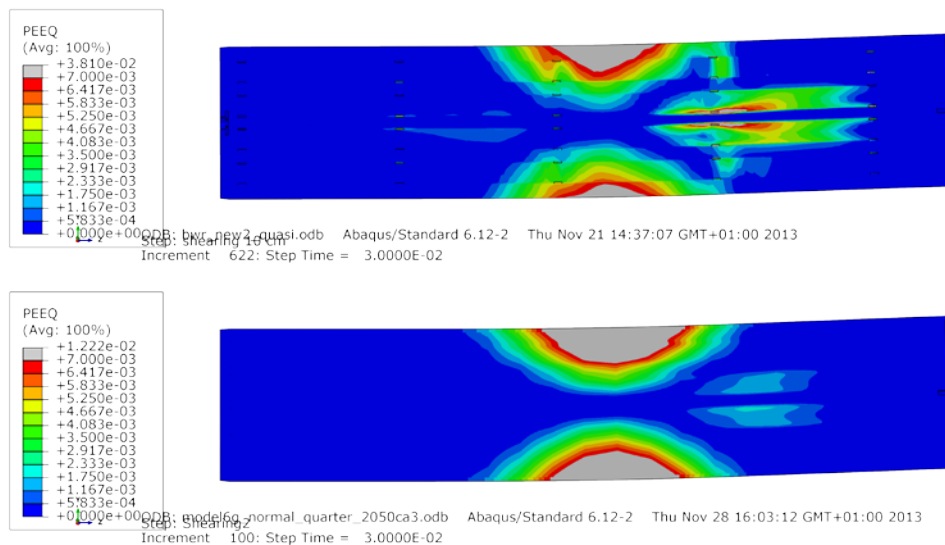


Figure 9-24 Plots showing plastic equivalent strain (PEEQ) for the insert after 8 cm shearing for detailed BWR model (top) and the reference BWR model (bottom).

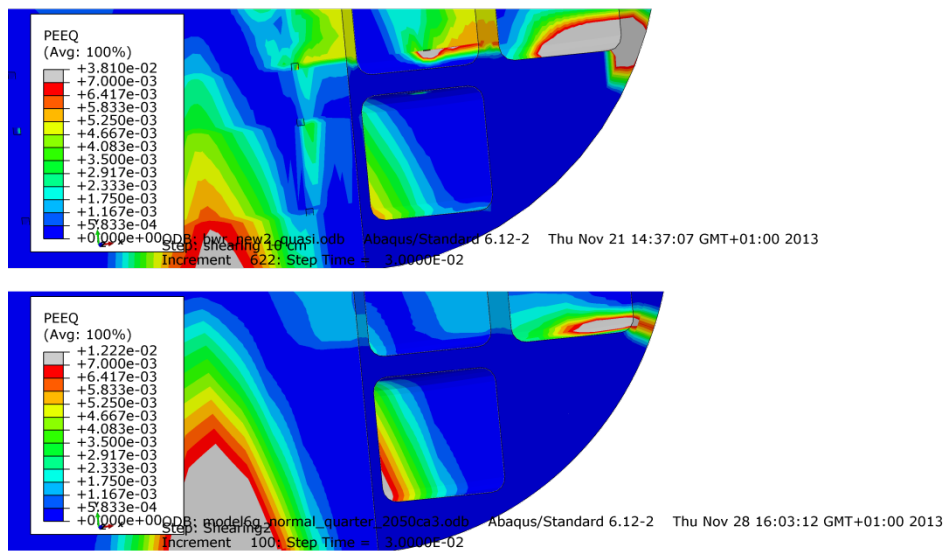


Figure 9-25 Plots showing plastic equivalent strain (PEEQ) for the insert after 8 cm shearing for detailed BWR model (top) and the reference BWR model (bottom).

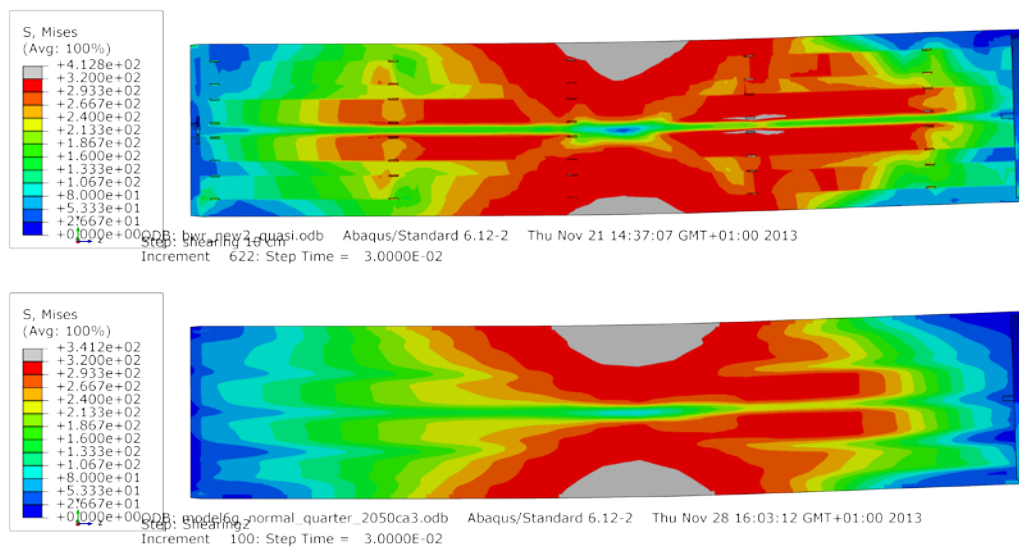


Figure 9-26 Plots showing Mises stress for the insert after 8 cm shearing for detailed BWR model (top) and the reference BWR model (bottom).

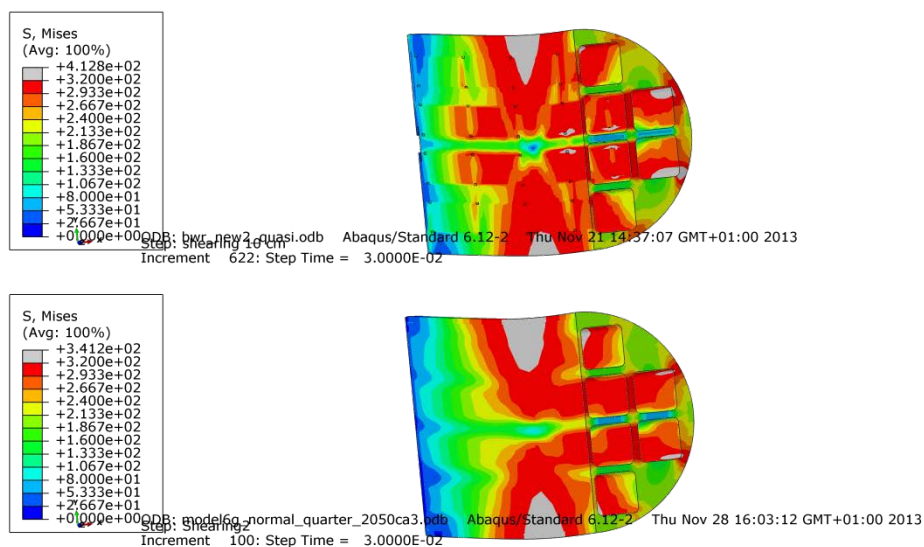


Figure 9-27 Plots showing Mises stress for the insert after 8 cm shearing for detailed BWR model (top) and the reference BWR model (bottom).

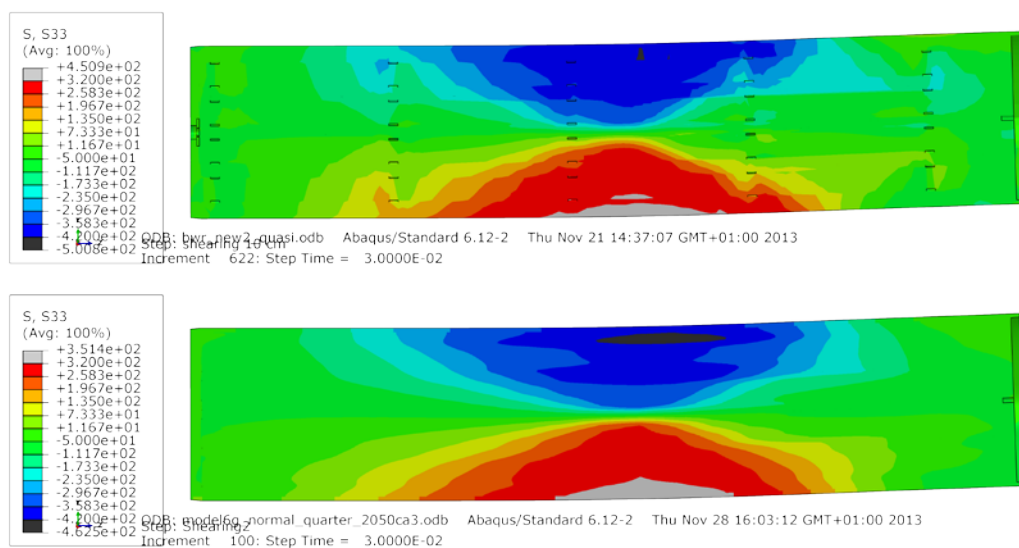


Figure 9-28 Plots showing axial stress (S33) for the insert after 8 cm shearing for detailed BWR model (top) and the reference BWR model (bottom).

9.2.3 Steel channel tubes

Figures 9-29 to 9-30 show differences between the detailed BWR-model and the reference model. One observation is that the global stress level is lower for the detailed model even though the maximum value is higher. The reason for the decreased stress level could be explained by the support plates which increase the bending stiffness.

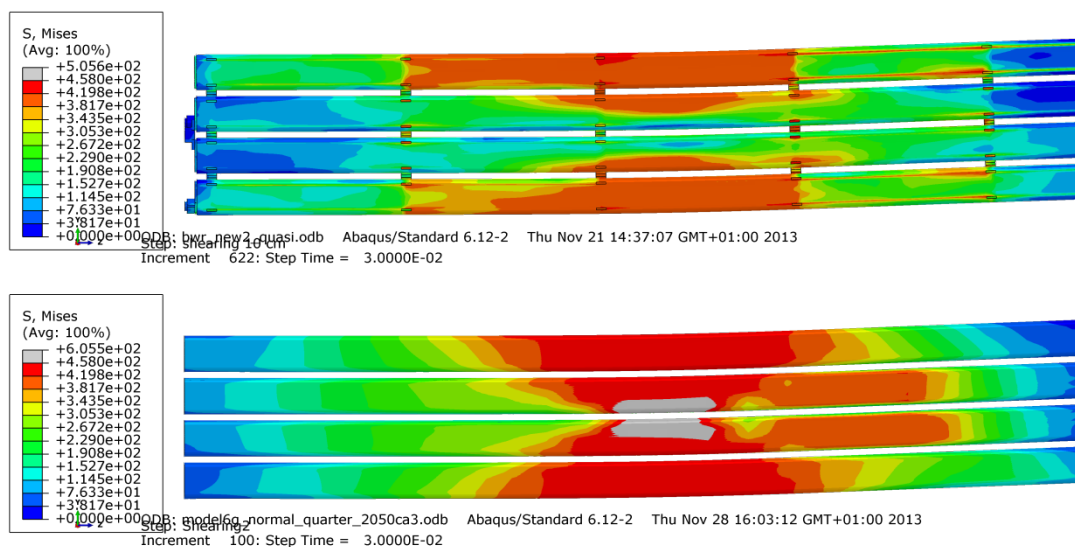


Figure 9-29 Plots showing Mises stress for the steel channel tubes after 8 cm shearing for detailed BWR model (top) and the reference BWR model (bottom).

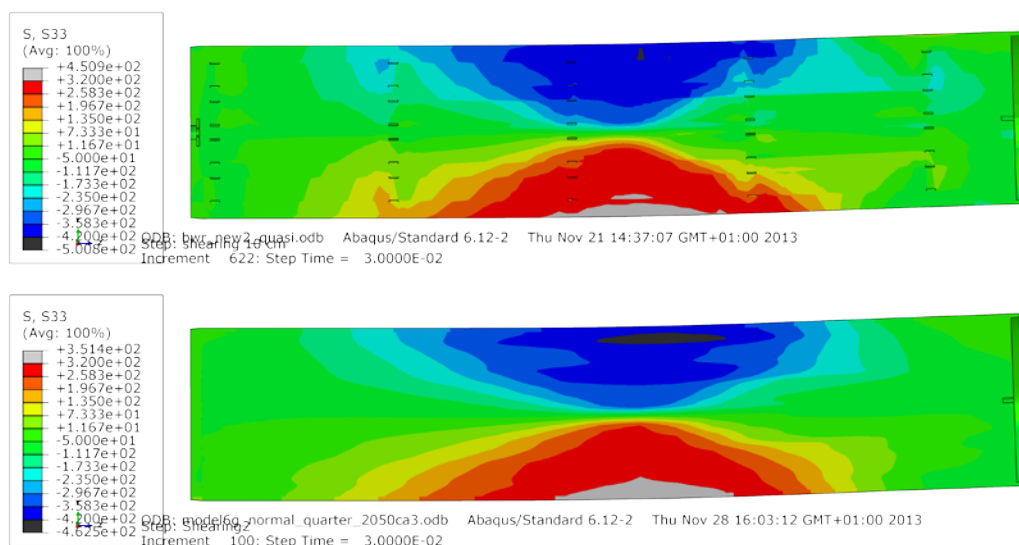


Figure 9-30 Plots showing axial stress (S33) for the steel channel tubes after 8 cm shearing for detailed BWR model (top) and the reference BWR model (bottom).

9.3 Steel lid fixed with central screw or welded to the PWR insert

One simplification made for the reference case is welding of the steel lid to the insert at the outer periphery. The current design instead uses a central screw to fix the steel lid to the insert. Figures 9-31 to 9-35 show differences between the reference case and new detailed model when a horizontal shearing is applied at the steel lid which is assumed to be the most severe location for impact from the steel lid. Figures 9-31 to 9-32 show that the plastic strain in the copper shell are close between the two models even though the compressive stresses in the steel lid is much higher for the model having the steel lid fixed by a screw (Figures 9-33 to 9-34). The screw also implies local stress increase (Figure 9-35) even though the stress level is rather low.

Figures 9-36 to 9-37 shows the results for the insert when shearing at the lid: The Mises stress plot, Figure 9-36, shows similar results even though the maximum value differs (306 respectively 393 MPa for the reference case). Figure 9-37 shows that only the case with fixing the lid with central screw implies equivalent plastic strain (PEEQ) but rather small, 0.24%.

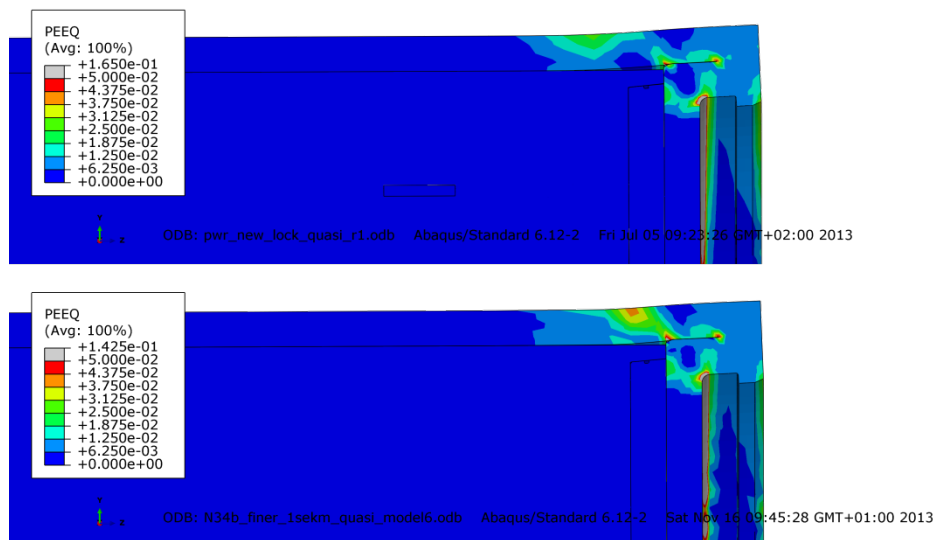


Figure 9-31 Plots showing equivalent plastic strain (PEEQ) at the top left corner after 8 cm shearing for detailed PWR model (top) and the reference PWR model (bottom).

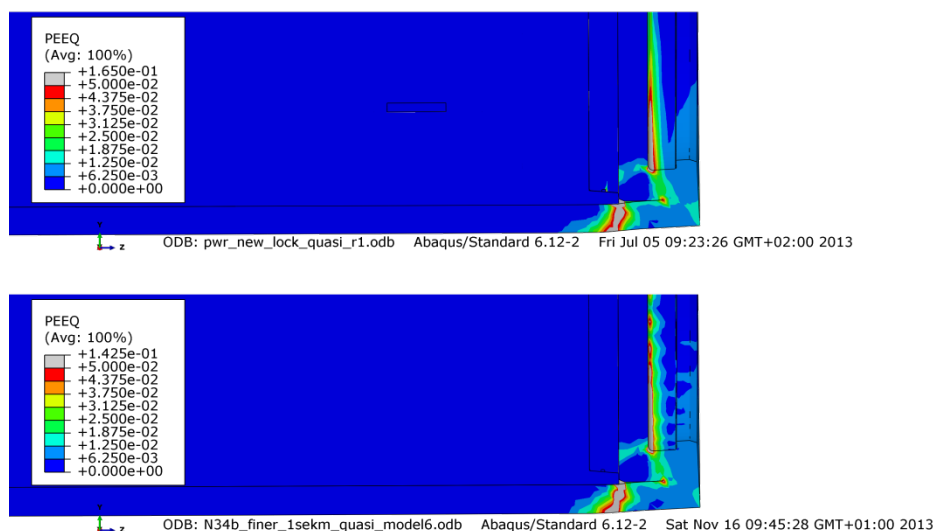


Figure 9-32 Plots showing equivalent plastic strain (PEEQ) at the top right corner after 8 cm shearing for detailed PWR model (top) and the reference PWR model (bottom).

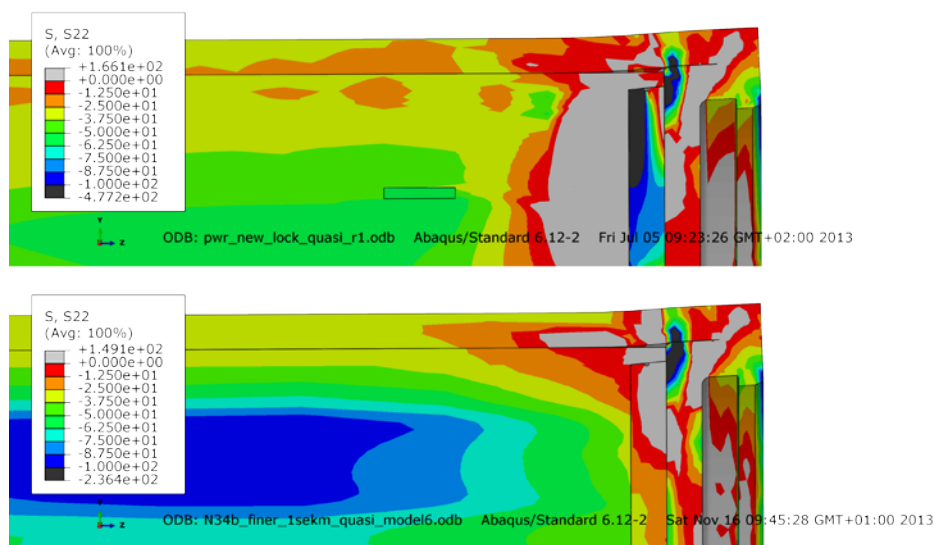


Figure 9-33 Plots showing lateral stress (S_{22}) at the top left corner after 8 cm shearing for detailed PWR model (top) and the reference PWR model (bottom).

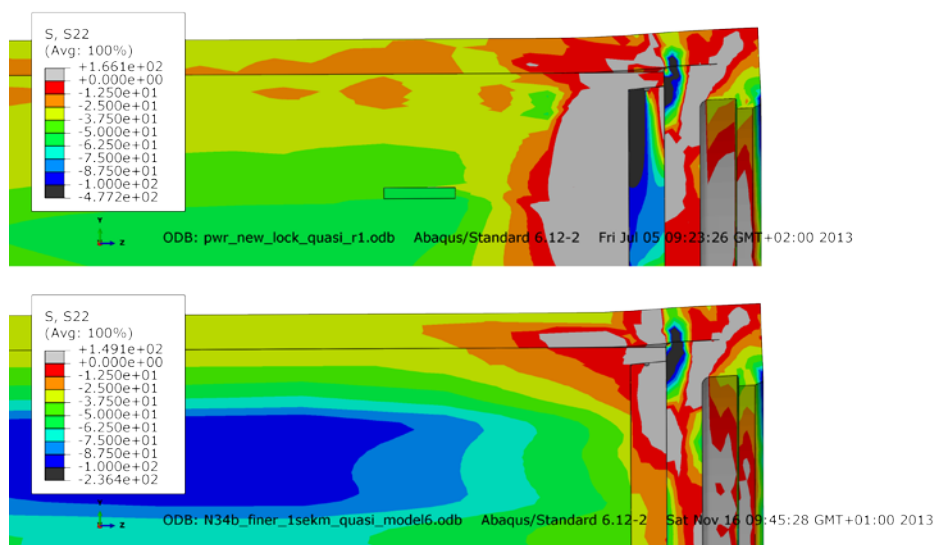


Figure 9-34 Plots showing lateral stress (S_{22}) at the top right corner after 8 cm shearing for detailed PWR model (top) and the reference PWR model (bottom).

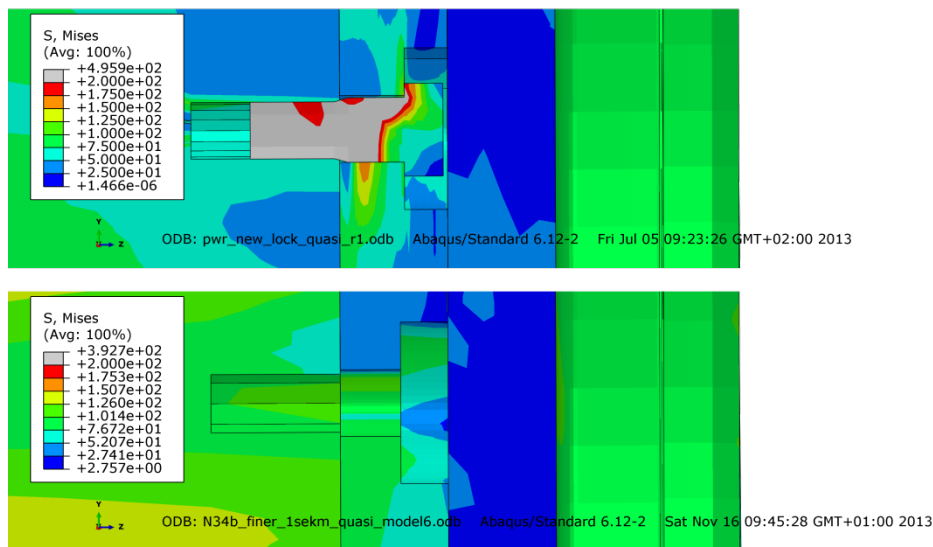


Figure 9-35 Plots showing Mises stress at the top around the fixing screw after 8 cm shearing for detailed PWR model (top) and the reference PWR model (bottom).

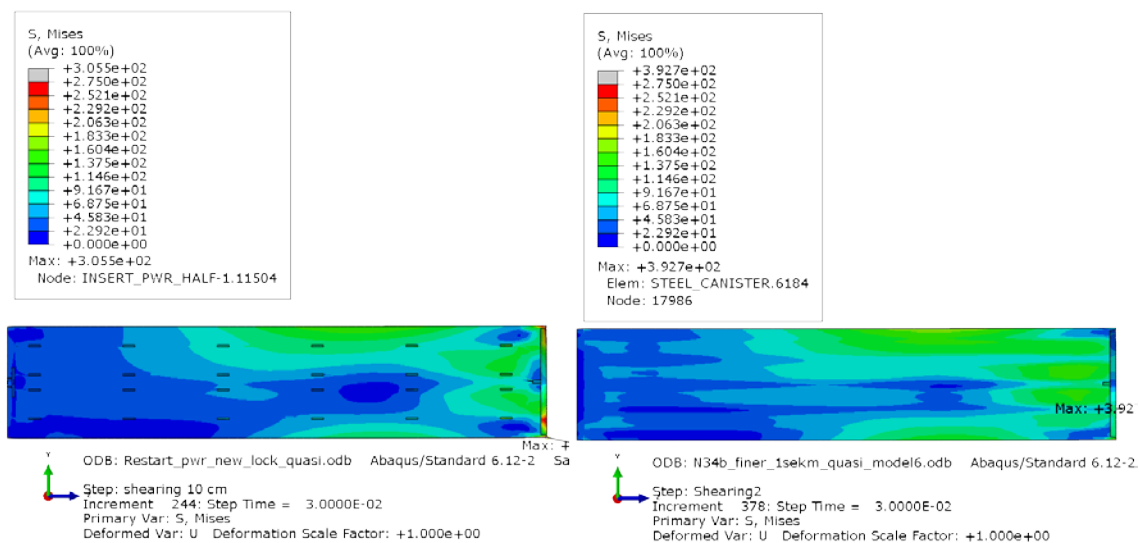


Figure 9-36 Plot showing Mises stress in the insert after 8 cm shearing at the lid for detailed PWR model (left) and the reference PWR model (right).

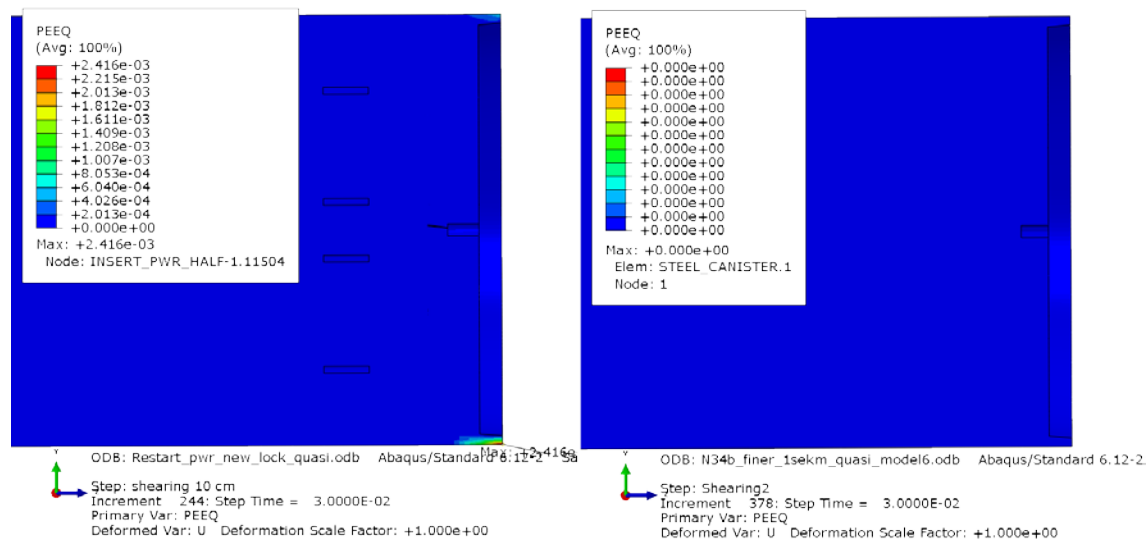


Figure 9-37 Plots showing equivalent plastic strain (PEEQ) in the insert after 8 cm shearing at the lid for detailed PWR model (left) and the reference PWR model (right).

9.4 Eccentric positioning of the steel channel tubes for the PWR insert

The reference case is based on nominal dimensions but the drawings also define allowable tolerances. One case of interest is when the tolerances imply that the steel channel tubes are placed as most eccentric as possible (10 mm) leading to decreased wall thickness at one corner. Figures 9-38 to 9-43 compare results using the detailed model for centric and eccentric positioning of the steel channel tubes when a horizontal shearing is applied at $\frac{3}{4}$ -distance from the insert base.

Figure 9-38 shows positioning of steel channel tubes with and without tolerances. Figures 9-39 to 9-40 show comparison of the Mises stress and equivalent plastic strain (PEEQ) where a slightly increase could be observed when eccentric positioning. The peak value for Mises stress increases from 426 to 454 MPa and plastic equivalent strain increases from 6.3 to 9.1%. However, visual inspection of the plots show very similar contours. Figures 9-41 to 9-42 show similar observation for the steel channel tubes. The peak value for axial stress (S33) increases from 416 to 429 MPa. The largest difference is for the equivalent plastic strain (PEEQ), 0.9 respectively 1.7%, at the corner radius of the insert for the thinnest wall thickness, Figure 9-43.

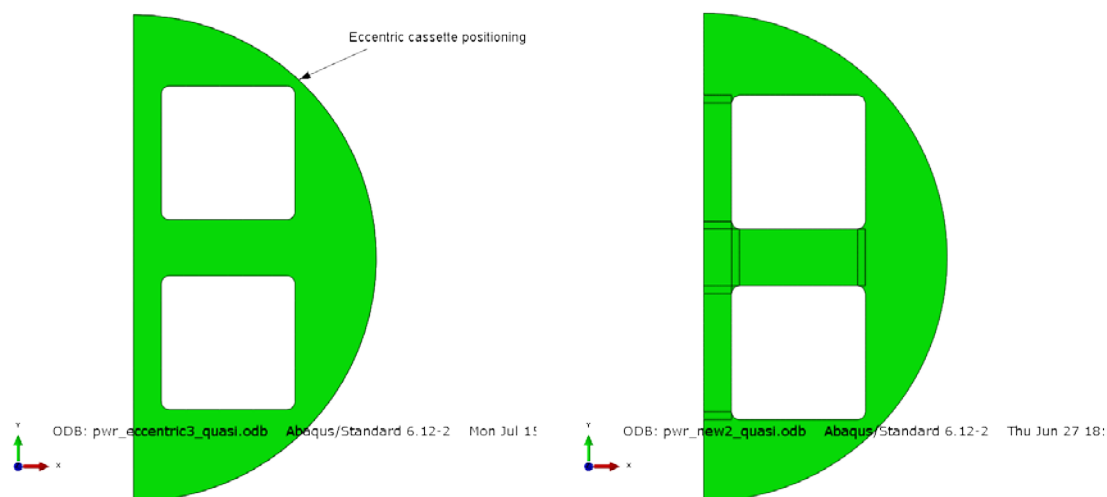


Figure 9-38 Plots showing positioning of steel channel tubes, eccentric (left) and centric (right).

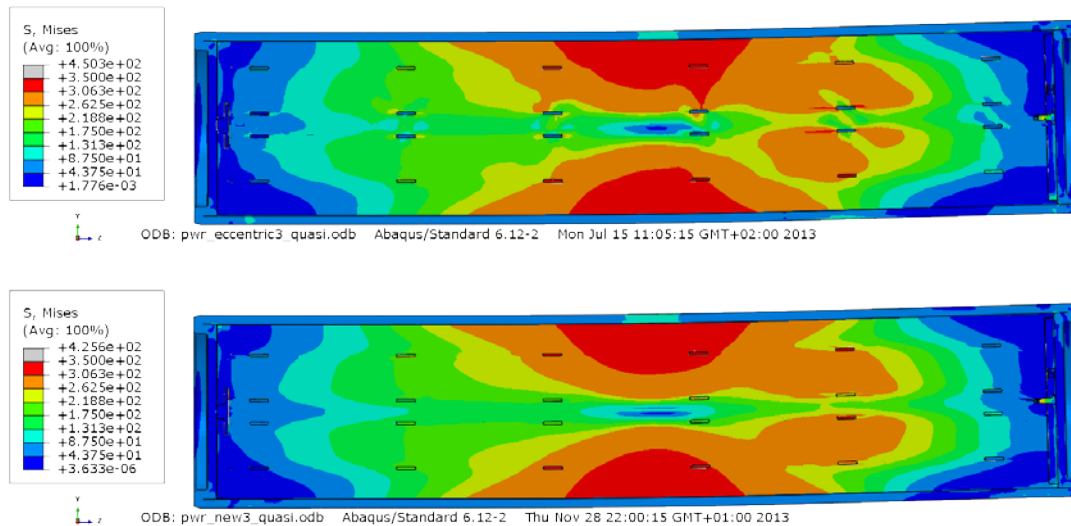


Figure 9-39 Plots showing Mises stress after 6 cm shearing for eccentric PWR model (top) and the centric PWR model (bottom).

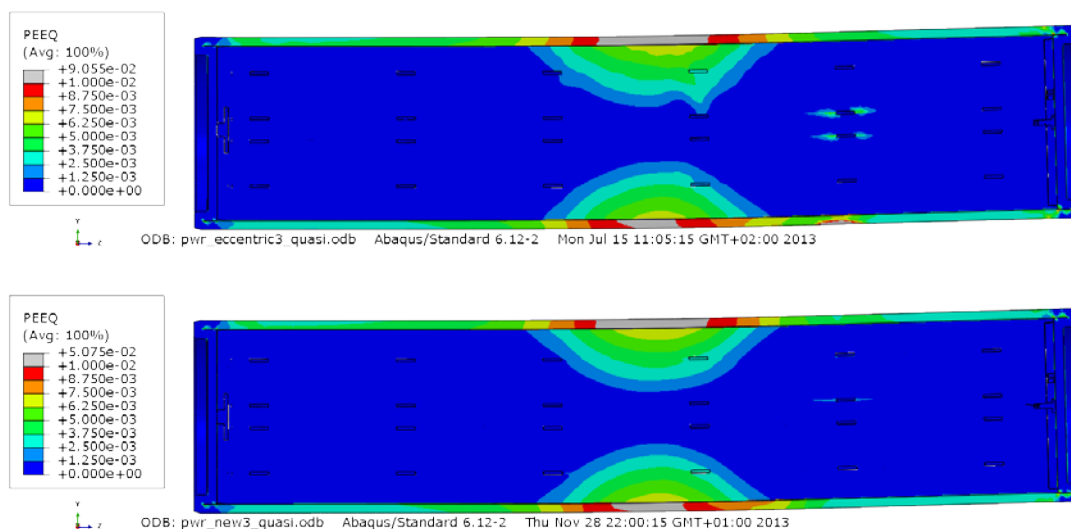


Figure 9-40 Plots showing equivalent plastic strain (PEEQ) after 6 cm shearing for eccentric PWR model (top) and the centric PWR model (bottom).

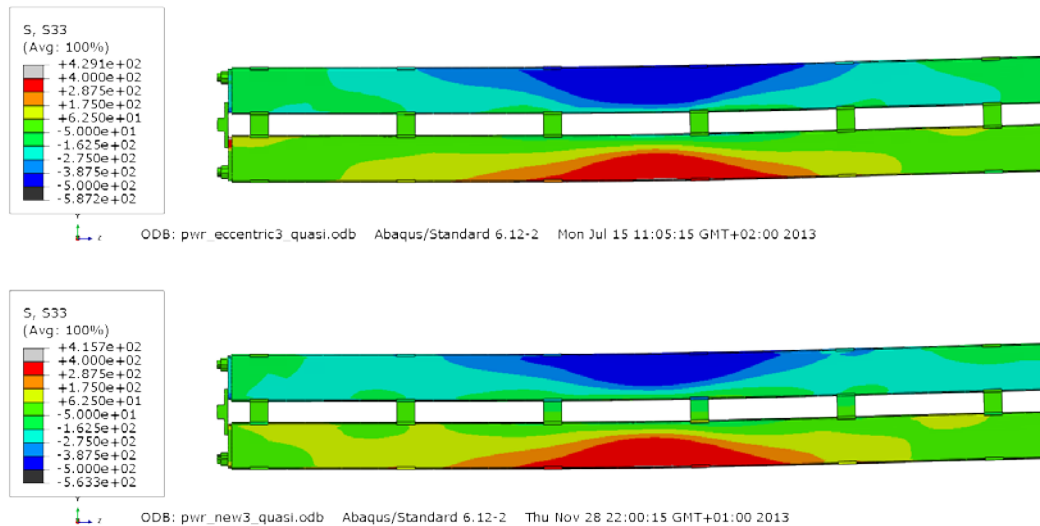


Figure 9-41 Plots showing axial stress for the steel channel tubes after 6 cm shearing for eccentric PWR model (top) and the centric PWR model (bottom).

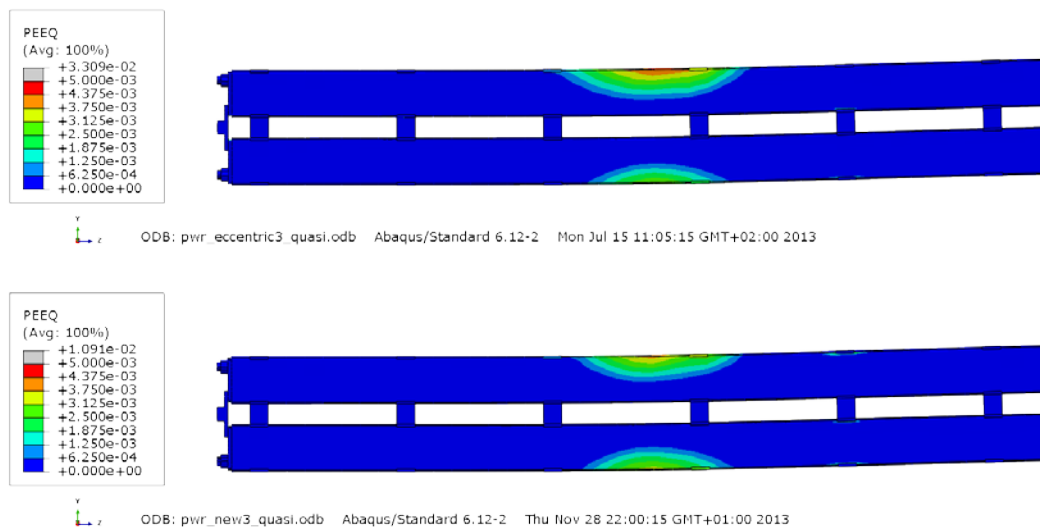


Figure 9-42 Plots showing equivalent plastic strain (PEEQ) for the steel channel tubes after 6 cm shearing for eccentric PWR model (top) and the centric PWR model (bottom).

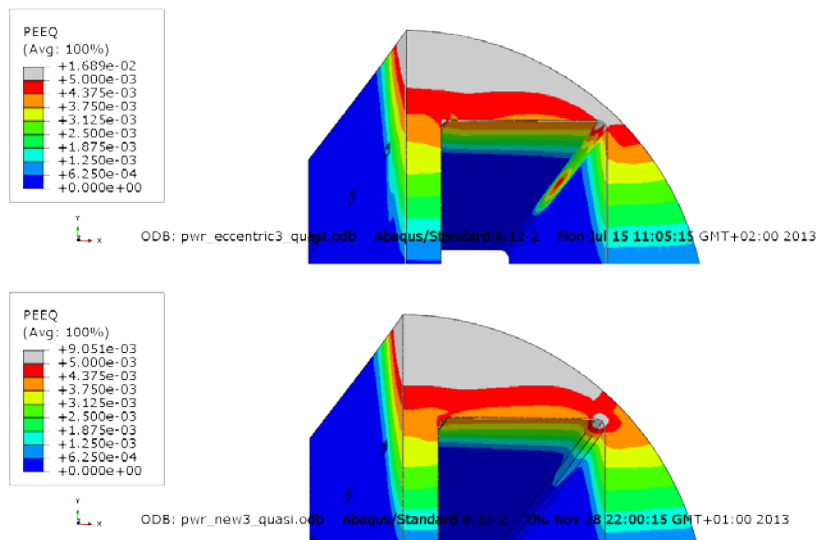


Figure 9-43 Plots showing equivalent plastic strain (PEEQ) for the insert after 6 cm shearing for eccentric PWR model (top) and the centric PWR model (bottom).

9.5 Initial insert/copper shell positioning for the PWR insert

The reference case assumes that the insert and the copper shell are co-axial but it is possible that the insert initially is in contact with the copper shell. Figures 9-44 to 9-47 compare the results using the detailed model for co-axial/no co-axial positioning when the horizontal shear plane is at $\frac{3}{4}$ -distance from the insert base. As can be seen from Figures 9-46 to 9-47 the initial position of the insert relative to the copper shell has extremely small effect. Figures 9-44 to 9-45 shows the initial positioned insert relative to the copper shell.

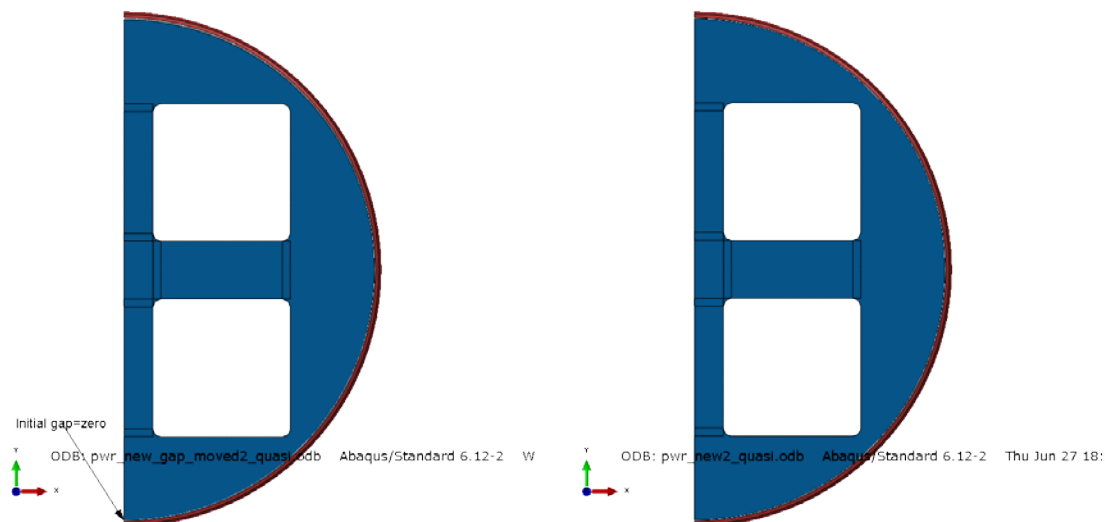


Figure 9-44 Plots showing geometry for eccentric placed insert (left) and co-axial insert (right) relative to the copper shell.

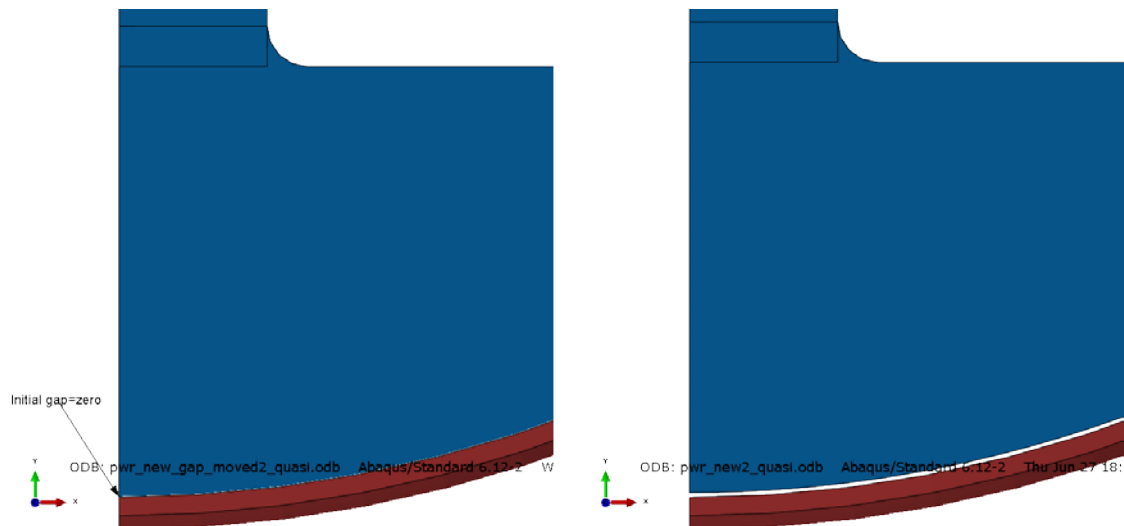


Figure 9-45 Plots showing geometry for eccentric placed insert (left) and co-axial insert (right) relative to the copper shell.

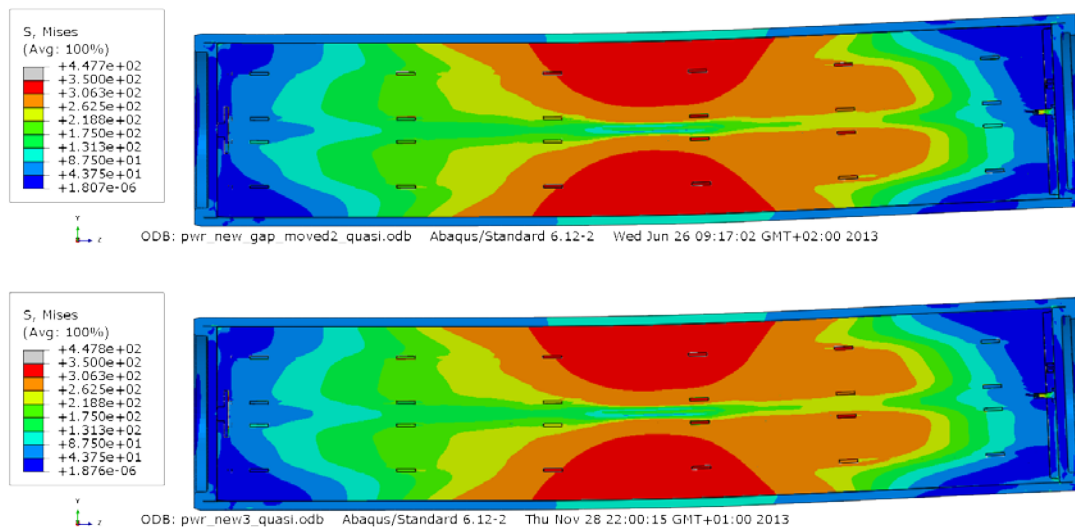


Figure 9-46 Plots showing Mises stress [MPa] after 10 cm shearing for eccentric placed insert (top) and co-axial insert (bottom) relative to the copper shell.

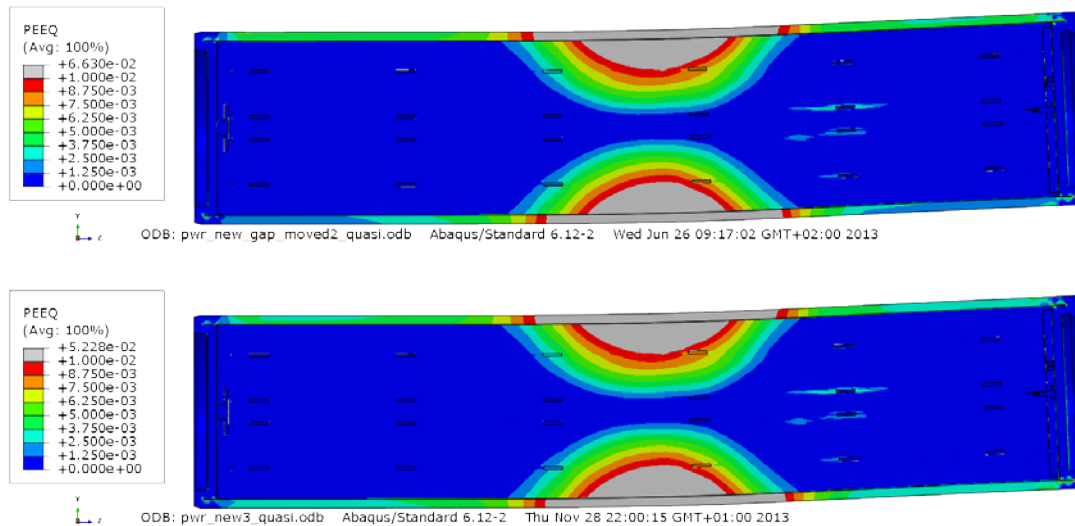


Figure 9-47 Plots showing equivalent plastic strain (PEEQ) after 10 cm shearing for eccentric placed insert (top) and co-axial insert (bottom) relative to the copper shell.

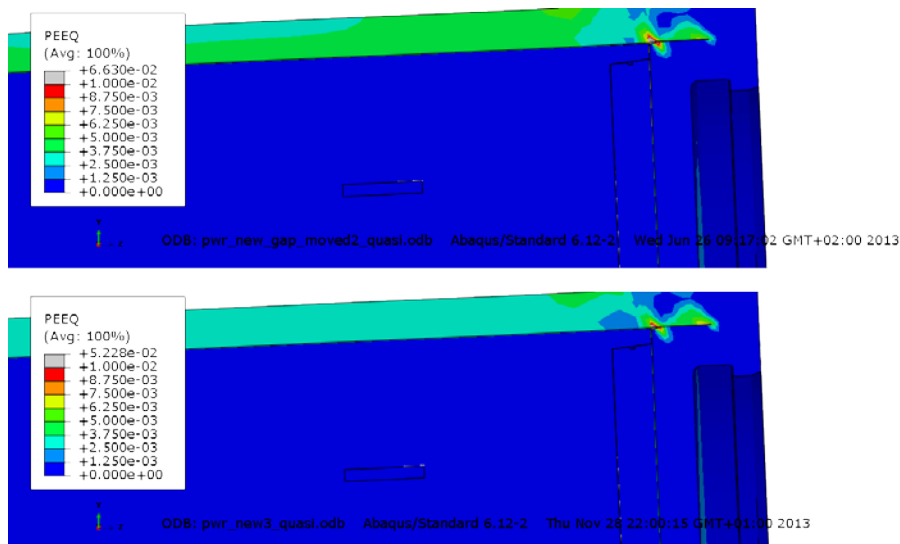


Figure 9-48 Plots showing equivalent plastic strain (PEEQ) after 10 cm shearing for eccentric placed insert (top) and co-axial insert (bottom) relative to the copper shell at the top left corner.

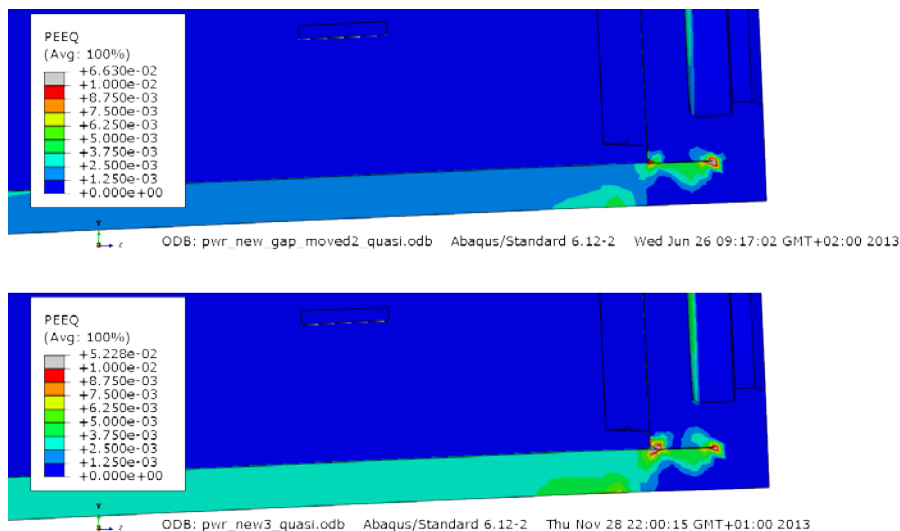


Figure 9-49 Plots showing equivalent plastic strain (PEEQ) after 10 cm shearing for eccentric placed insert (top) and co-axial insert (bottom) relative to the copper shell at the top right corner.

9.6 Stress concentrations for the detailed analyses for the PWR insert

The reference case have several simplifications such as neglecting screw holes, base plates with screws and support plates fixing the steel channel tubes. The detailed model includes these features. Figures 9-50 to 9-54 show some of the achieved results when the horizontal shear plane at $\frac{3}{4}$ -distance from the insert base has been chosen. However, even though a lot of details are included the global model is not intended to pick-up detailed stress concentrations (which require a much more dense mesh). The detailed model only indicates if stress concentrations need to be studied more in detail by e.g. using a sub-model technique. Figure 9-50 shows equivalent plastic strain (PEEQ) for the insert where the maximum strain is found at outer surface in mid insert but some increased strains could also be found where the support plates are imbedded into the insert.

Other areas of interest are at the insert base where the steel channel tubes base plates are located (Figure 9-51) and at the top of the insert where screw holes for lifting purposes are located (Figure 9-52). The base plates for the steel channel tubes are plotted (Figure 9-53) and finally the neighbourhood to the steel lid fixing screw (Figure 9-54). None of the plots show any significant stress/strain increase related to the geometry discontinuities.

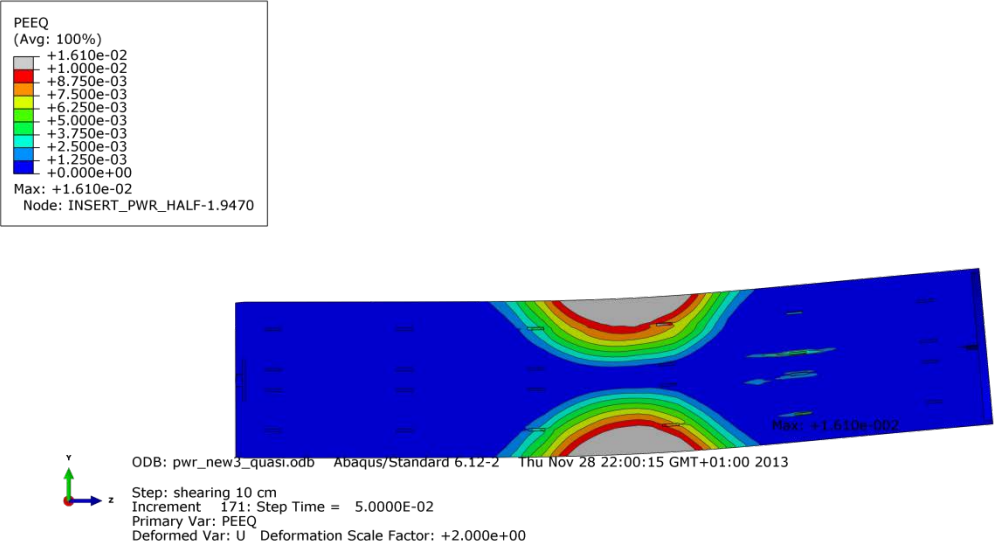


Figure 9-50 Plot showing equivalent plastic strain (PEEQ) for the insert after 10 cm shearing at $\frac{3}{4}$ -distance from the insert base.

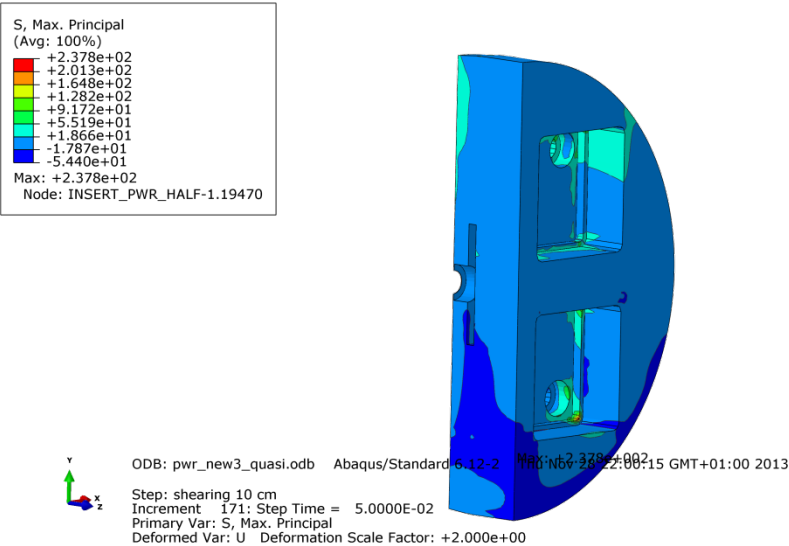


Figure 9-51 Plot showing maximum principal stress [MPa] for the insert base after 10 cm shearing at $\frac{3}{4}$ -distance from the insert base.

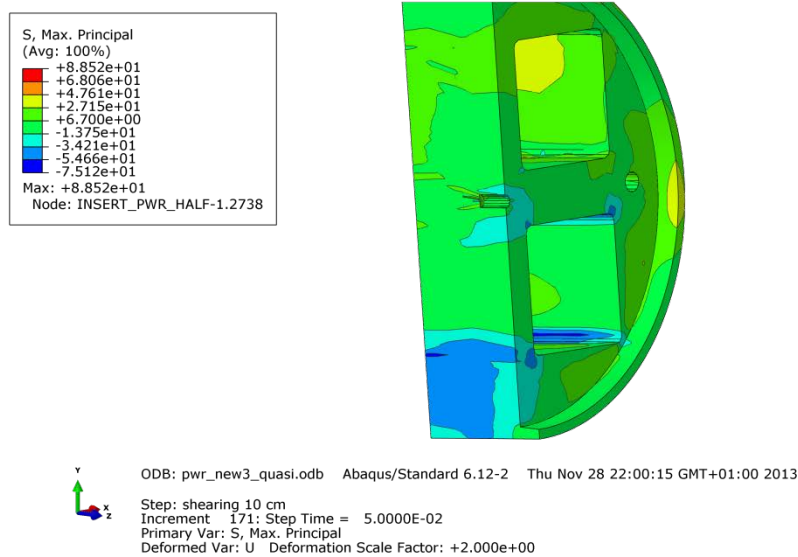


Figure 9-50 Plot showing maximum principal stress [MPa] for the insert top after 10 cm shearing at $\frac{3}{4}$ -distance from the insert base.

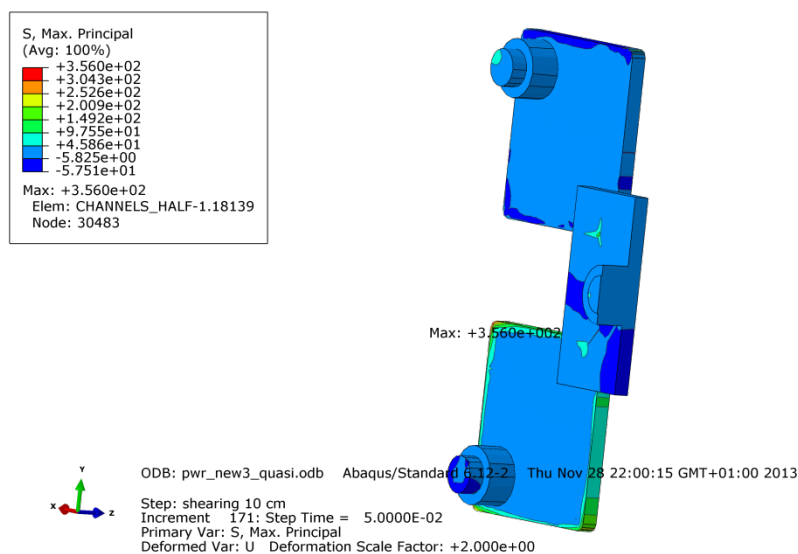


Figure 9-51 Plot showing maximum principal stress [MPa] for the steel channel tube plates at the base after 10 cm shearing at $\frac{3}{4}$ -distance from the insert base.

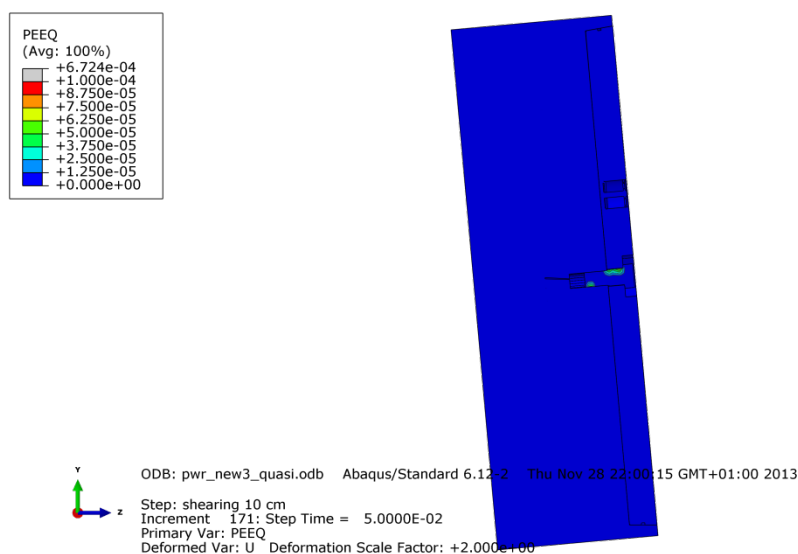


Figure 9-54 Plot showing equivalent plastic strain (PEEQ) at the top close to the fixing screw after 10 cm shearing at $\frac{3}{4}$ -distance from the insert base.

9.7 Washer and steel lid fixing screw

All analyses with the detailed model with horizontal shearing at $\frac{3}{4}$ -distance from the insert base includes the steel lid fixing screw which also is defined with an initial axial stress corresponding to the yield stress for the screw (355 MPa) – exceptions from this are models including the washer where the final pre-stress in the screw is specified. The screw is tied to the inner insert hole and have traditional contact (simulating opening/closing) between screw shaft and steel lid hole.

The approach using initial stress for the screw works fine if the surrounding parts (insert and steel lid are stiff compared to the screw). However, if the washer is included the initial stress in the screw is lost at equilibrium since the washer is much softer and accordingly deforms when iterations are made to have equilibrium.

Horizontal shearing at the lid has been analyzed with the initial stress method with two different magnitudes for the initial stress (335 MPa and 175 MPa) and with washer the prescribed screw stress has been defined to 81 MPa and 230 MPa (with 230 MPa the washer compresses too much with the existing model preventing the analysis to complete).

Figure 9-55 shows the axial stress after established equilibrium. It could be observed that the initial screw stress decreases almost a factor of two at equilibrium and thus the expected pre stress in the screw became too low. For the washer models the defined screw stress is retained.

Figure 9-56 shows the plastic equivalent strain after established equilibrium and only the washer models have significant strains (the case with 230 MPa obviously imply a highly compressed washer).

Figure 9-57 shows the equivalent plastic strain after 5 cm shearing and only the case with initial stress 355 MPa shows any significant strain (however not considered to be high).

Figure 9-58 shows the lateral stress after 5 cm shearing and it could be noticed that the steel lid has negative lateral stress (contact) for shearing at $\frac{3}{4}$ -distance from the insert base and positive lateral stress (no contact) in the same region when shearing at the lid. This is confirmed also by the lateral displacement (U2), Figure 9-59 where it is observed that without washer there is a slip between screw head and steel lid but with washer the slip is zero (or small) – another observation is that shearing at the lid imply much smaller displacement at the insert (about a factor of 10) compared to shearing at $\frac{3}{4}$ -distance from the insert base. Figure 9-60 – 9-61 show the corresponding results for 8 cm shearing.

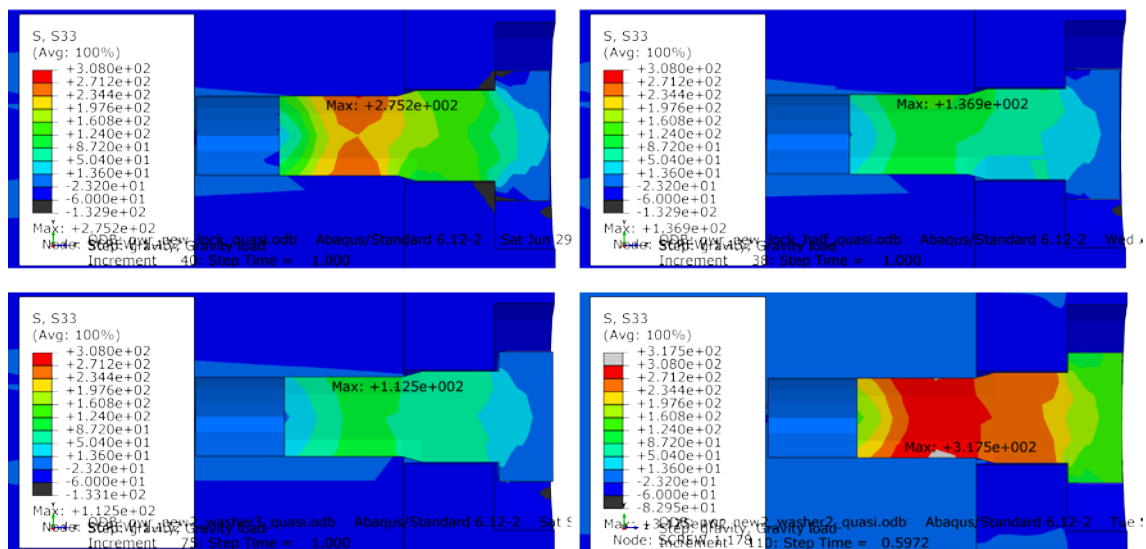


Figure 9-55 Plots showing axial stress (S33) in the screw after established initial equilibrium. Top left shows shearing at the lid using initial stress 355 MPa, top right shows shearing at the lid using initial stress 177.5 MPa, bottom left shows shearing at $\frac{3}{4}$ -distance from the insert base when screw stress is specified to 81 MPa and bottom right shows shearing at $\frac{3}{4}$ -distance from the insert base when screw stress is specified to 230 MPa.

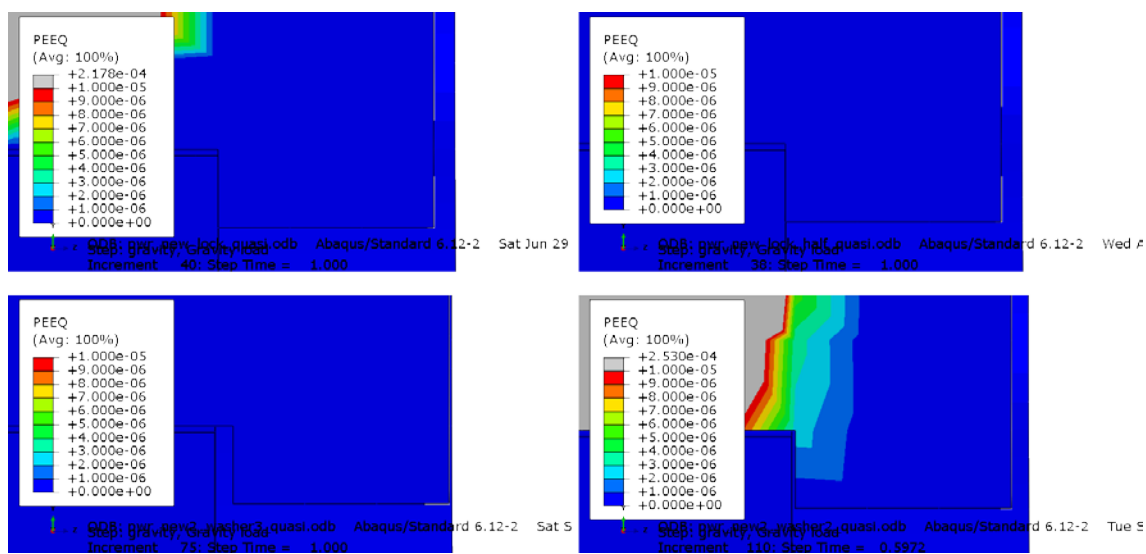


Figure 9-56 Plots showing plastic equivalent strain (PEEQ) in the screw after established initial equilibrium. Top left shows shearing at the lid using initial stress 355 MPa, top right shows shearing at the lid using initial stress 177.5 MPa, bottom left shows shearing at $\frac{3}{4}$ -distance from the insert base when screw stress is specified to 81 MPa and bottom right shows shearing at $\frac{3}{4}$ -distance from the insert base when screw stress is specified to 230 MPa.

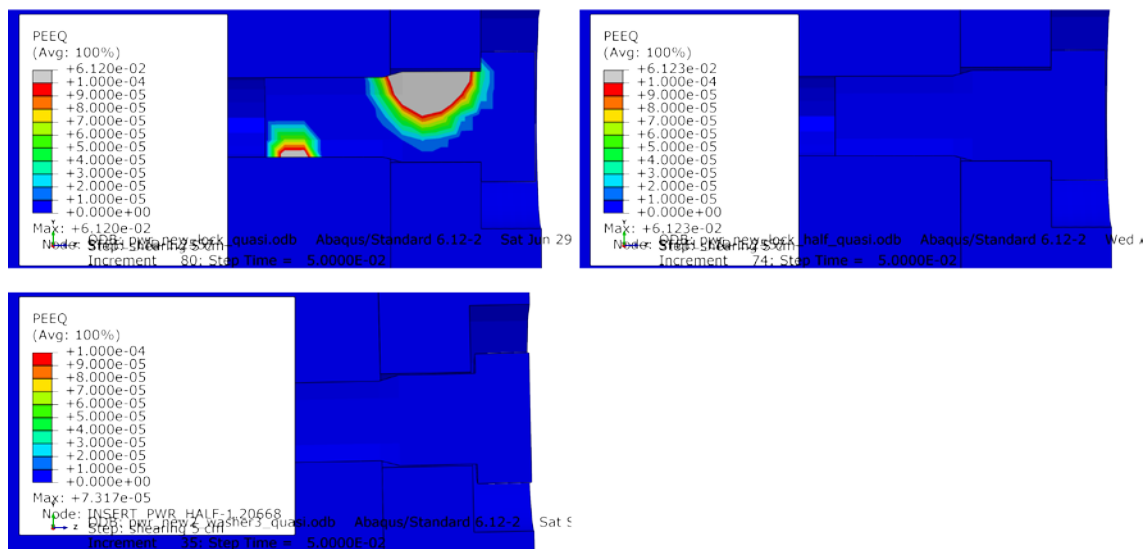


Figure 9-57 Plots showing plastic equivalent strain (PEEQ) in the screw after 5 cm shearing. Top left shows shearing at the lid using initial stress 355 MPa, top right shows shearing at the lid using initial stress 177.5 MPa and bottom left shows shearing at 3/4-distance from the insert base when screw stress is specified to 81 MPa.

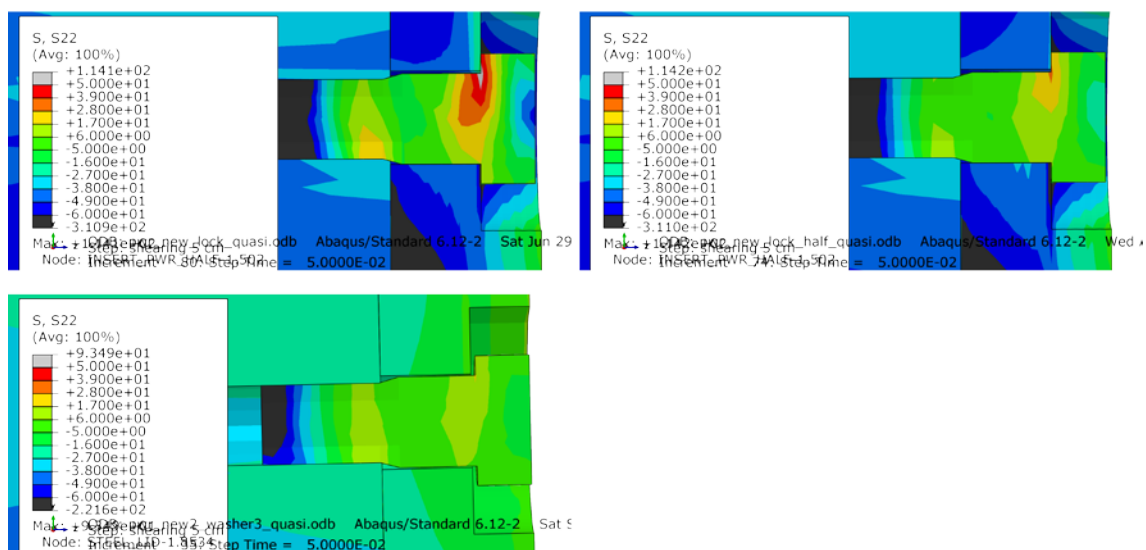


Figure 9-58 Plots showing lateral stress (S22) in the screw after 5 cm shearing. Top left shows shearing at the lid using initial stress 355 MPa, top right shows shearing at the lid using initial stress 177.5 MPa and bottom left shows shearing at 3/4-distance from the insert base when screw stress is specified to 81 MPa.

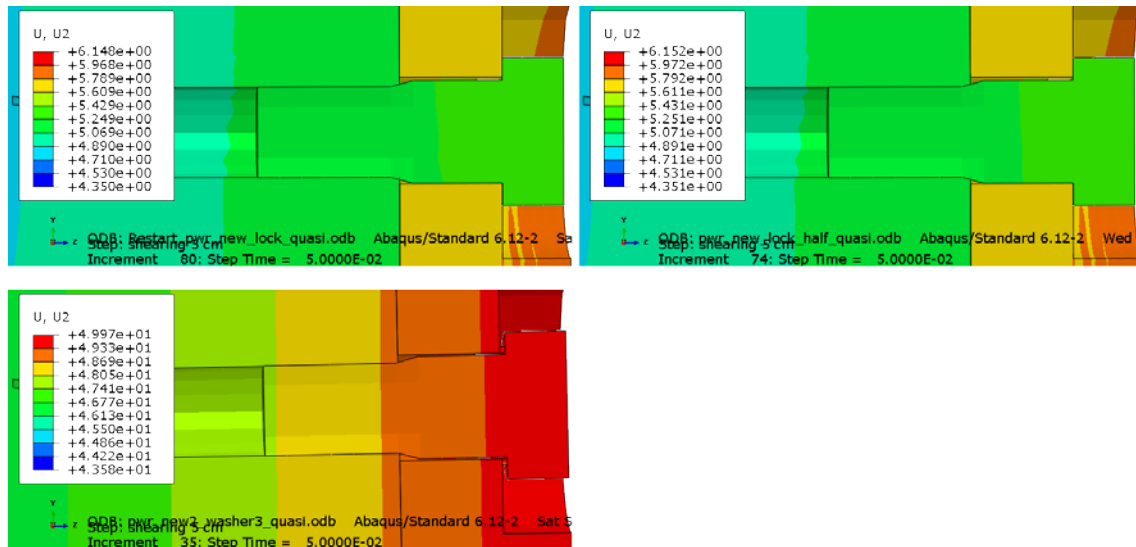


Figure 9-59 Plots showing lateral displacement (U2) in the screw after 5 cm shearing. Top left shows shearing at the lid using initial stress 355 MPa, top right shows shearing at the lid using initial stress 177.5 MPa and bottom left shows shearing at $\frac{3}{4}$ -distance from the insert base when screw stress is specified to 81 MPa.

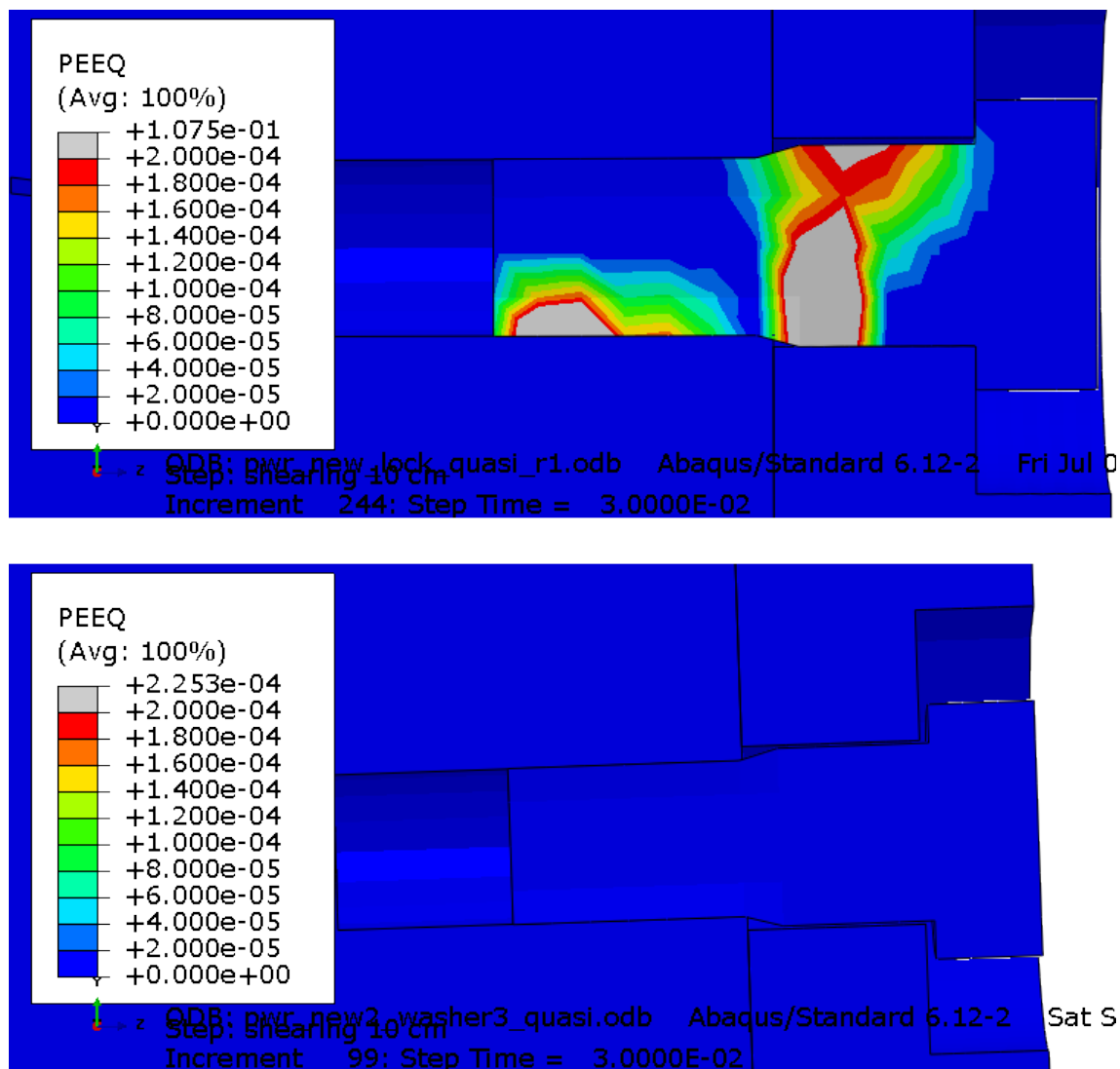


Figure 9-60 Plots showing plastic equivalent strain (PEEQ) in the screw after 8 cm shearing. Top plot shows shearing at the lid using initial stress 355 MPa and bottom plot shows shearing at $\frac{3}{4}$ -distance from the insert base when screw stress is specified to 81 MPa.

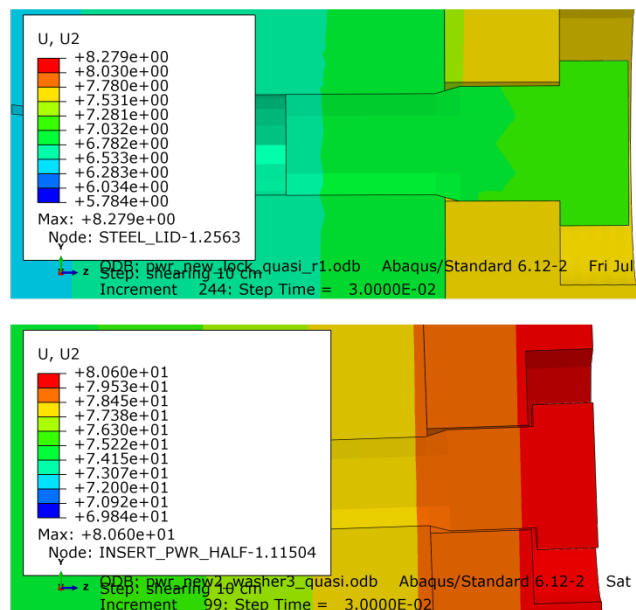


Figure 9-61 Plots showing lateral displacement (U2) in the screw after 8 cm shearing. Top plot shows shearing at the lid using initial stress 355 MPa and bottom plot shows shearing at $\frac{3}{4}$ -distance from the insert base when screw stress is specified to 81 MPa.

The Mises stress and equivalent plastic strain (PEEQ) in the steel lid when are plotted in Figures 9-62 to 9-63.

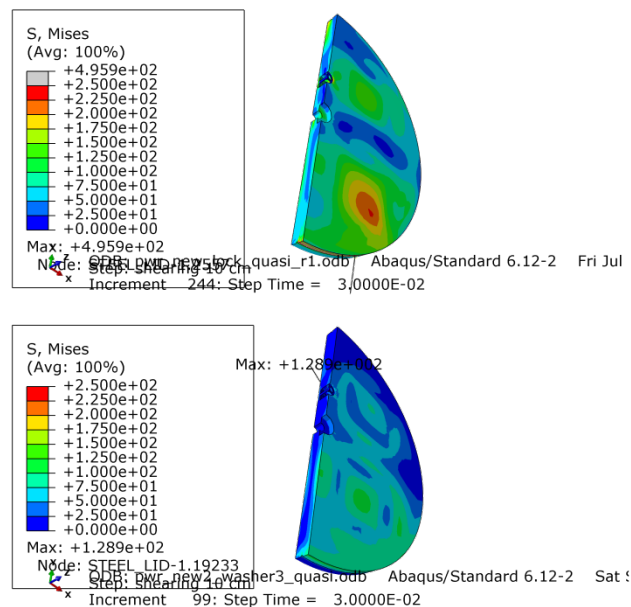


Figure 9-62 Plots showing Mises stress in the steel lid after 8 cm shearing. Top plot shows shearing at the lid using initial stress 355 MPa and bottom plot shows shearing at $\frac{3}{4}$ -distance from the insert base when screw stress is specified to 81 MPa.

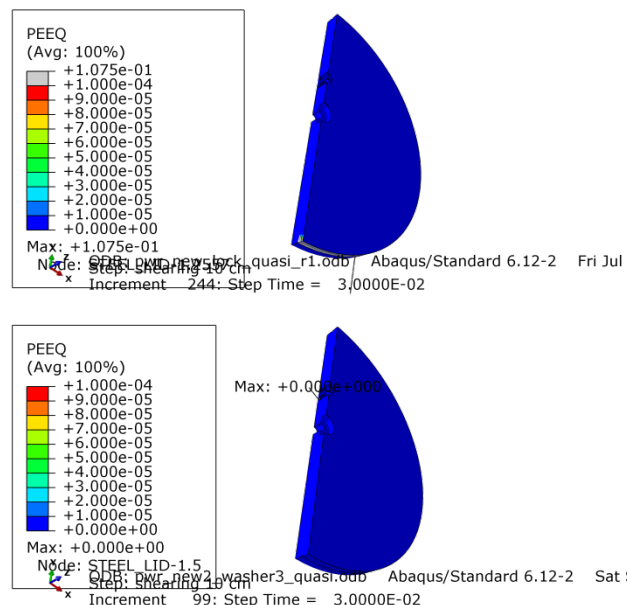


Figure 9-63 Plots showing equivalent plastic strain (PEEQ) in the steel lid after 8 cm shearing. Left shows shearing at the lid using initial stress 355 MPa and right shows shearing at $\frac{3}{4}$ -distance from the insert base when screw stress is specified to 81 MPa.

9.8 Eccentric positioning of the steel channel tubes for the BWR insert

The reference case is based on nominal dimensions but the drawings also define allowable tolerances. One case of interest is when the tolerances imply that the steel channel tubes are placed as most eccentric as possible (should be 10 mm but the model has 20 mm by mistake) leading to decreased wall thickness at one corner. Figures 9-64 to 9-69 compare results using the detailed model for centric and eccentric positioning of the steel channel tubes when a horizontal shearing is applied at $\frac{3}{4}$ -distance from the insert base.

Figure 9-64 shows positioning of steel channel tubes with and without tolerances. Figures 9-65 to 9-66 show comparison of the Mises stress and equivalent plastic strain (PEEQ) where a slightly increase could be observed when eccentric positioning. The peak value for Mises stress increases from 473 to 483 MPa and plastic equivalent strain increases from 5.5 to 5.7%. However, visual inspection of the plots show very similar contours. Figures 9-67 to 9-68 show similar observation for the steel channel tubes. The peak value for axial stress (S33) decreases from 417 to 415 MPa. The largest difference is for the equivalent plastic strain (PEEQ), 2.2 respectively 4.1%, at the corner radius of the insert for the thinnest wall thickness, Figure 9-69.

Note! Even though the eccentricity is modelled as 20 mm instead of the correct value of 10 mm the increase of equivalent plastic strain is rather small.

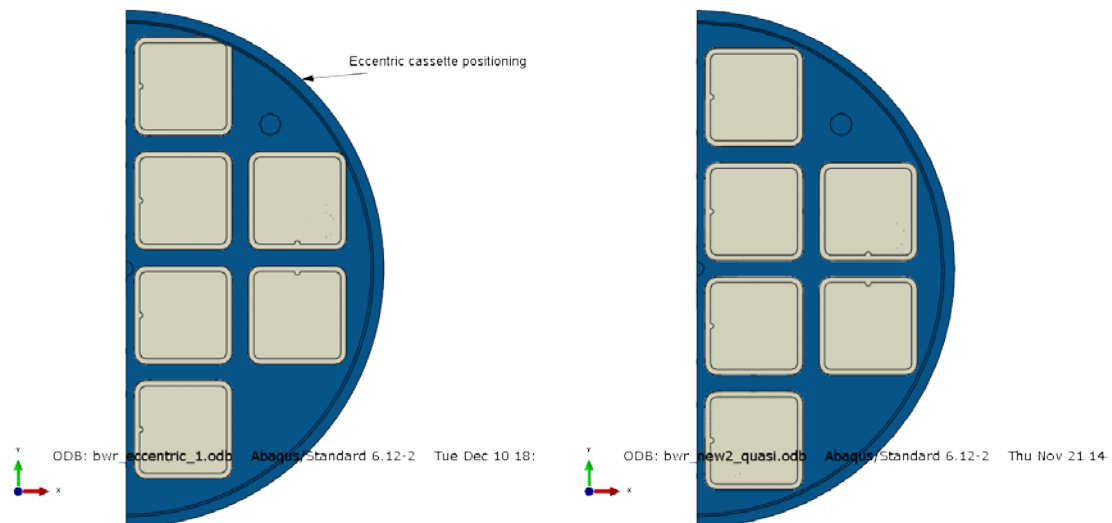


Figure 9-64 Plots showing positioning of steel channel tubes, eccentric (left) and centric (right).

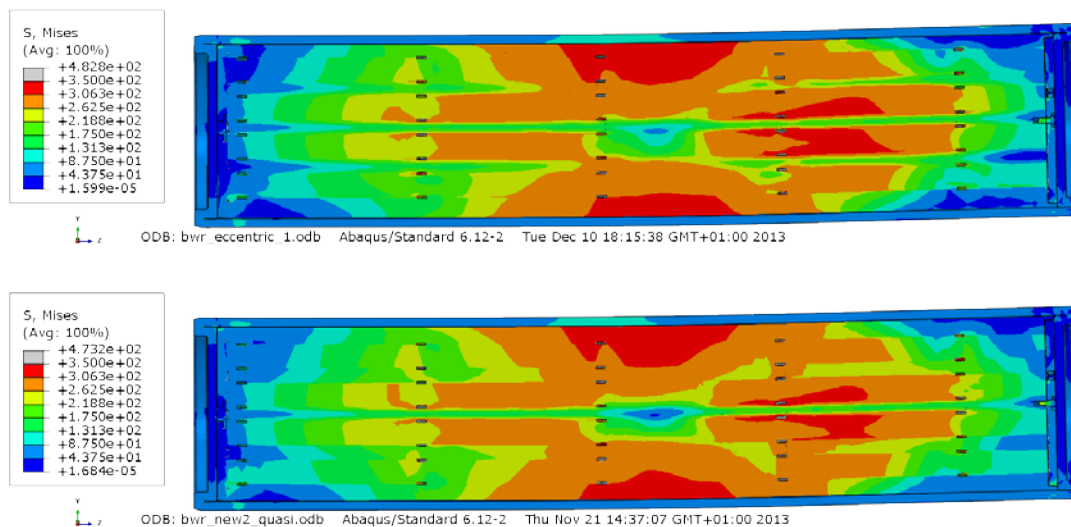


Figure 9-65 Plots showing Mises stress after 6 cm shearing for eccentric BWR model (top) and the centric BWR model (bottom).

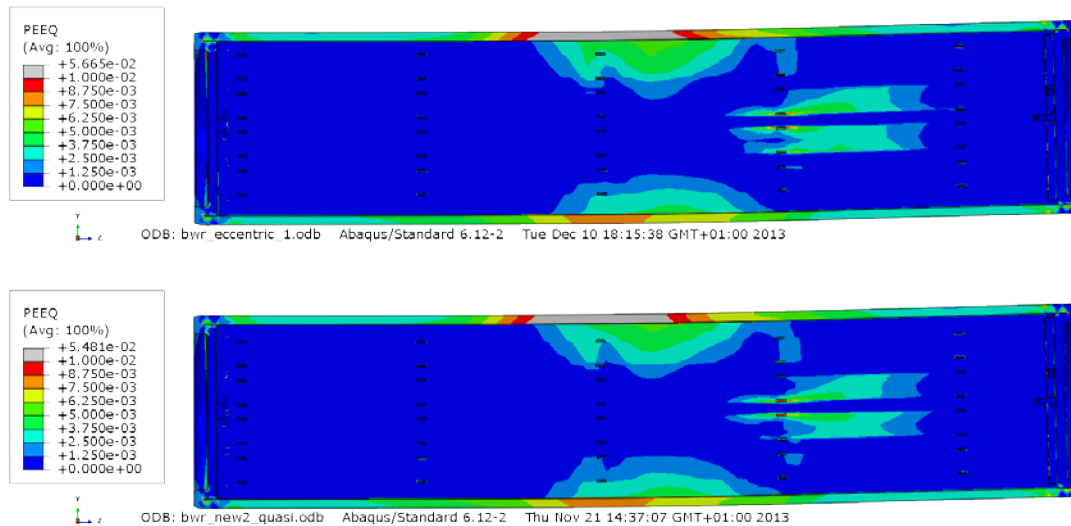


Figure 9-66 Plots showing equivalent plastic strain (PEEQ) after 6 cm shearing for eccentric BWR model (top) and the centric BWR model (bottom).

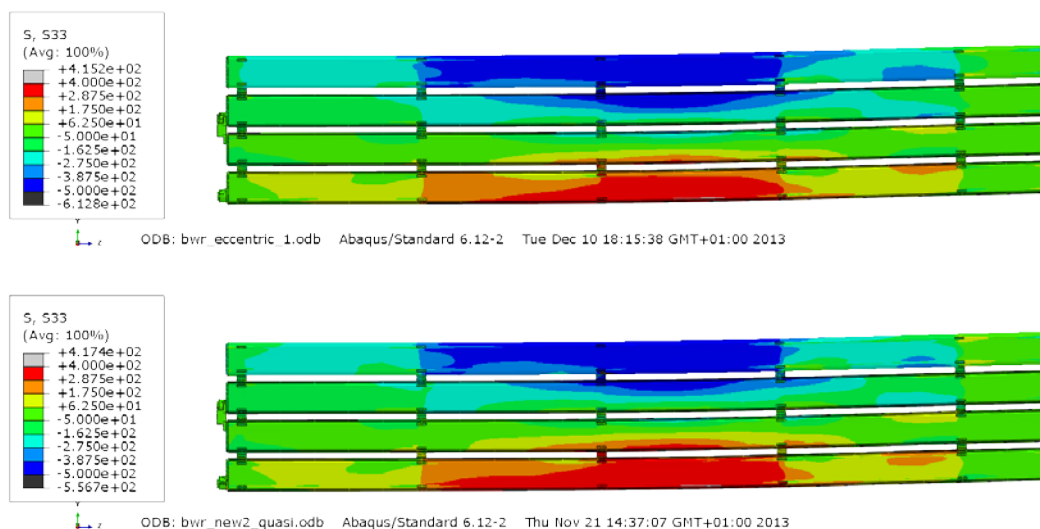


Figure 9-67 Plots showing axial stress for the steel channel tubes after 6 cm shearing for eccentric BWR model (top) and the centric BWR model (bottom).

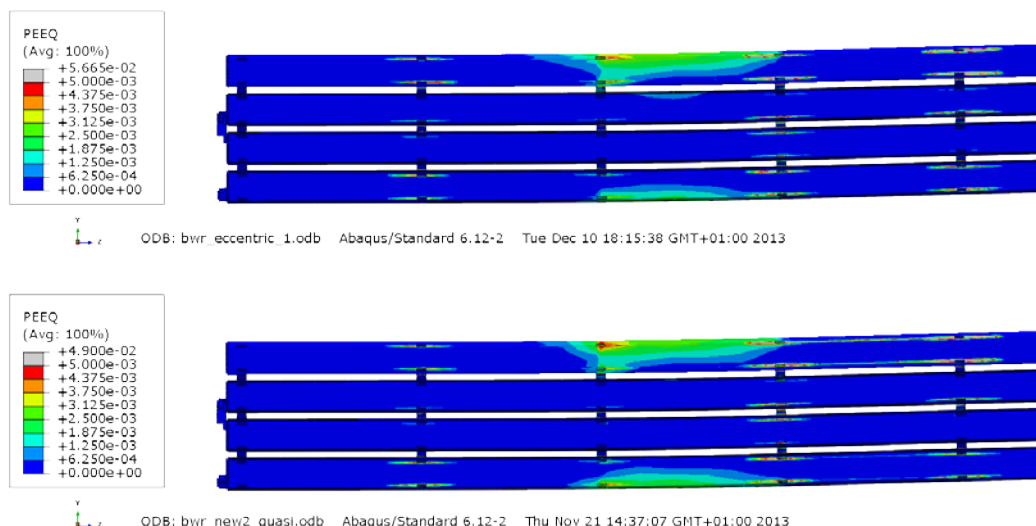


Figure 9-68 Plots showing equivalent plastic strain (PEEQ) for the steel channel tubes after 6 cm shearing for eccentric PWR model (top) and the centric PWR model (bottom).

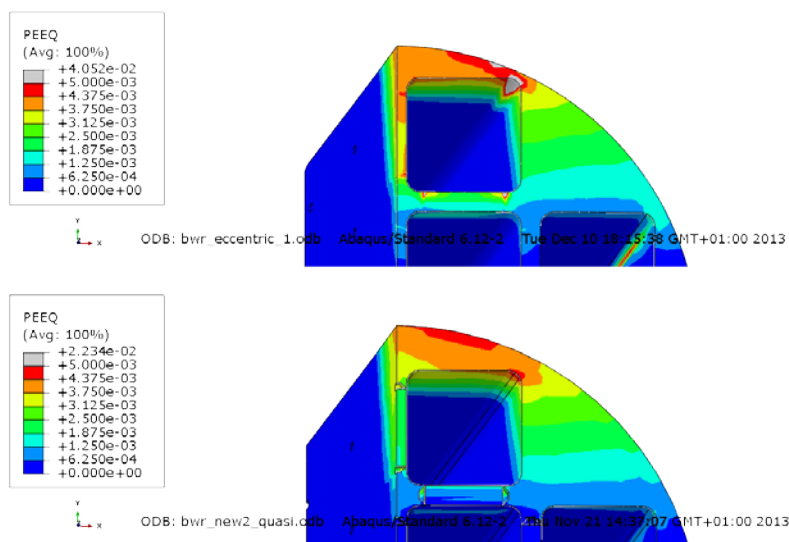


Figure 9-69 Plots showing equivalent plastic strain (PEEQ) for the insert after 6 cm shearing for eccentric BWR model (top) and the centric BWR model (bottom).

Below the obtained results are summarized in Tables 9-1 to 9-21. The tables show maximum values for Mises stress, PEEQ (plastic equivalent strain) and for the insert and channel tubes also maximum and minimum axial stress (S33). These values are not always representative since the extreme values could be caused by badly shaped elements or discontinuities in the geometry and furthermore the values are taken from the corresponding contour plots which are based on extrapolated values. If the yield surface has been reached then the Mises stress should be defined from PEEQ at the integration points.

Tables 9-1 to 9-6 show the results for the PWR-insert with shearing of 5 and 10 cm at $\frac{3}{4}$ -distance from the base. The Mises stress, Table 9-1 and 9-2, show similar values for insert, channel tubes and the steel lid (except for the eccentric case where the stress is significantly higher). However, the response is elastic for the steel lid. The Mises stress show lower values when the washer is included probably due to a lower initial pre-stress in the screw to avoid too distorted washer.

The same conclusion holds for PEEQ, Table 9-3 and 9-4, which also shows very small values for the screw regardless of initial pre-stress.

The maximum/minimum values for the axial stress (S33), Table 9-5 and 9-6, are very similar for all cases.

Table 9-1. Maximum Mises stress [MPa] for PWR-insert with shearing of 5 cm at $\frac{3}{4}$ -distance.

Model name	Copper shell	Insert	Channel tubes	Steel lid	Screw	Washer
Reference (Hernelind 2010) – model6g_PWR_normal_quarter_2050ca3	203	319	416	148	-	-
pwr_new3_quasi	202	329	422	137	325	-
pwr_eccentric3_quasi	135	349	445	209	335	-
pwr_new_gap_moved2_quasi	184	326	422	150	324	-
pwr_new2_washer	170	321	420	127	269	123
pwr_new2_washer3	171	321	420	127	149	266

Table 9-2. Maximum Mises stress [MPa] for PWR-insert with shearing of 10 cm at $\frac{3}{4}$ -distance.

Model name	Copper shell	Insert	Channel tubes	Steel lid	Screw	Washer
Reference (Hernelind 2010) – model6g_PWR_normal_quarter_2050ca3	206	326	418	173	-	-
pwr_new3_quasi	206	329	426	152	328	-
pwr_eccentric3_quasi	208	356	450	217	334	-
pwr_new_gap_moved2_quasi	184	350	448	148	326	-
pwr_new2_washer	176	348	442	154	275	117
pwr_new2_washer3	177	348	442	154	152	255

Table 9-3. Maximum PEEQ (plastic equivalent strain) [%] for PWR-insert with shearing of 5 cm at $\frac{3}{4}$ -distance.

Model name	Copper shell	Insert	Channel tubes	Steel lid	Screw	Washer
Reference (Hernelind 2010) – model6g_PWR_normal_quarter_2050ca3	9.8	0.51	1.1	0	-	-
pwr_new3_quasi	5	0.74	0.77	0	0.01	-
pwr_eccentric3_quasi	4.2	1.4	2.6	0	0.02	-
pwr_new_gap_moved2_quasi	6.6	0.73	0.77	0	0.02	-
pwr_new2_washer	3.3	0.62	0.72	0	0.01	4.1
pwr_new2_washer3	3.3	0.62	0.72	0	0	30

Table 9-4. Maximum PEEQ (plastic equivalent strain) [%] for PWR-insert with shearing of 10 cm at ¾-distance.

Model name	Copper shell	Insert	Channel tubes	Steel lid	Screw	Washer
Reference (Hernelind 2010) – model6g_PWR_normal_quarter_2050ca3	9.9	0.8	1.1	0	-	-
pwr_new3_quasi	5.1	0.91	2.9	0	0.01	-
pwr_eccentric3_quasi	9.1	1.7	3.3	0	0.02	-
pwr_new_gap_moved2_quasi	6.6	1.6	2.9	0	0.02	-
pwr_new2_washer	3.9	1.5	2.4	0	0.01	4.1
pwr_new2_washer3	3.9	1.5	2.4	0	0	30

Table 9-5. Axial stress, S33 [MPa] for PWR-insert with shearing of 5 cm at ¾-distance.

Model name	Insert		Channel tubes	
	maximum	minimum	maximum	minimum
Reference (Hernelind 2010) – model6g_PWR_normal_2050ca3	327	-413	437	-542
pwr_new3_quasi	333	-423	405	-554
pwr_eccentric3_quasi	330	-459	400	-574
pwr_new_gap_moved2_quasi	331	-423	403	-554
pwr_new2_washer	331	-415	401	-544
pwr_new2_washer3	331	-415	401	-544

Table 9-6. Axial stress, S33 [MPa] for PWR-insert with shearing of 10 cm at ¾-distance.

Model name	Insert		Channel tubes	
	maximum	minimum	maximum	minimum
Reference (Hernelind 2010) – model6g_PWR_normal_2050ca3	334	-422	449	-547
pwr_new3_quasi	346	-434	416	-563
pwr_eccentric3_quasi	350	-466	429	-521
pwr_new_gap_moved2_quasi	370	-474	440	-535
pwr_new2_washer	373	-461	441	-588
pwr_new2_washer3	373	-461	440	-588

When shearing at the insert lid the most significant finding is the increase of stresses and strains for the steel lid, Tables 9-7 and 9-8. The steel lid shows very locally some plasticity and is judged to not cause any severe damage. The axial stress shows as expected lower values, Tables 9-5, 9-6 and 9-9, when shearing at the insert lid compared to shearing at $\frac{3}{4}$ -distance from the base.

Table 9-7. Maximum Mises stress [MPa] for PWR-insert with shearing of 5 cm at the insert lid.

Model name	Copper shell	Insert	Channel tubes	Steel lid	Screw	Washer
Reference (SKBdoc 1339902) – N34b_finer_1sekm_normal_quasi_model6	183	178	322	160	-	-
pwr_new_lock_quasi	203	297	418	427	332	-
pwr_new_lock_half_quasi	203	297	418	427	205	-
pwr_new2_lock_washer0_quasi	202	298	420	437	95	88
pwr_new2_lock_washer3_quasi	202	298	420	437	185	271
pwr_new2_lock2_quasi	203	297	418	427	378	-
pwr_new2_lock2b_quasi	203	297	418	427	259	-

Table 9-8. Maximum PEEQ (plastic equivalent strain) [%] for PWR-insert with shearing of 5 cm at the insert lid.

Model name	Copper shell	Insert	Channel tubes	Steel lid	Screw	Washer
Reference (SKBdoc 1339902) – N34b_finer_1sekm_normal_quasi_model6	9.0	0	0	0	-	-
pwr_new_lock_quasi	9.7	0.068	0.47	6.1	0.021	-
pwr_new_lock_half_quasi	9.7	0.067	0.48	6.1	0	-
pwr_new2_lock_washer0_quasi	9.9	0.11	0.63	6.8	0	1.2
pwr_new2_lock_washer3_quasi	9.8	0.11	0.63	6.8	0	30
pwr_new2_lock2_quasi	9.7	0.067	0.47	6.1	3.4	-
pwr_new2_lock2b_quasi	9.7	0.067	0.47	6.1	0	-

Table 9-9. Axial stress, S33 [MPa] for PWR-insert with shearing of 5 cm at the insert lid.

Model name	Insert		Channel tubes	
	maximum	minimum	maximum	minimum
Reference (SKBdoc 1339902) – N34b_finer_1sekm_normal_quasi_model6	88	-184	85	-253
pwr_new_lock_quasi	156	-253	75	-251
pwr_new_lock_half_quasi	157	-253	74	-251
pwr_new2_lock_washer0_quasi	156	-258	81	-268
pwr_new2_lock_washer3_quasi	155	-258	81	-268
pwr_new2_lock2_quasi	156	-253	74	-251
pwr_new2_lock2b_quasi	156	-253	74	-251

Tables 9-10 to 9-15 show the results for the BWR-insert for 5 and 8 cm shearing at $\frac{3}{4}$ -distance from the insert base. The highest value for Mises stress in the insert occurs for the eccentric case, Table 9-10 and 9-11, even though that analysis stopped already at 6 cm shearing. The plastic strains are also higher for the detailed model mostly related to discontinuities close to the connection with the support plates (the weld has not been included which will increase stresses/strains).

Table 9-10. Maximum Mises stress [MPa] for BWR-insert with shearing of 5 cm at $\frac{3}{4}$ -distance.

Model name	Copper shell	Insert	Channel tubes	Steel lid	Screw
Reference (Hernelind 2010) – model6g_normal_quarter_2050ca3	201	321	470	103	-
bwr_new2_quasi	153	392	458	340	301
bwr_eccentric_1	152	401	468	270	291

Table 9-11. Maximum Mises stress [MPa] for BWR-insert with shearing of 8 cm at $\frac{3}{4}$ -distance.

Model name	Copper shell	Insert	Channel tubes	Steel lid	Screw
Reference (Hernelind 2010) – model6g_normal_quarter_2050ca3	199	341	606	122	-
bwr_new2_quasi	172	413	506	344	306
bwr_eccentric_1 (6 cm)	157	417	483	258	296

Table 9-12. Maximum PEEQ (plastic equivalent strain) [%] for BWR-insert with shearing of 5 cm at $\frac{3}{4}$ -distance.

Model name	Copper shell	Insert	Channel tubes	Steel lid	Screw
Reference (Hernelind 2010) – model6g_normal_quarter_2050ca3	9.1	0.54	0.88	0	-
bwr_new2_quasi	5.1	1.5	3.7	0.35	0.001
bwr_eccentric_1	5	2.7	4.5	0.23	0

Table 9-13. Maximum PEEQ (plastic equivalent strain) [%] for BWR-insert with shearing of 8 cm at $\frac{3}{4}$ -distance.

Model name	Copper shell	Insert	Channel tubes	Steel lid	Screw
Reference (Hernelind 2010) – model6g_normal_quarter_2050ca3	9.1	1.2	2.2	0	
bwr_new2_quasi	6.0	3.8	7.5	0.68	0.0015
bwr_eccentric_1 (6 cm)	5.5	4.1	5.7	0.23	0

Table 9-14. Axial stress, S33 [MPa] for BWR-insert with shearing of 5 cm at $\frac{3}{4}$ -distance.

Model name	Insert		Channel tubes	
	maximum	minimum	maximum	minimum
Reference (Hernelind 2010) – model6g_normal_quarter_2050ca3	333	-439	452	-599
bwr_new2_quasi	395	-441	414	-526
bwr_eccentric_1	395	-524	406	-580

Table 9-15. Axial stress, S33 [MPa] for BWR-insert with shearing of 8 cm at $\frac{3}{4}$ -distance.

Model name	Insert		Channel tubes	
	maximum	minimum	maximum	minimum
Reference (Hernelind 2010) – model6g_normal_quarter_2050ca3	351	-463	463	-617
bwr_new2_quasi	451	-501	430	-593
bwr_eccentric_1 (6 cm)	438	-569	415	-613

Tables 9-16 to 9-21 show the results for the BWR-insert with 5 and 6 cm shearing at the insert lid where it can be observed that especially the Mises stress for the steel lid is significantly higher for the detailed model, Table 9-16 and 9-17 but the plastic strain is rather low, Table 9-18 and 9-19.

Table 9-16. Maximum Mises stress [MPa] for BWR-insert with shearing of 5 cm at insert lid.

Model name	Copper shell	Insert	Channel tubes	Steel lid	Screw
Reference (SKBdoc 1339902) – N34b_finer_1sekm_normal_quasi_model6	183	178	322	160	-
bwr_eccentric_lock	216	355	425	350	341

Table 9-17. Maximum Mises stress [MPa] for BWR-insert with shearing of 6 cm at insert lid.

Model name	Copper shell	Insert	Channel tubes	Steel lid	Screw
Reference (SKBdoc 1339902) – N34b_finer_1sekm_normal_quasi_model6	187	201	349	169	-
bwr_eccentric_lock	227	365	427	355	349

Table 9-18. Maximum PEEQ (plastic equivalent strain) [%] for BWR-insert with shearing of 5 cm at insert lid.

Model name	Copper shell	Insert	Channel tubes	Steel lid	Screw
Reference (SKBdoc 1339902) – N34b_finer_1sekm_normal_quasi_model6	9	0	0	0	-
bwr_eccentric_lock	15.5	1.1	1.1	0.98	0.42

Table 9-19. Maximum PEEQ (plastic equivalent strain) [%] for BWR-insert with shearing of 6 cm at insert lid.

Model name	Copper shell	Insert	Channel tubes	Steel lid	Screw
Reference (SKBdoc 1339902) – N34b_finer_1sekm_normal_quasi_model6	11	0	0	0	-
bwr_eccentric_lock	17	1.4	1.3	1.3	0.93

Table 9-20. Axial stress, S33 [MPa] for BWR-insert with shearing of 5 cm at insert lid.

Model name	Insert		Channel tubes	
	maximum	minimum	maximum	minimum
Reference (SKBdoc 1339902) – N34b_finer_1sekm_normal_quasi_model6	89	-184	85	-253
bwr_eccentric_lock	382	-266	82	-237

Table 9-21. Axial stress, S33 [MPa] for BWR-insert with shearing of 6 cm at insert lid.

Model name	Insert		Channel tubes	
	maximum	minimum	maximum	minimum
Reference (SKBdoc 1339902) – N34b_finer_1sekm_normal_quasi_model6	202	-198	99	-270
bwr_eccentric_lock	389	-272	91	-255

10 Uncertainties

The obtained results are based on several assumptions regarding loads and material properties. Also the discretization in the computer model will affect the results. Some of these influencing factors are addressed below:

- All experiments used for material calibration have a spread which will imply a range for the properties defining each material model.
- Material properties for bentonite and nodular cast iron depends on hydrostatic pressure but in this study the material definitions are based on Mises plasticity theory using tensile properties except for the bentonite where typical tests are triaxial compression and oedometer tests. Same assumptions have been used for material properties as in previous analyses, e.g. Hernelind (2010).
- Swelling pressure for the bentonite will affect the material stiffness. The experimental results have a spread in the results and the used data should be conservative in the sense that the obtained stress and strain magnitudes are overestimated.
- Element mesh is rather fine but nevertheless it is too coarse in some regions, especially at the welds and regions with geometric discontinuities. A more refined mesh will probably increase the maximum stress and strain levels. Fortunately, the use of non-linear material properties (such as plasticity) will decrease the sensitivity on the used mesh. The used mesh has been judged to be accurate enough considering also the required computer resources to obtain the results.

11 Evaluation and conclusions

The results obtained from the rock shear analyses could be summarized as follows.

- General findings
 - The maximum plastic strain in the copper shell, 15.5%, occurs in fillets (besides regions containing singularities) for the case bwr_eccentric_lock.
 - The maximum plastic strains in the insert result from bending, case bwr_eccentric_1 at 6 cm shearing. However, the magnitude is small (2.7%) compared to ultimate strains (>16%) and is considered not to threaten the mechanical integrity.
 - The maximum principal stress in the insert, 395 MPa, mainly comes from bending of the shell, case bwr_eccentric_1 at 6 cm shearing– the level depends mainly on material properties for the insert (and dimensions) and the stiffness of the buffer.
 - The maximum plastic strain in the steel tubes, 4.5%, occurs at the corners of a specific steel tube. However, the magnitude is small compared to ultimate strains (>16%) and is considered not to cause any failure.
 - Strain rate effects for bentonite, copper and iron will affect the results. Strain rate dependency is included for the buffer and the cast iron. The copper shell will have the strain rate effect included when the creep model is used but in this study all analyzes have been performed by using Mises plasticity theory.
 - The nodular cast iron material has pressure dependent properties but data from tensile tests has been used which is considered to be conservative.

- Effect on modelling steel tubes with support plates and contact surfaces
 - The approach used for connecting the steel tubes to the insert (tied connection) in previous analyses imply very similar results as when modelling the connection with steel plates welded to the steel tubes. E.g. the axial stress (S33) differ less than 2% at 5 cm shearing for the insert compared with the reference case (Hernelind 2010). The peak values for Mises stress differ more where the support plates between the steel tubes are tied to the insert. Another finding is that the channel tubes have decreased stress magnitudes due to increased stiffness when including the support plates.
- Effect of modelling the steel lid with a fixing screw in the centre
 - Modelling the steel lid with a fixing screw in the centre will change the stress distribution in the steel lid ends as well at the peripheral insert top but the strain/strain-level is still not considered to cause any severe damage. The stresses in the steel lid are in the elastic range except for a small region close to the contact with the insert – small equivalent plastic strains less than 0.001. Also the screw shows stresses in the elastic range except locally close to the contact with the steel lid. Low pre-stress in the screw implies slip between screw head and steel lid - the screw takes the load by almost pure elastic shear stresses. High pre-stress in the screw prevents slip and the screw takes the load by bending causing some plasticity (equivalent plastic strain less than 0.001). Using a washer distributes the contact stresses more smoothly but doesn't change the conclusions above.
- Effect of including small details
 - Neglecting small details (screw holes, steel tube bottom plates, screws and nuts) does not cause any visible stress concentrations (except for the support plates). The Mises stress is in the elastic range at the insert base and steel tubes base (containing plates, screws and nuts) which is also the case for the insert top (containing a small screw hole). However, the mesh is not fine enough to have the correct stress distribution. A sub-model based on the obtained global displacement solution could be used to obtain more accurate results for these regions.
- Effect of production tolerances
 - Considering tolerances when creating the model increases stresses/strains in regions where the wall thickness have been reduced but the magnitude for stress/strain will not cause any failure. At the corner where the wall thickness is smallest the equivalent plastic strain (PEEQ) increases at most from 1.5% to 2.7%, comparing bwr_new2_quasi with bwr_eccentric_1.

The plastic equivalent strains are low for all cases (except for the washer which should have large plastic deformation – with high pre-stress almost 30%) and occurs at localized regions, except for the insert when shearing at $\frac{3}{4}$ -distance from the base where the highest strain of 4.1% at 6 cm shearing and 2.7% at 5 cm shearing is found. However, also this strain level is considered to be low and will not break the insert.

The steel lid have for most cases a pure elastic response and when plastic strains occur (as most about 6%), they are very localized and will not cause any failure.

Maximum equivalent plastic strain in the copper shell, 15.5%, is found at a geometric discontinuity and is much localized. This strain level is not considered to cause any failure of the copper shell.

The used material definitions are valid for the strain levels obtained in the reported analyses and the strains are all far below any necking (or softening of the material when looking at engineering stresses/strains).

References

ABAQUS, 2013. Version 6.12.1. Dassault Systèmes Simulia Corp.

Börgeßson L, Hernelind J, 2006. Earthquake induced rock shear through a deposition hole. Influence of shear plane inclination and location as well as buffer properties on the damage caused to the canister. SKB TR-06-43, Svensk Kärnbränslehantering AB.

Börgeßson L, Johannesson L-E, Sandén T, Hernelind J, 1995. Modeling of the physical behavior of water saturated clay barriers. Laboratory tests, material models and finite element application. SKB TR 95-20, Svensk Kärnbränslehantering AB.

Börgeßson L, Johannesson L-E, Hernelind J, 2004. Earthquake induced rock shear through a deposition hole. Effect on the canister and the buffer. SKB TR-04-02, Svensk Kärnbränslehantering AB.

Börgeßson L, Dueck A, Johannesson L-E, 2010. Material model for shear of the buffer – evaluation of laboratory test results. SKB TR-10-31, Svensk Kärnbränslehantering AB.

Hernelind J, 2010. Modelling and analysis of canister and buffer for earthquake induced rock shear and glacial load. SKB TR-10-34, Svensk Kärnbränslehantering AB.

Jin L-Z, Sandström R, 2008. Creep of copper canisters in power-law breakdown. Computational Materials Science 43, 403–416.

Raiko H, Sandström R, Rydén H, Johansson M, 2010. Design analysis report for the canister. SKB TR-10-28, Svensk Kärnbränslehantering AB.

Sandström R, Andersson H C M, 2008. Creep in phosphorus alloyed copper during power-law breakdown. Journal of Nuclear Materials 372, 76–88.

Sandström R, Hallgren J, Burman G, 2009. Stress strain flow curves for Cu-OFP. SKB R-09-14, Svensk Kärnbränslehantering AB.

SSABDirekt, 2008. Steelfacts Domex 355 MC. Available at <http://www.ssabdirect.com>. [19 September 2008].

SS-EN 10025-2:2004. Varmvalsade konstruktionsstål – Del 2: Tekniska leveransbestämmelser för olegerade stål (Hot rolled products of structural steels - Part 2: Technical delivery conditions for non-alloy structural steels). Stockholm: Swedish Standards Institute.

Unpublished documents

SKBdoc id, version	Title	Issuer, year
1201865 ver 1.0	Dragprovning av gjutjärn. (In Swedish.)	KTH, 2009
1203875 ver 1.0	Ritningsförteckning för kapselkomponenter. (In Swedish.)	SKB, 2009
1203875 ver 2.0	Ritningsförteckning för kapselkomponenter. (In Swedish.)	SKB, 2014
1339902 ver 1.0	Global simulation of copper canister – final deposition	SKB, 2013
1407337 ver 1.0	Earthquake induced rock shear through a deposition hole – Part 2. Additional calculations of the influence of inhomogeneous buffer on the stresses in the canister.	Clay Technology/ 5T Engineering, 2013

Revision audit trail

Version	Date	Description	Author	Reviewed	Approved
2.0	See first pageheader	Reference"Earthquake induced rock shear through a deposition hole – Part 2. Additional calculations of the influence of inhomogeneous buffer on the stresses in the canister" (SKBdoc 1407337) on page 23 corrected. Headlines for Table 9-18 and Table 9-19 corrected to BWR, previous PWR in the headlines.	Jan Hernelind/5T Engineering AB	See first pageheader	See first pageheader
1.0	2014-01-30	New report.	Jan Hernelind/5T Engineering AB	Sabina Hammarberg	Jan SarnetJan Sarnet

Appendix 1 – Plots for pwr_new3_quasi

Plots showing deformed geometry as contour plots for all parts at shearing magnitude 5 and 10 cm for case pwr_new3_quasi (horizontal shearing at $\frac{3}{4}$ -distance from base of the insert). The view shows the symmetry plane and all deformations are scaled by a factor of two.

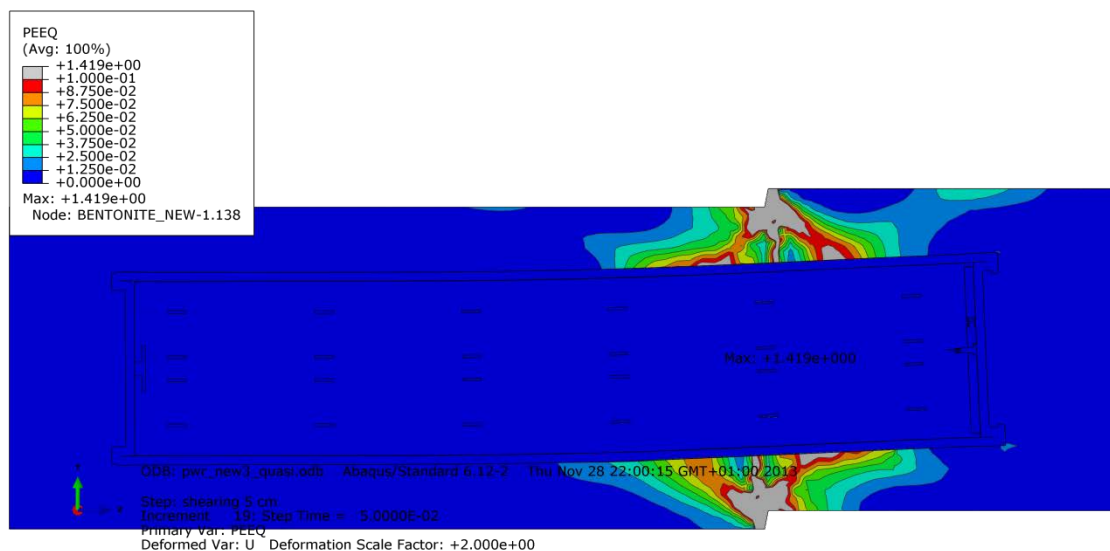


Figure A1-1 Plot showing equivalent plastic strain (PEEQ) after 5 cm shearing.

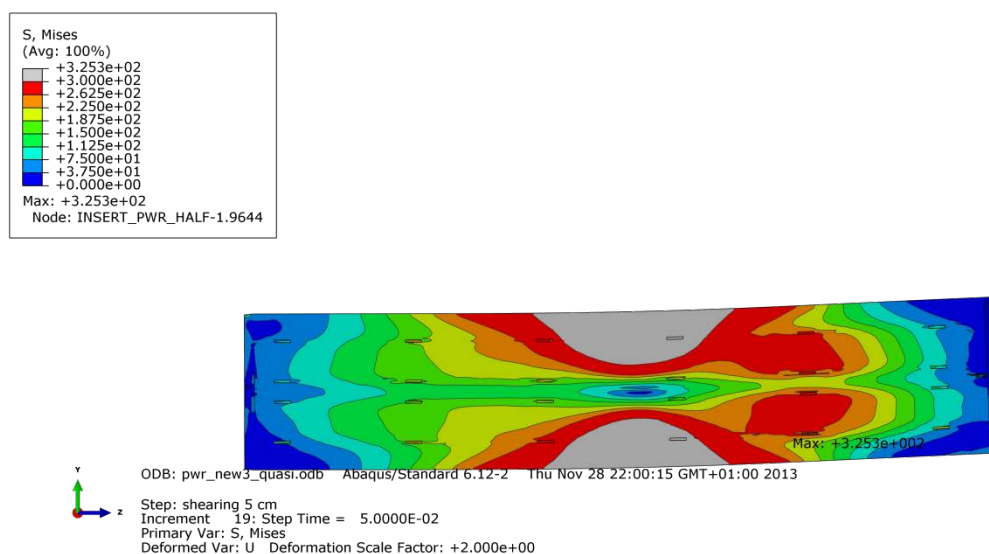


Figure A1-2 Plot showing Mises stress [MPa] for the insert after 5 cm shearing.

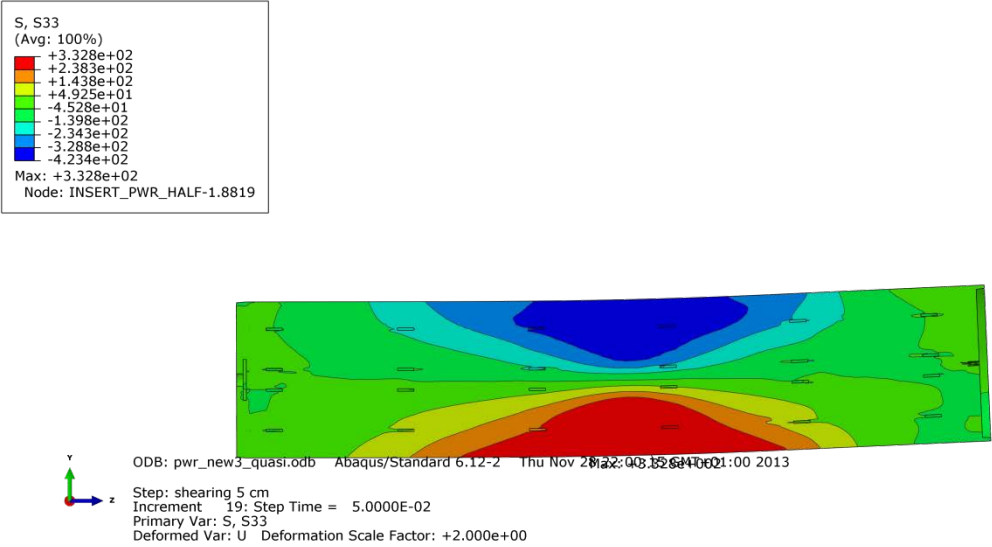


Figure A1-3 Plot showing axial stress [MPa] for the insert after 5 cm shearing.

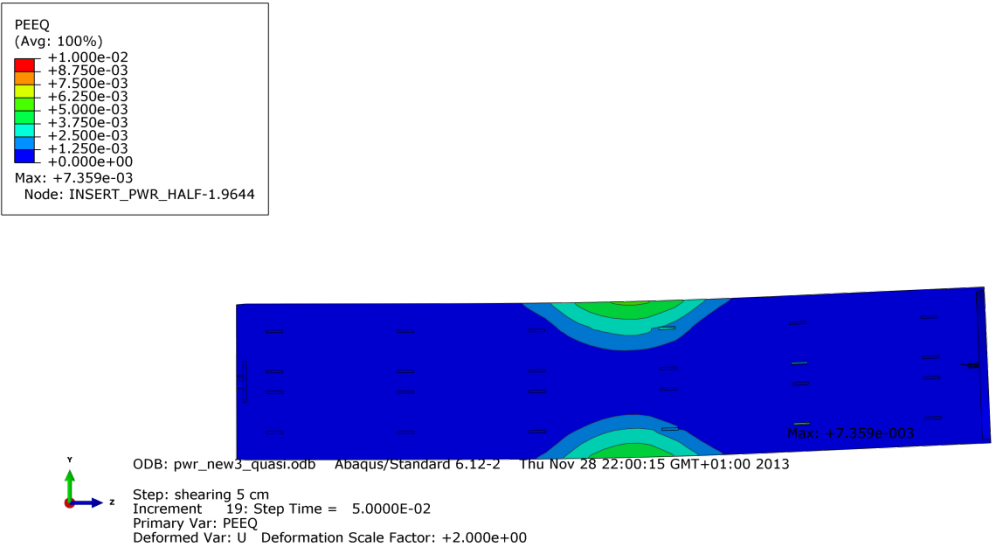


Figure A1-4 Plot showing equivalent plastic strain (PEEQ) for the insert after 5 cm shearing.

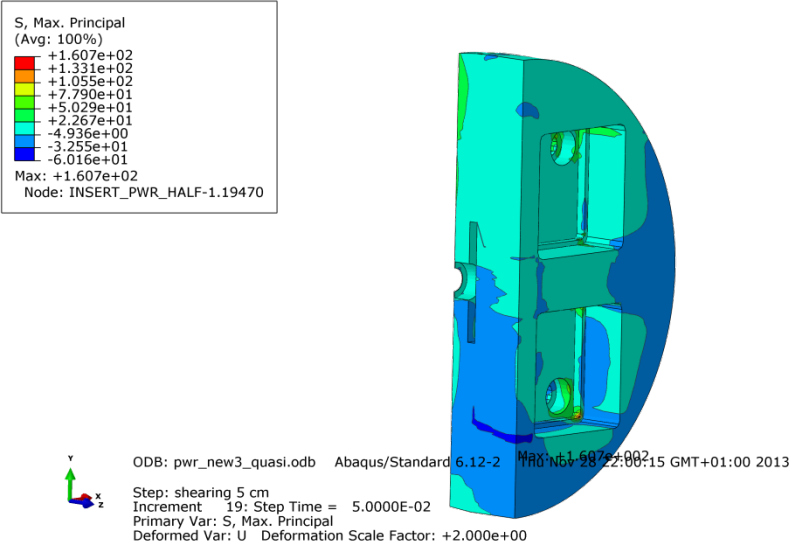


Figure A1-5 Plot showing maximum principal stress [MPa] for the insert base after 5 cm shearing.

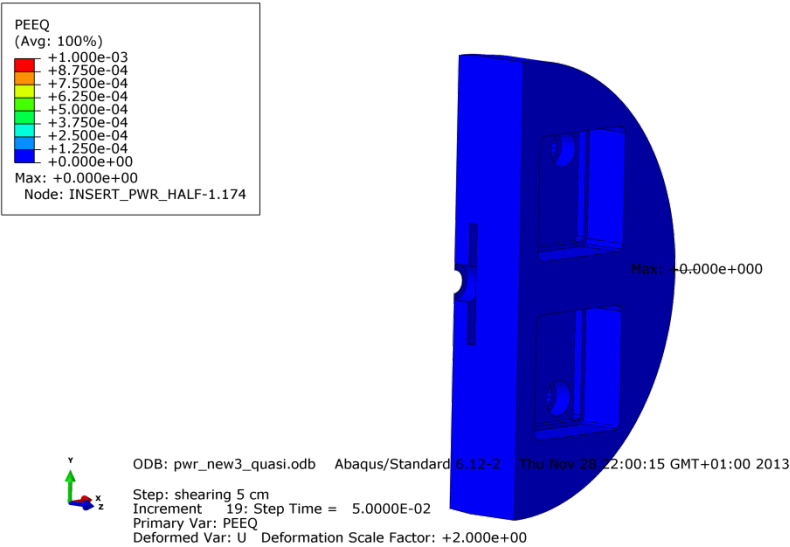


Figure A1-6 Plot showing equivalent plastic strain (PEEQ) for the insert base after 5 cm shearing.

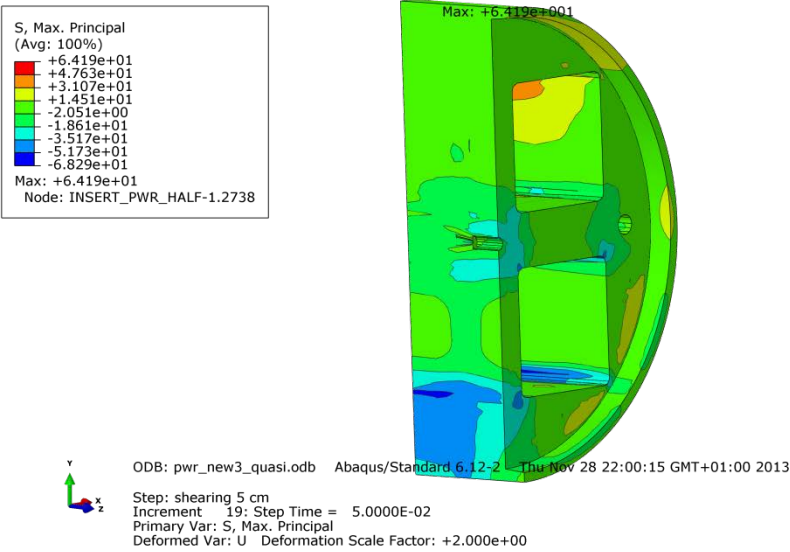


Figure A1-7 Plot showing maximum principal stress [MPa] for the insert top after 5 cm shearing.

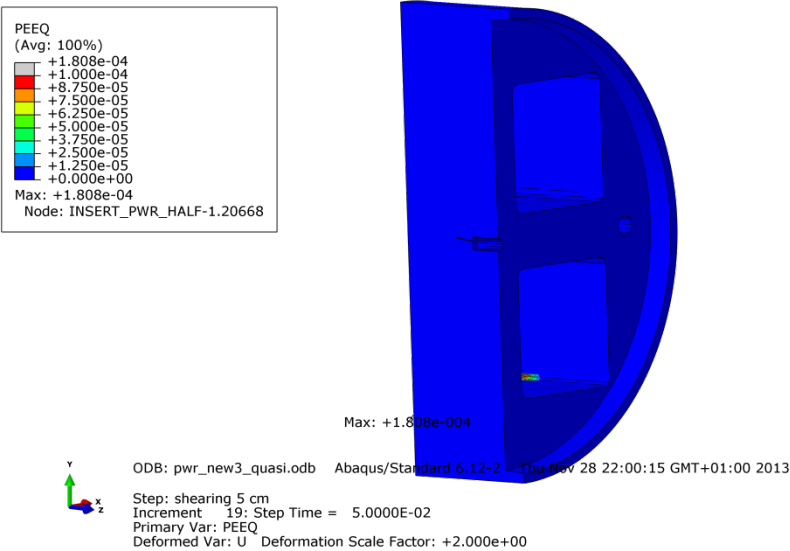


Figure A1-8 Plot showing equivalent plastic strain (PEEQ) for the insert top after 5 cm shearing.

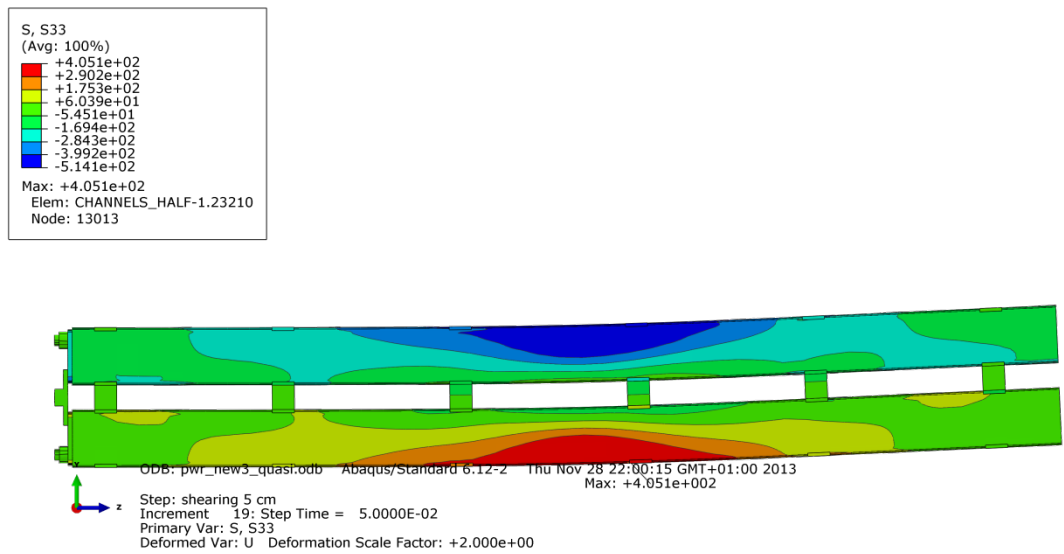


Figure A1-9 Plot showing axial stress [MPa] for the steel channel tubes after 5 cm shearing.

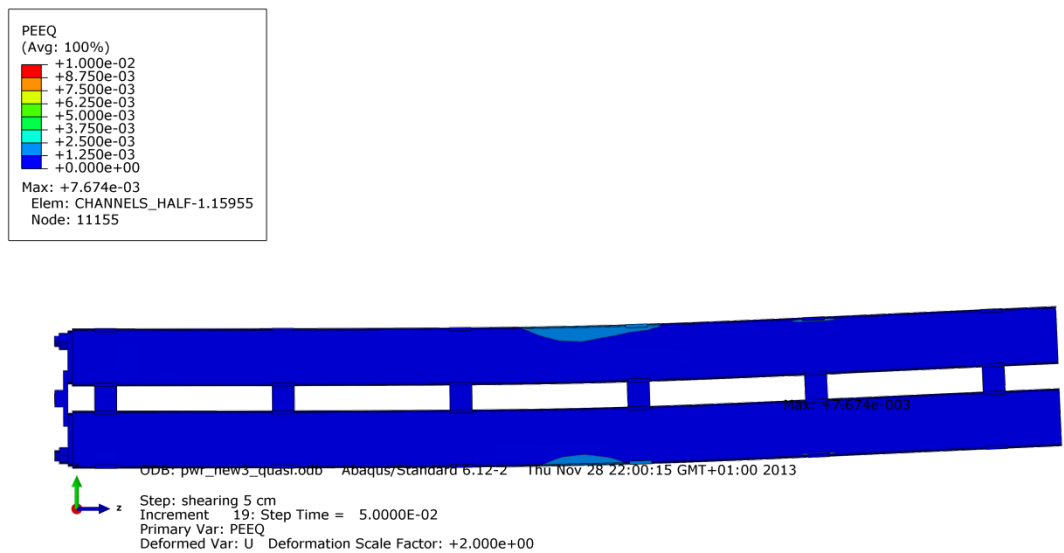


Figure A1-10 Plot showing equivalent plastic strain (PEEQ) for the steel channel tubes after 5 cm shearing.

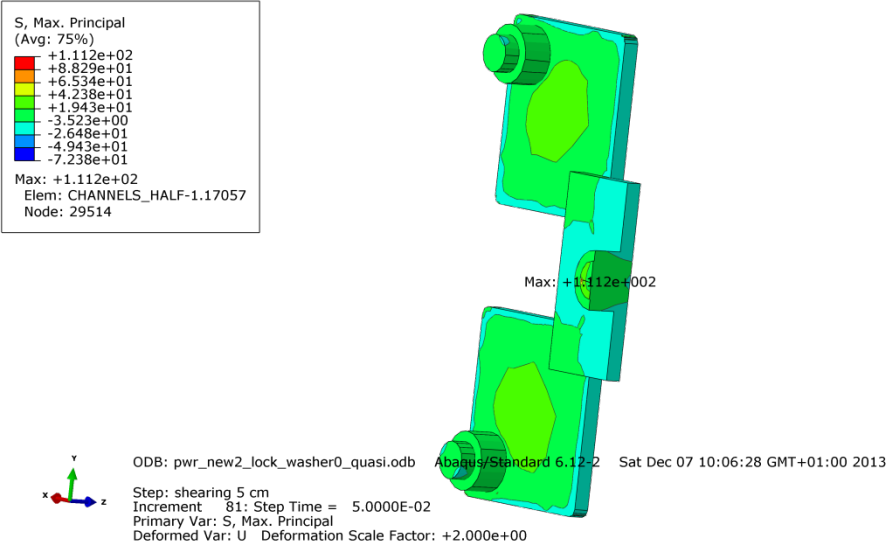


Figure A1-11 Plot showing maximum principal stress [MPa] for the steel channel tubes base plates after 5 cm shearing.

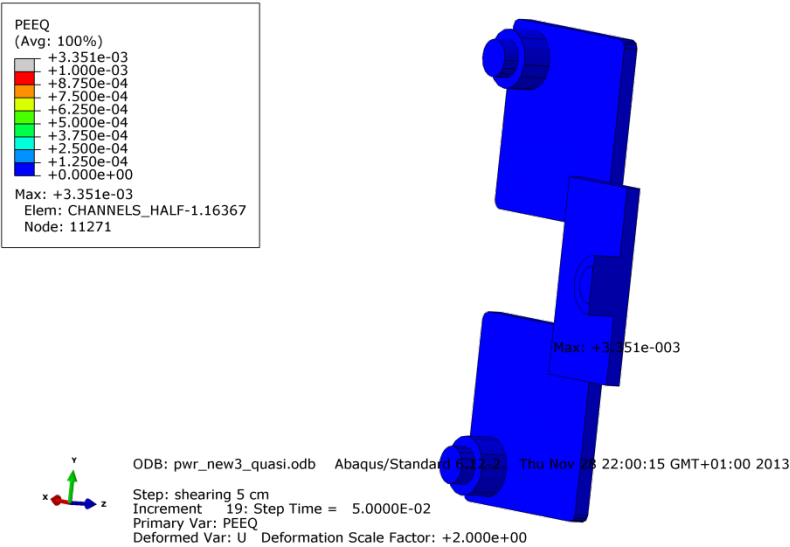


Figure A1-12 Plot showing equivalent plastic strain (PEEQ) for the steel channel tubes base plates after 5 cm shearing.

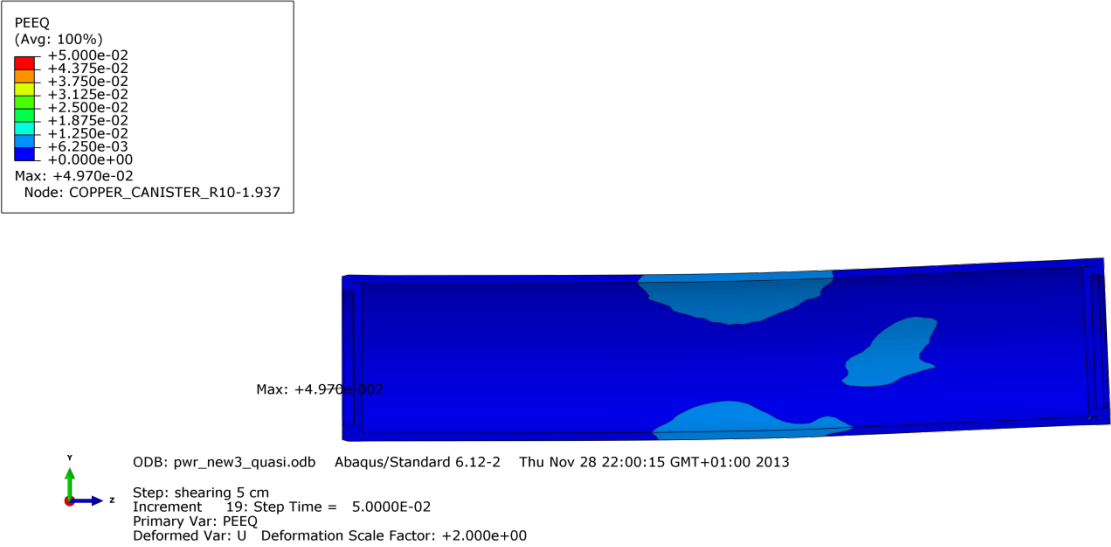


Figure A1-13 Plot showing equivalent plastic strain (PEEQ) for the steel copper shell after 5 cm shearing.

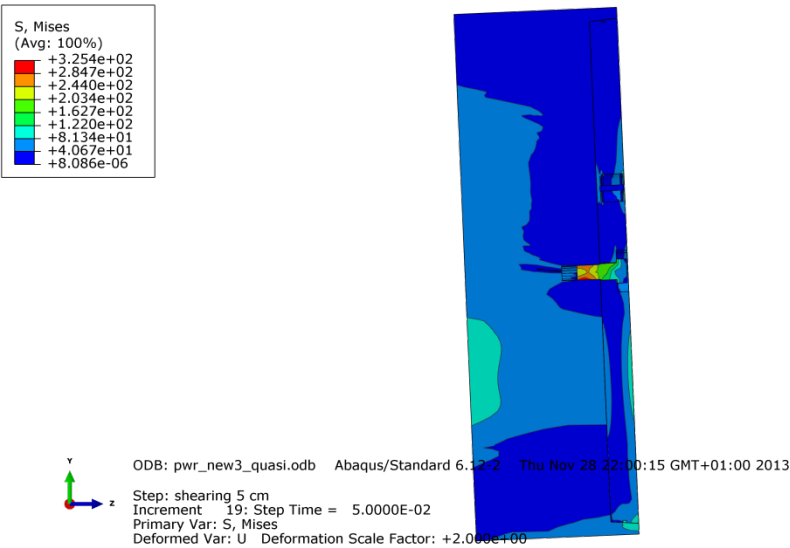


Figure A1-14 Plot showing Mises stress [MPa] close to the steel lid fixing screw after 5 cm shearing.

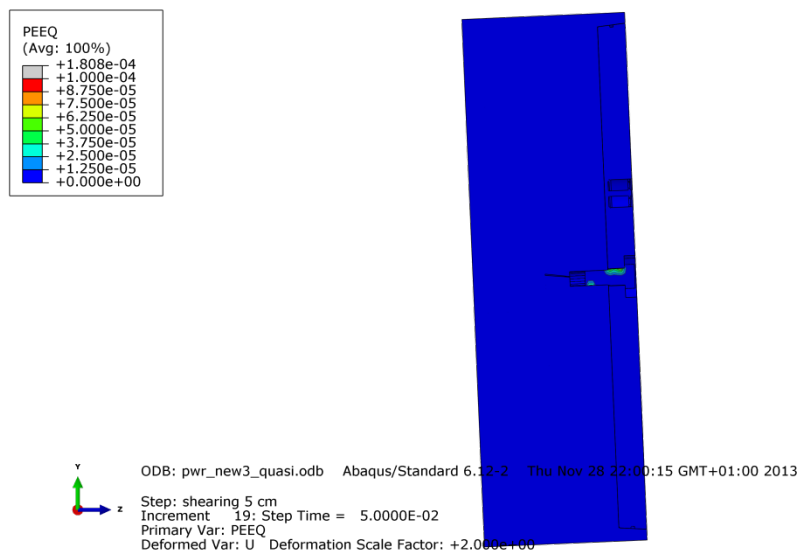


Figure A1-15 Plot showing equivalent plastic strain (PEEQ) close to the steel lid fixing screw after 5 cm shearing.

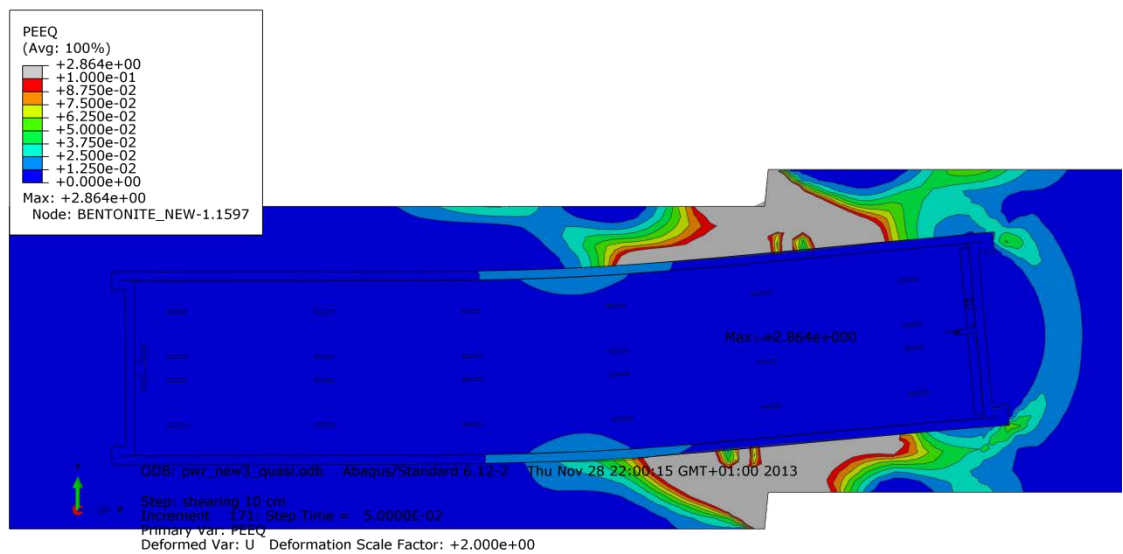


Figure A1-16 Plot showing equivalent plastic strain (PEEQ) after 10 cm shearing.

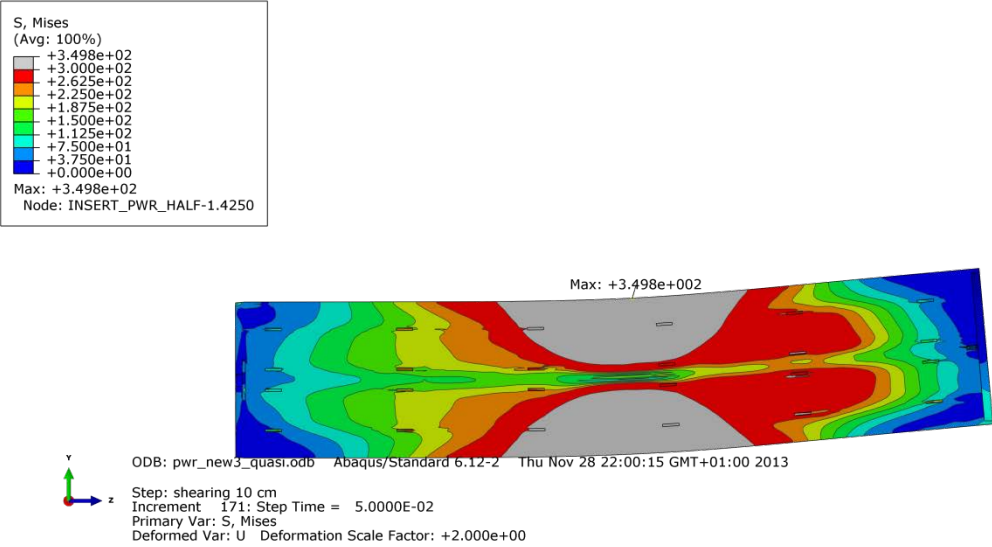


Figure A1-17 Plot showing Mises stress[MPa] for the insert after 10 cm shearing.

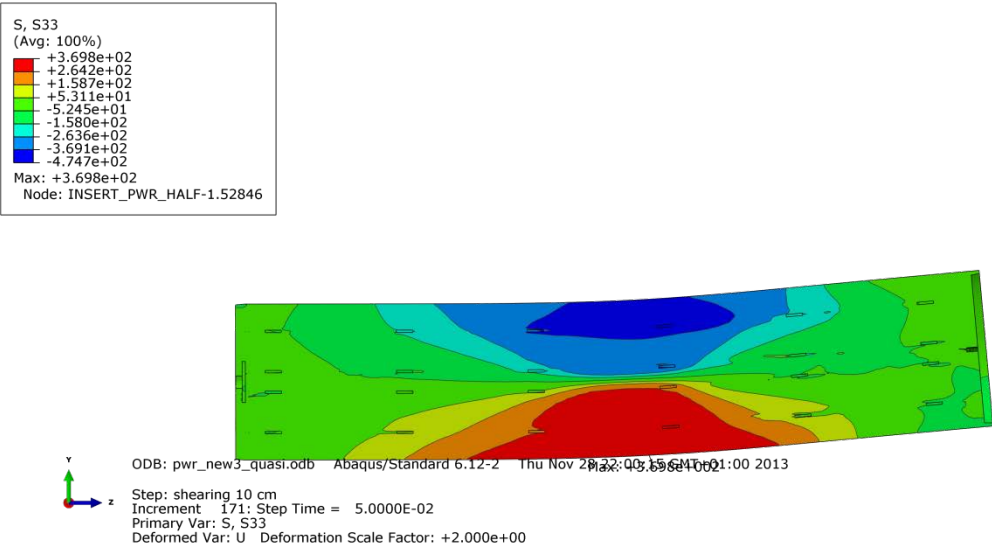


Figure A1-18 Plot showing axial stress [MPa] for the insert after 10 cm shearing.

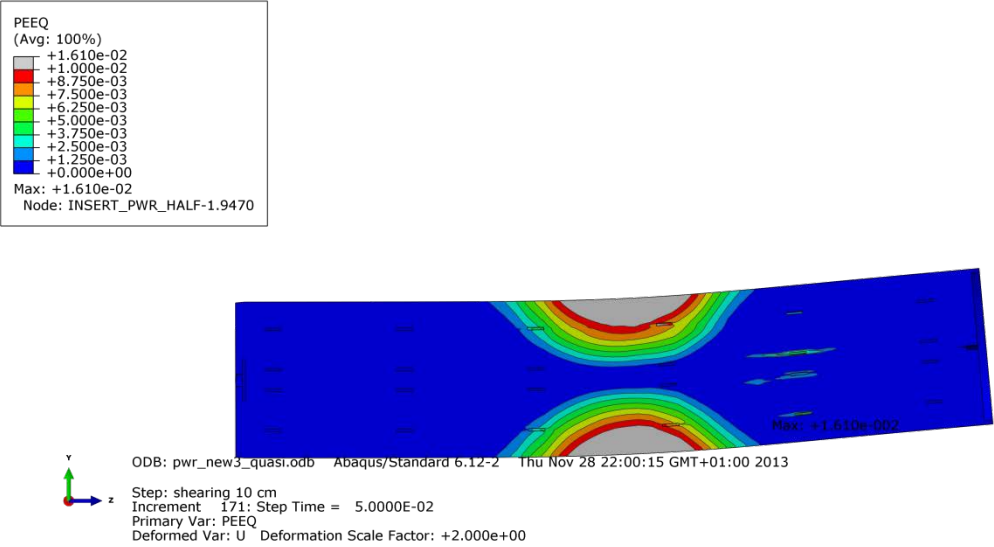


Figure A1-19 Plot showing equivalent plastic strain (PEEQ) for the insert after 10 cm shearing.

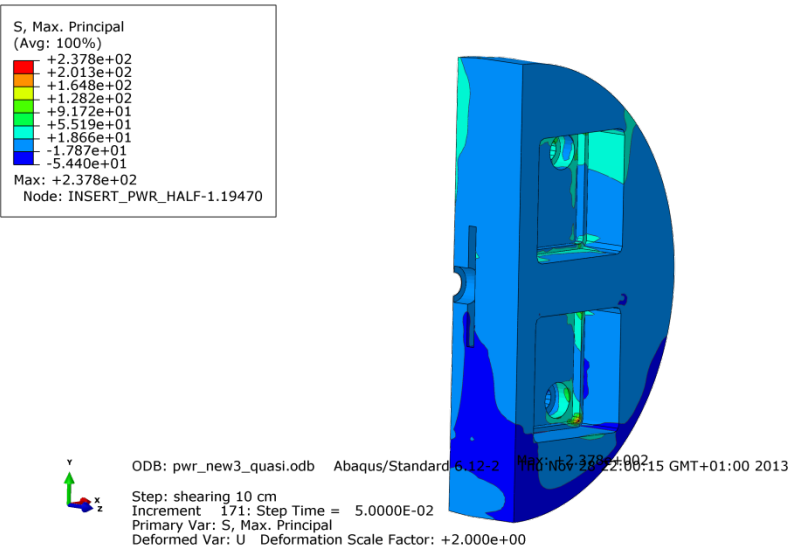


Figure A1-20 Plot showing maximum principal stress [MPa] for the insert base after 10 cm shearing.

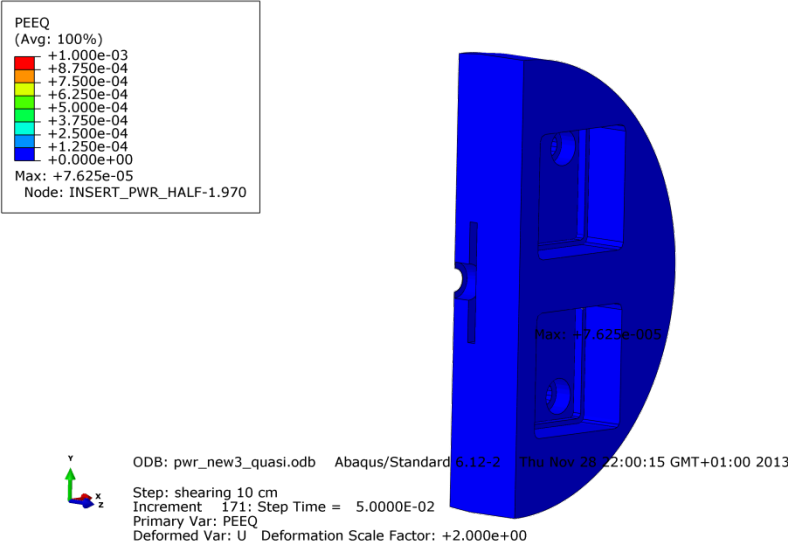


Figure A1-21 Plot showing equivalent plastic strain (PEEQ) for the insert base after 10 cm shearing.

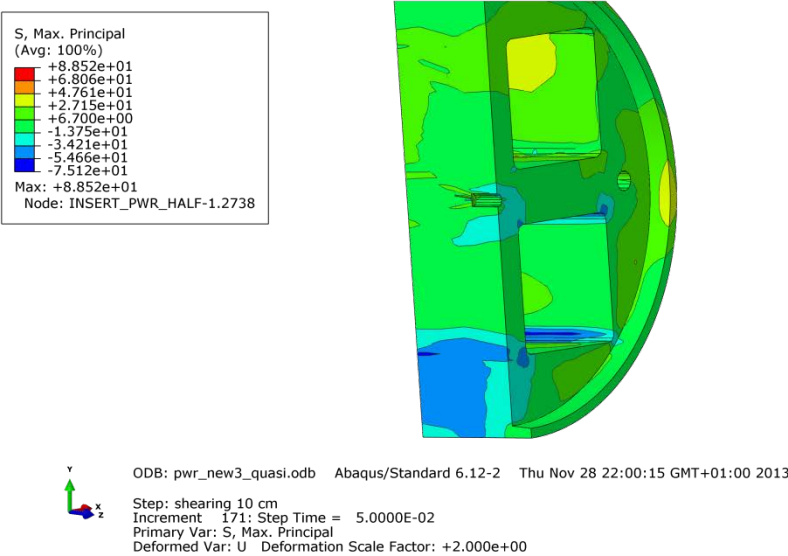


Figure A1-22 Plot showing maximum principal stress [MPa] for the insert top after 10 cm shearing.

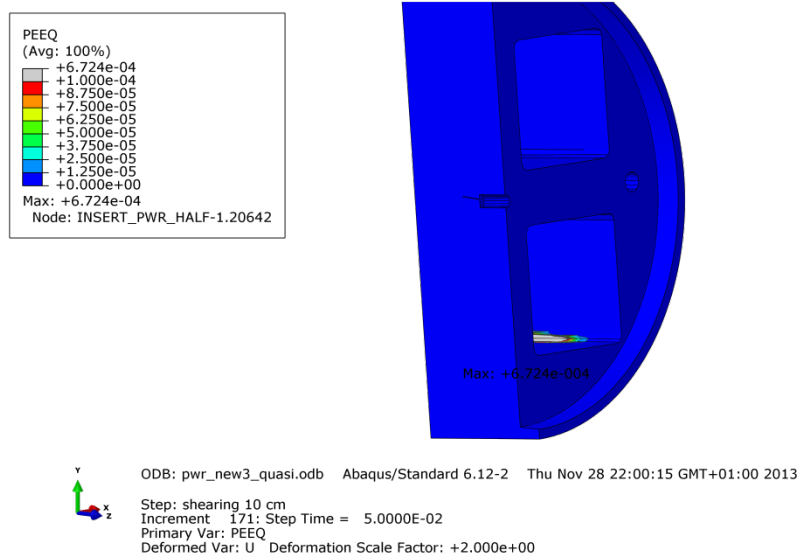


Figure A1-23 Plot showing equivalent plastic strain (PEEQ) for the insert top after 10 cm shearing.

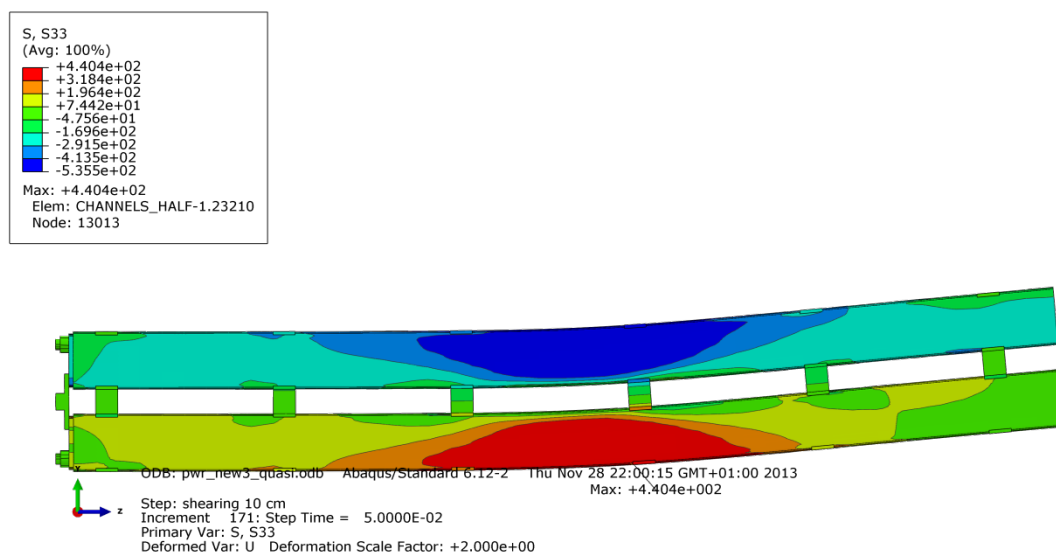


Figure A1-24 Plot showing axial stress [MPa] for the steel channel tubes after 10 cm shearing.

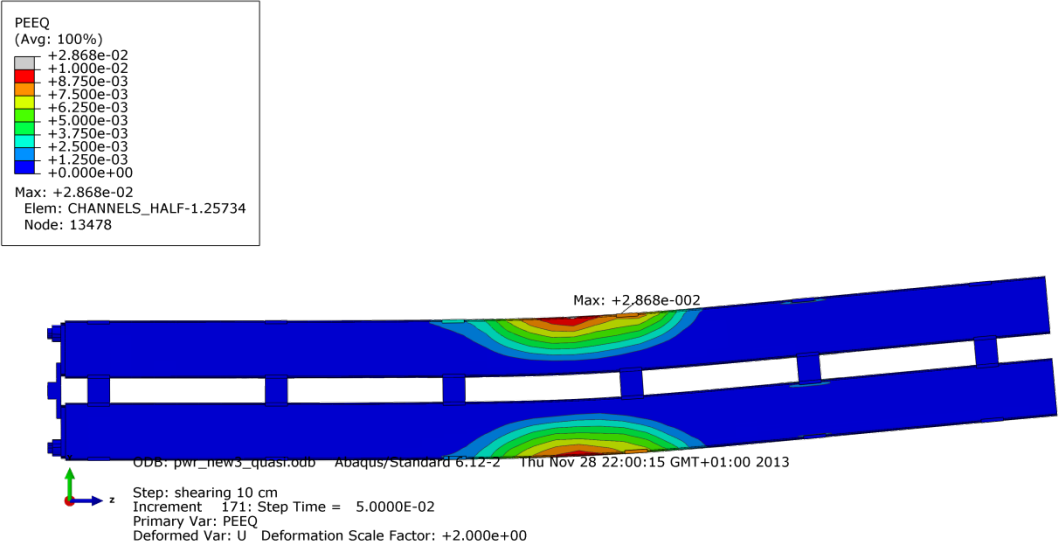


Figure A1-25 Plot showing equivalent plastic strain (PEEQ) for the steel channel tubes after 10 cm shearing.

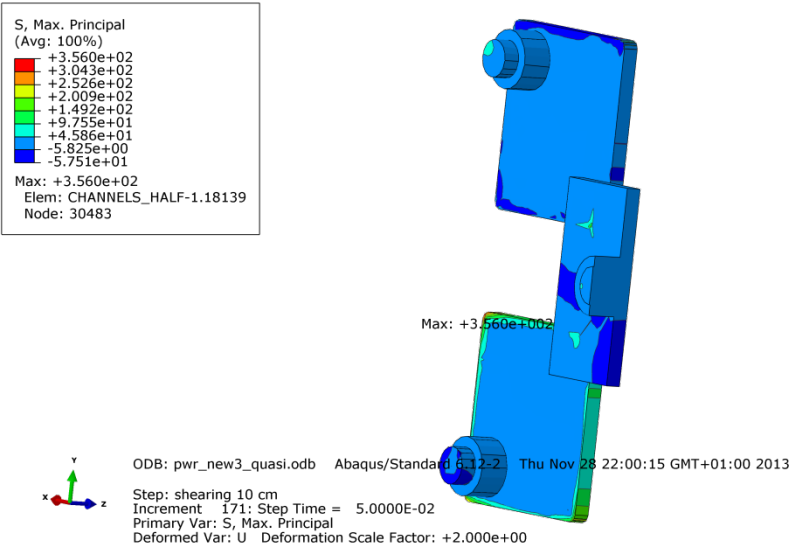


Figure A1-26 Plot showing maximum principal stress [MPa] for the steel channel tubes base plates after 10 cm shearing.

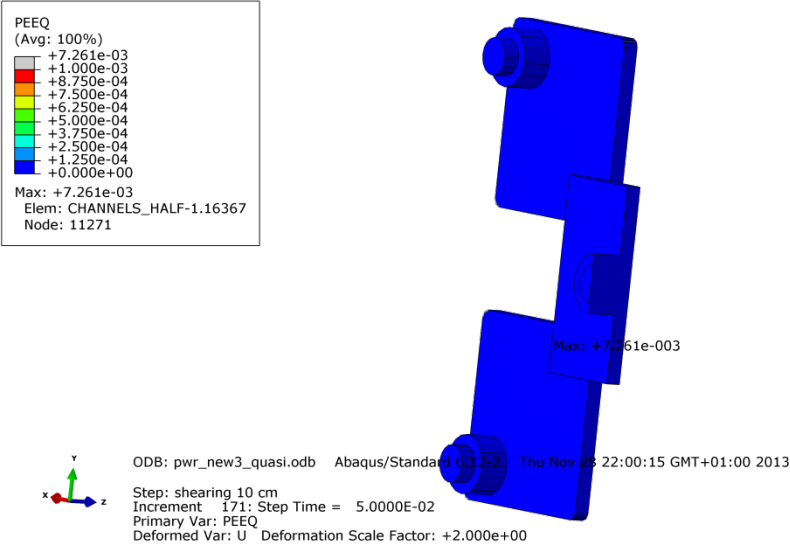


Figure A1-27 Plot showing equivalent plastic strain (PEEQ) for the steel channel tubes base plates after 10 cm shearing.

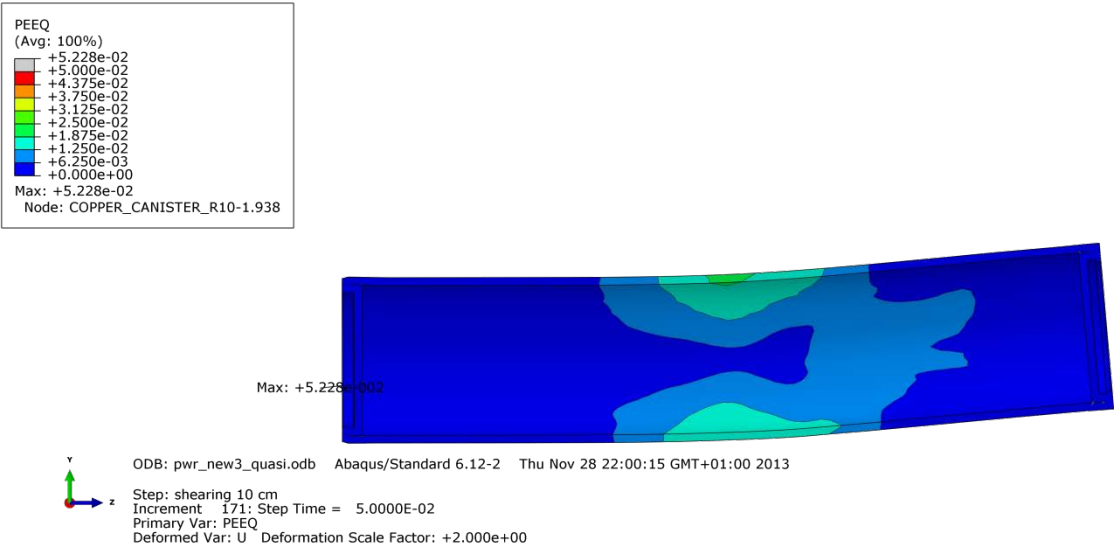


Figure A1-28 Plot showing equivalent plastic strain (PEEQ) for the copper shell after 10 cm shearing.

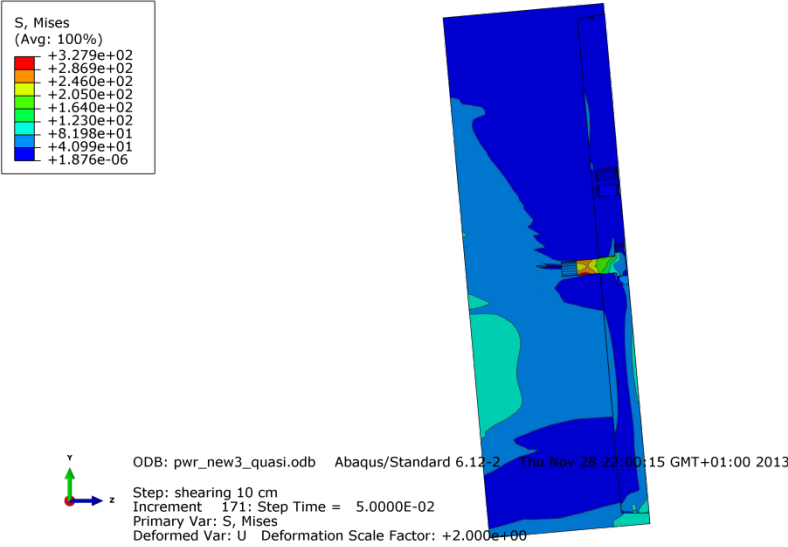


Figure A1-29 Plot showing Mises stress [MPa] close to the steel lid fixing screw after 10 cm shearing.

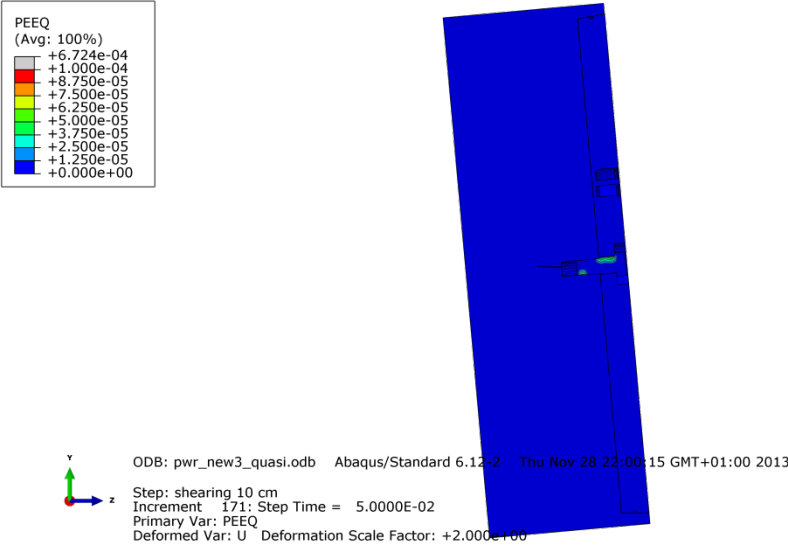


Figure A1-30 Plot showing equivalent plastic strain (PEEQ) close to the steel lid fixing screw after 10 cm shearing.

Appendix 2 – Plots for pwr_eccentric3_quasi

Plots showing deformed geometry as contour plots for all parts at shearing magnitude 5 and 10 cm for case pwr_eccentric3_quasi (horizontal shearing at $\frac{3}{4}$ -distance from base of the insert) when the insert is placed eccentric in respect to the steel channel tubes taking tolerances into account. The view shows the symmetry plane and all deformations are scaled by a factor of two.

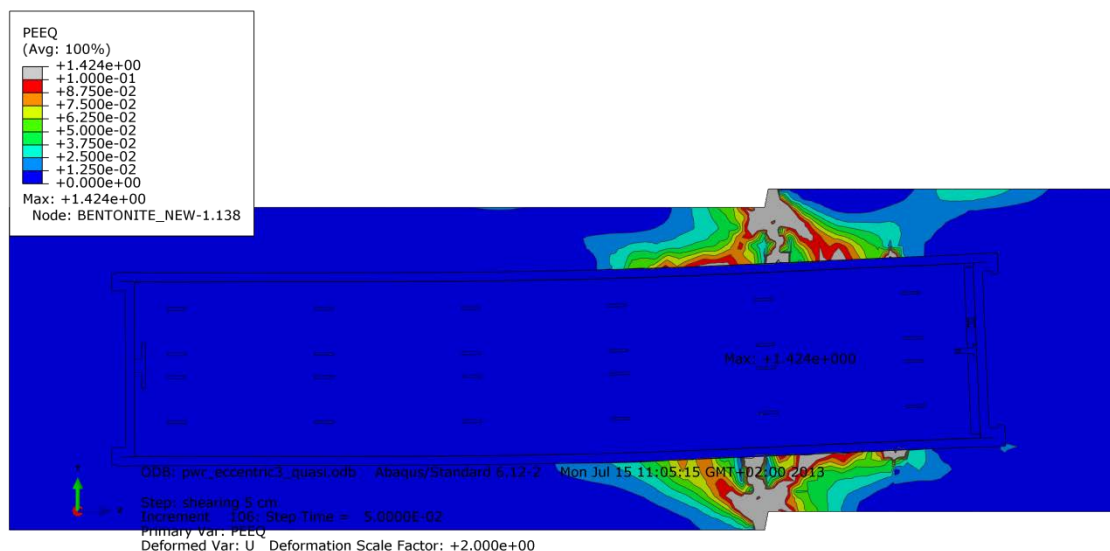


Figure A2-1 Plot showing equivalent plastic strain (PEEQ) after 5 cm shearing.

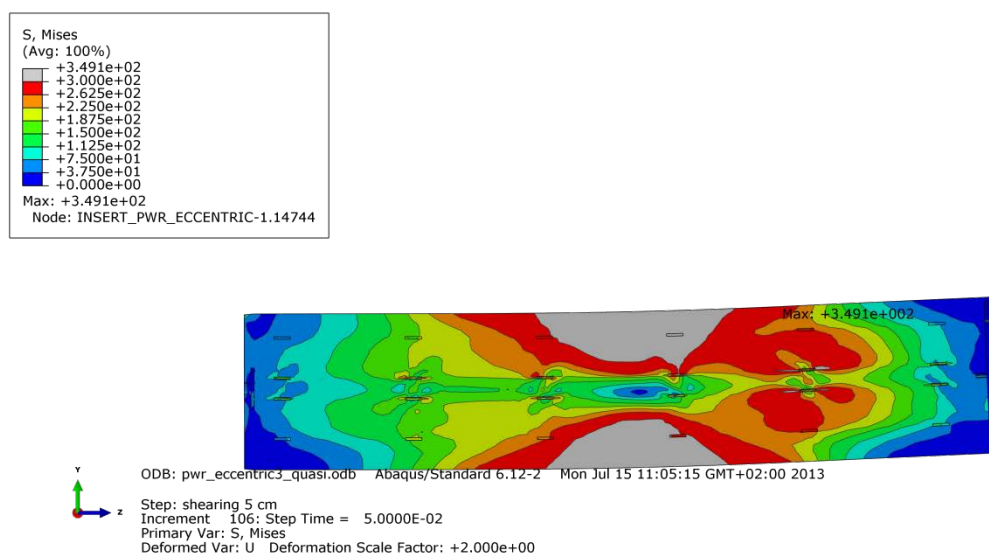


Figure A2-2 Plot showing Mises stress [MPa] for the insert after 5 cm shearing.

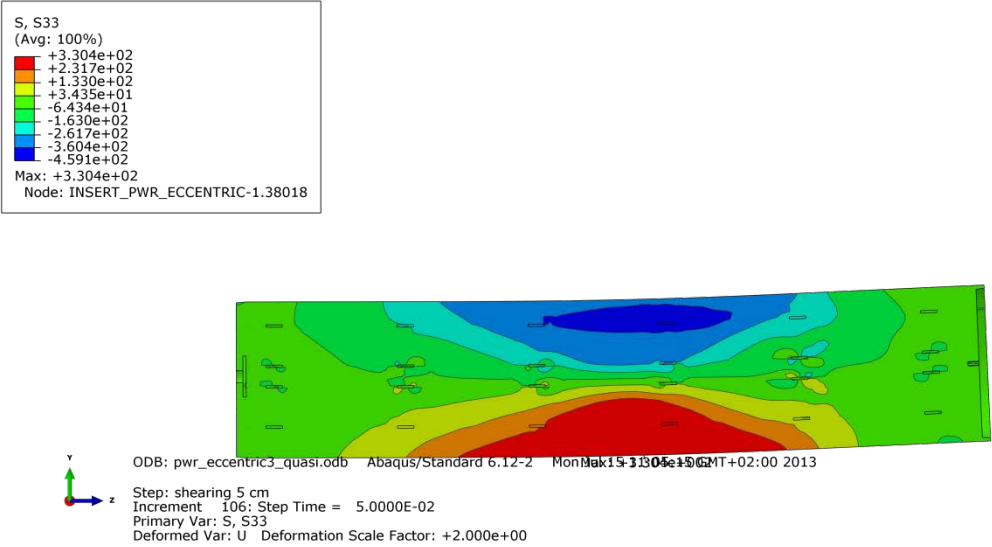


Figure A2-3 Plot showing axial stress [MPa] for the insert after 5 cm shearing.

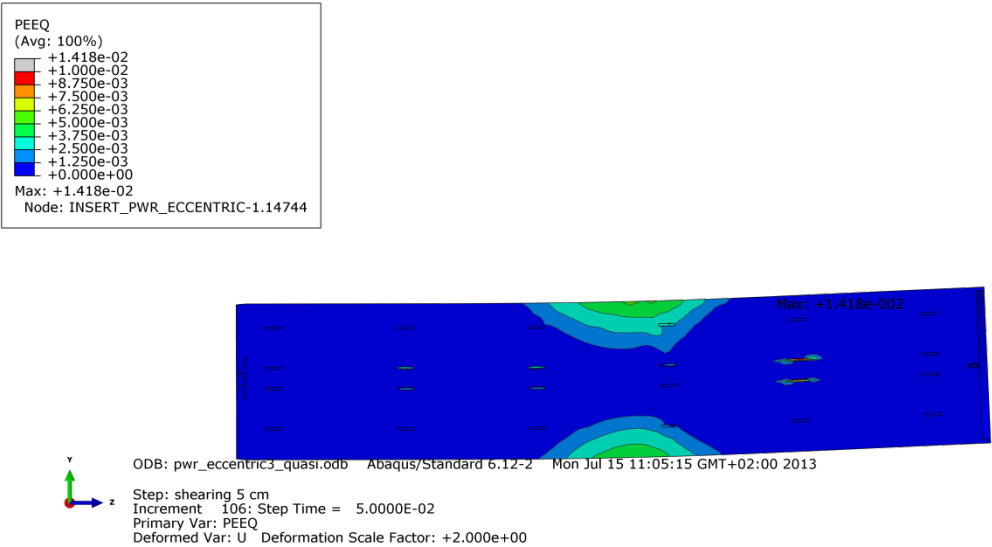


Figure A2-4 Plot showing equivalent plastic strain (PEEQ) for the insert after 5 cm shearing.

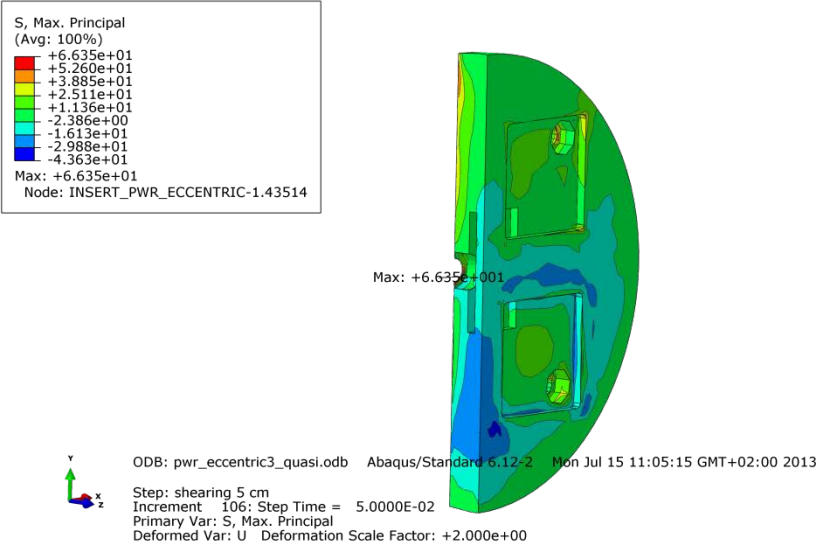


Figure A2-5 Plot showing maximum principal stress [MPa] for the insert base after 5 cm shearing.

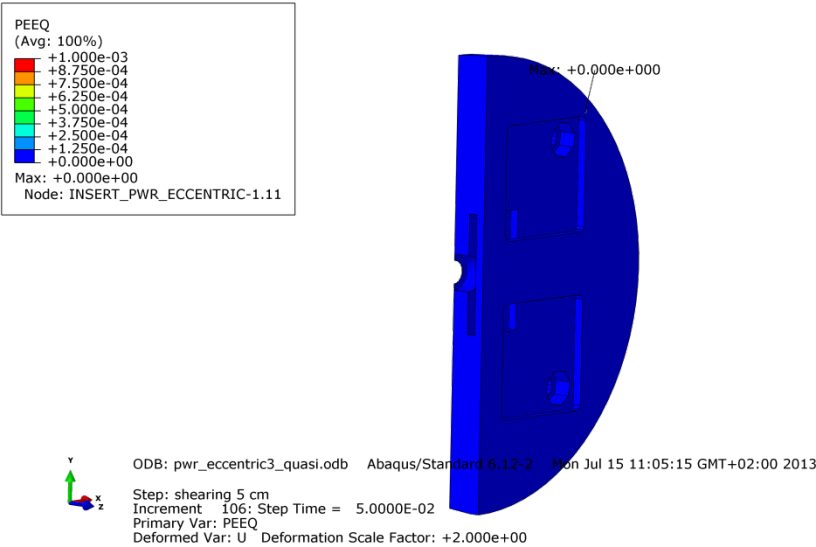


Figure A2-6 Plot showing equivalent plastic strain (PEEQ) for the insert base after 5 cm shearing.

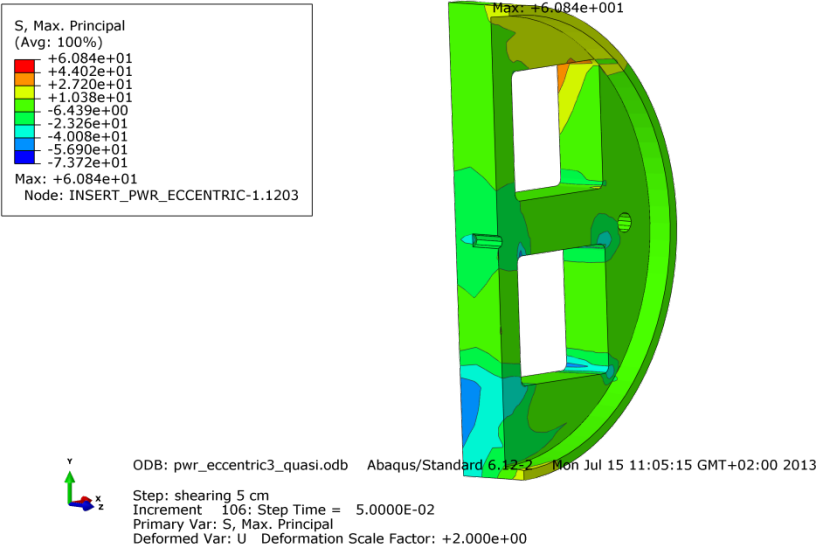


Figure A2-7 Plot showing maximum principal stress [MPa] for the insert top after 5 cm shearing.

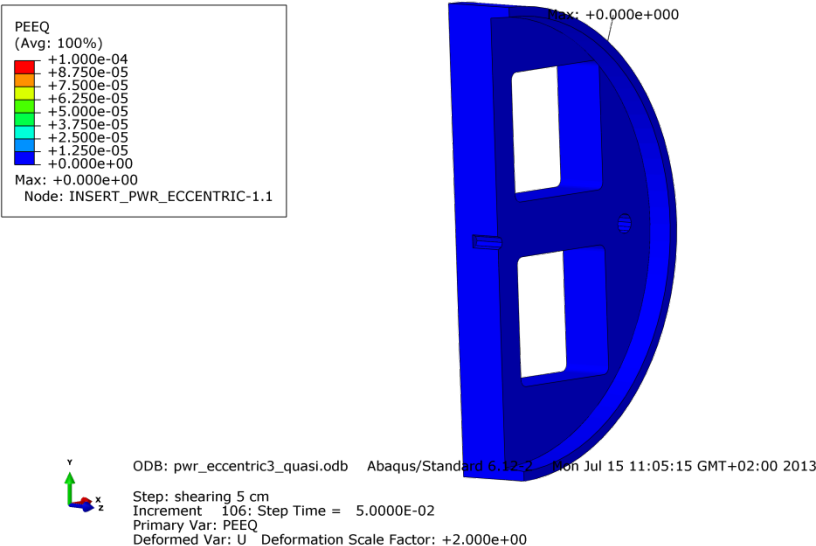


Figure A2-8 Plot showing equivalent plastic strain (PEEQ) for the insert top after 5 cm shearing.

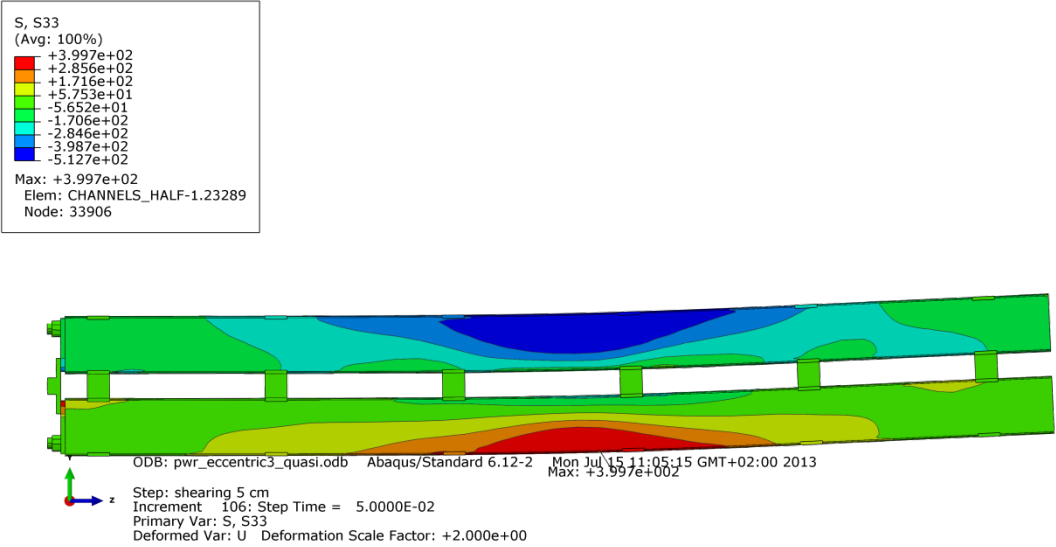


Figure A2-9 Plot showing axial stress [MPa] for the steel channel tubes after 5 cm shearing.

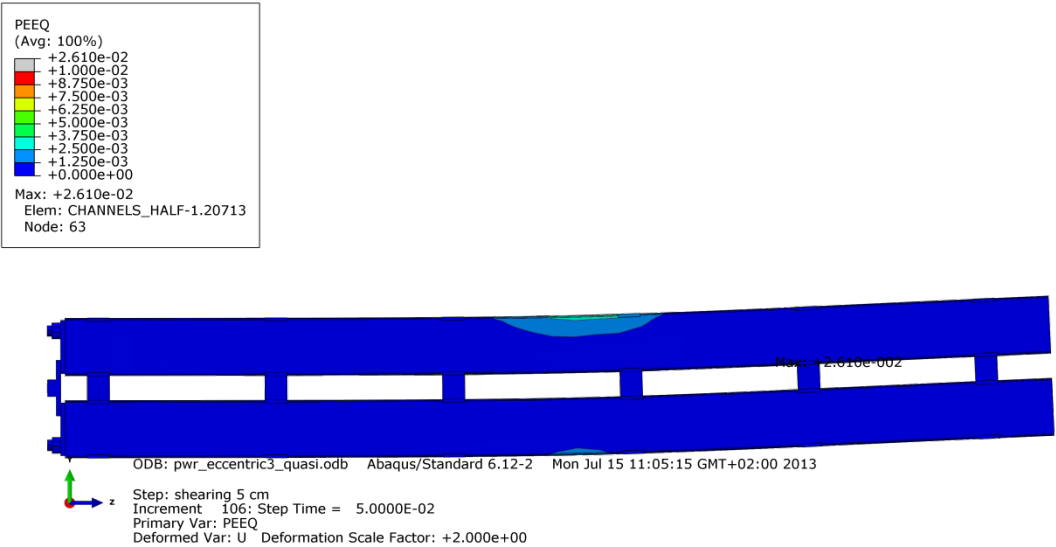


Figure A2-10 Plot showing equivalent plastic strain (PEEQ) for the steel channel tubes after 5 cm shearing.

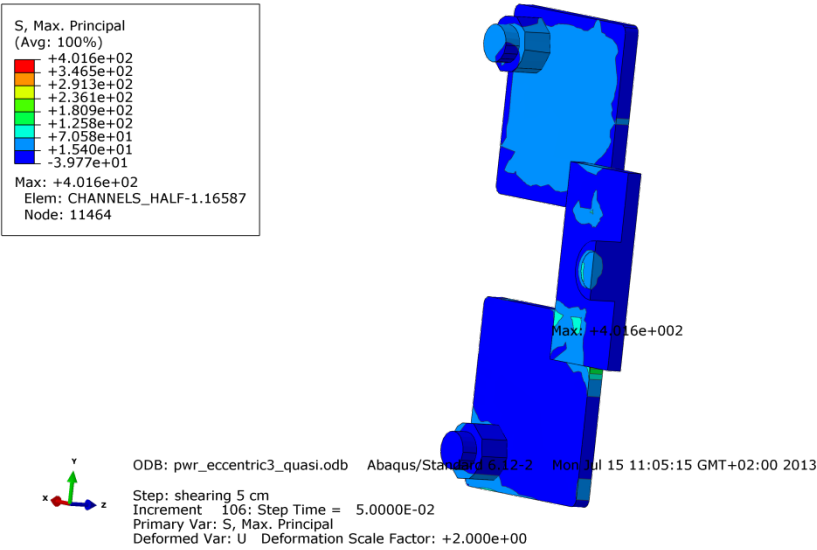


Figure A2-11 Plot showing maximum principal stress [MPa] for the steel channel tubes base plates after 5 cm shearing.

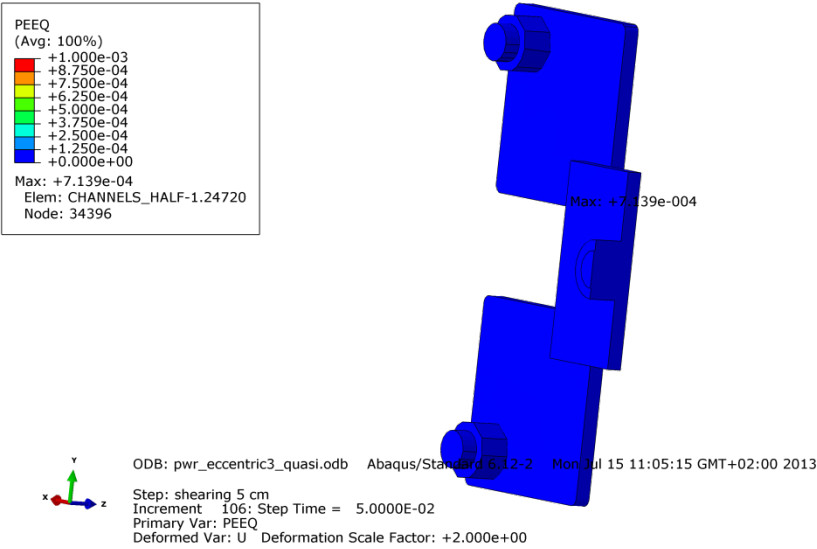


Figure A2-12 Plot showing equivalent plastic strain (PEEQ) for the steel channel tubes base plates after 5 cm shearing.

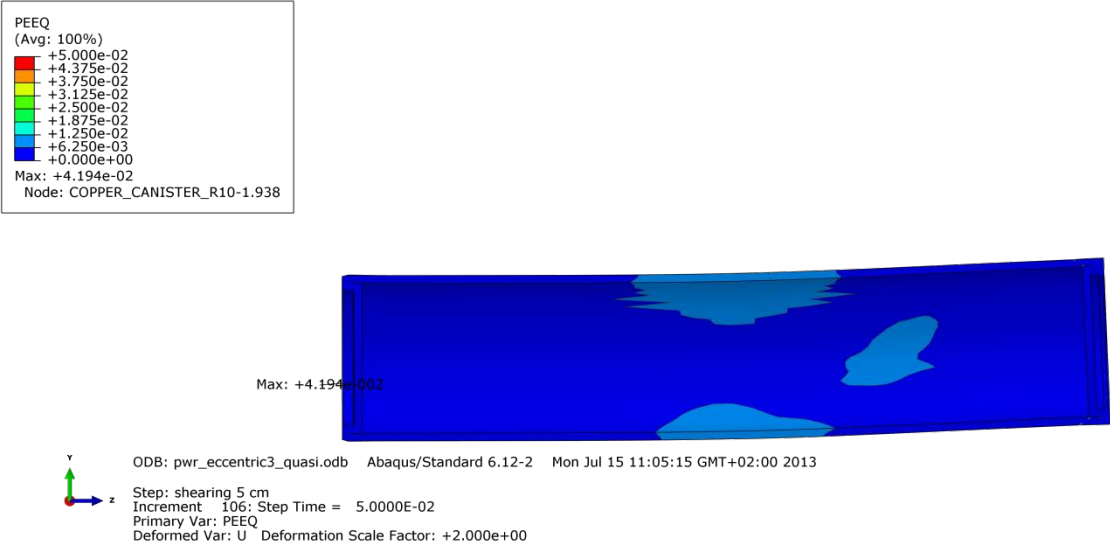


Figure A2-13 Plot showing equivalent plastic strain (PEEQ) for the copper shell after 5 cm shearing.

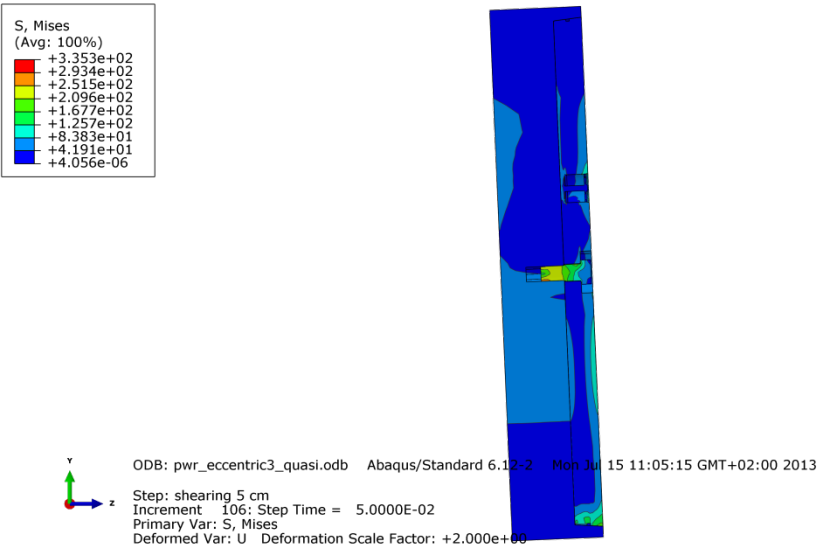


Figure A2-14 Plot showing Mises stress [MPa] close to the steel lid fixing screw after 5 cm shearing.

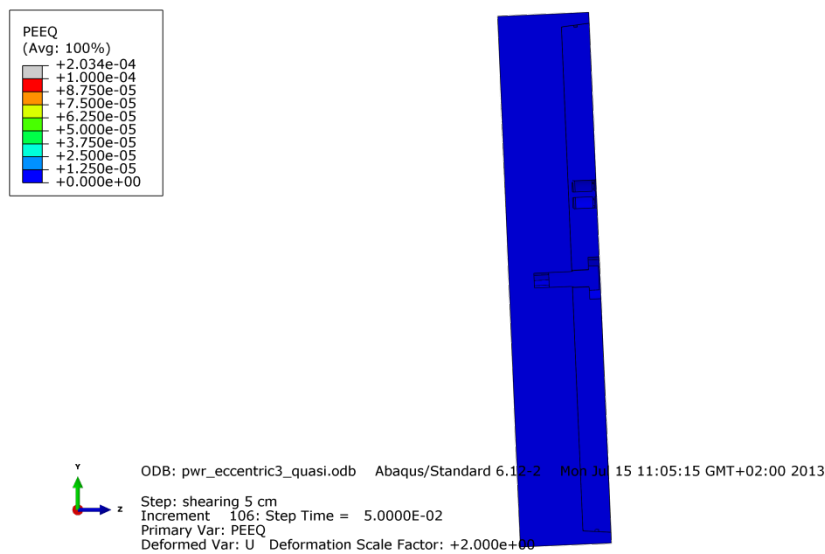


Figure A2-15 Plot showing equivalent plastic strain (PEEQ) close to the steel lid fixing screw after 5 cm shearing.

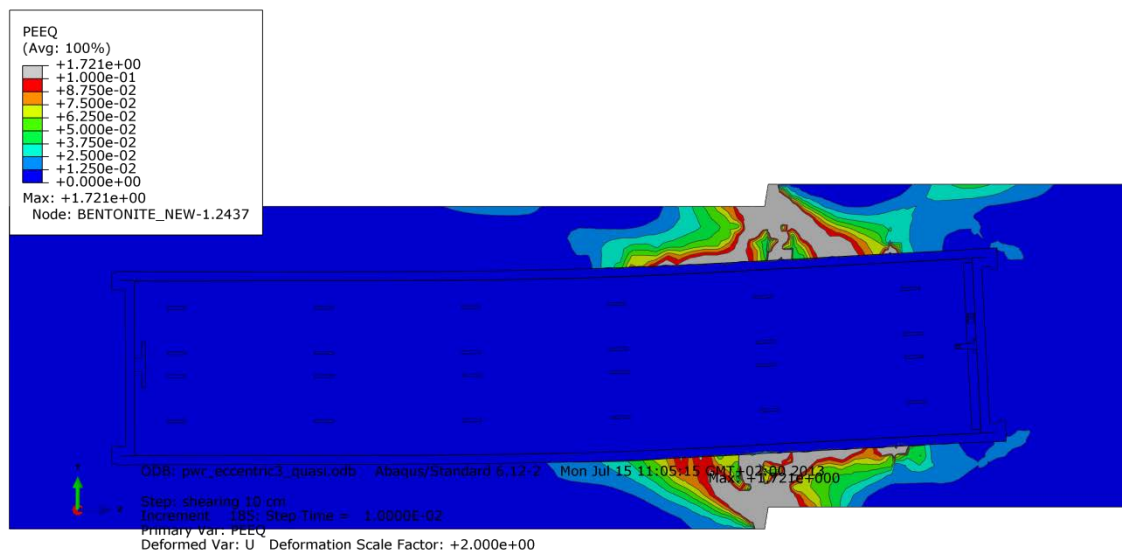


Figure A2-16 Plot showing equivalent plastic strain (PEEQ) after 10 cm shearing.

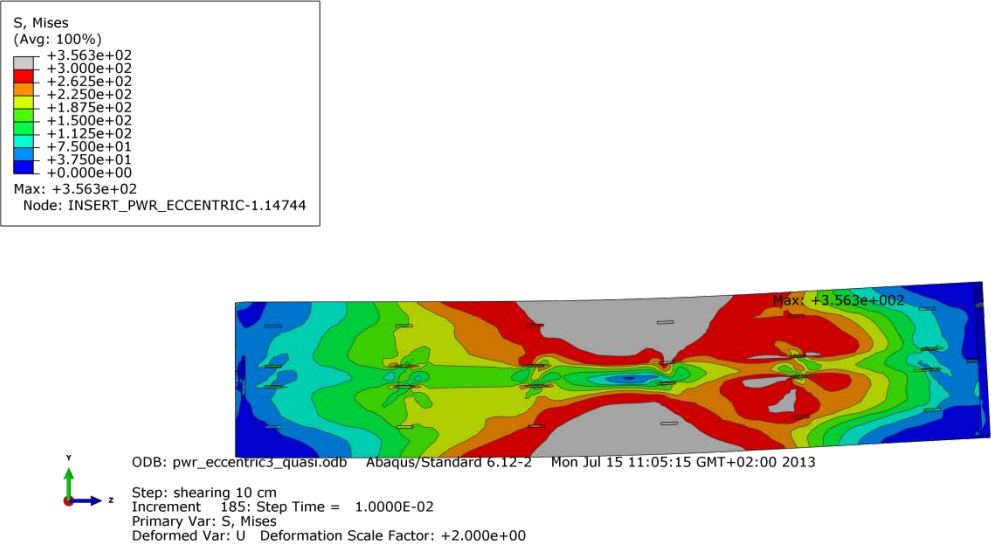


Figure A2-17 Plot showing Mises stress [MPa] for the insert after 10 cm shearing.

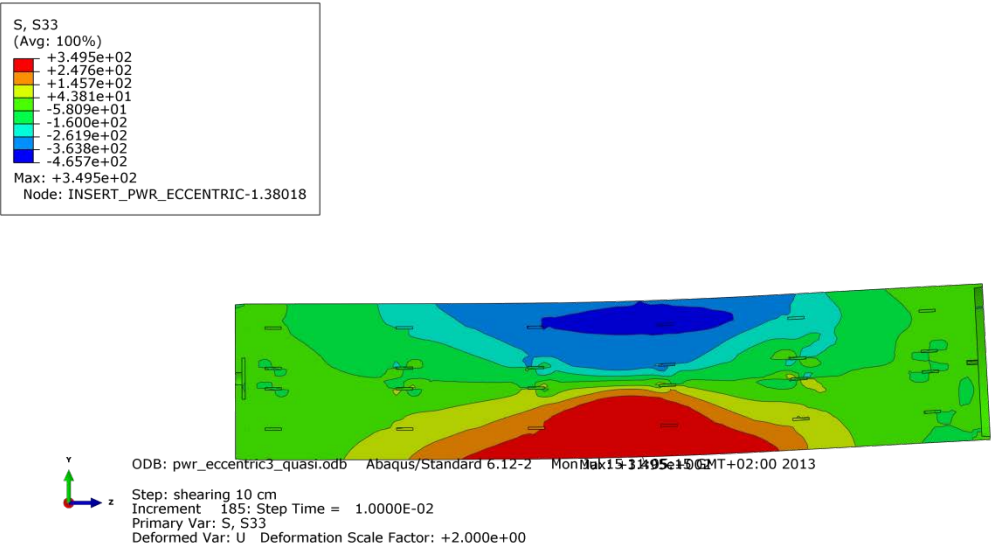


Figure A2-18 Plot showing axial stress [MPa] for the insert after 10 cm shearing.

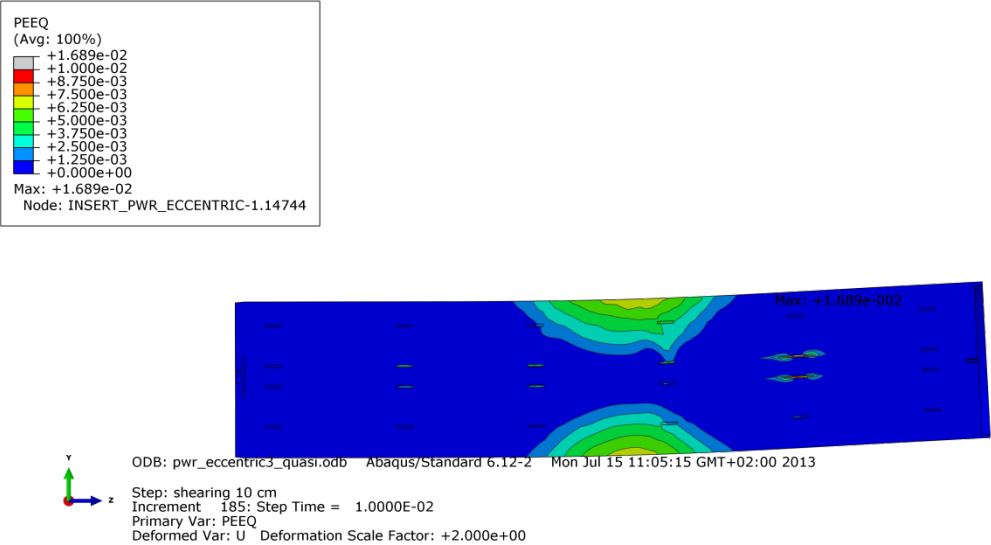


Figure A2-19 Plot showing equivalent plastic strain (PEEQ) for the insert after 10 cm shearing.

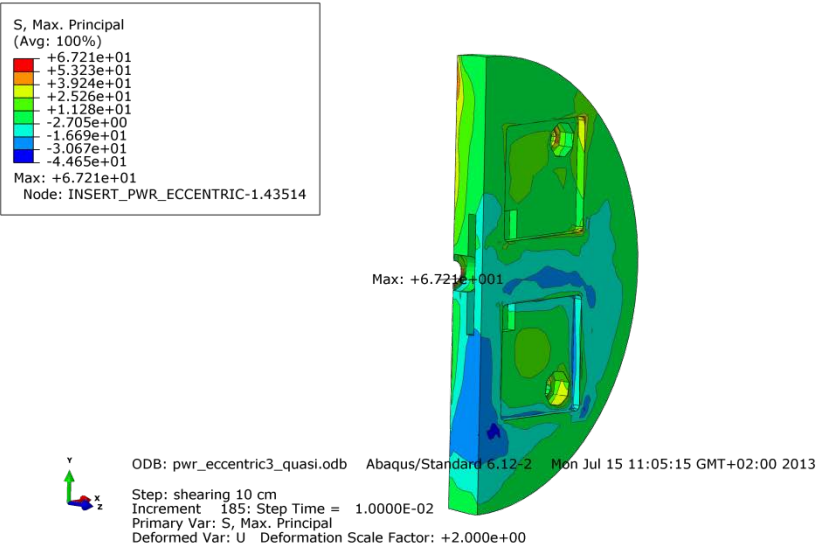


Figure A2-20 Plot showing maximum principal stress [MPa] for the insert base after 10 cm shearing.

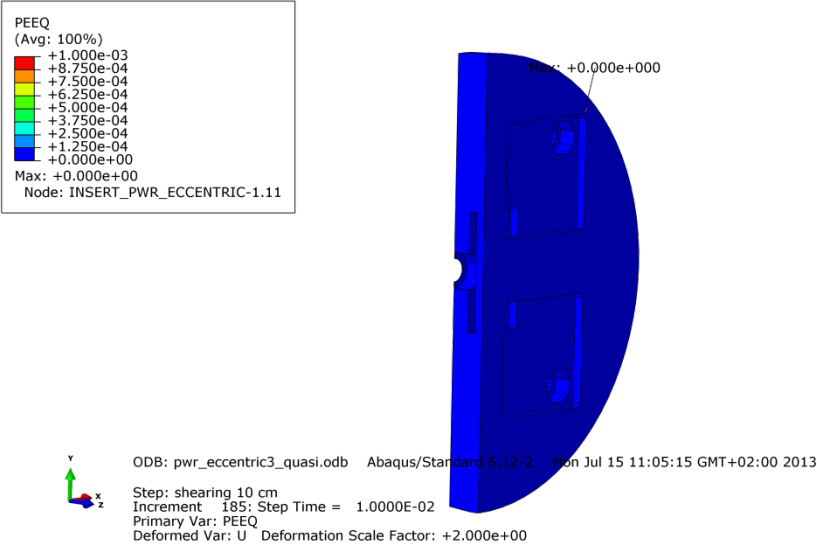


Figure A2-21 Plot showing equivalent plastic strain (PEEQ) for the insert base after 10 cm shearing.

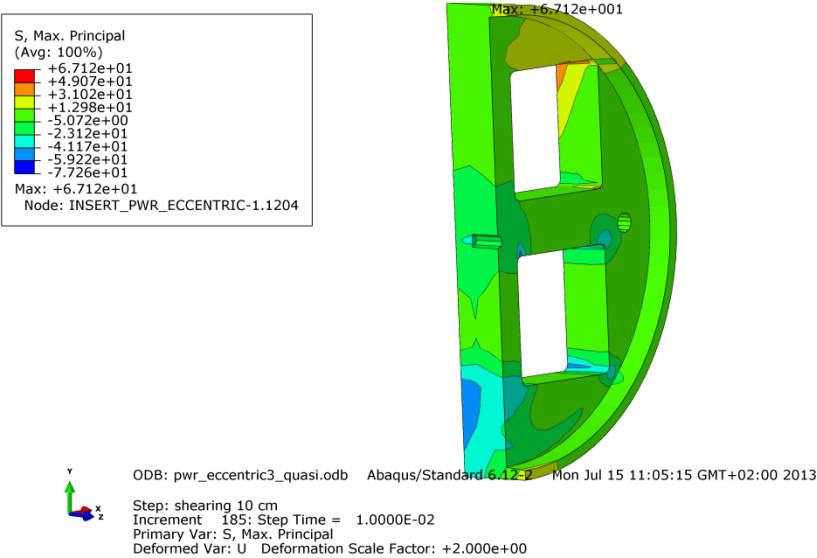


Figure A2-22 Plot showing maximum principal stress [MPa] for the insert top after 10 cm shearing.

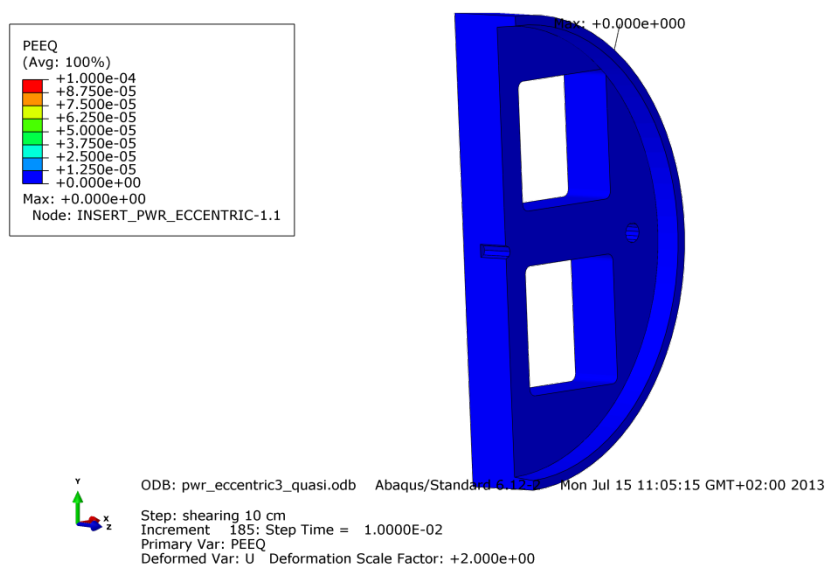


Figure A2-23 Plot showing equivalent plastic strain (PEEQ) for the insert top after 10 cm shearing.

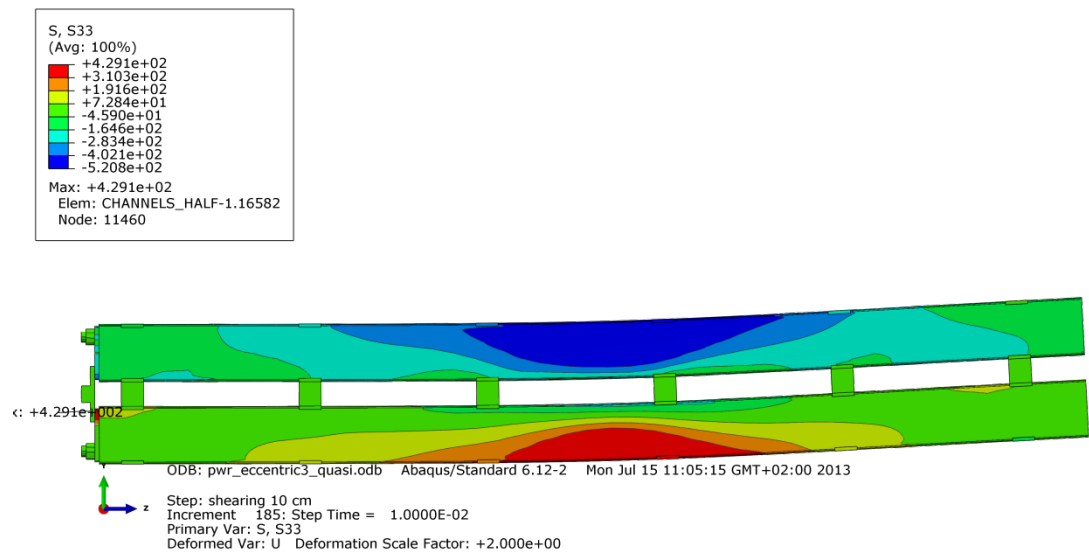


Figure A2-24 Plot showing axial stress [MPa] for the steel channel tubes after 10 cm shearing.

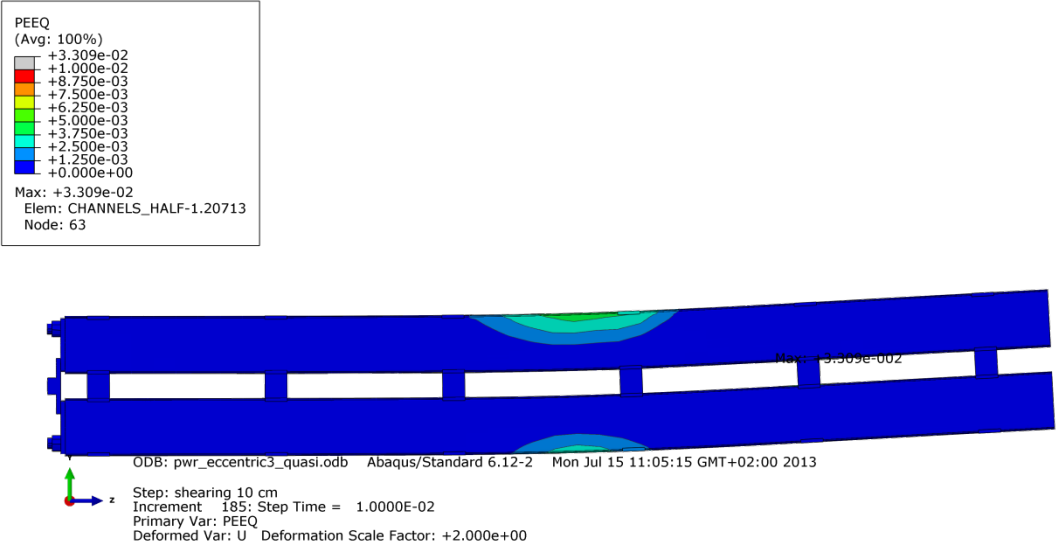


Figure A2-25 Plot showing equivalent plastic strain (PEEQ) for the steel channel tubes after 10 cm shearing.

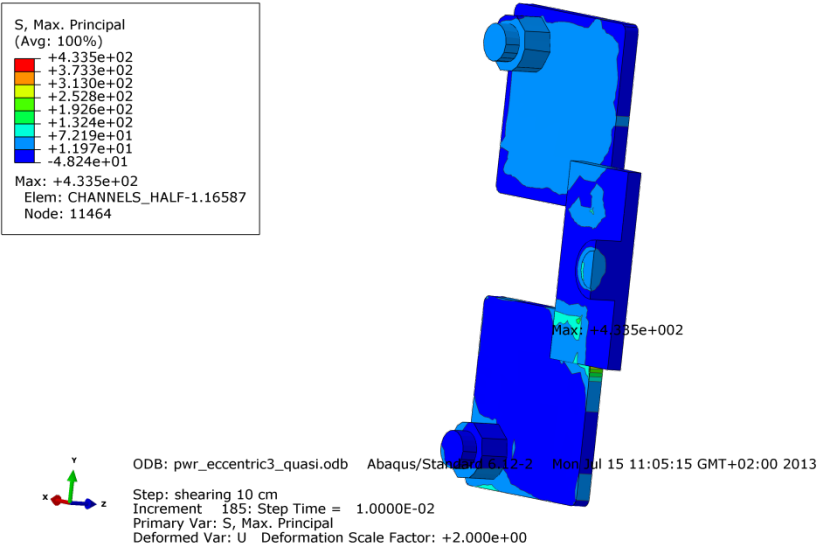


Figure A2-26 Plot showing maximum principal stress [MPa] for the steel channel tubes base plates after 10 cm shearing.

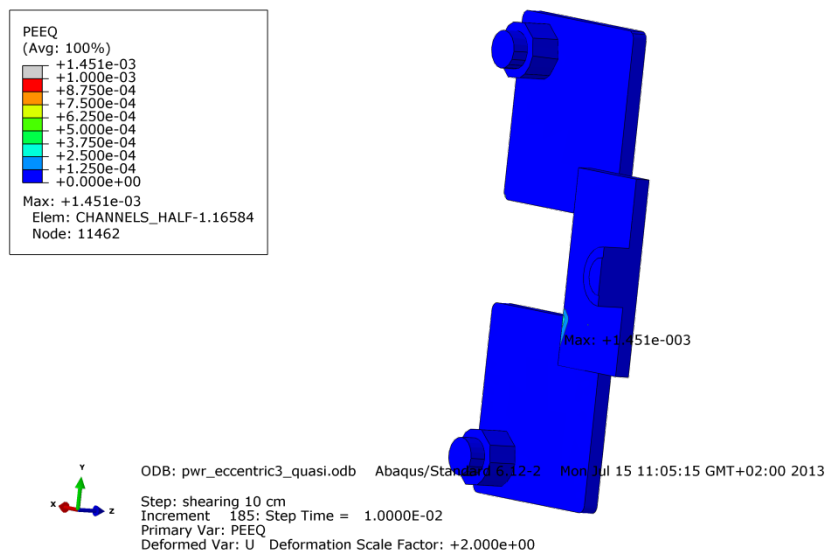


Figure A2-27 Plot showing equivalent plastic strain (PEEQ) for the steel channel tubes base plates after 10 cm shearing.

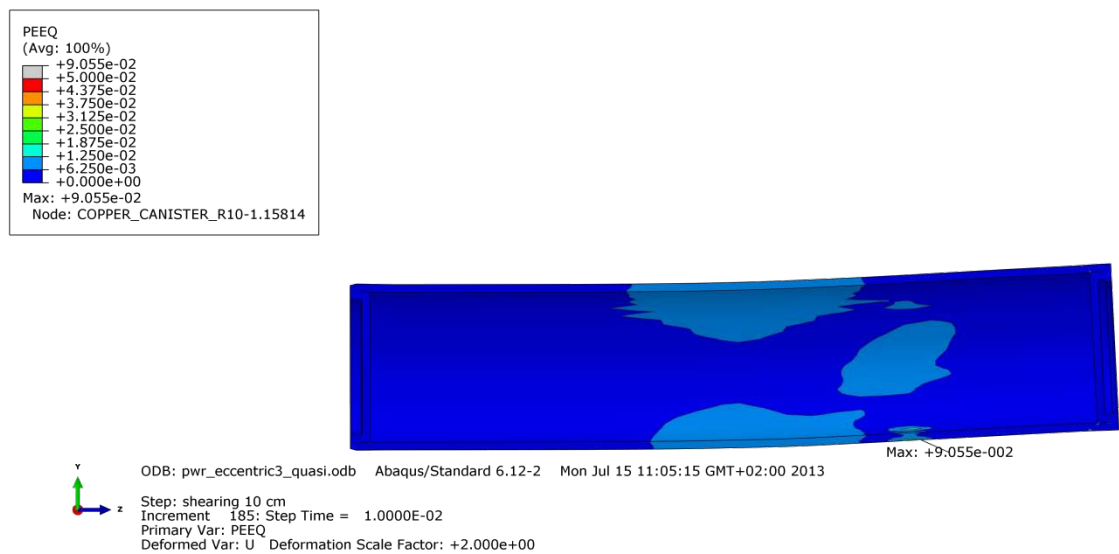


Figure A2-28 Plot showing equivalent plastic strain (PEEQ) for the copper shell after 10 cm shearing.

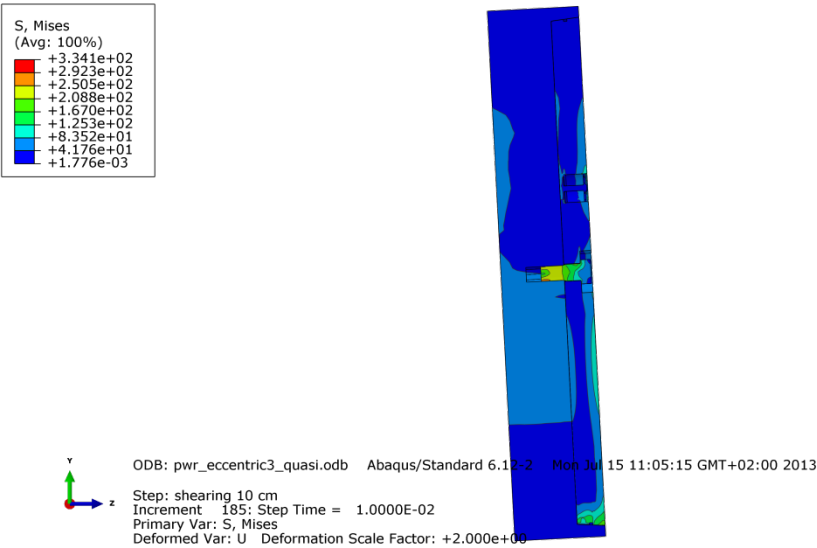


Figure A2-29 Plot showing Mises stress [MPa] close to the steel lid fixing screw after 10 cm shearing.

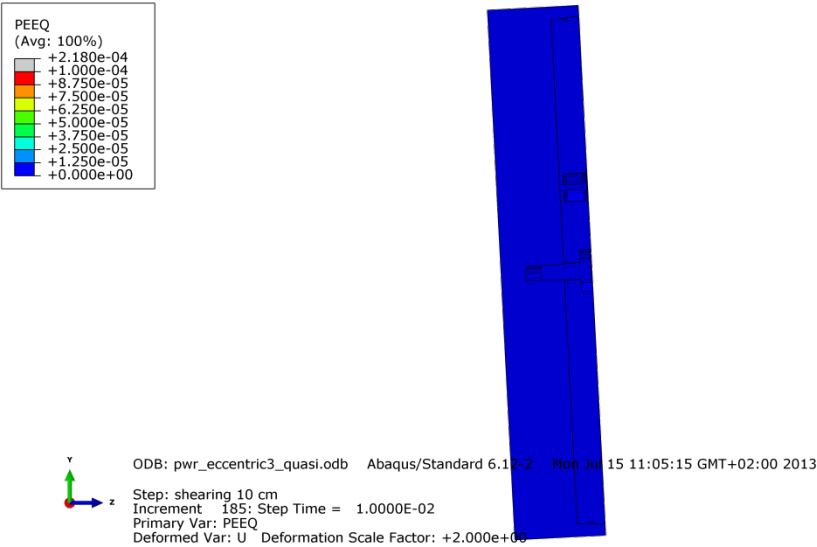


Figure A2-30 Plot showing equivalent plastic strain (PEEQ) close to the steel lid fixing screw after 10 cm shearing.

Appendix 3 – Plots for pwr_new_gap_moved2_quasi

Plots showing deformed geometry as contour plots for all parts at shearing magnitude 5 and 10 cm for case pwr_new_gap_moved2_quasi (horizontal shearing at $\frac{3}{4}$ -distance from base of the insert) when the insert is placed eccentric in respect to the copper shell and in contact at one line. The view shows the symmetry plane and all deformations are scaled by a factor of two.

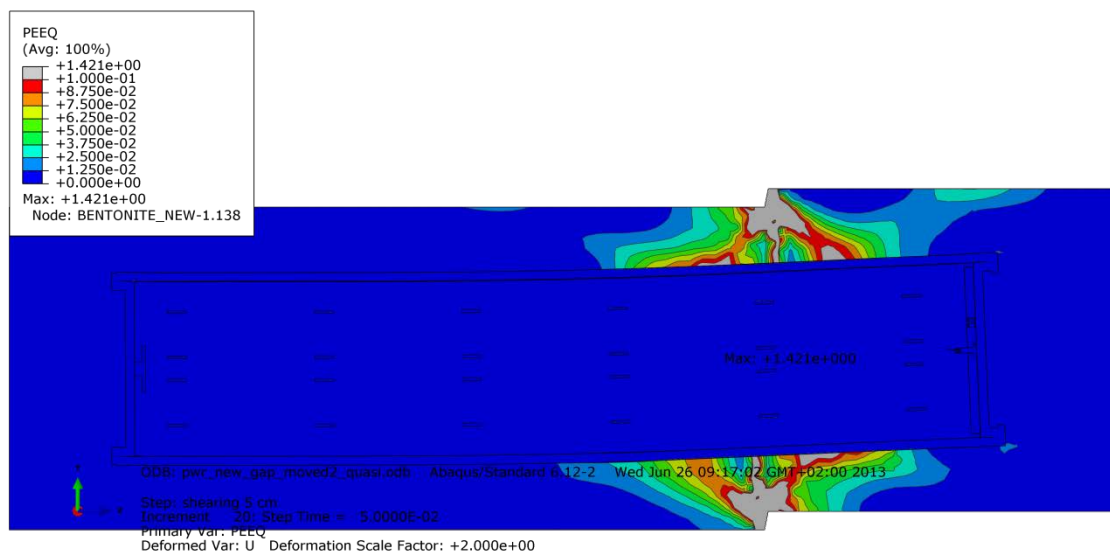


Figure A3-1 Plot showing equivalent plastic strain (PEEQ) after 5 cm shearing.

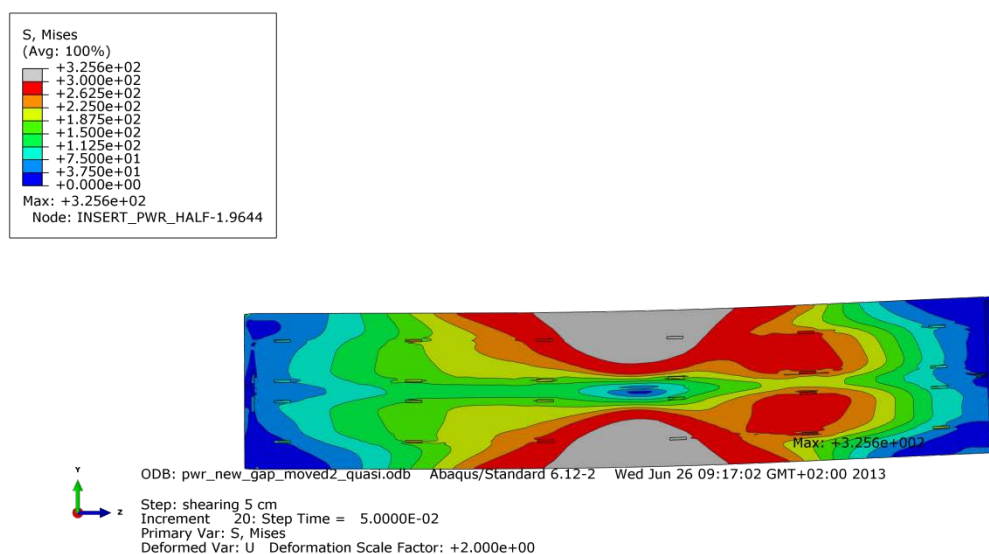


Figure A3-2 Plot showing Mises stress [MPa] for the insert after 5 cm shearing.

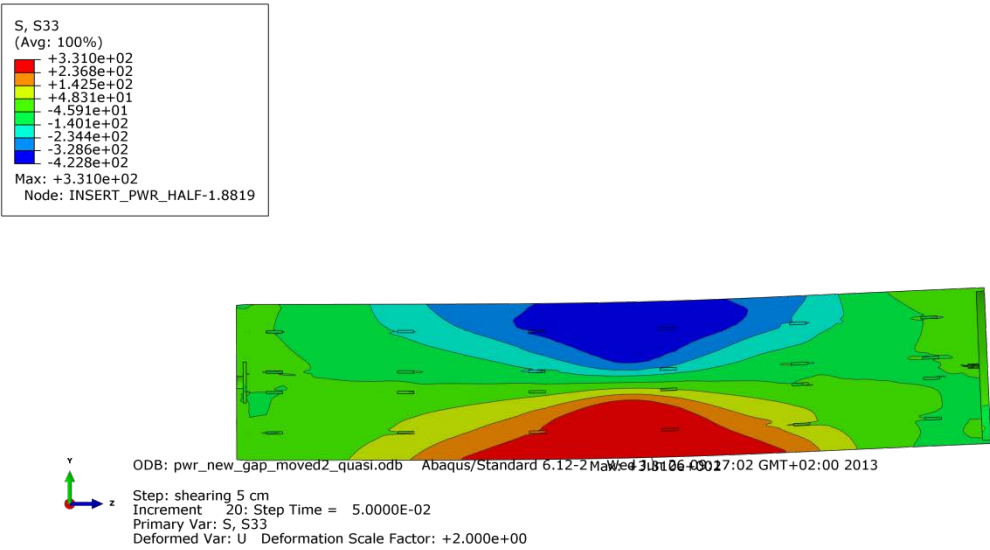


Figure A3-3 Plot showing axial stress [MPa] for the insert after 5 cm shearing.

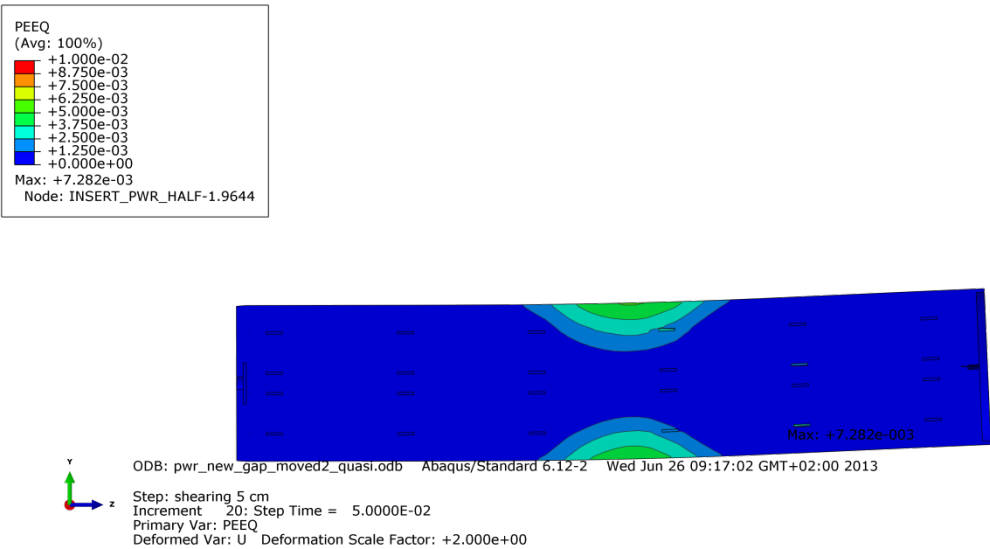


Figure A3-4 Plot showing equivalent plastic strain (PEEQ) for the insert after 5 cm shearing.

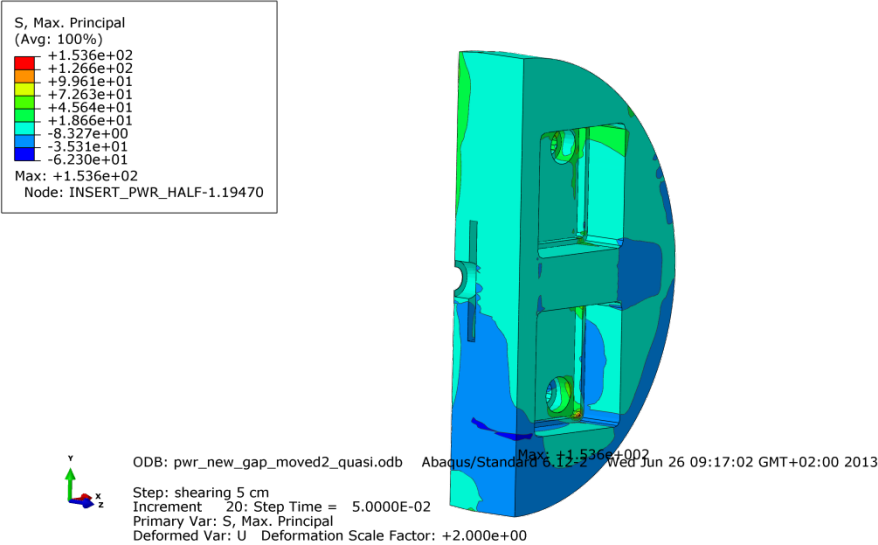


Figure A3-5 Plot showing maximum principal stress [MPa] for the insert base after 5 cm shearing.

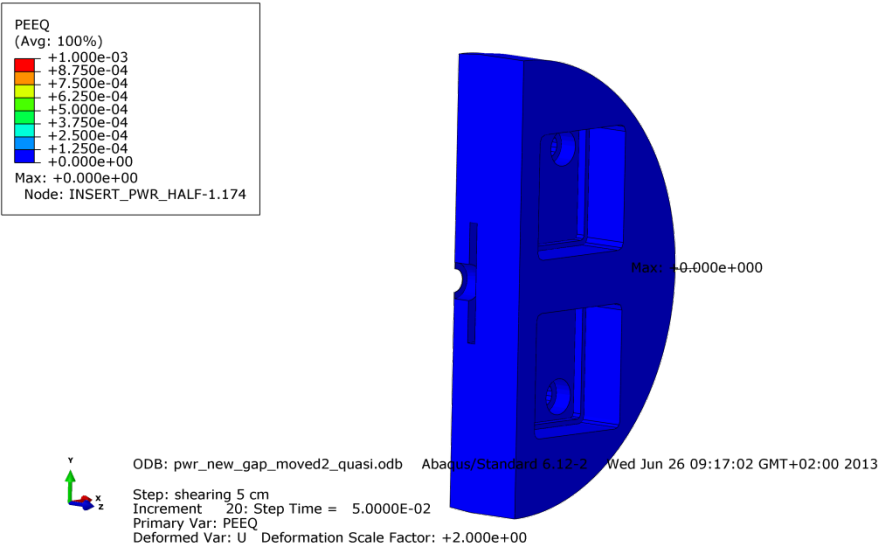


Figure A3-6 Plot showing equivalent plastic strain (PEEQ) for the insert base after 5 cm shearing.

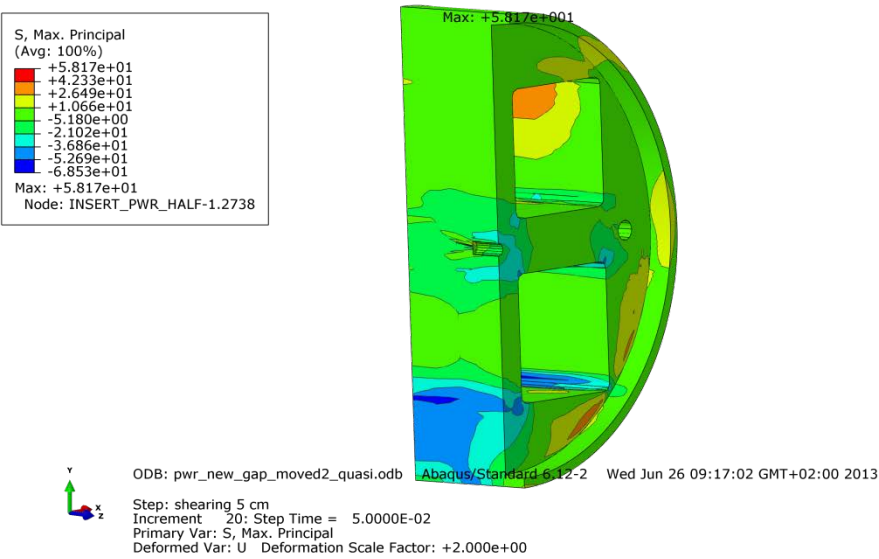


Figure A3-7 Plot showing maximum principal stress [MPa] for the insert top after 5 cm shearing.

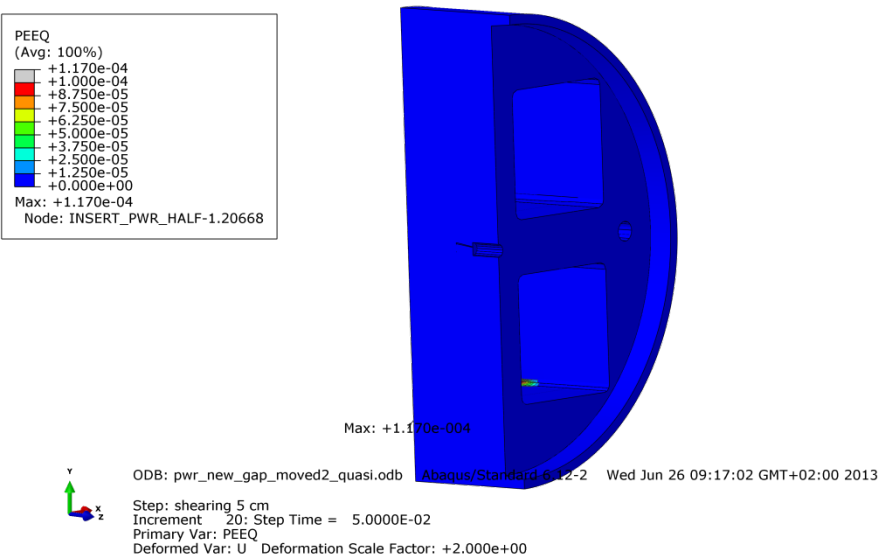


Figure A3-8 Plot showing equivalent plastic strain (PEEQ) for the insert top after 5 cm shearing.

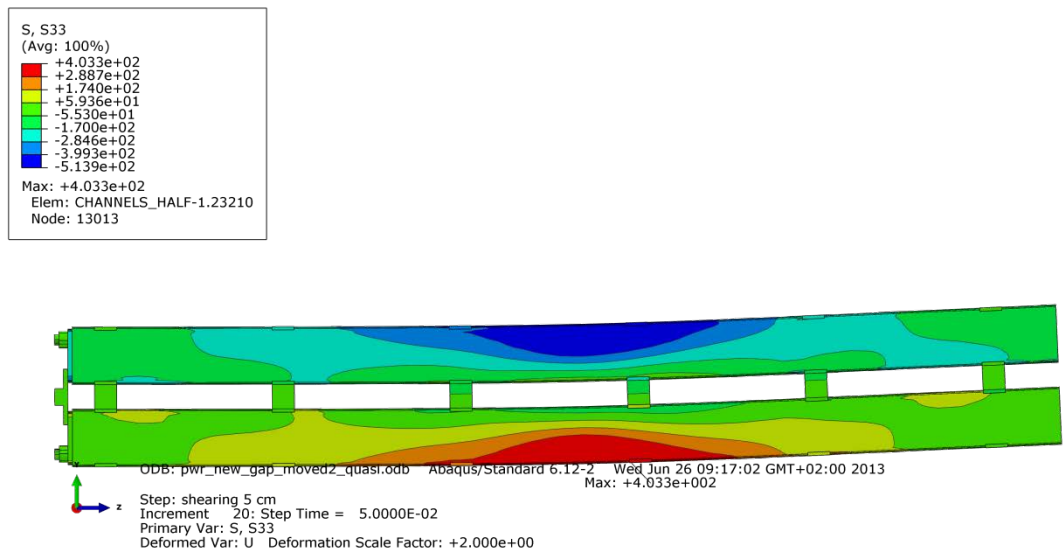


Figure A3-9 Plot showing axial stress [MPa] for the steel channel tubes after 5 cm shearing.

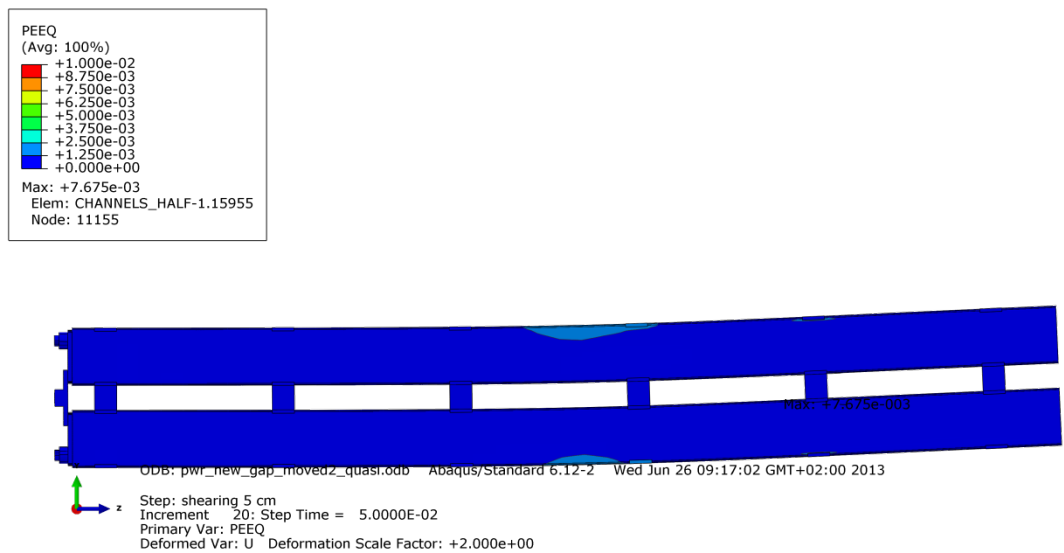


Figure A3-10 Plot showing equivalent plastic strain (PEEQ) for the steel channel tubes after 5 cm shearing.

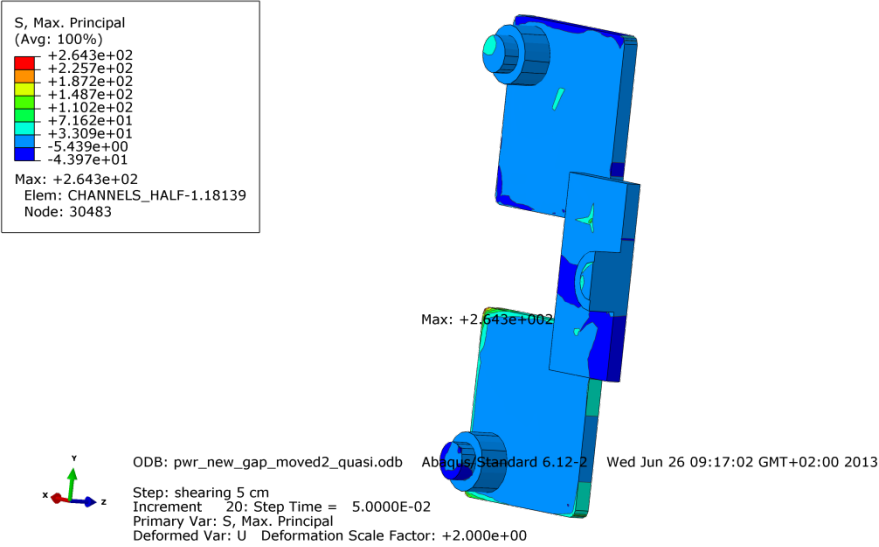


Figure A3-11 Plot showing maximum principal stress [MPa] for the steel channel tubes base plates after 5 cm shearing.

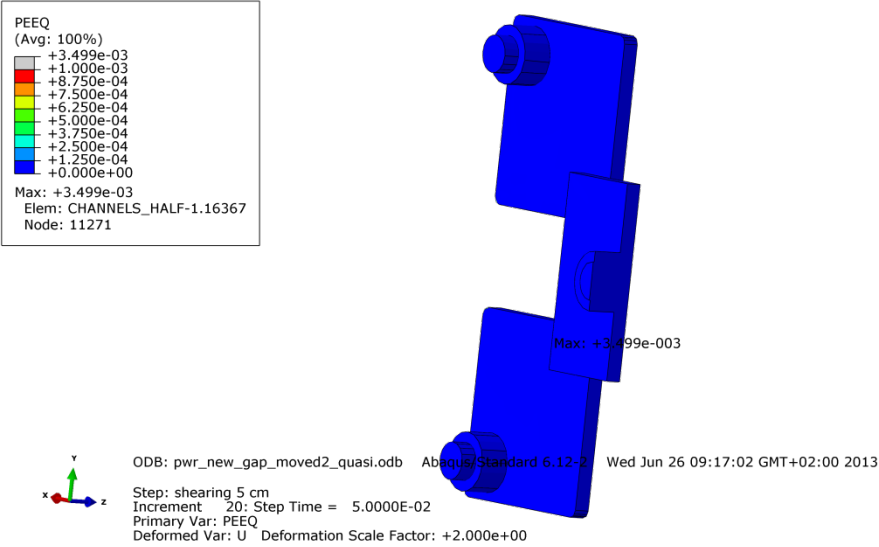


Figure A3-12 Plot showing equivalent plastic strain (PEEQ) for the steel channel tubes base plates after 5 cm shearing.

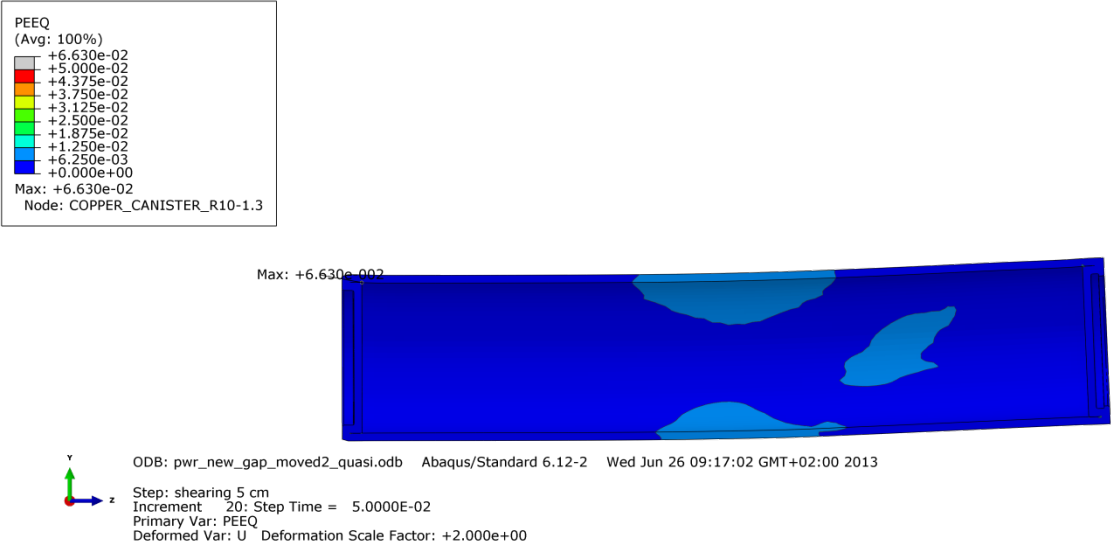


Figure A3-13 Plot showing equivalent plastic strain (PEEQ) for the copper shell after 5 cm shearing.

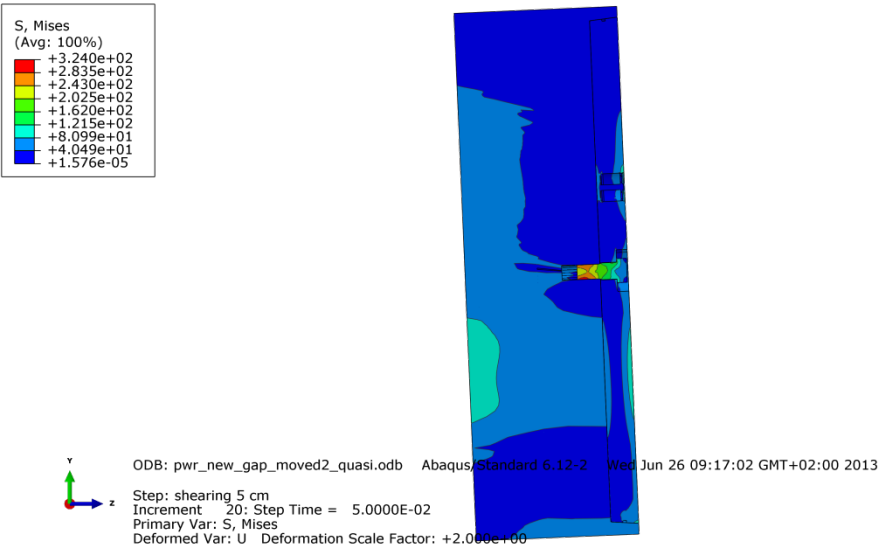


Figure A3-14 Plot showing Mises stress [MPa] close to the steel lid fixing screw after 5 cm shearing.

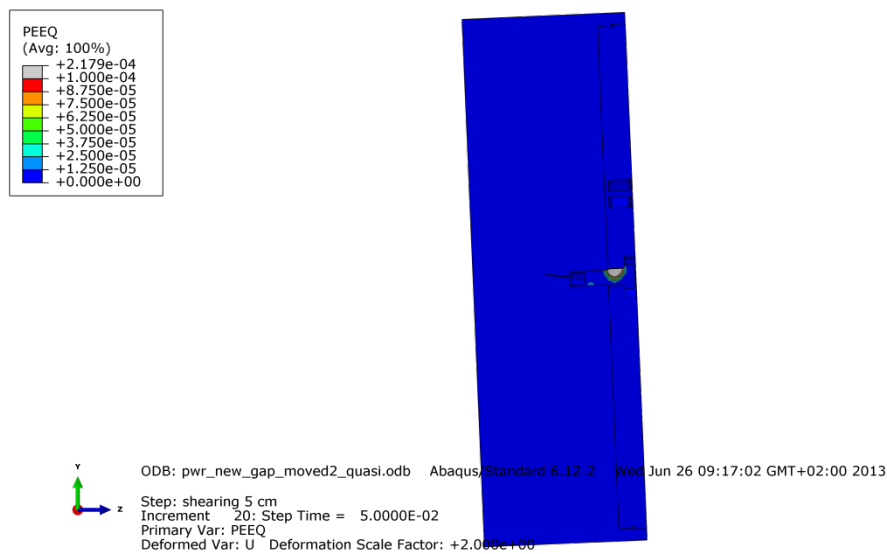


Figure A3-15 Plot showing equivalent plastic strain (PEEQ) close to the steel lid fixing screw after 5 cm shearing.

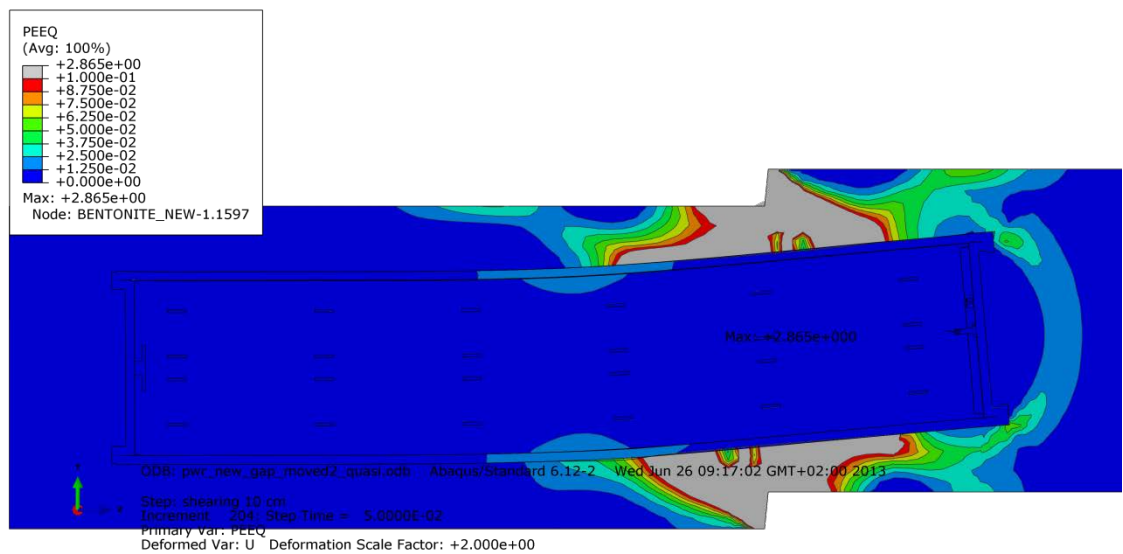


Figure A3-16 Plot showing equivalent plastic strain (PEEQ) after 10 cm shearing.

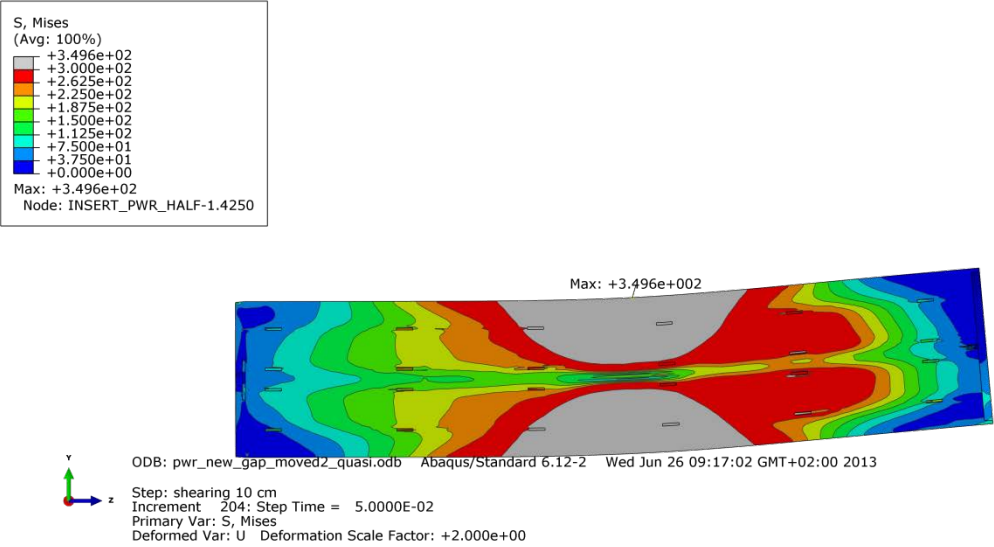


Figure A3-17 Plot showing Mises stress [MPa] for the insert after 10 cm shearing.

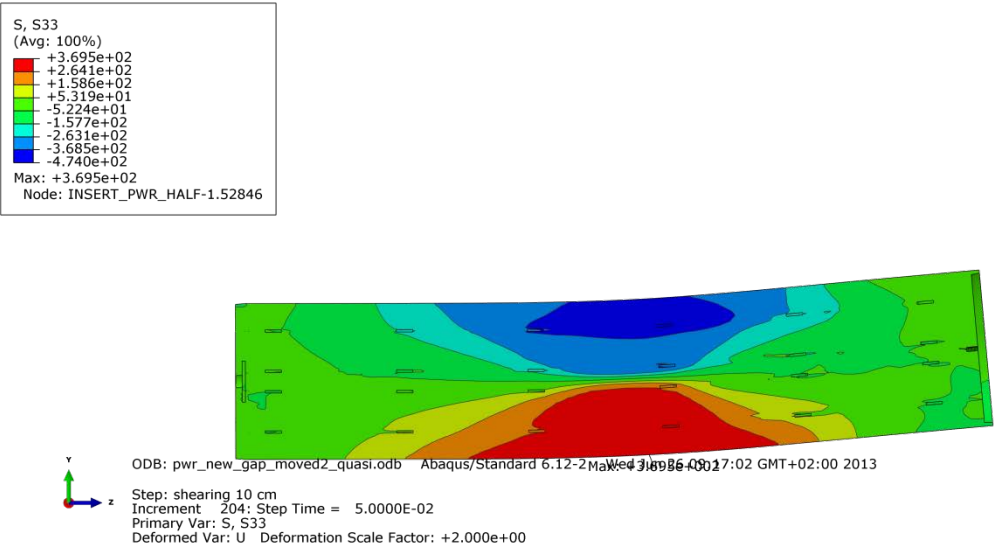


Figure A3-18 Plot showing axial stress [MPa] for the insert after 10 cm shearing.

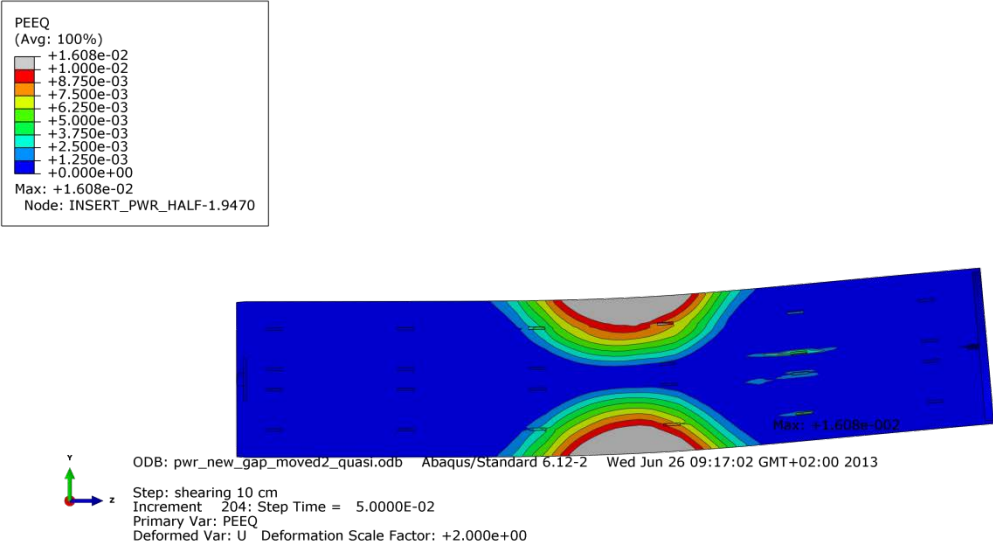


Figure A3-19 Plot showing equivalent plastic strain (PEEQ) for the insert after 10 cm shearing.

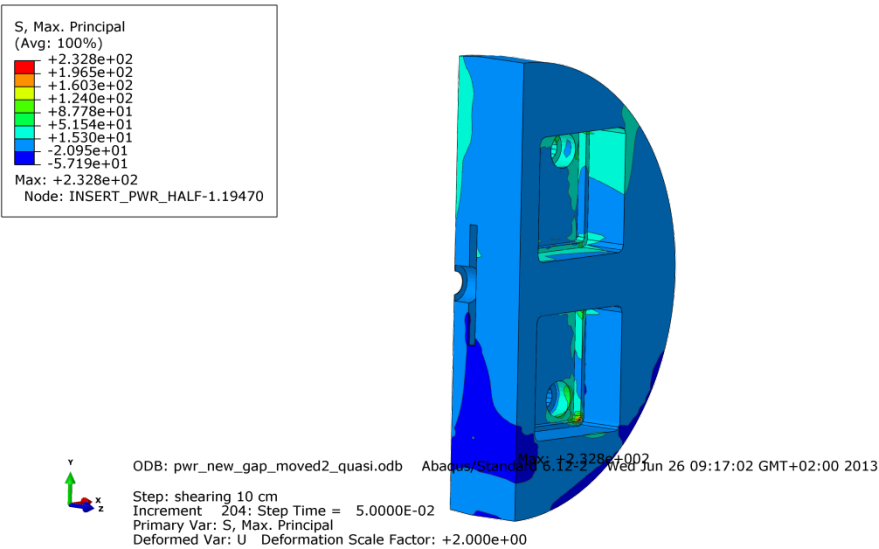


Figure A3-20 Plot showing maximum principal stress [MPa] for the insert base after 10 cm shearing.

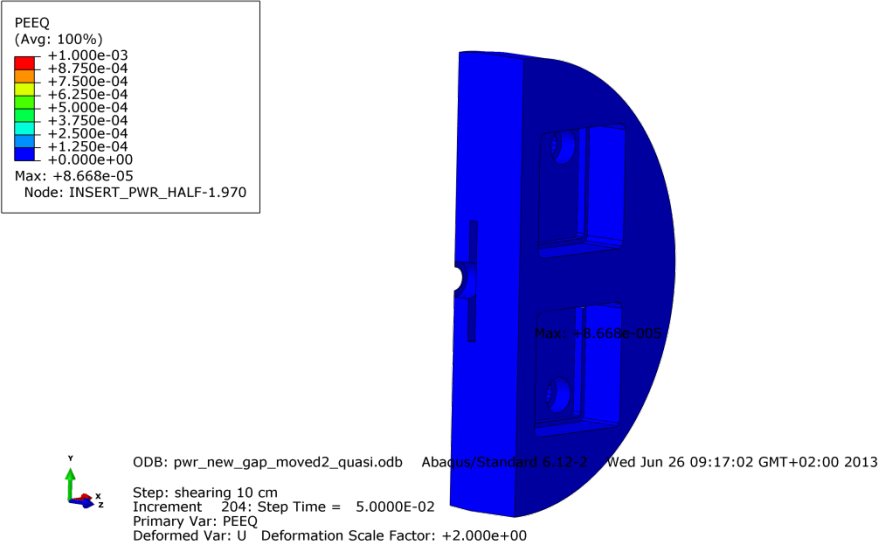


Figure A3-21 Plot showing equivalent plastic strain (PEEQ) for the insert base after 10 cm shearing.

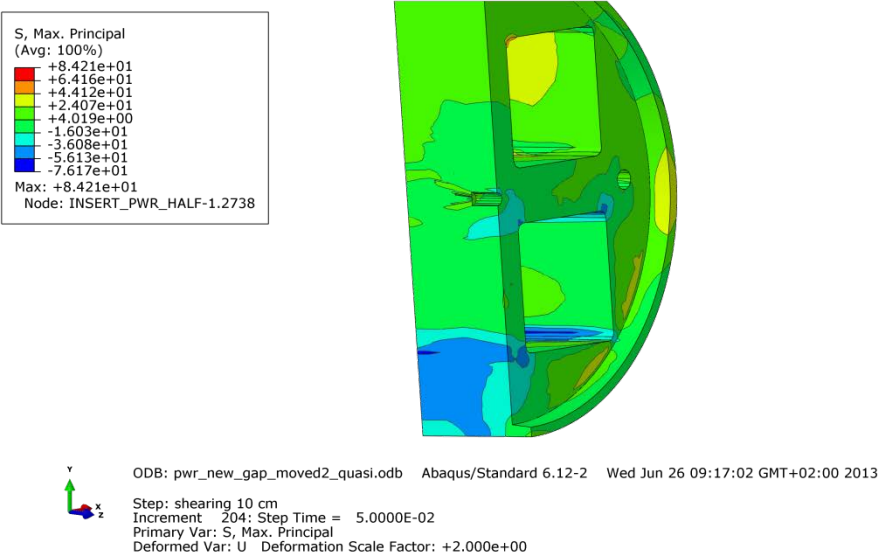


Figure A3-22 Plot showing maximum principal stress [MPa] for the insert top after 10 cm shearing.

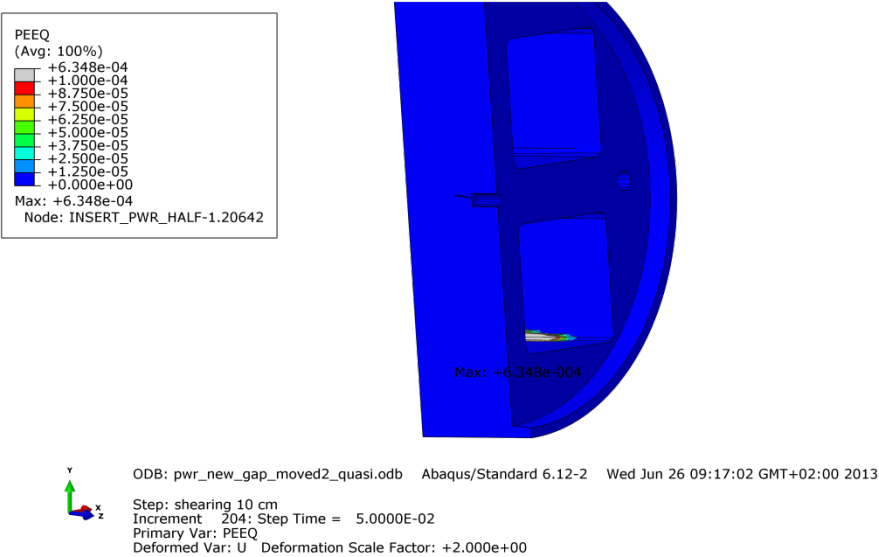


Figure A3-23 Plot showing equivalent plastic strain (PEEQ) for the insert top after 10 cm shearing.

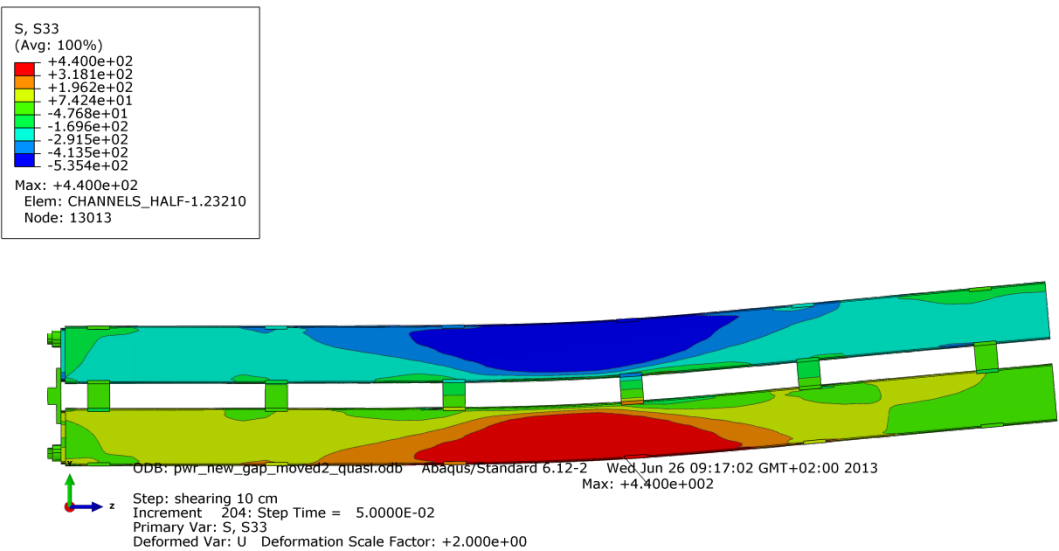


Figure A3-24 Plot showing axial stress [MPa] for the steel channel tubes after 10 cm shearing.

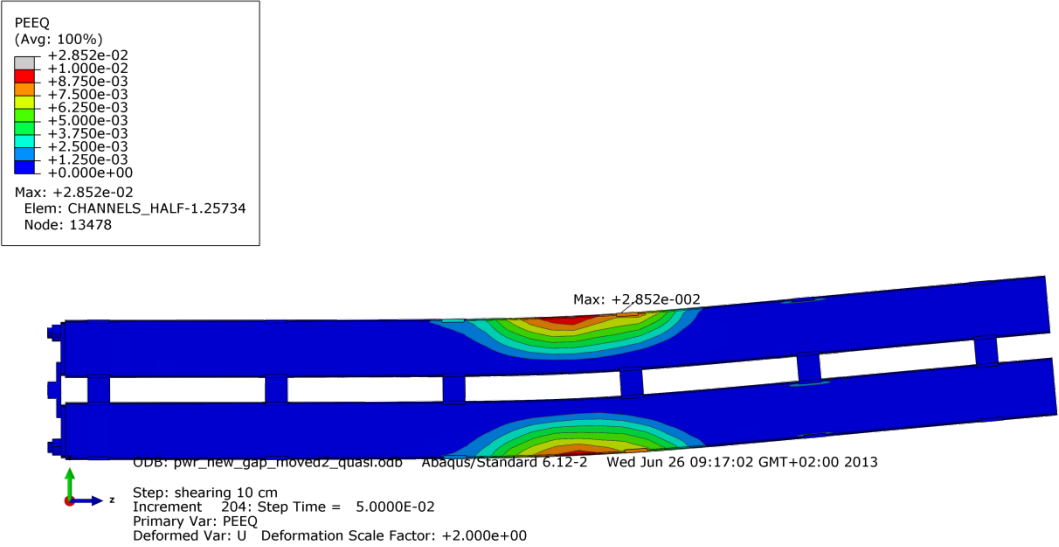


Figure A3-25 Plot showing equivalent plastic strain (PEEQ) for the steel channel tubes after 10 cm shearing.

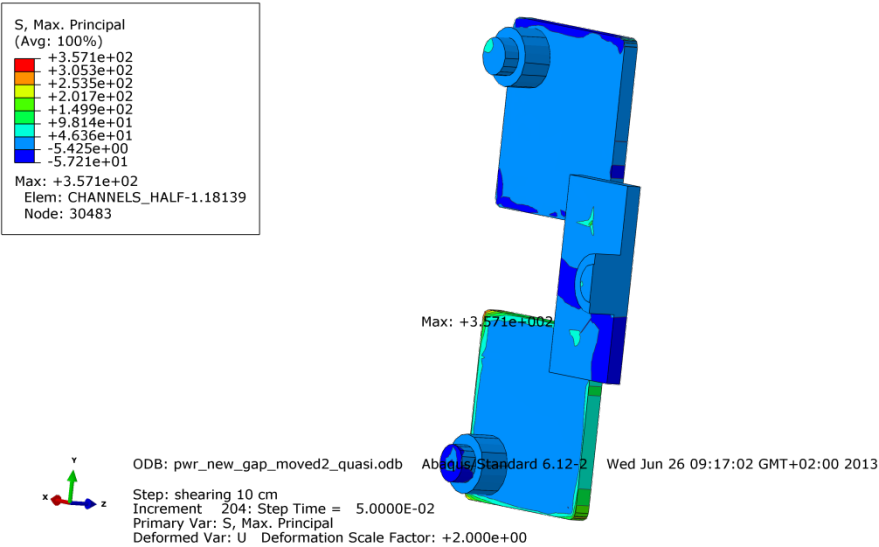


Figure A3-26 Plot showing maximum principal stress [MPa] for the steel channel tubes base plates after 10 cm shearing.

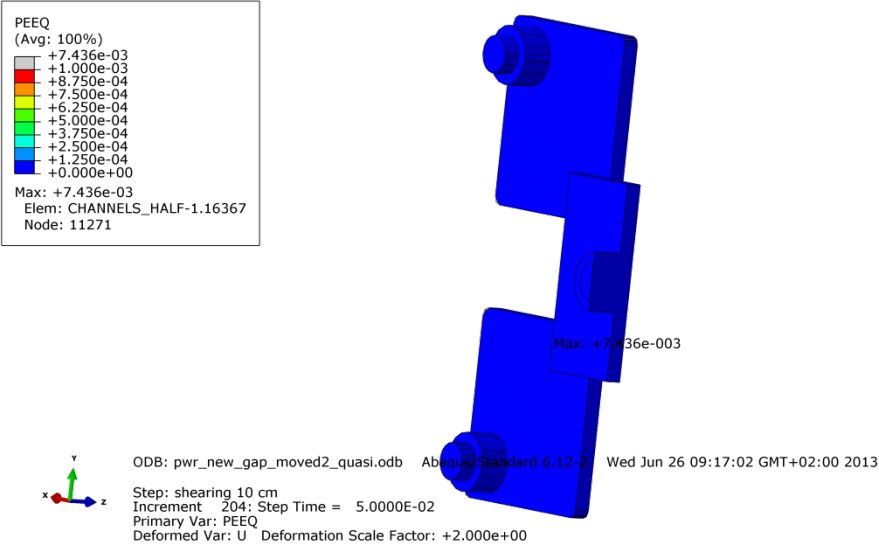


Figure A3-27 Plot showing equivalent plastic strain (PEEQ) for the steel channel tubes base plates after 10 cm shearing.

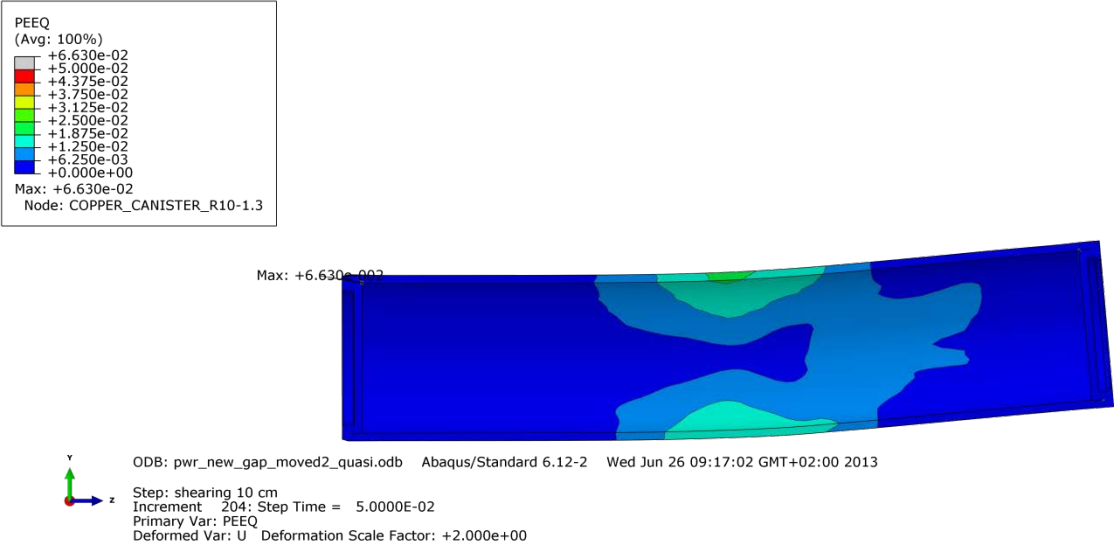


Figure A3-28 Plot showing equivalent plastic strain (PEEQ) for the copper shell after 10 cm shearing.

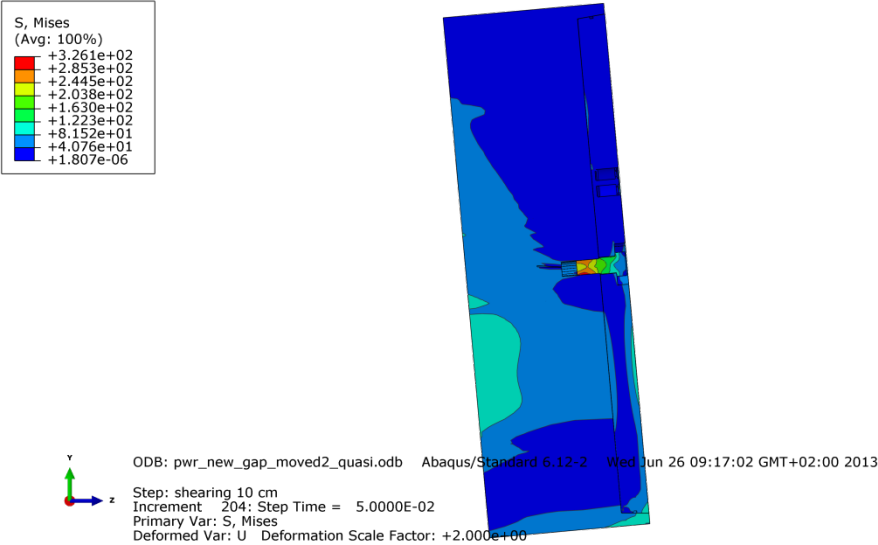


Figure A3-29 Plot showing Mises stress [MPa] close to the steel lid fixing screw after 10 cm shearing.

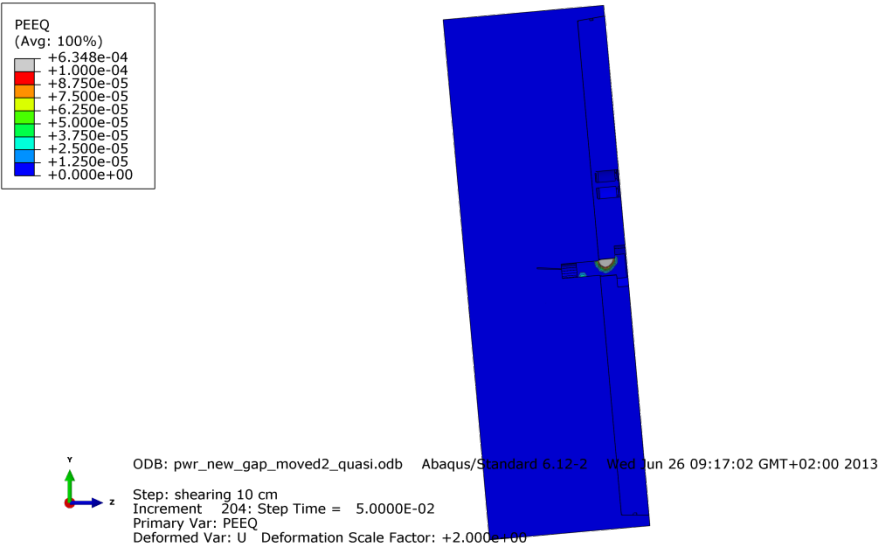


Figure A3-30 Plot showing equivalent plastic strain (PEEQ) close to the steel lid fixing screw after 10 cm shearing.

Appendix 4 – Plots for pwr_new_lock_quasi

Plots show deformed geometry as contour plots for all parts at shearing magnitude 5 and 8 cm for case pwr_new_lock_quasi (horizontal shearing at the steel lid) using pre-stress in the screw corresponding to yield stress. The view shows the symmetry plane and all deformations are scaled by a factor of two. Note! The analysis failed to complete 10 cm shearing.

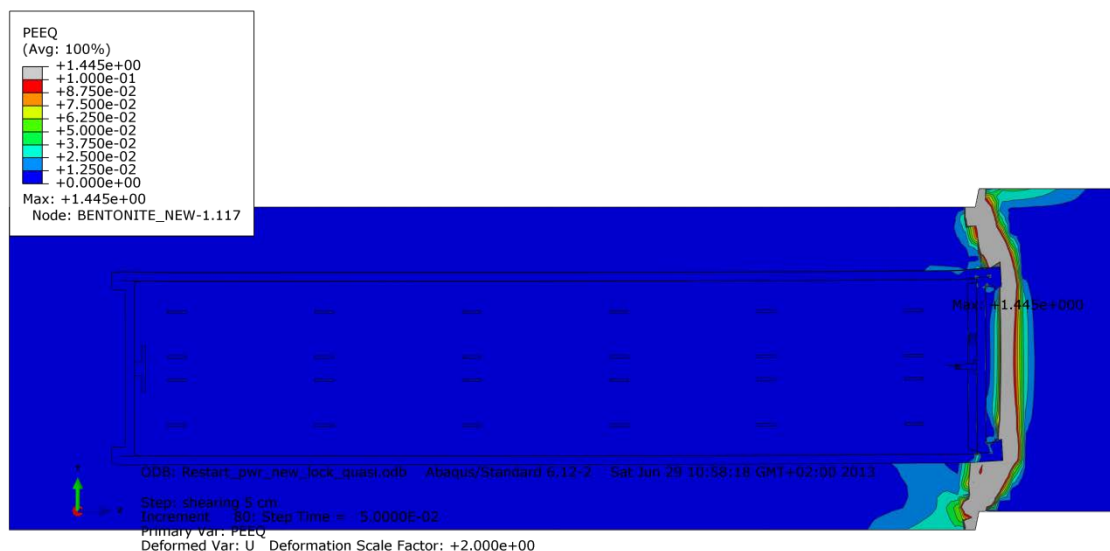


Figure A4-1 Plot showing equivalent plastic strain (PEEQ) after 5 cm shearing.

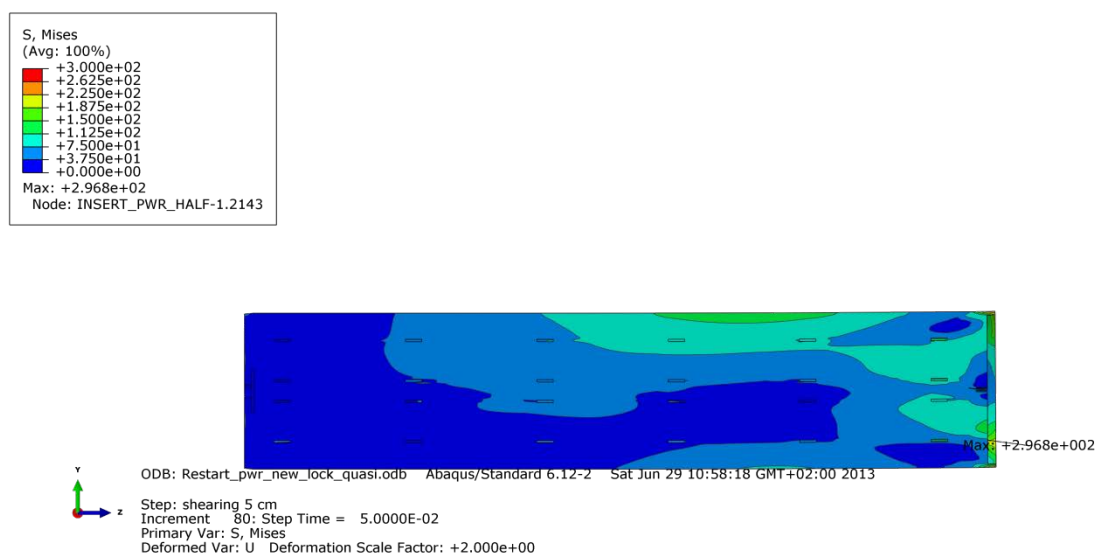


Figure A4-2 Plot showing Mises stress [MPa] for the insert after 5 cm shearing.

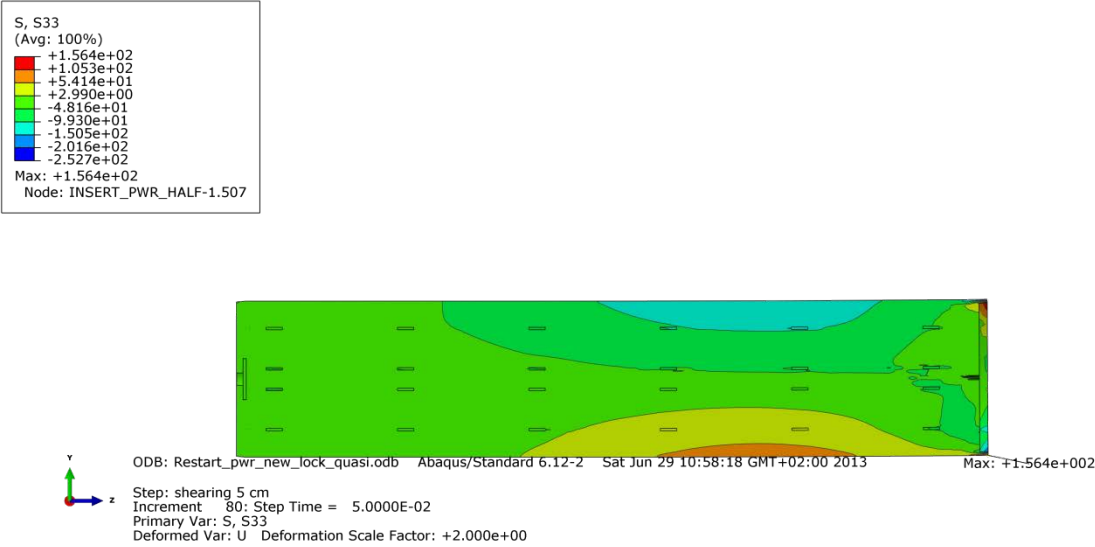


Figure A4-3 Plot showing axial stress [MPa] for the insert after 5 cm shearing.

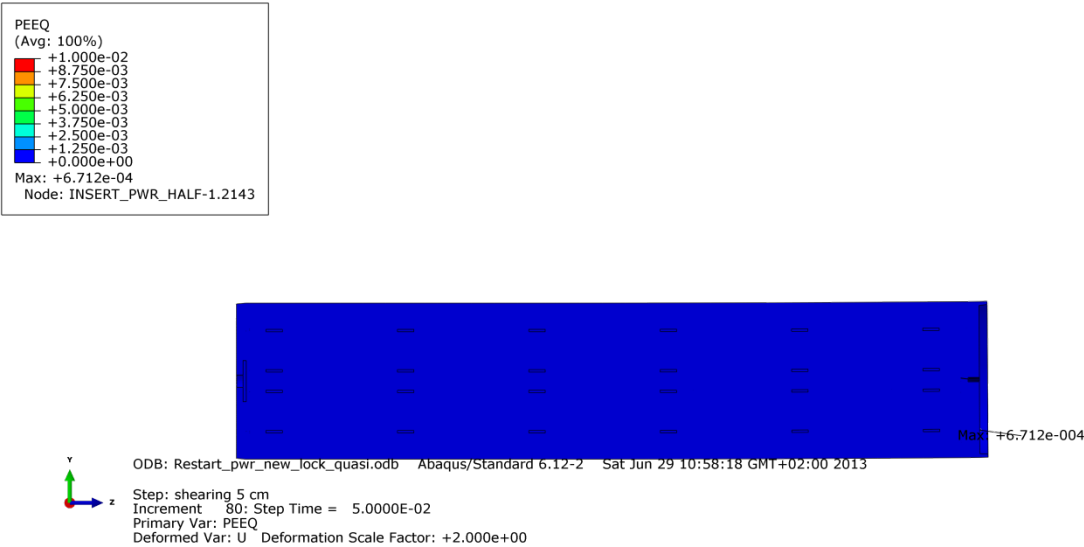


Figure A4-4 Plot showing equivalent plastic strain (PEEQ) for the insert after 5 cm shearing.

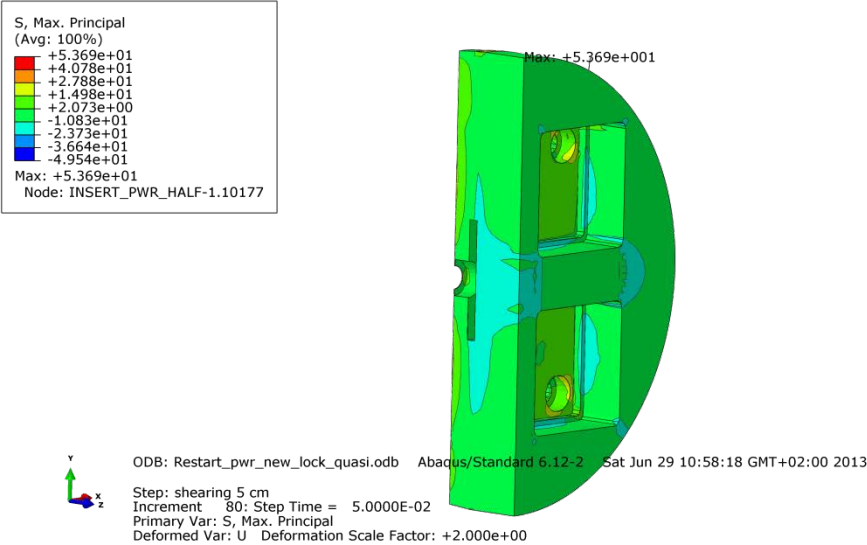


Figure A4-5 Plot showing maximum principal stress [MPa] for the insert base after 5 cm shearing.

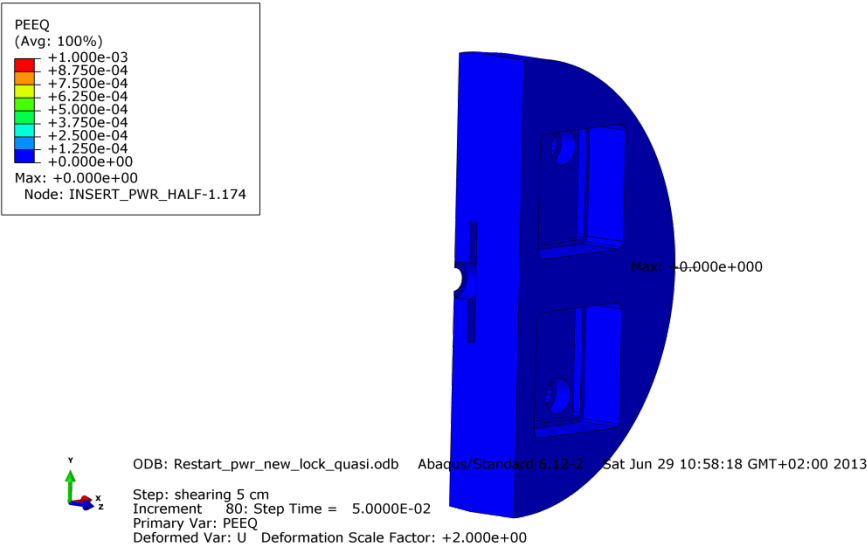


Figure A4-6 Plot showing equivalent plastic strain (PEEQ) for the insert base after 5 cm shearing.

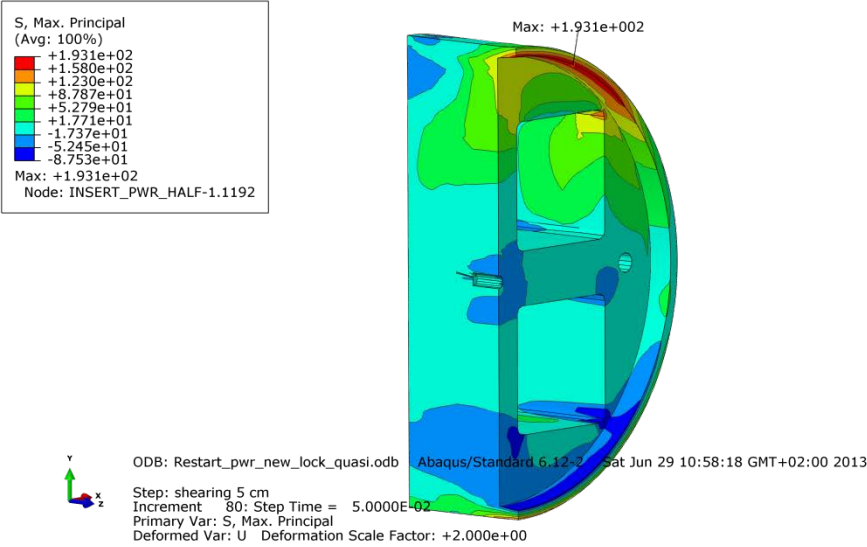


Figure A4-7 Plot showing maximum principal stress [MPa] for the insert top after 5 cm shearing.

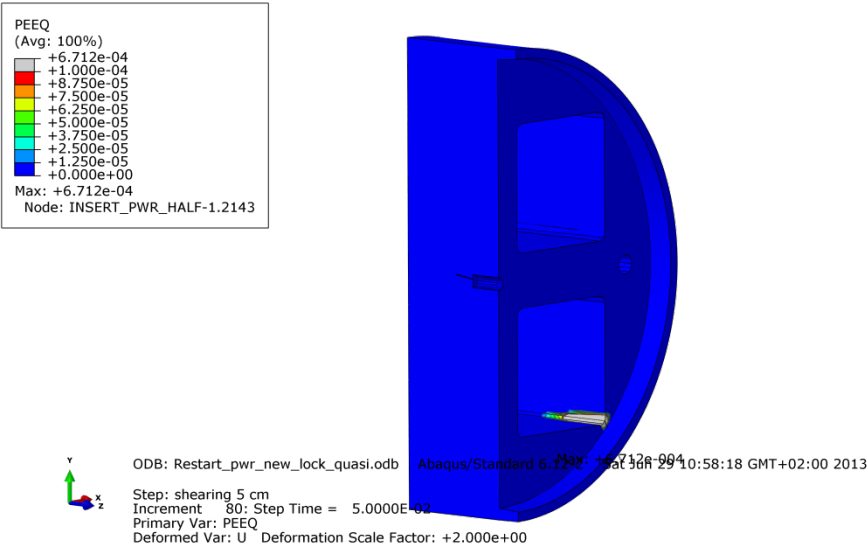


Figure A4-8 Plot showing equivalent plastic strain (PEEQ) for the insert top after 5 cm shearing.

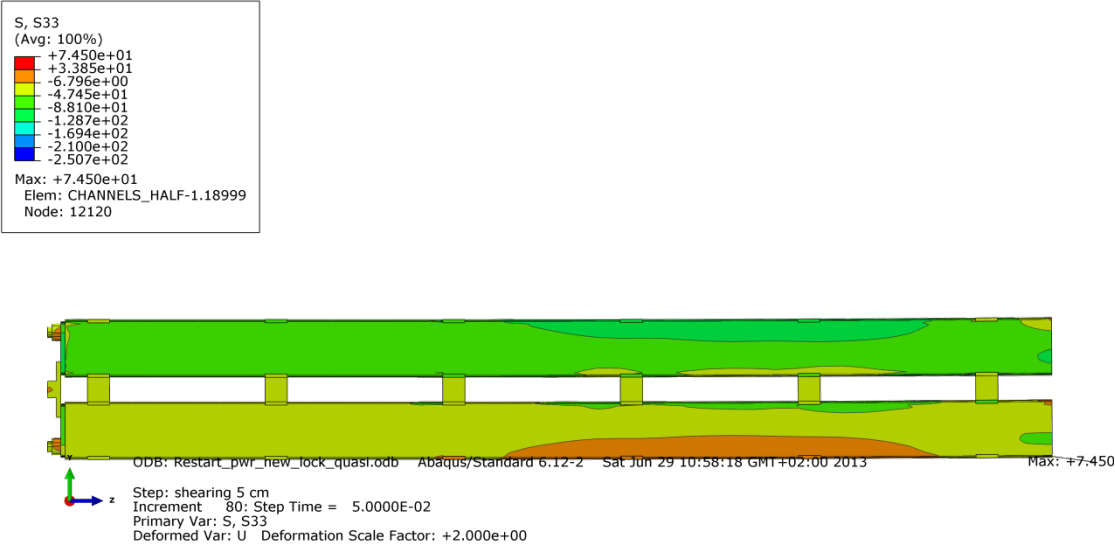


Figure A4-9 Plot showing axial stress [MPa] for the steel channel tubes after 5 cm shearing.

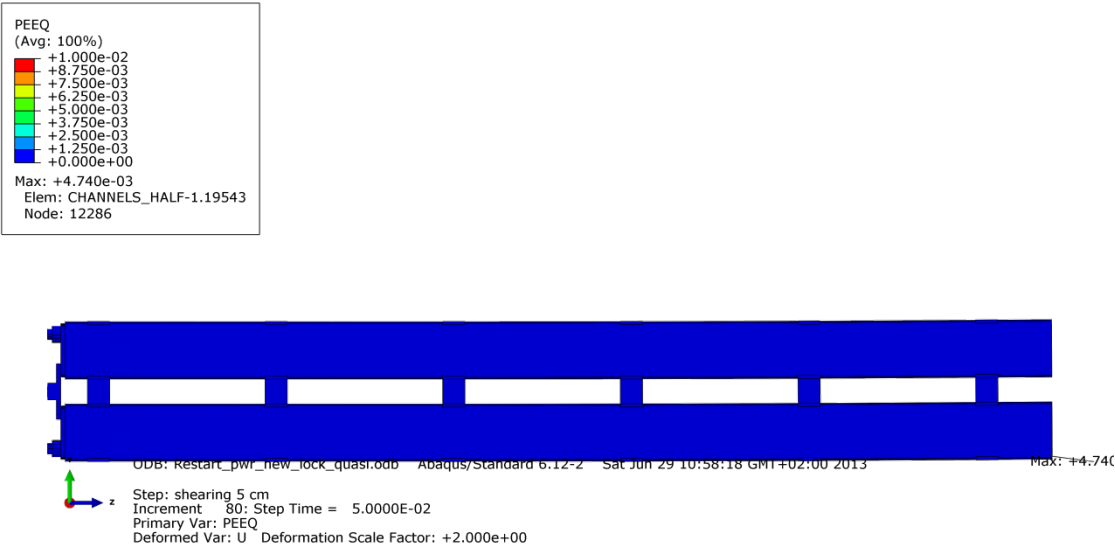


Figure A4-10 Plot showing equivalent plastic strain (PEEQ) for the steel channel tubes after 5 cm shearing.

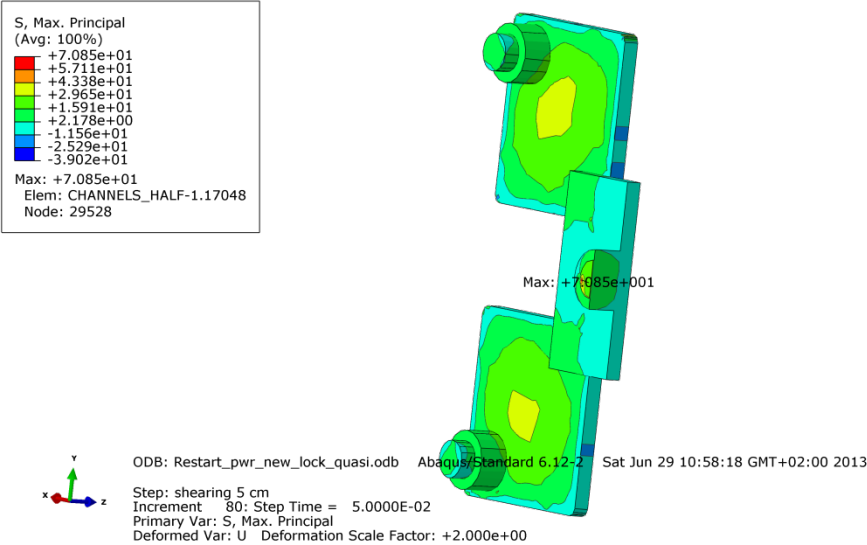


Figure A4-11 Plot showing maximum principal stress [MPa] for the steel channel tubes base plates after 5 cm shearing.

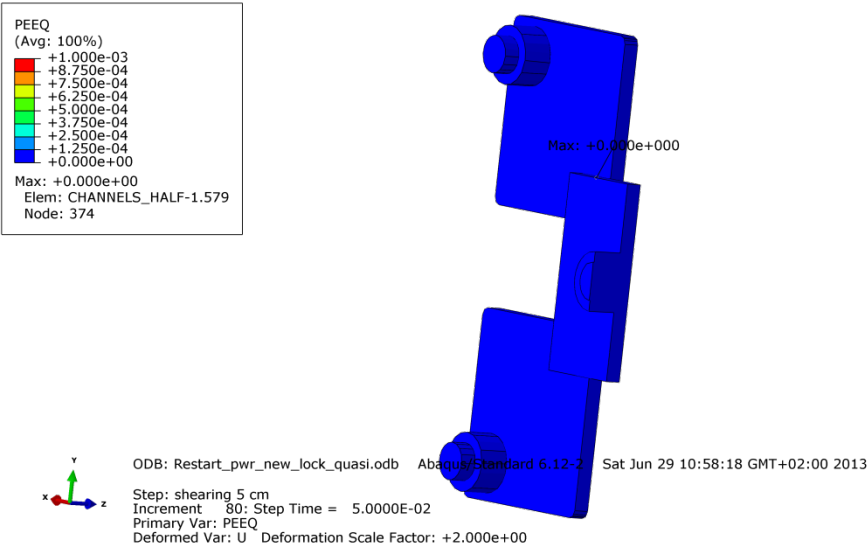


Figure A4-12 Plot showing equivalent plastic strain (PEEQ) for the steel channel tubes base plates after 5 cm shearing.

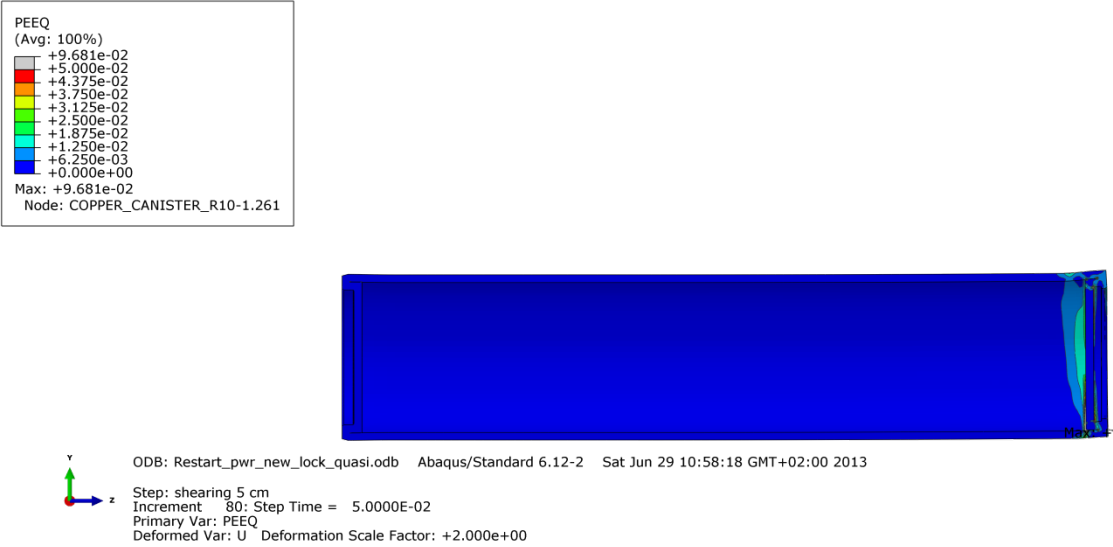


Figure A4-13 Plot showing equivalent plastic strain (PEEQ) for the copper shell after 5 cm shearing.

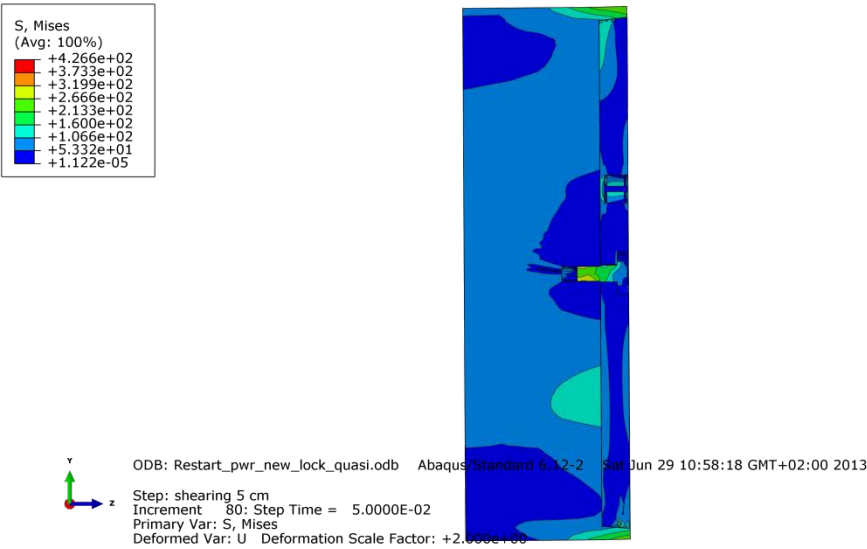


Figure A4-14 Plot showing Mises stress [MPa] close to the steel lid fixing screw after 5 cm shearing.

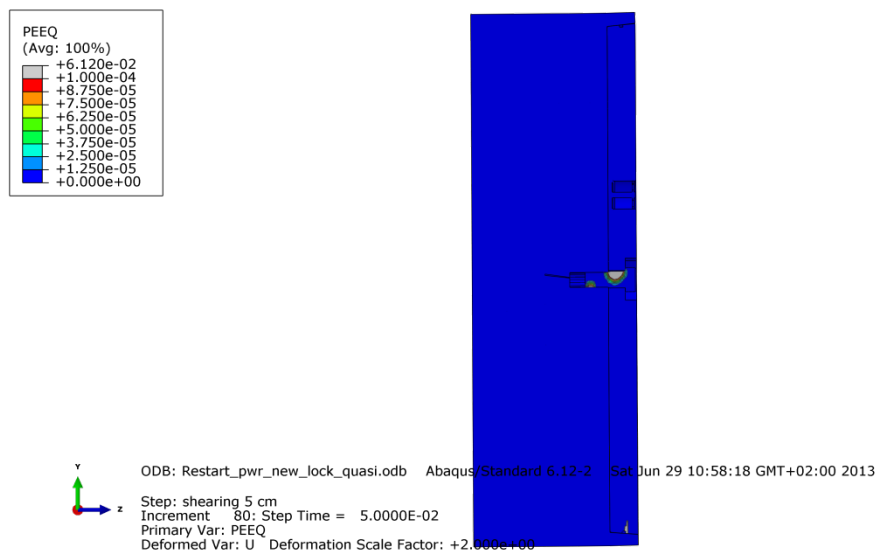


Figure A4-15 Plot showing equivalent plastic strain (PEEQ) close to the steel lid fixing screw after 5 cm shearing.

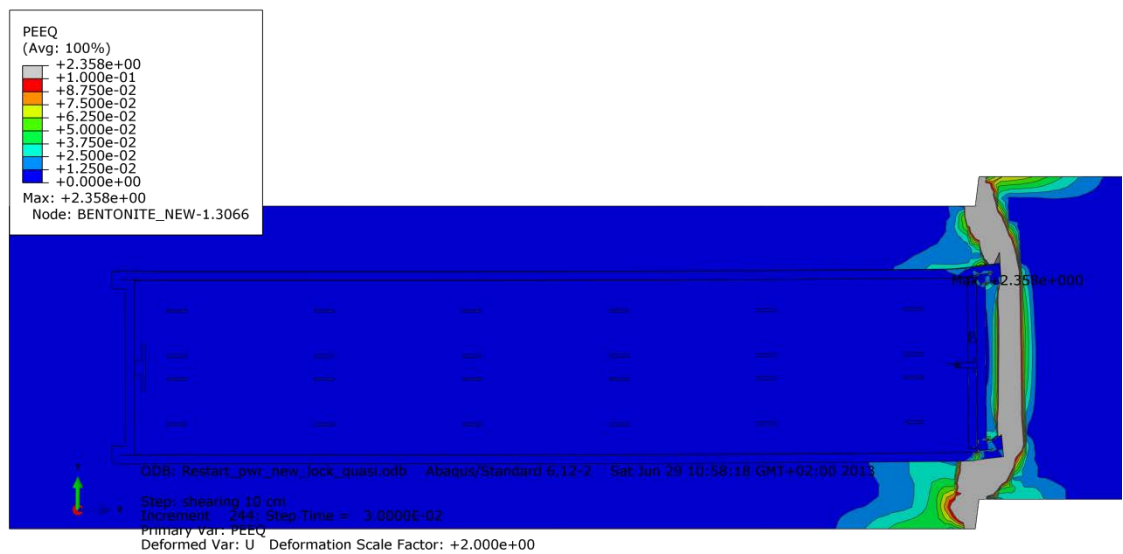


Figure A4-16 Plot showing equivalent plastic strain (PEEQ) after 8 cm shearing.

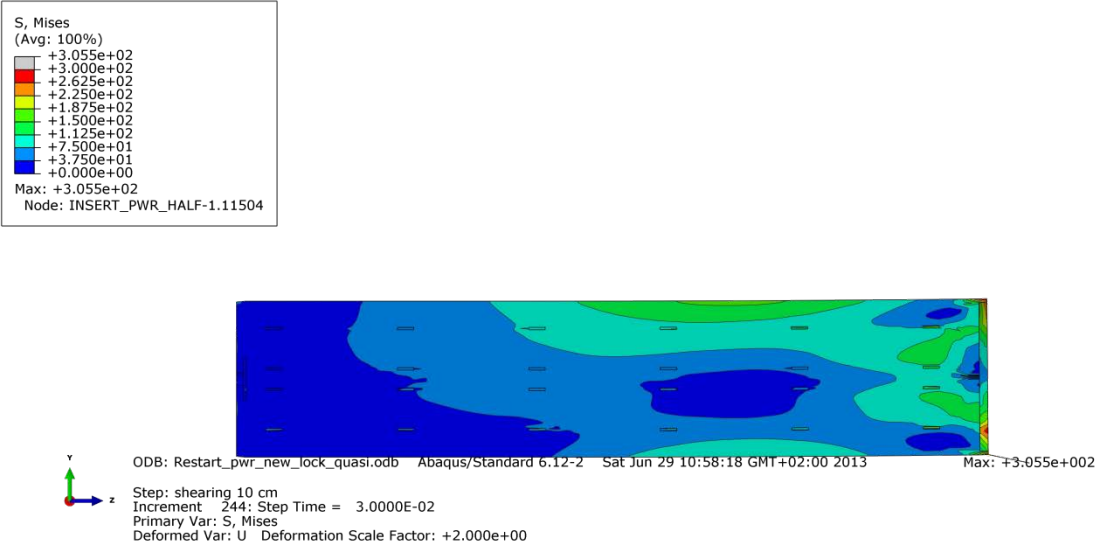


Figure A4-17 Plot showing Mises stress [MPa] for the insert after 8 cm shearing.

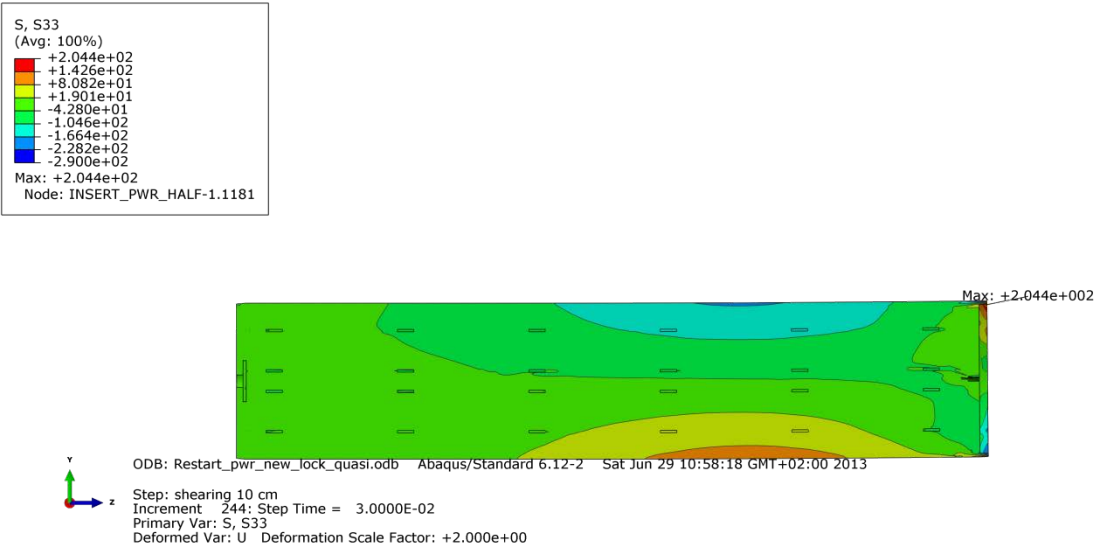


Figure A4-18 Plot showing axial stress [MPa] for the insert after 8 cm shearing.

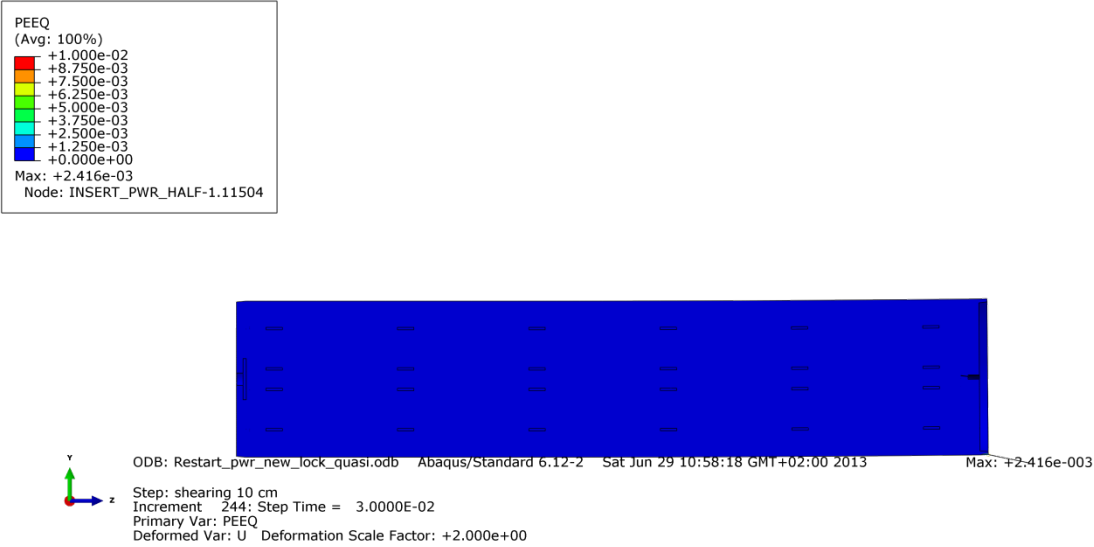


Figure A4-19 Plot showing equivalent plastic strain (PEEQ) for the insert after 8 cm shearing.

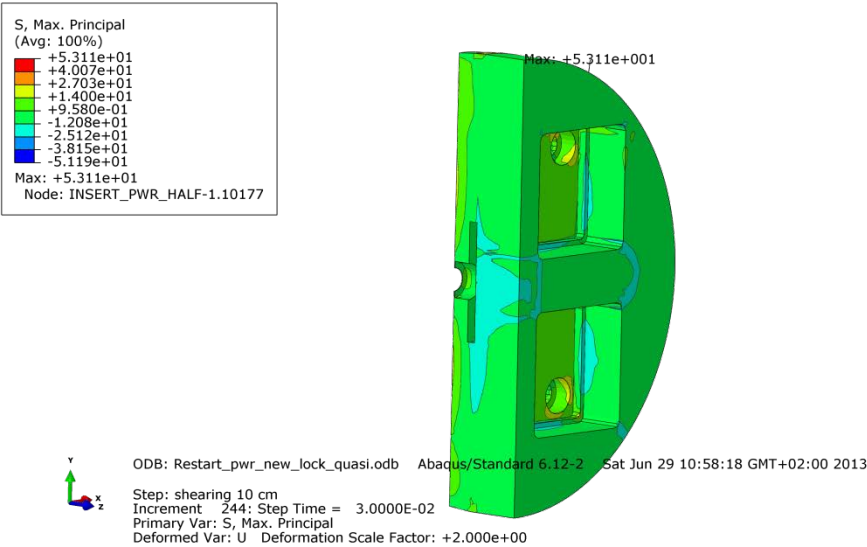


Figure A4-20 Plot showing maximum principal stress [MPa] for the insert base after 8 cm shearing.

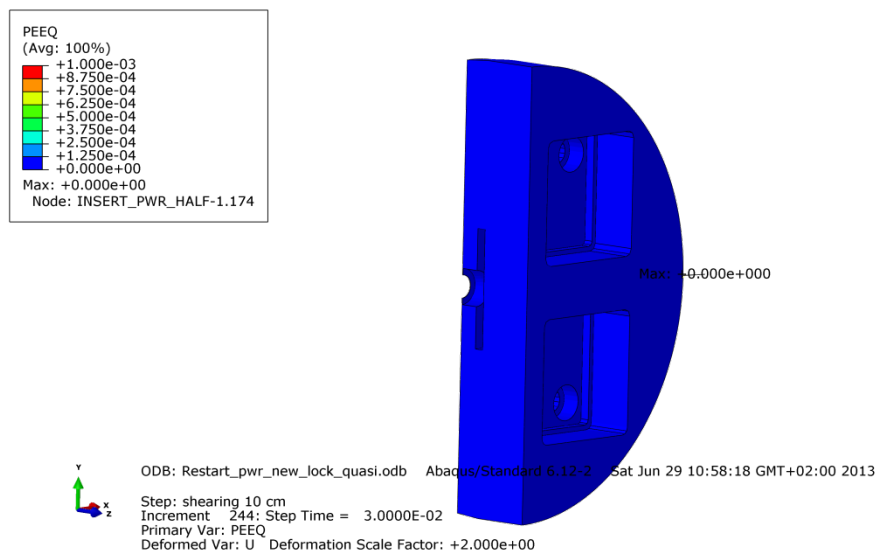


Figure A4-21 Plot showing equivalent plastic strain (PEEQ) for the insert base after 8 cm shearing.

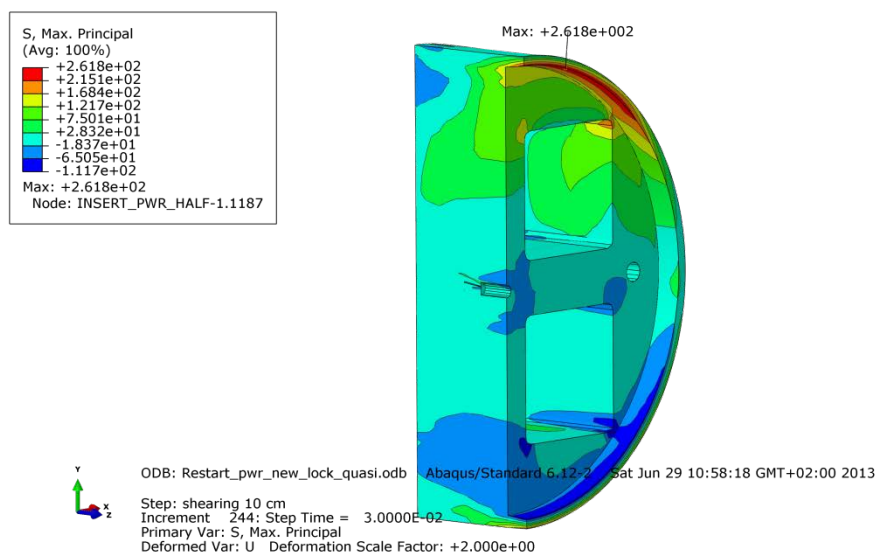


Figure A4-22 Plot showing maximum principal stress [MPa] for the insert top after 8 cm shearing.

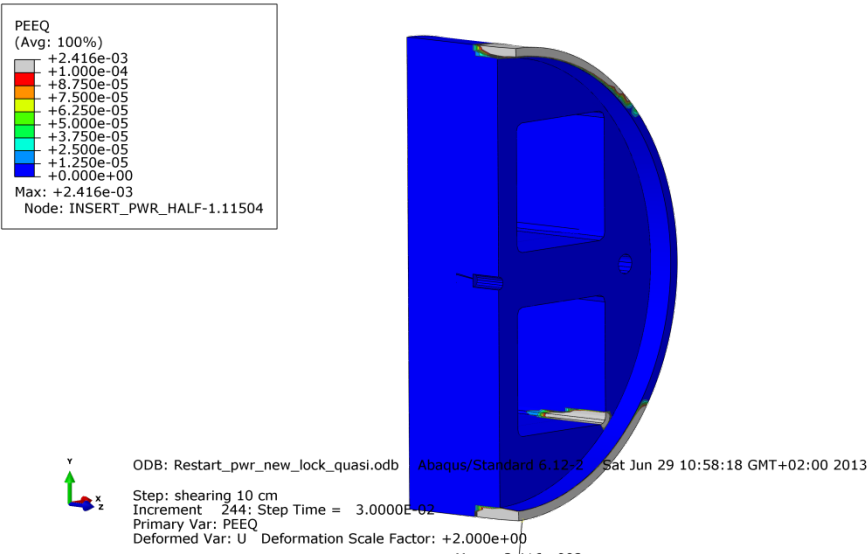


Figure A4-23 Plot showing equivalent plastic strain (PEEQ) for the insert top after 8 cm shearing.

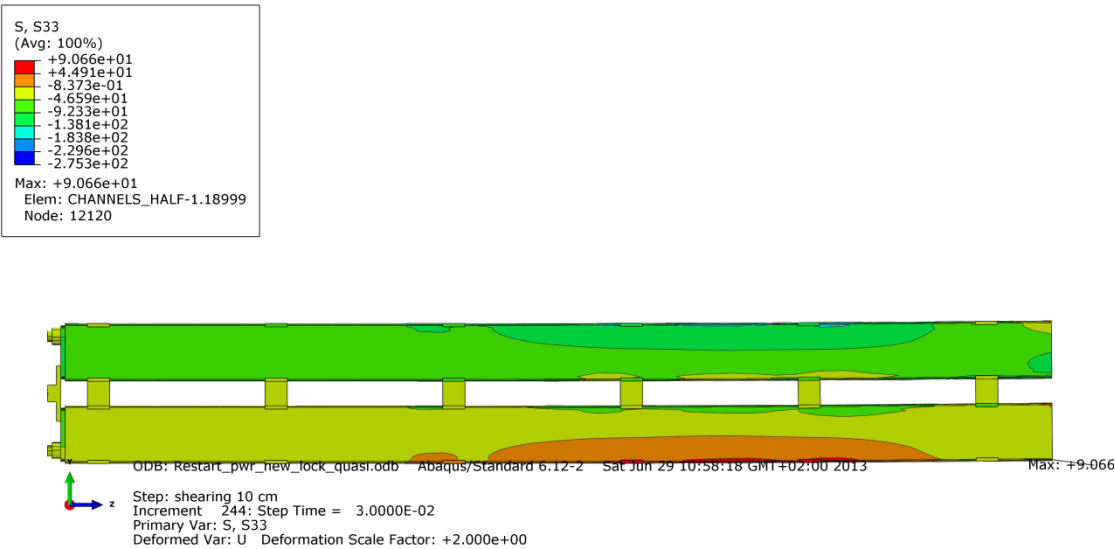


Figure A4-24 Plot showing axial stress [MPa] for the steel channel tubes after 8 cm shearing.

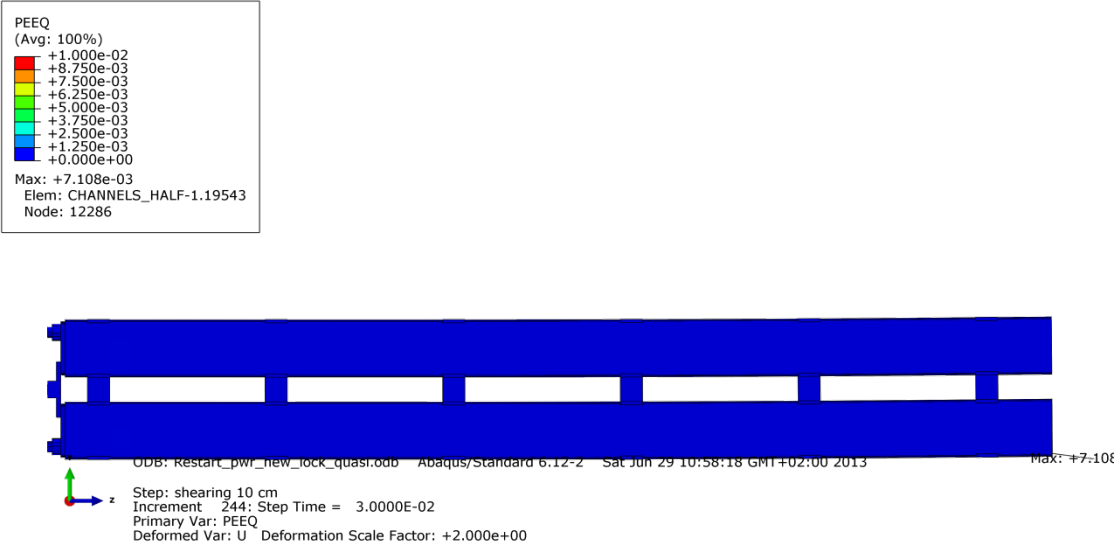


Figure A4-25 Plot showing equivalent plastic strain (PEEQ) for the steel channel tubes after 8 cm shearing.

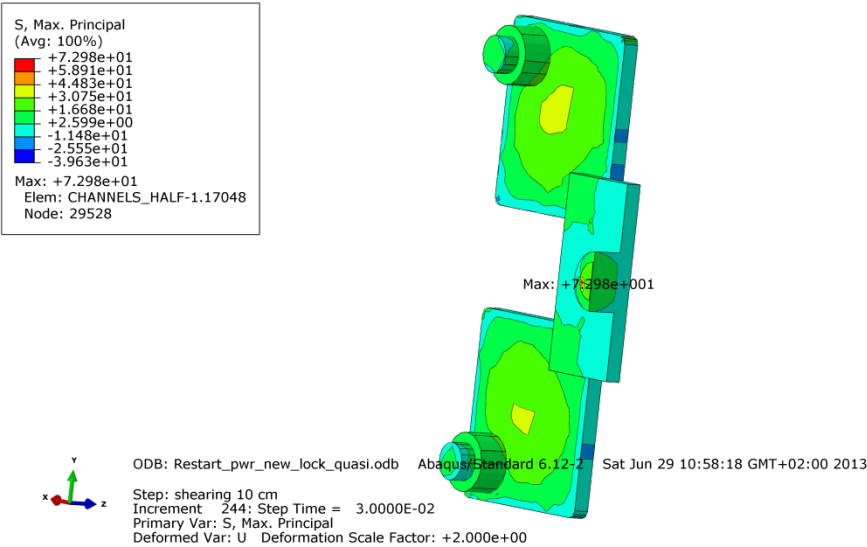


Figure A4-26 Plot showing maximum principal stress [MPa] for the steel channel tubes base plates after 8 cm shearing.

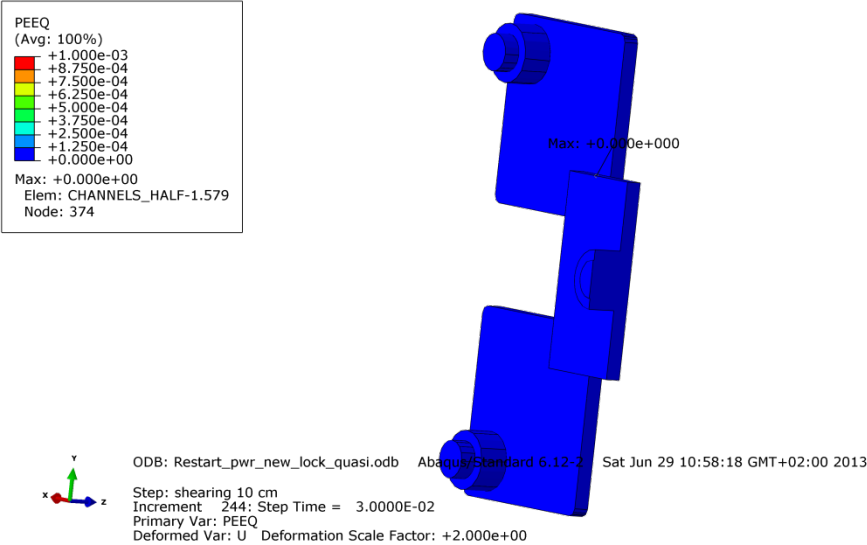


Figure A4-27 Plot showing equivalent plastic strain (PEEQ) for the steel channel tubes base plates after 8 cm shearing.

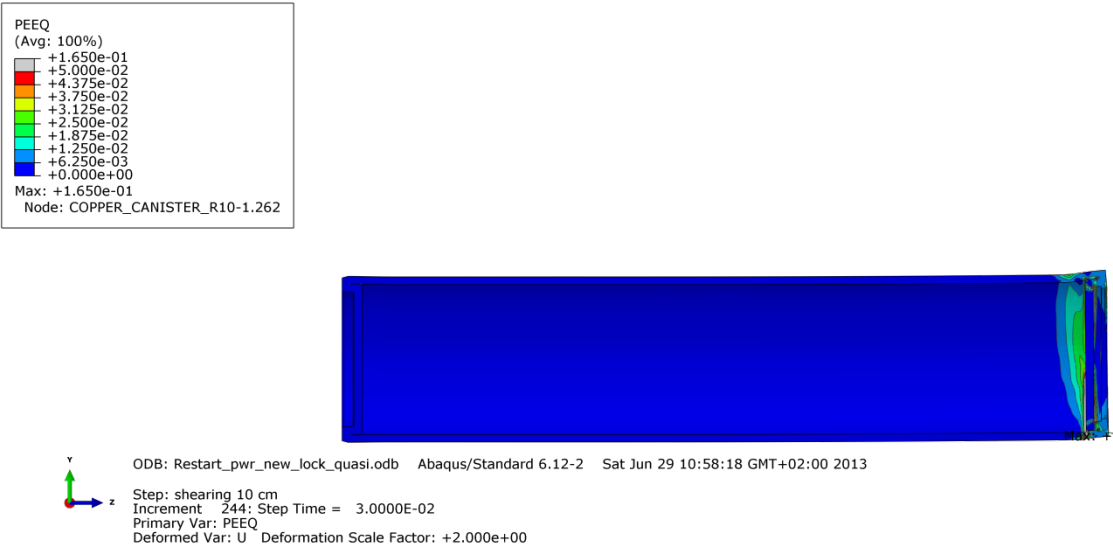


Figure A4-28 Plot showing equivalent plastic strain (PEEQ) for the copper shell after 8 cm shearing.

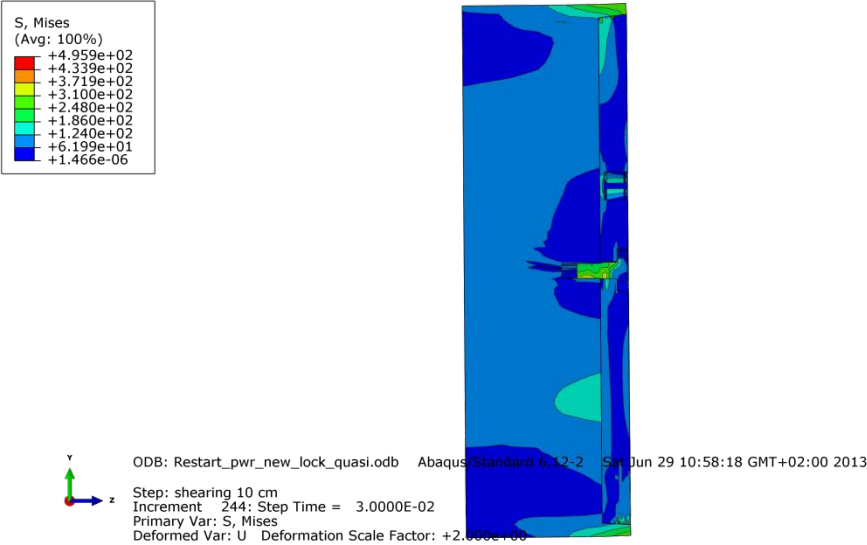


Figure A4-29 Plot showing Mises stress [MPa] close to the steel lid fixing screw after 8 cm shearing.

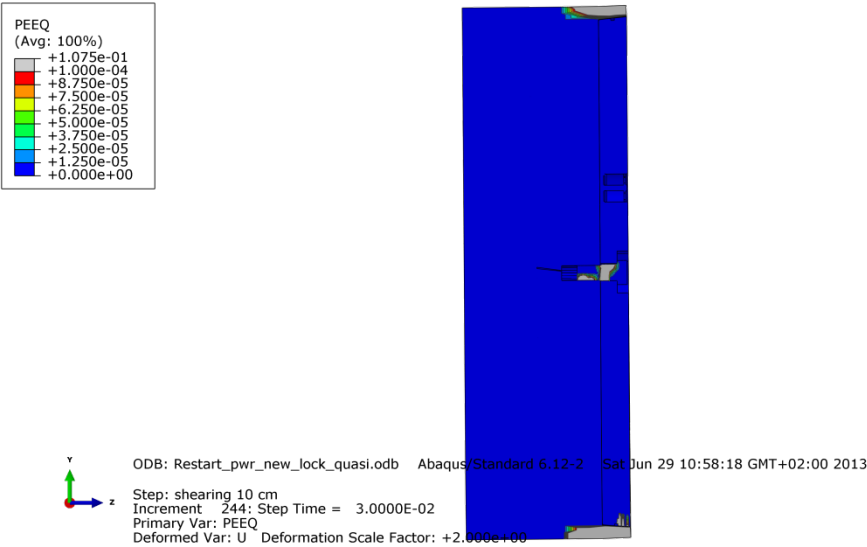


Figure A4-30 Plot showing equivalent plastic strain (PEEQ) close to the steel lid fixing screw after 8 cm shearing.

Appendix 5 – Plots for pwr_new_lock_half_quasi

Plots showing deformed geometry as contour plots for all parts at shearing magnitude 5 cm for case pwr_new_lock_half_quasi (horizontal shearing at the steel lid) using pre-stress in the screw corresponding to half yield stress. The view shows the symmetry plane and all deformations are scaled by a factor of two. Note! The analysis failed to converge for shearing displacement > 5 cm.

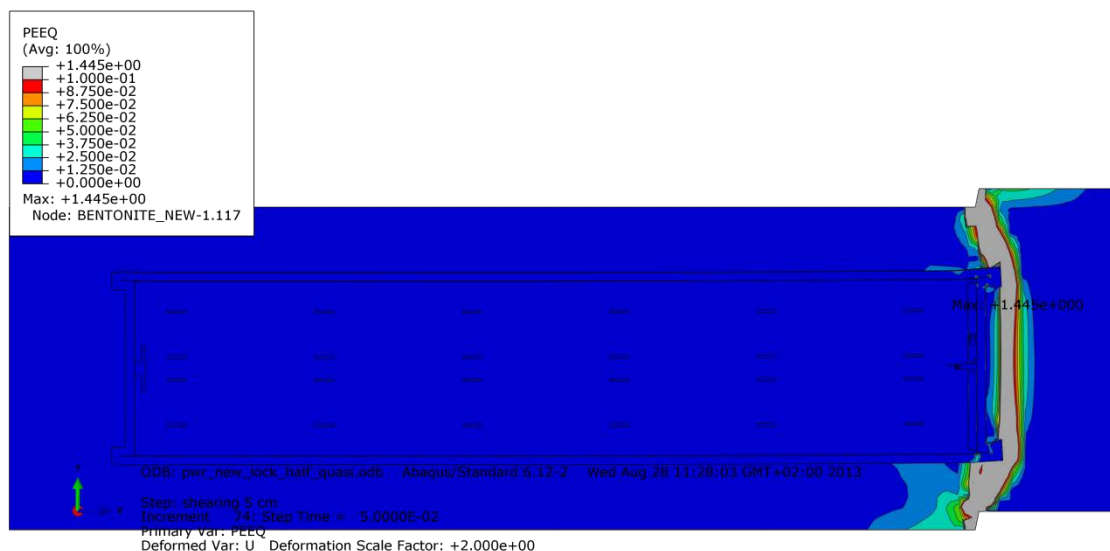


Figure A5-1 Plot showing equivalent plastic strain (PEEQ) after 5 cm shearing.

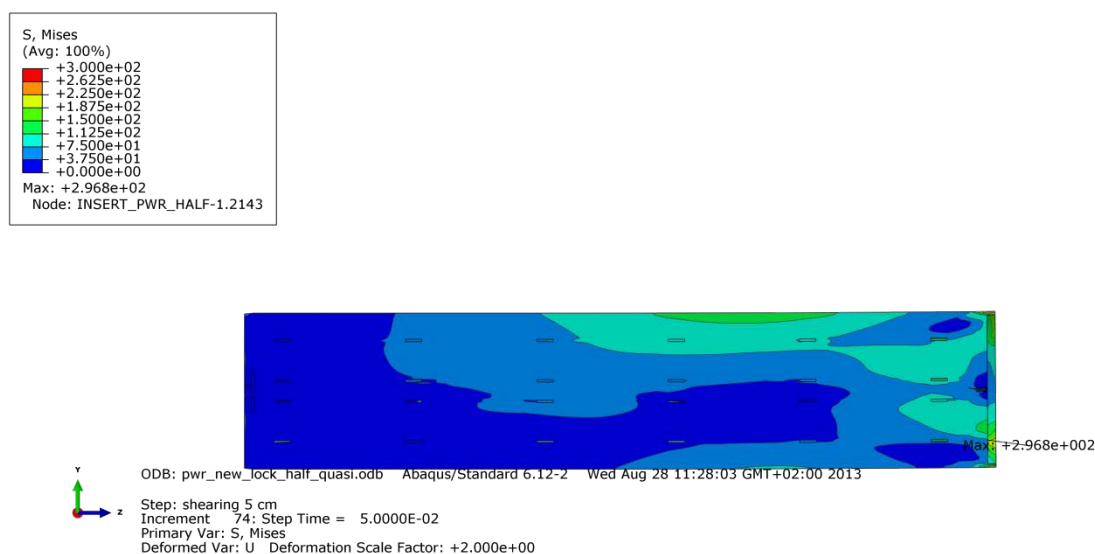


Figure A5-2 Plot showing Mises stress [MPa] for the insert after 5 cm shearing.

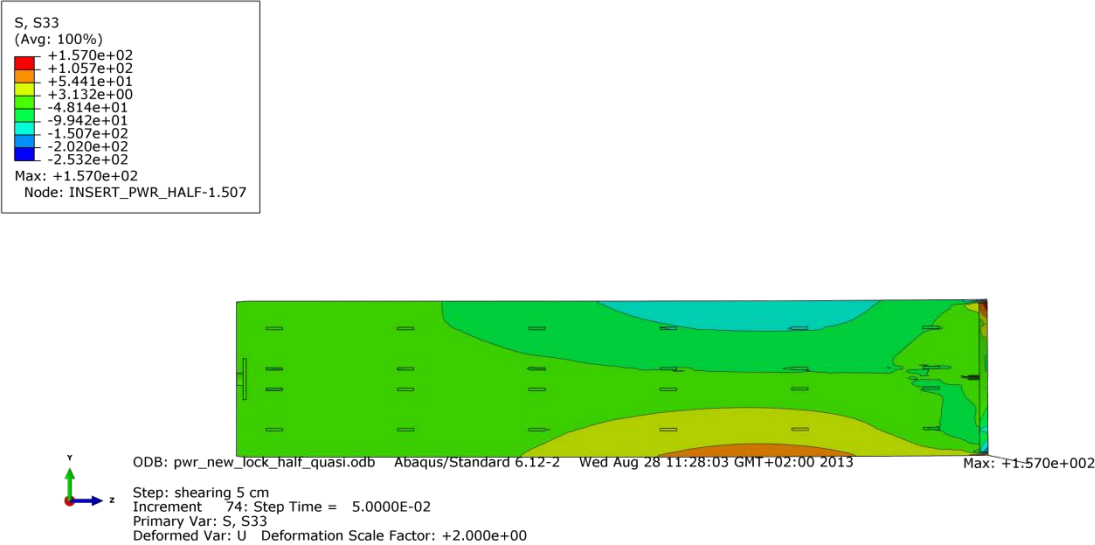


Figure A5-3 Plot showing axial stress [MPa] for the insert after 5 cm shearing.

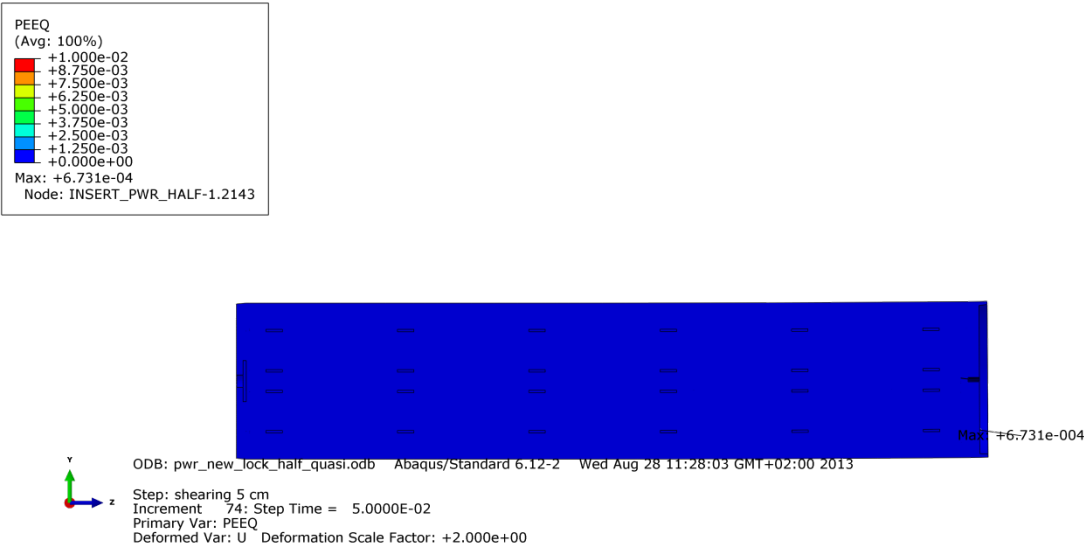


Figure A5-4 Plot showing equivalent plastic strain (PEEQ) for the insert after 5 cm shearing.

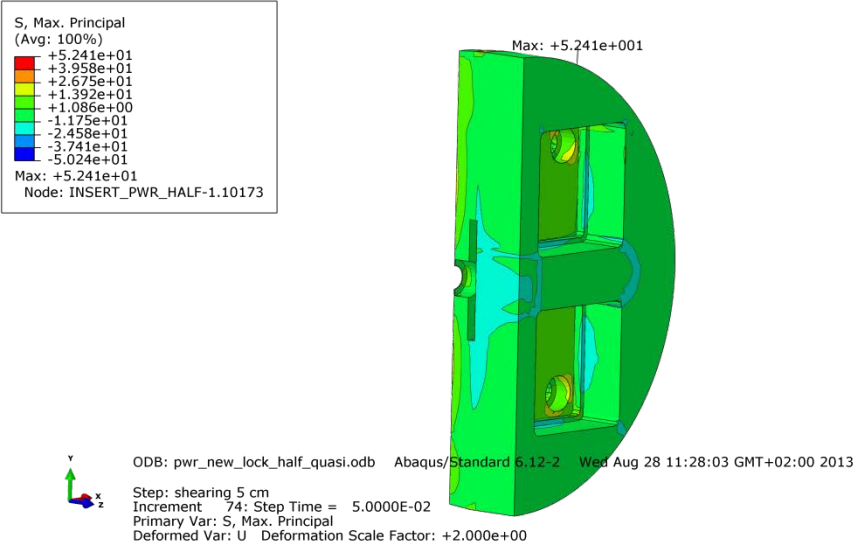


Figure A5-5 Plot showing maximum principal stress [MPa] for the insert base after 5 cm shearing.

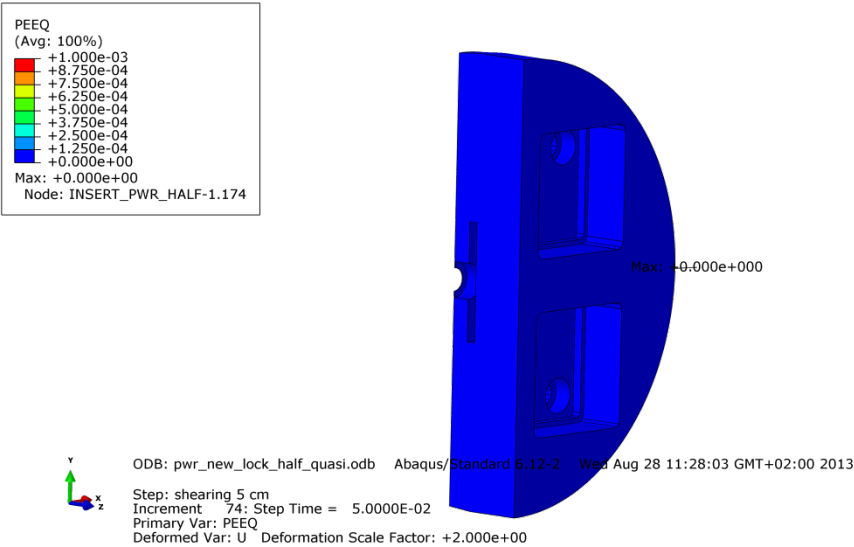


Figure A5-6 Plot showing equivalent plastic strain (PEEQ) for the insert base after 5 cm shearing.

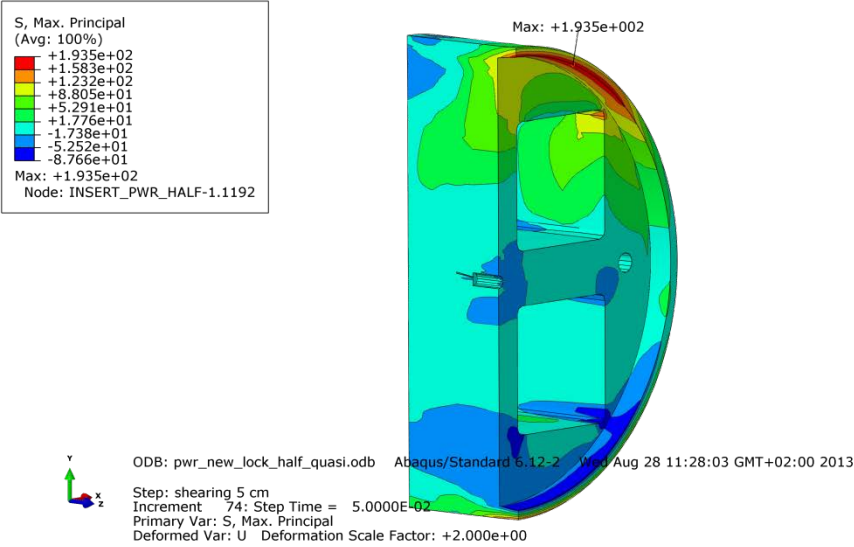


Figure A5-7 Plot showing maximum principal stress [MPa] for the insert top after 5 cm shearing.

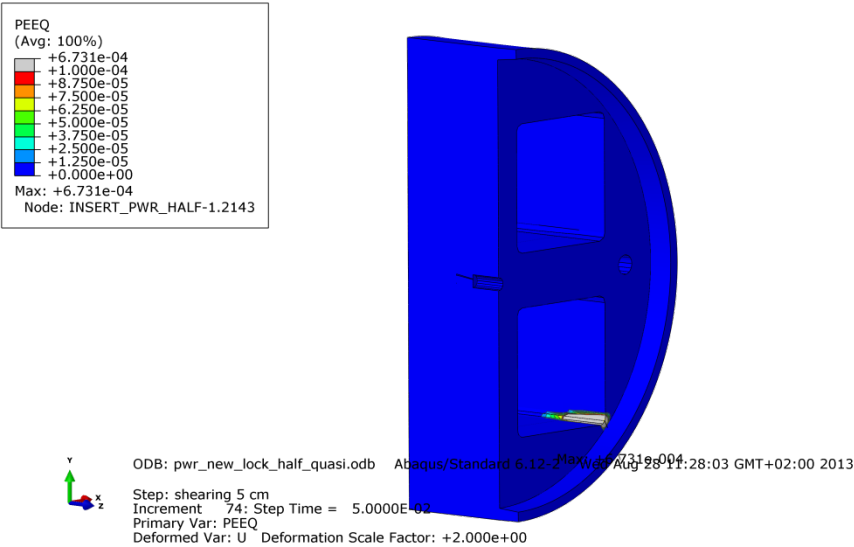


Figure A5-8 Plot showing equivalent plastic strain (PEEQ) for the insert top after 5 cm shearing.

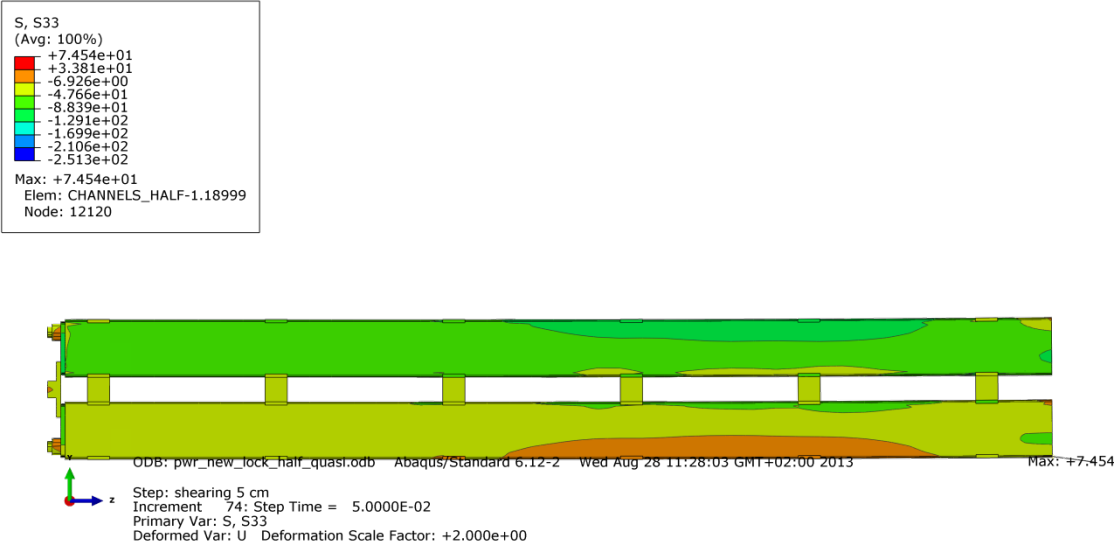


Figure A5-9 Plot showing axial stress [MPa] for the steel channel tubes after 5 cm shearing.

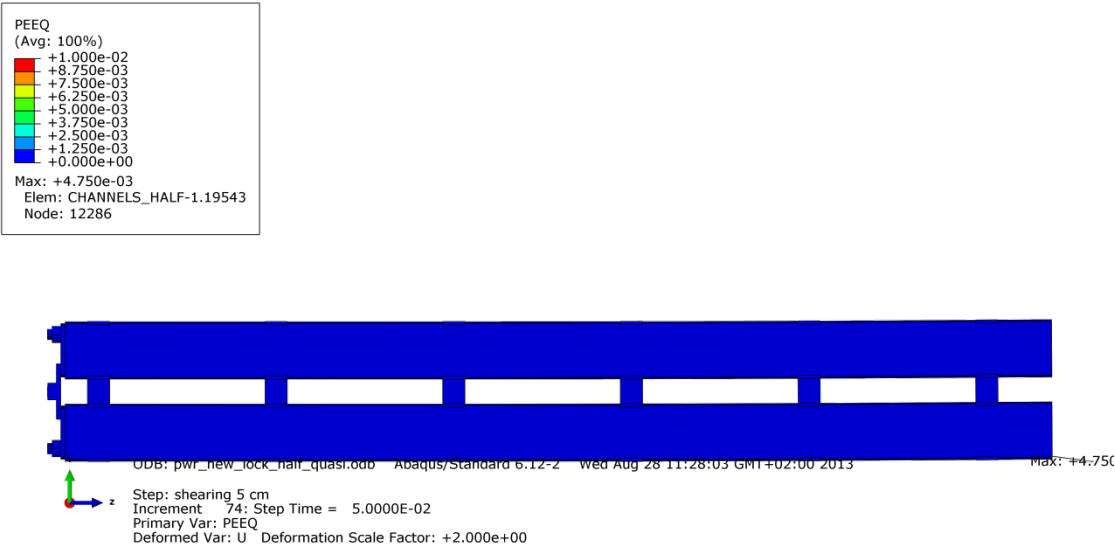


Figure A5-10 Plot showing equivalent plastic strain (PEEQ) for the steel channel tubes after 5 cm shearing.

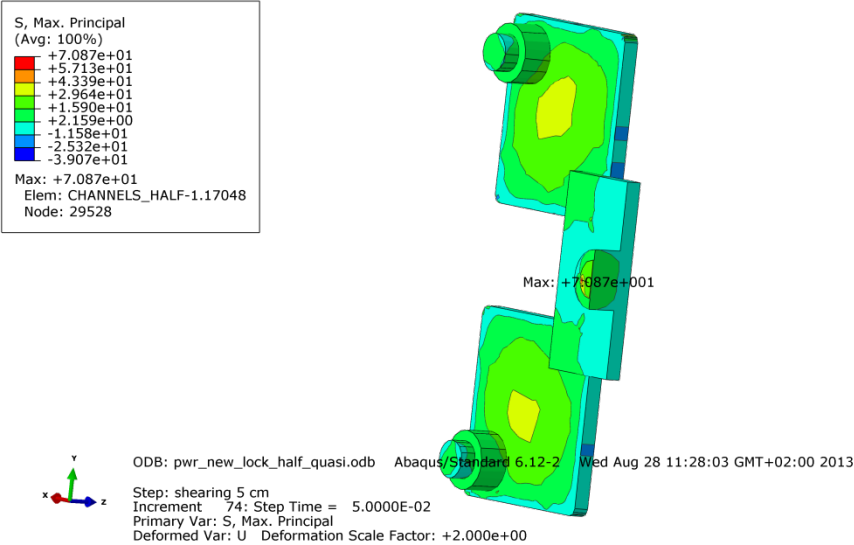


Figure A5-11 Plot showing maximum principal stress [MPa] for the steel channel tubes base plates after 5 cm shearing.

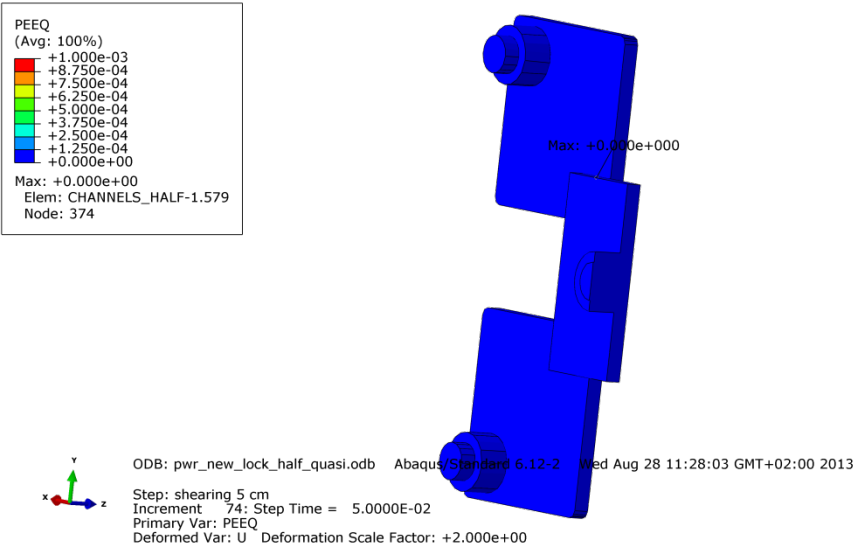


Figure A5-12 Plot showing equivalent plastic strain (PEEQ) for the steel channel tubes base plates after 5 cm shearing.

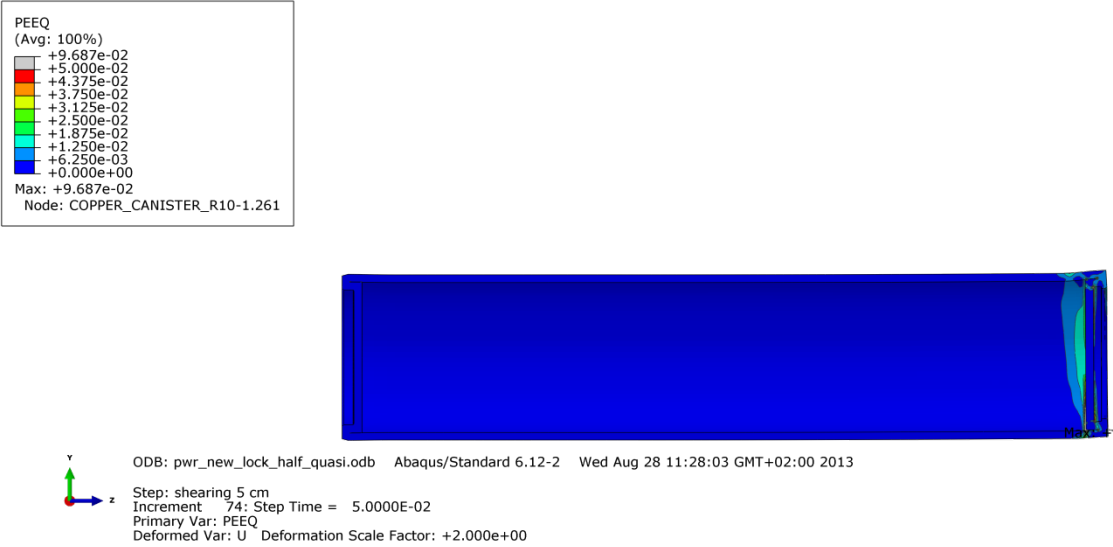


Figure A5-13 Plot showing equivalent plastic strain (PEEQ) for the copper shell after 5 cm shearing.

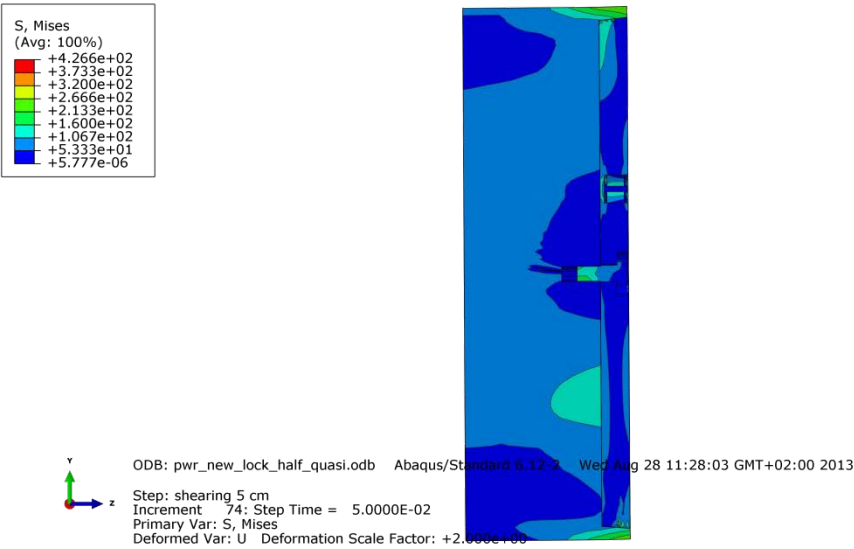


Figure A5-14 Plot showing Mises stress [MPa] close to the steel lid fixing screw after 5 cm shearing.

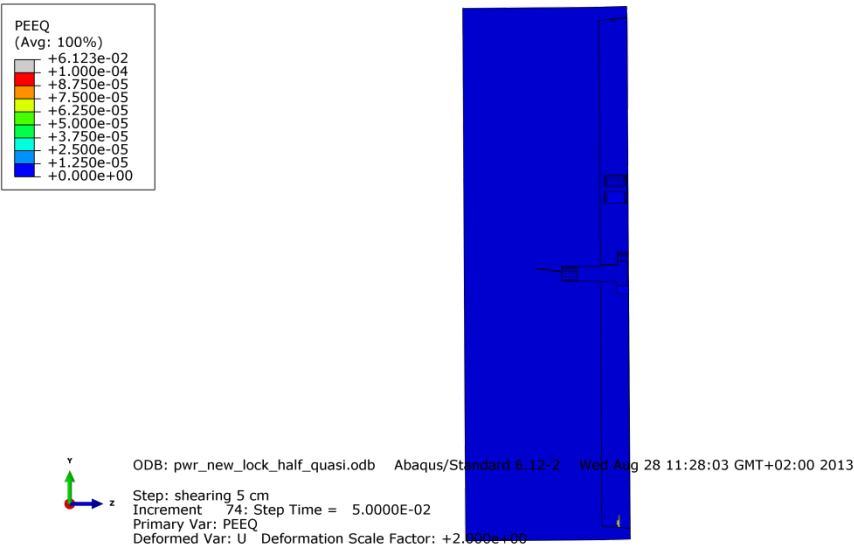


Figure A5-15 Plot showing equivalent plastic strain (PEEQ) close to the steel lid fixing screw after 5 cm shearing.

Appendix 6 – Plots for pwr_new2_washer3_quasi

Plots showing deformed geometry as contour plots for all parts at shearing magnitude 5 and 10 cm for case pwr_new2_washer3_quasi (horizontal shearing at $\frac{3}{4}$ -distance from base of the insert) when the washer between the screw head and steel lid is included. The view shows the symmetry plane and all deformations are scaled by a factor of two.

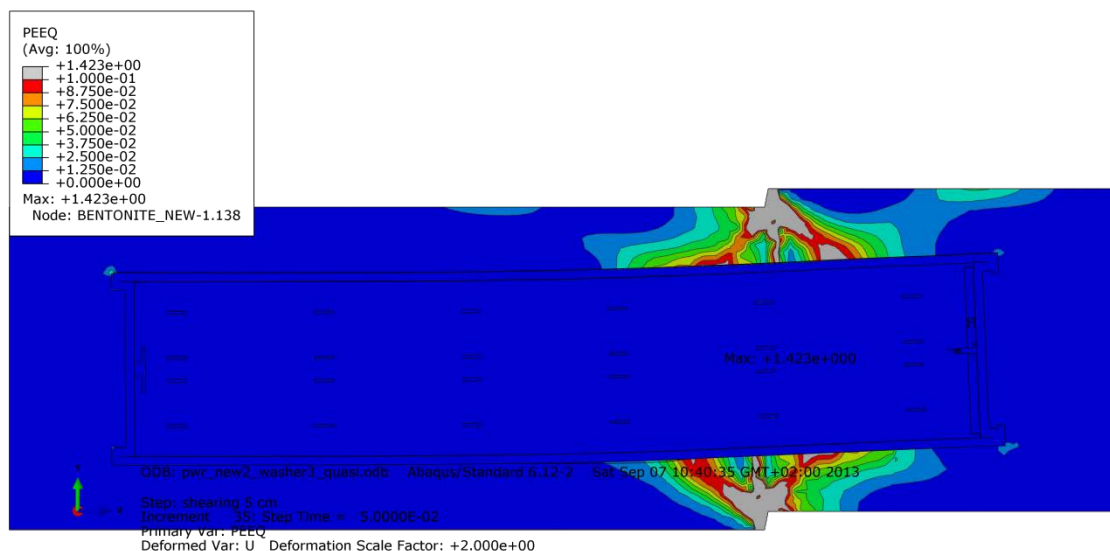


Figure A6-1 Plot showing equivalent plastic strain (PEEQ) after 5 cm shearing.

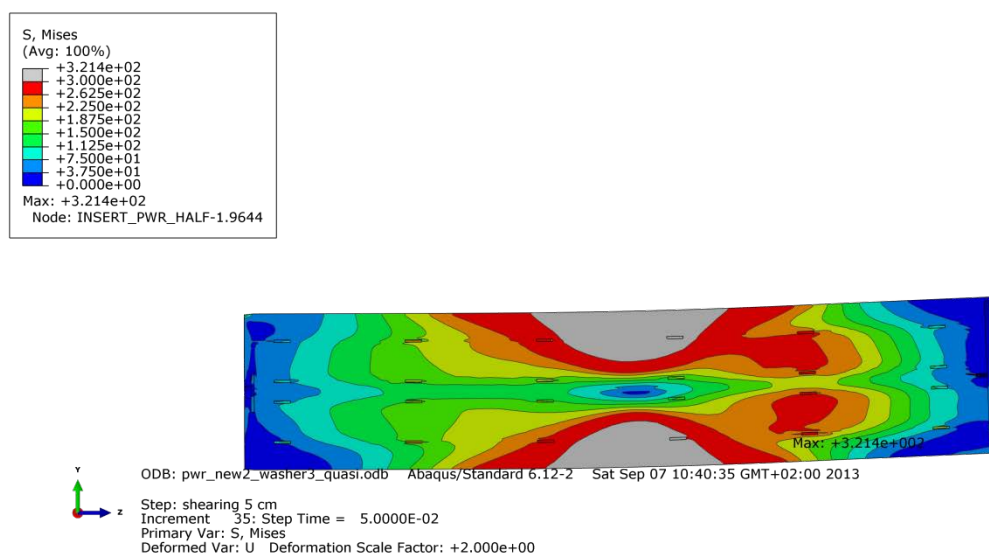


Figure A6-2 Plot showing Mises stress [MPa] for the insert after 5 cm shearing.

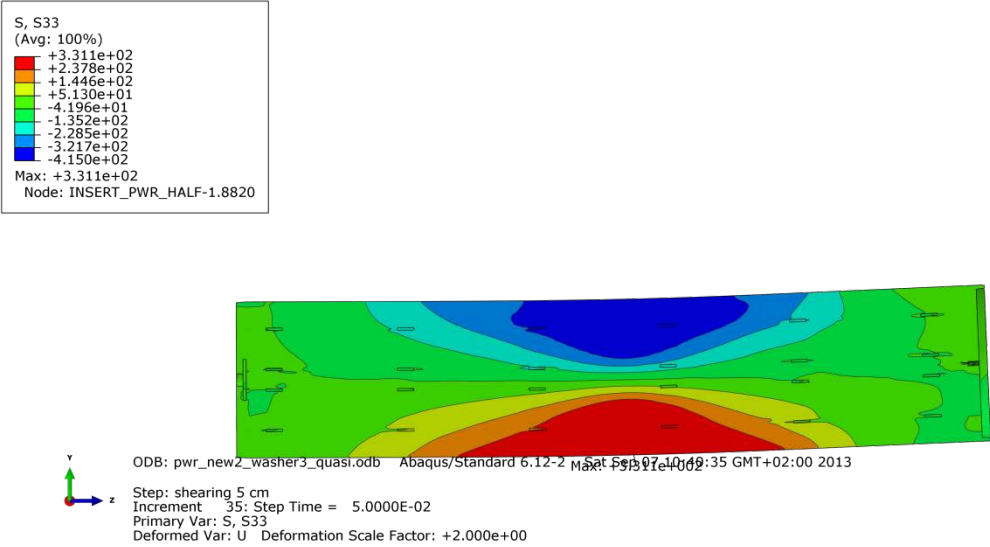


Figure A6-3 Plot showing axial stress [MPa] for the insert after 5 cm shearing.

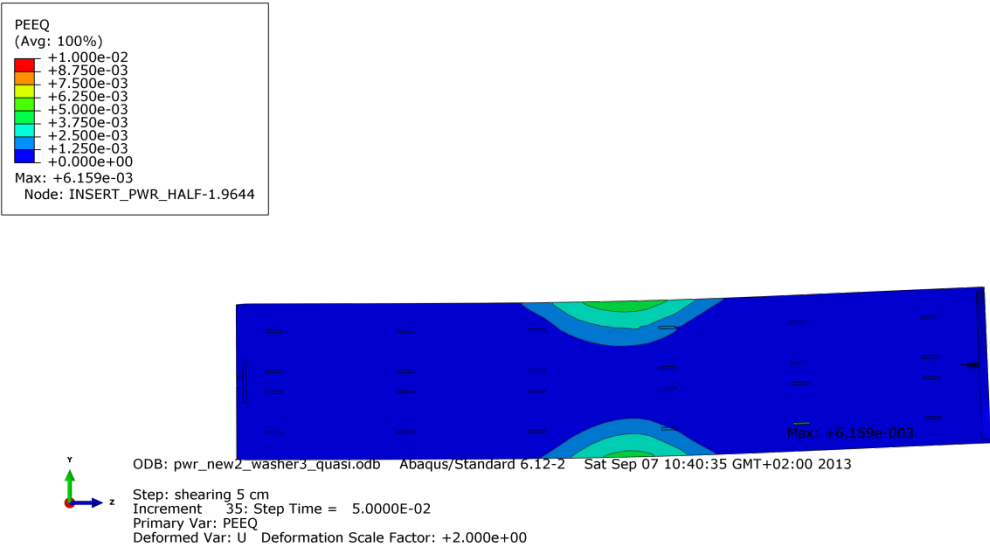


Figure A6-4 Plot showing equivalent plastic strain (PEEQ) for the insert after 5 cm shearing.

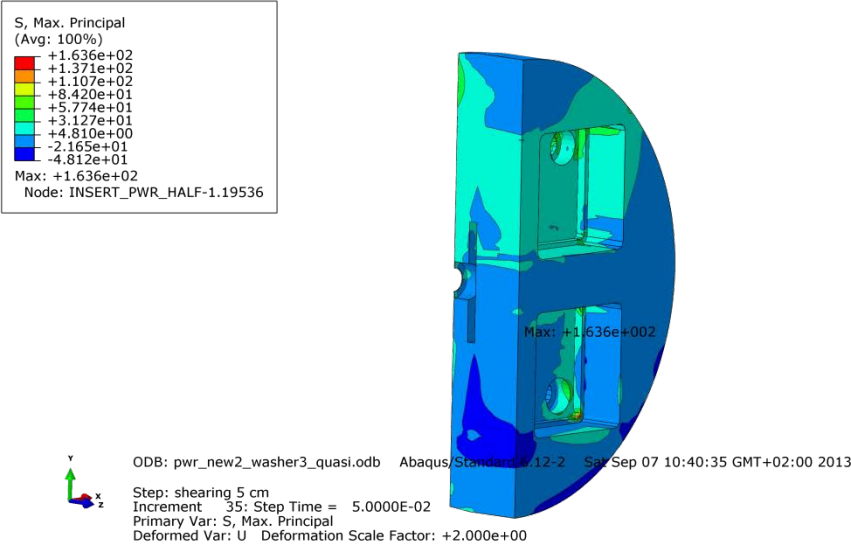


Figure A6-5 Plot showing maximum principal stress [MPa] for the insert base after 5 cm shearing.

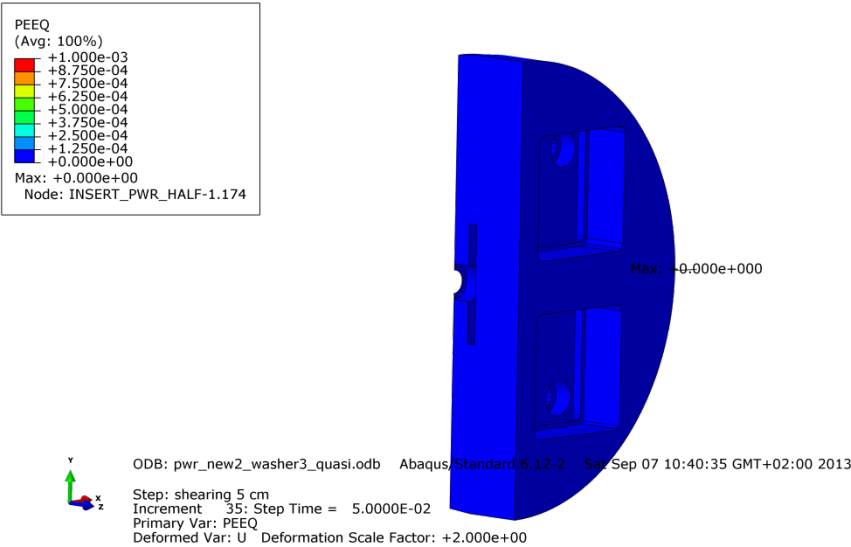


Figure A6-6 Plot showing equivalent plastic strain (PEEQ) for the insert base after 5 cm shearing.

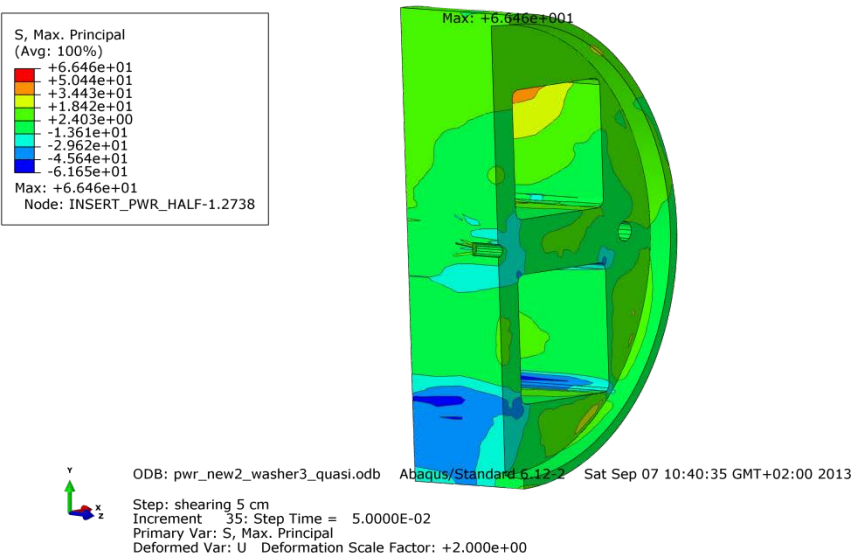


Figure A6-7 Plot showing maximum principal stress [MPa] for the insert top after 5 cm shearing.

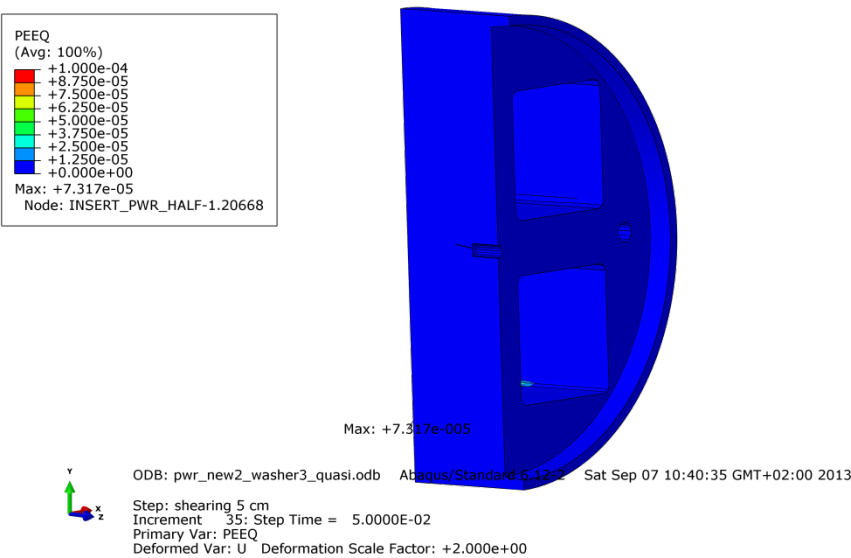


Figure A6-8 Plot showing equivalent plastic strain (PEEQ) for the insert top after 5 cm shearing.

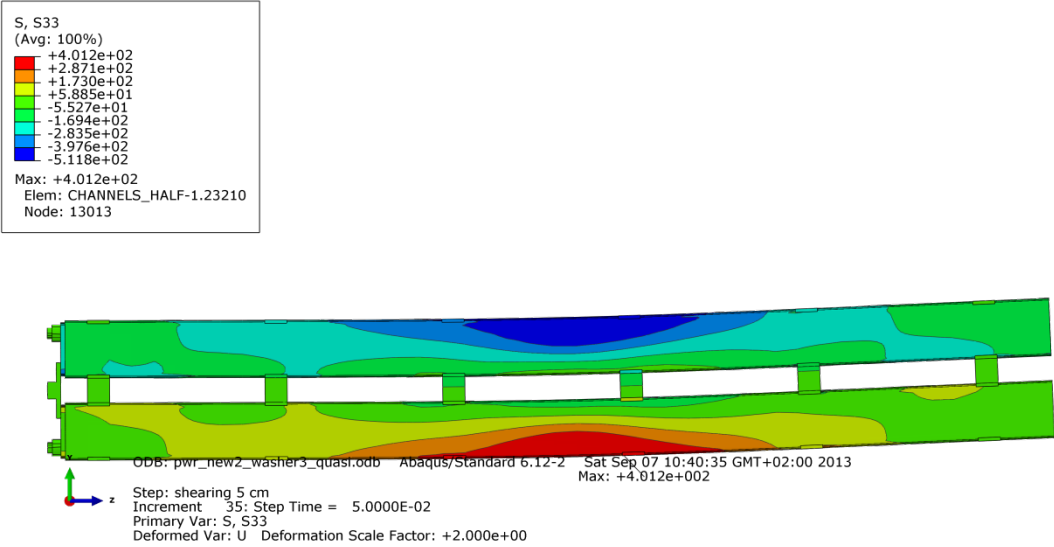


Figure A6-9 Plot showing axial stress [MPa] for the steel channel tubes after 5 cm shearing.

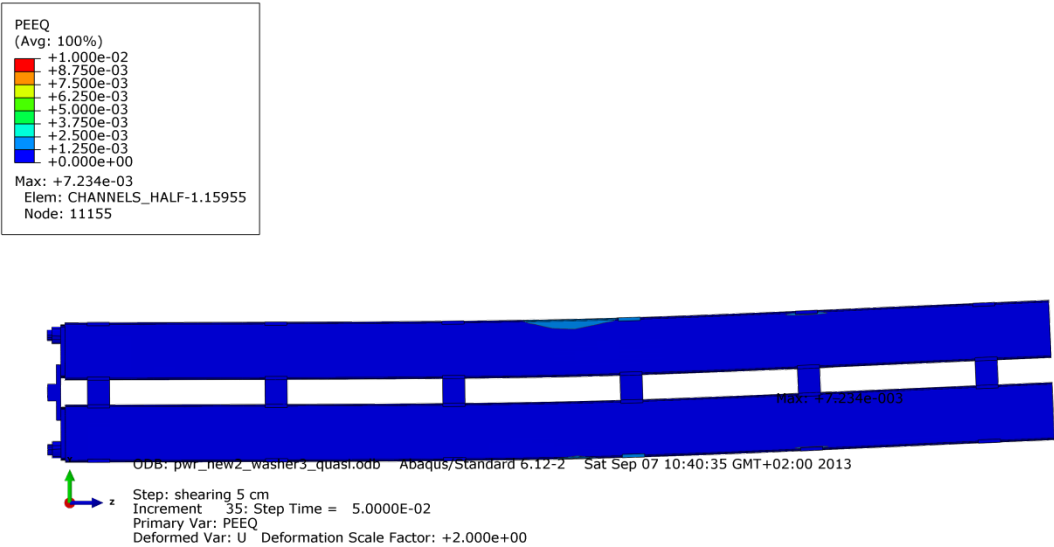


Figure A6-10 Plot showing equivalent plastic strain (PEEQ) for the steel channel tubes after 5 cm shearing.

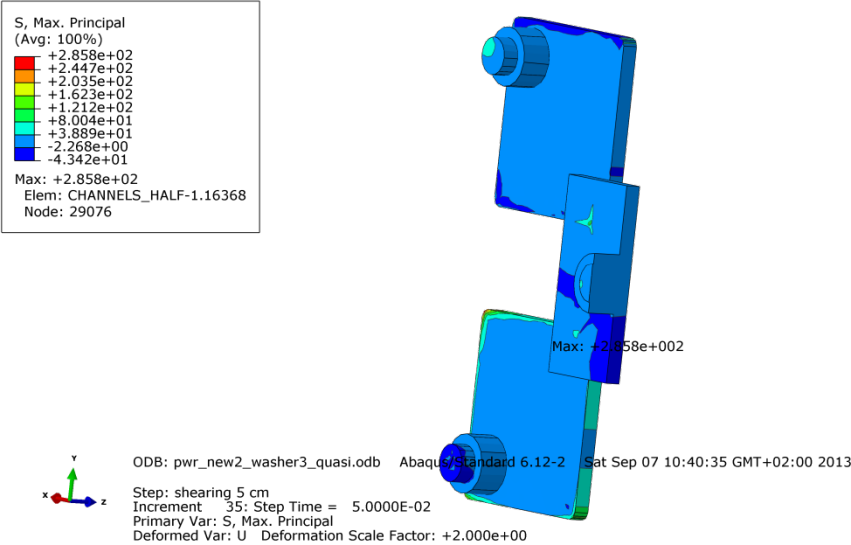


Figure A6-11 Plot showing maximum principal stress [MPa] for the steel channel tubes base plates after 5 cm shearing.

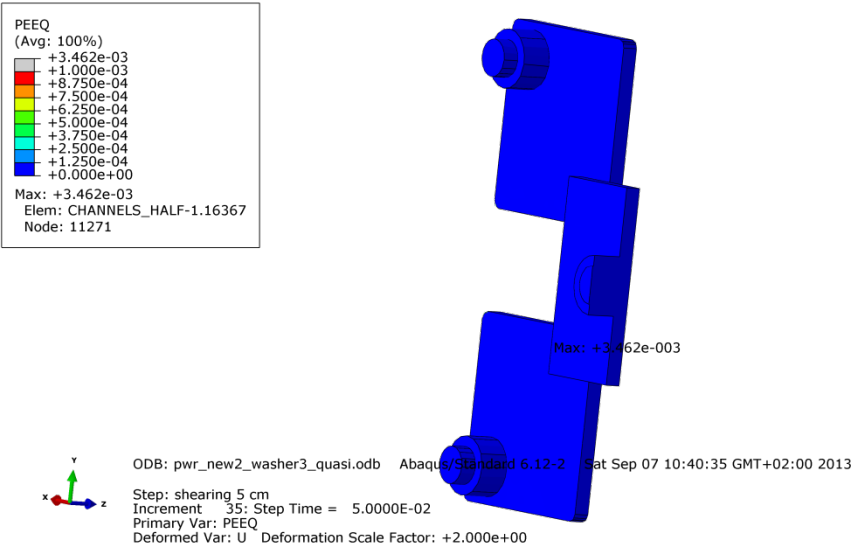


Figure A6-12 Plot showing equivalent plastic strain (PEEQ) for the steel channel tubes base plates after 5 cm shearing.

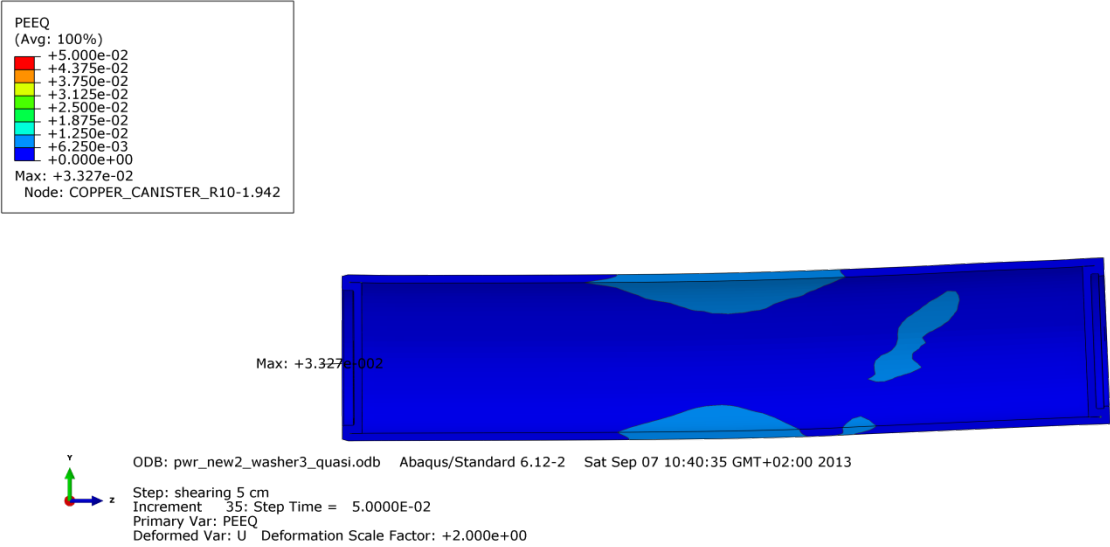


Figure A6-13 Plot showing equivalent plastic strain (PEEQ) for the copper shell after 5 cm shearing.

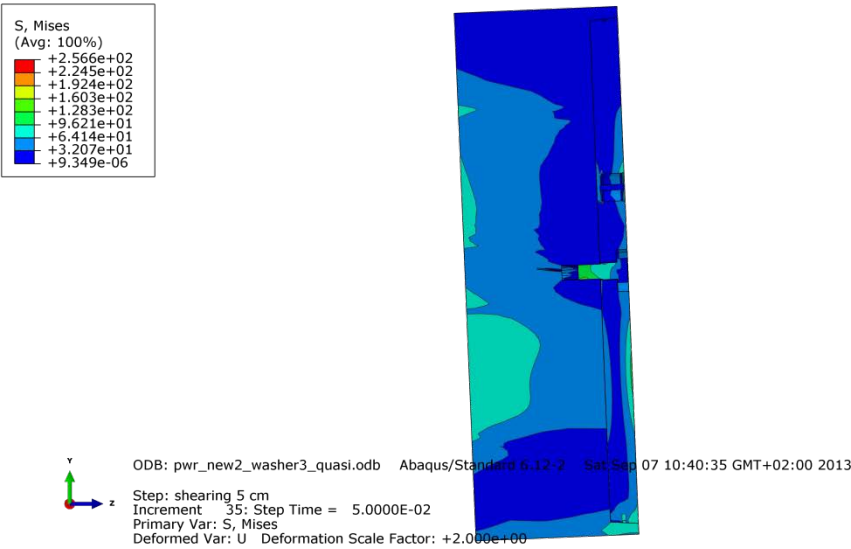


Figure A6-14 Plot showing Mises stress [MPa] close to the steel lid fixing screw after 5 cm shearing.

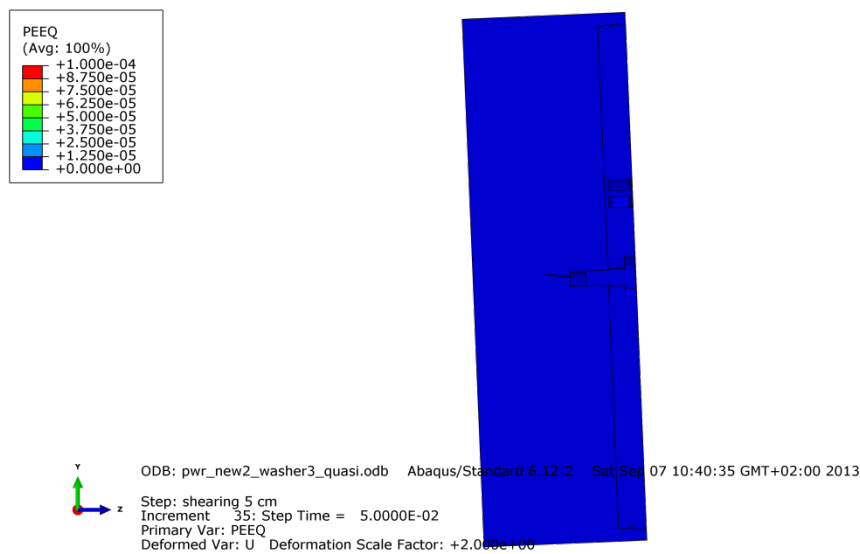


Figure A6-15 Plot showing equivalent plastic strain (PEEQ) close to the steel lid fixing screw after 5 cm shearing.

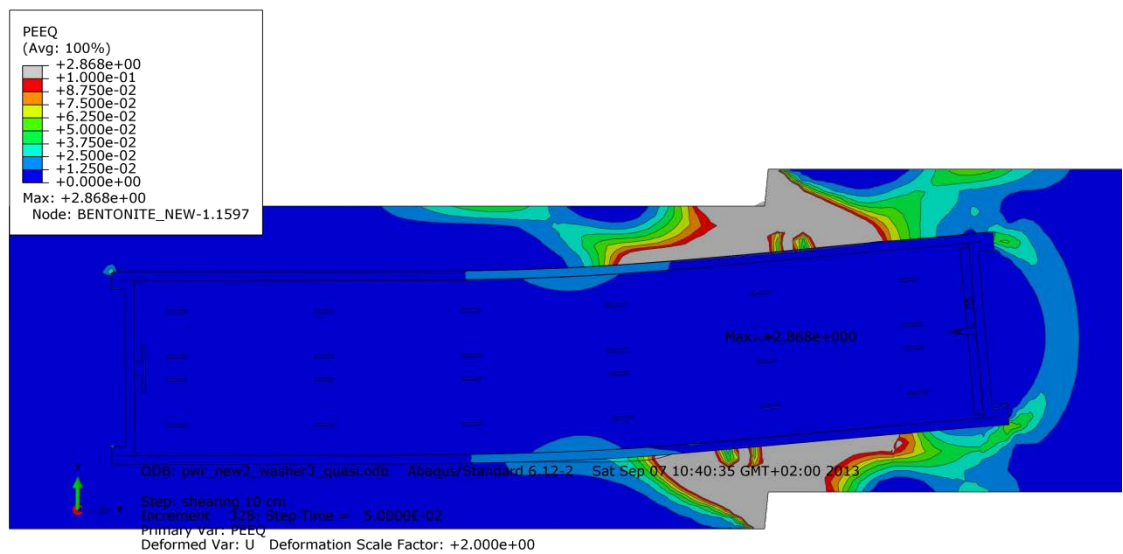


Figure A6-16 Plot showing equivalent plastic strain (PEEQ) after 10 cm shearing.

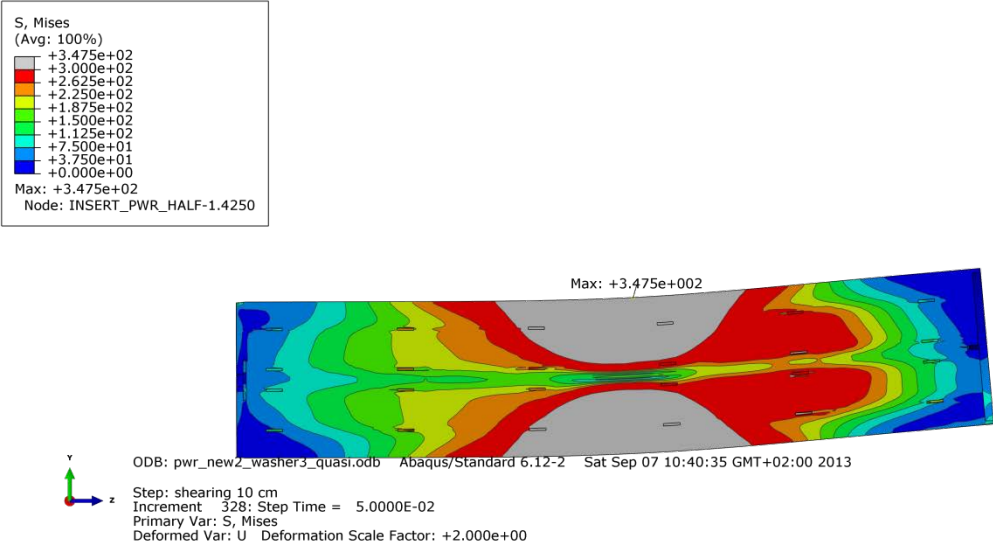


Figure A6-17 Plot showing Mises stress [MPa] for the insert after 10 cm shearing.

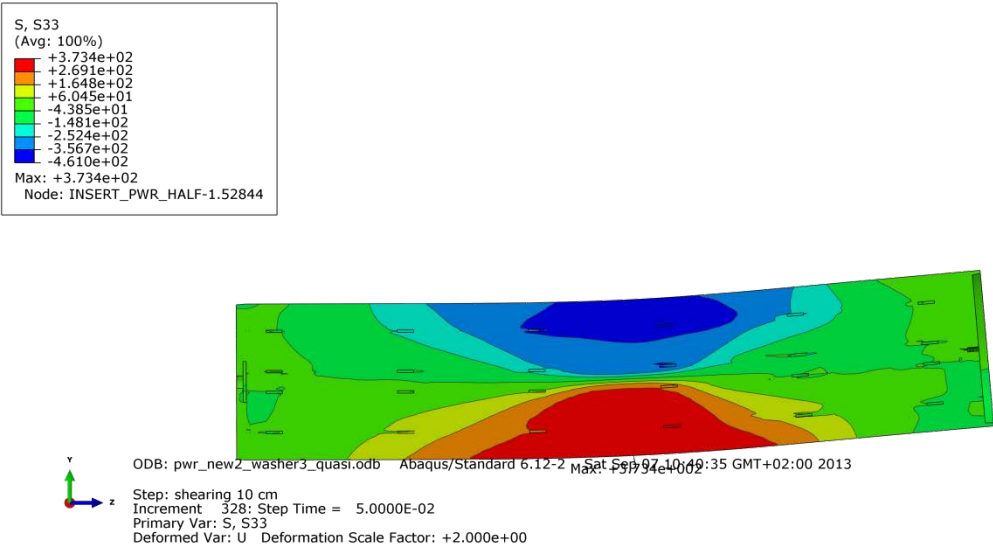


Figure A6-18 Plot showing axial stress [MPa] for the insert after 10 cm shearing.

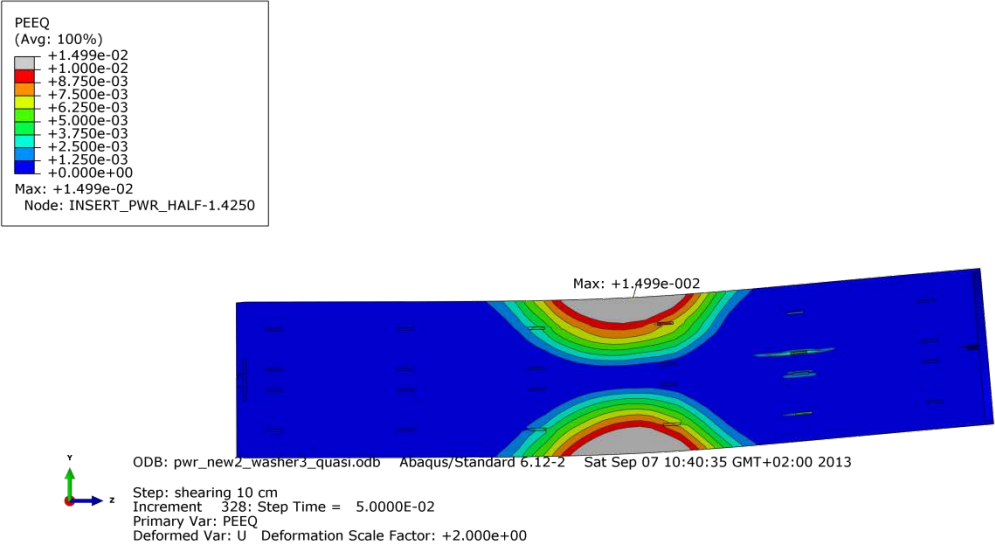


Figure A6-19 Plot showing equivalent plastic strain (PEEQ) for the insert after 10 cm shearing.

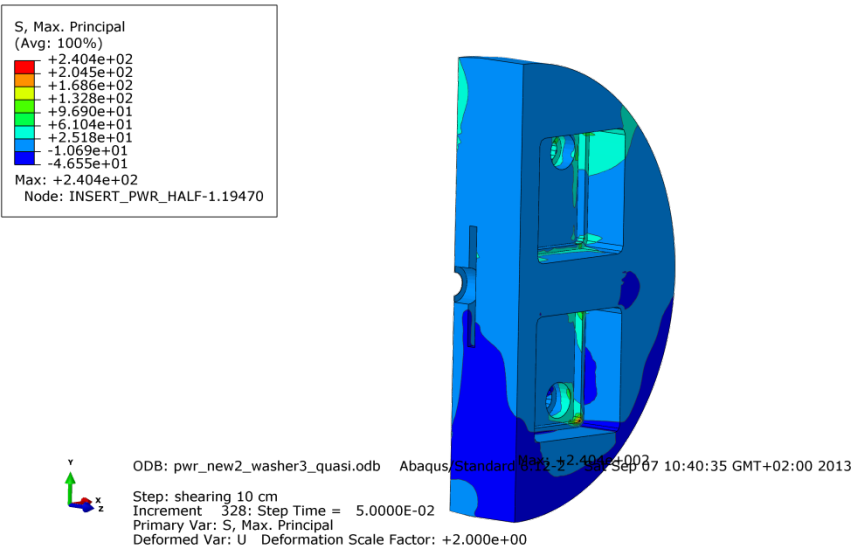


Figure A6-20 Plot showing maximum principal stress [MPa] for the insert base after 10 cm shearing.

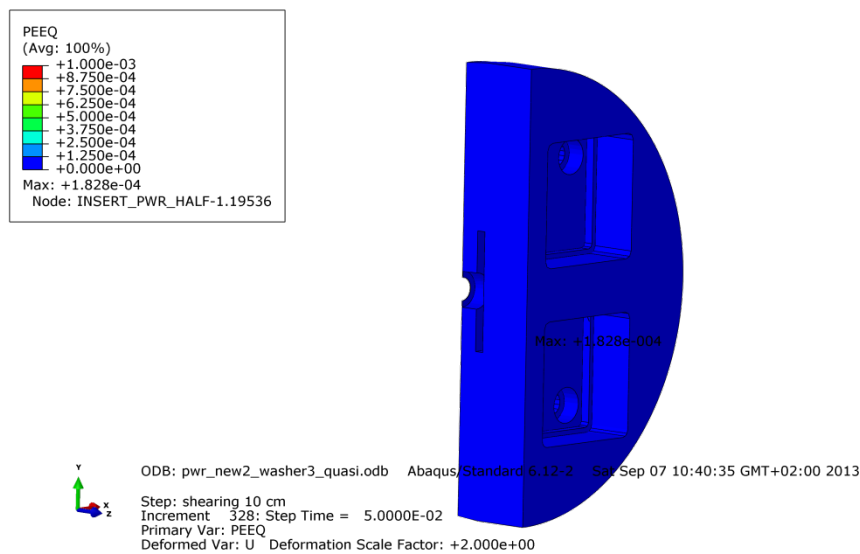


Figure A6-21 Plot showing equivalent plastic strain (PEEQ) for the insert base after 10 cm shearing.

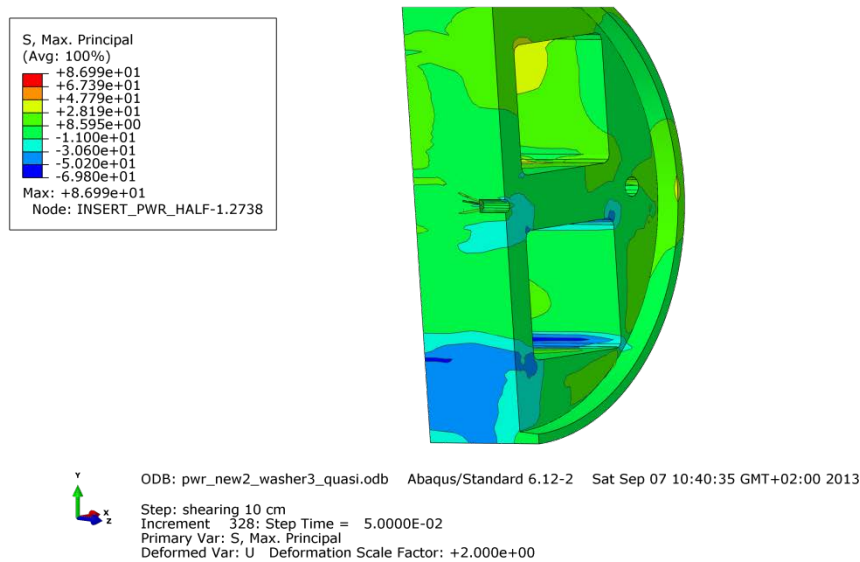


Figure A6-22 Plot showing maximum principal stress [MPa] for the insert top after 10 cm shearing.

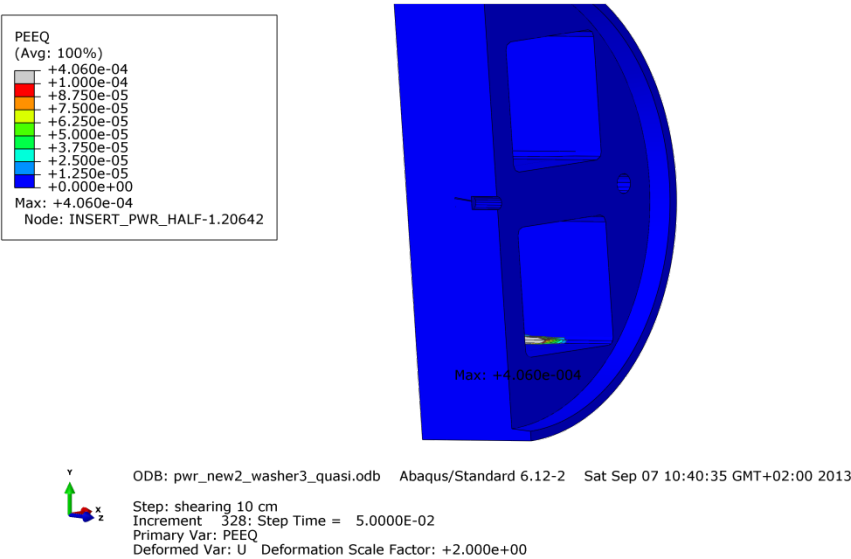


Figure A6-23 Plot showing equivalent plastic strain (PEEQ) for the insert top after 10 cm shearing.

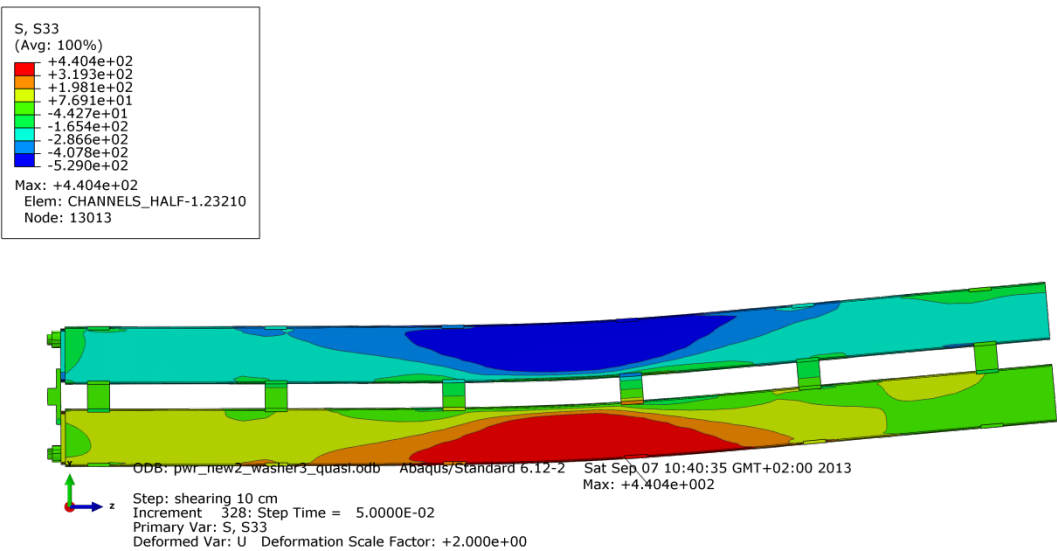


Figure A6-24 Plot showing axial stress [MPa] for the steel channel tubes after 10 cm shearing.

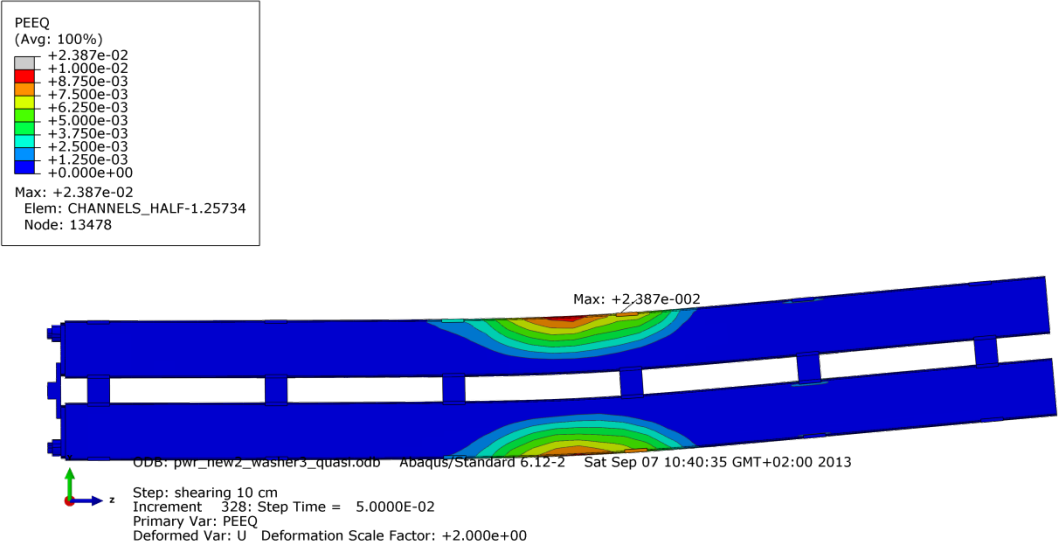


Figure A6-25 Plot showing equivalent plastic strain (PEEQ) for the steel channel tubes after 10 cm shearing.

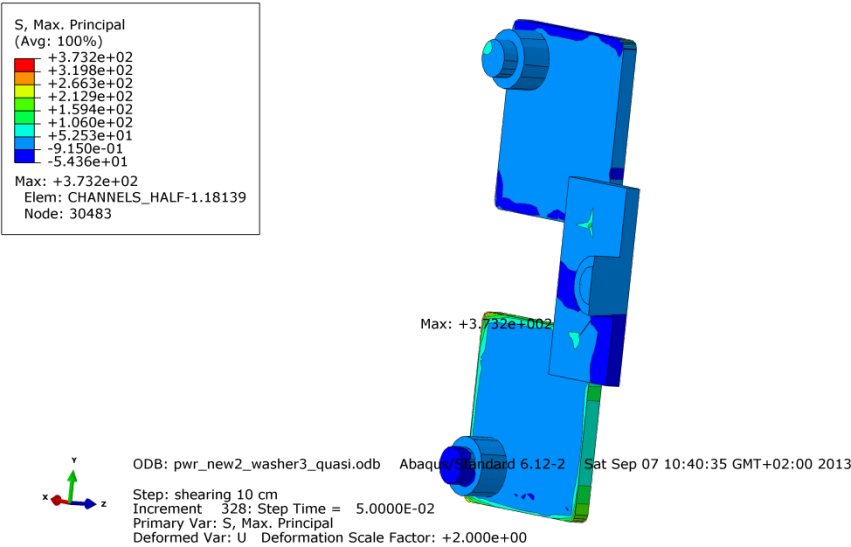


Figure A6-26 Plot showing maximum principal stress [MPa] for the steel channel tubes base plates after 10 cm shearing.

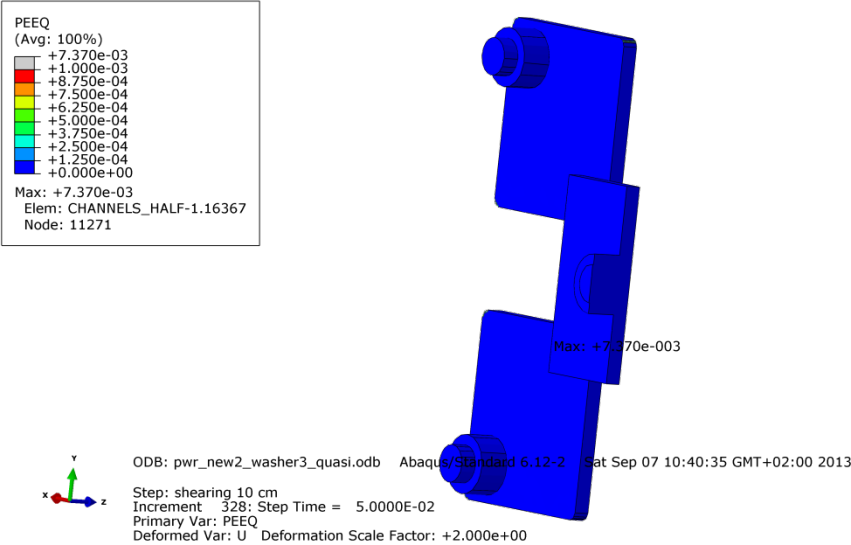


Figure A6-27 Plot showing equivalent plastic strain (PEEQ) for the steel channel tubes base plates after 10 cm shearing.

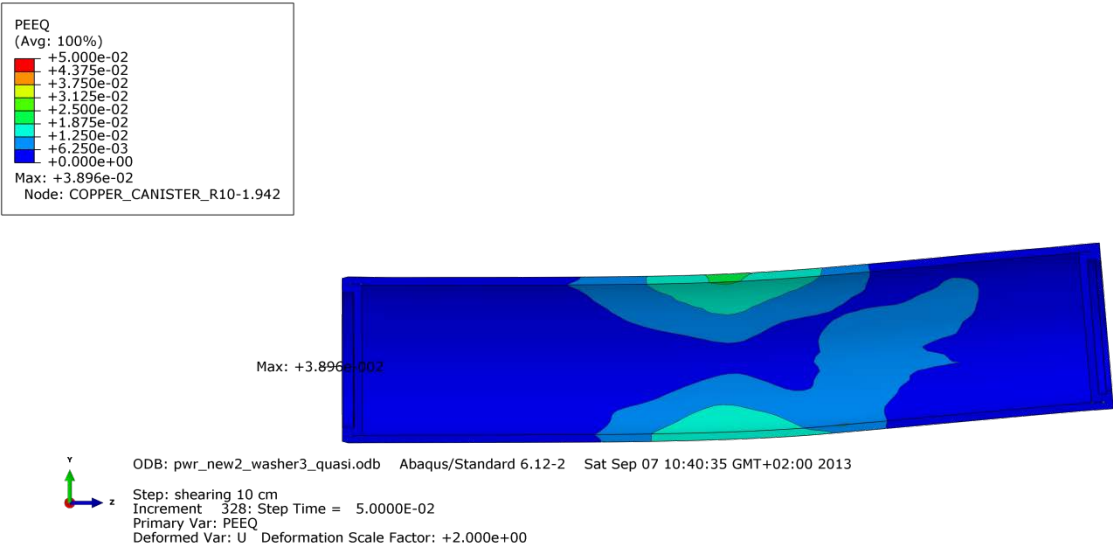


Figure A6-28 Plot showing equivalent plastic strain (PEEQ) for the copper shell after 10 cm shearing.

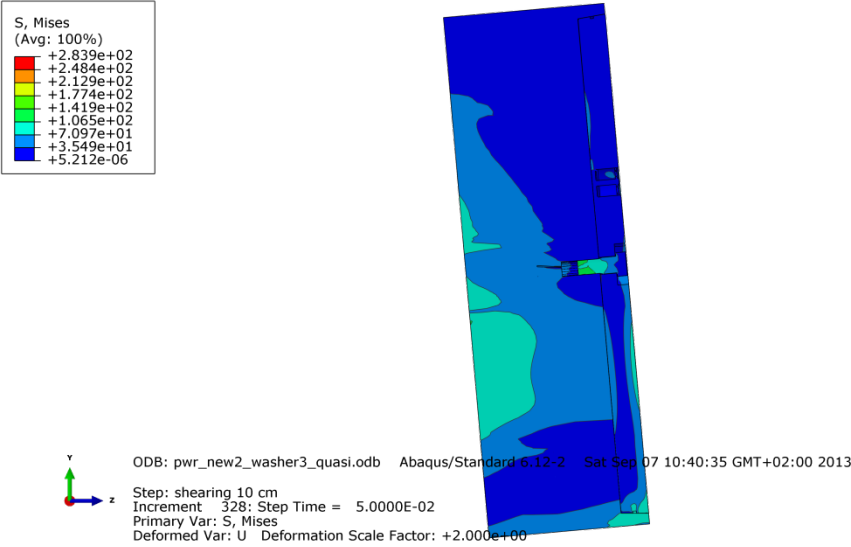


Figure A6-29 Plot showing Mises stress [MPa] close to the steel lid fixing screw after 10 cm shearing.

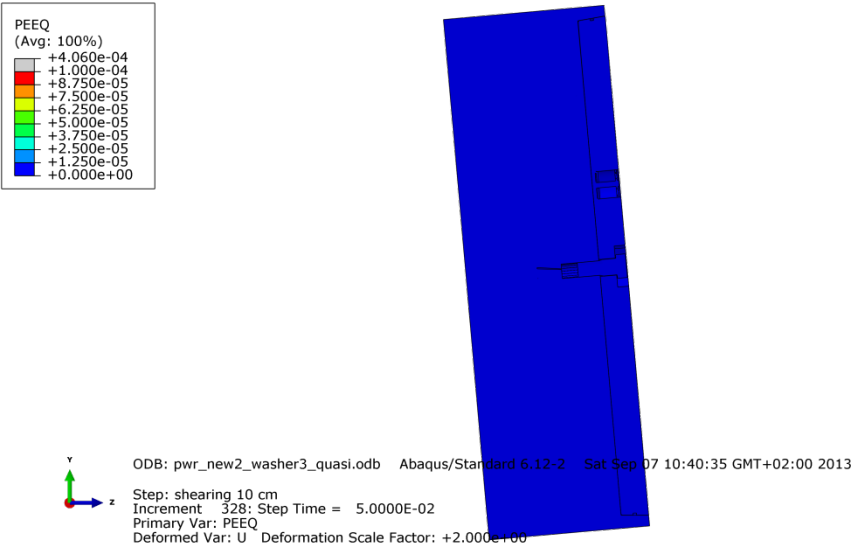


Figure A6-30 Plot showing equivalent plastic strain (PEEQ) close to the steel lid fixing screw after 10 cm shearing.

Appendix 7 – Plots for bwr_new2_quasi

Plots showing deformed geometry as contour plots for all parts at shearing magnitude 5 and 8 cm for case bwr_new2_quasi (horizontal shearing at $\frac{3}{4}$ distance from insert base). The view shows the symmetry plane and all deformations are scaled by a factor of two. Note! The analysis failed to converge for shearing displacement > 8 cm.

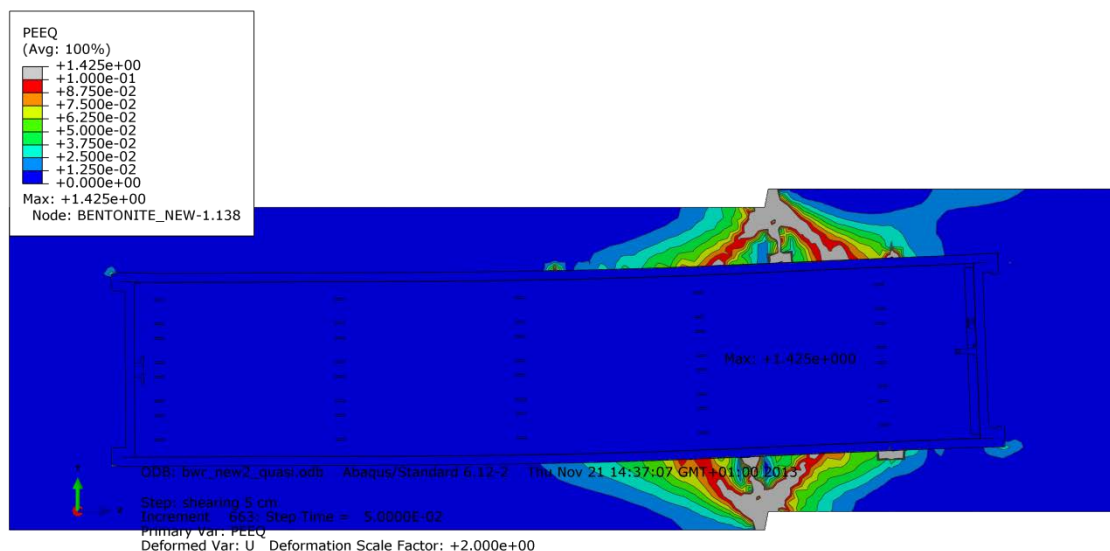


Figure A7-1 Plot showing equivalent plastic strain (PEEQ) after 5 cm shearing.

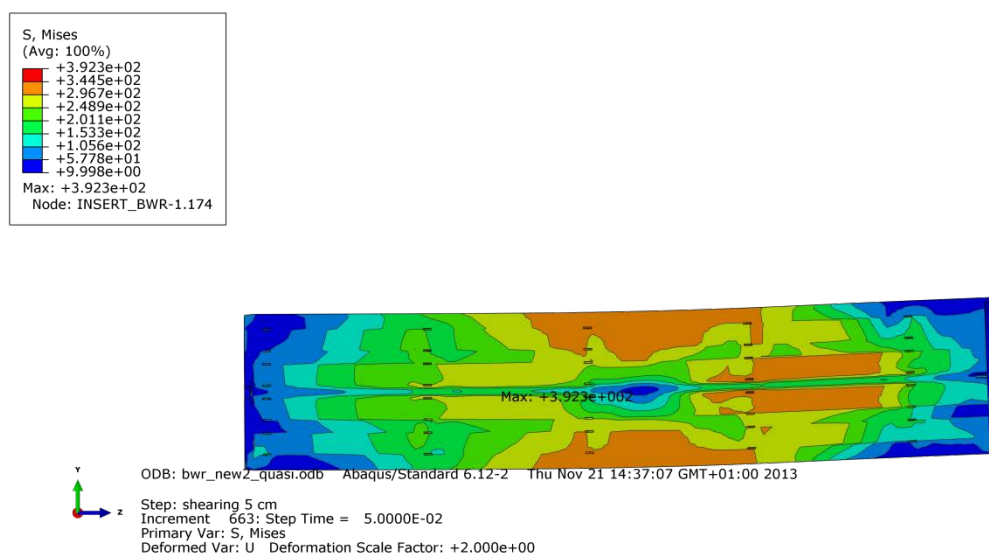


Figure A7-2 Plot showing Mises stress [MPa] for the insert after 5 cm shearing.

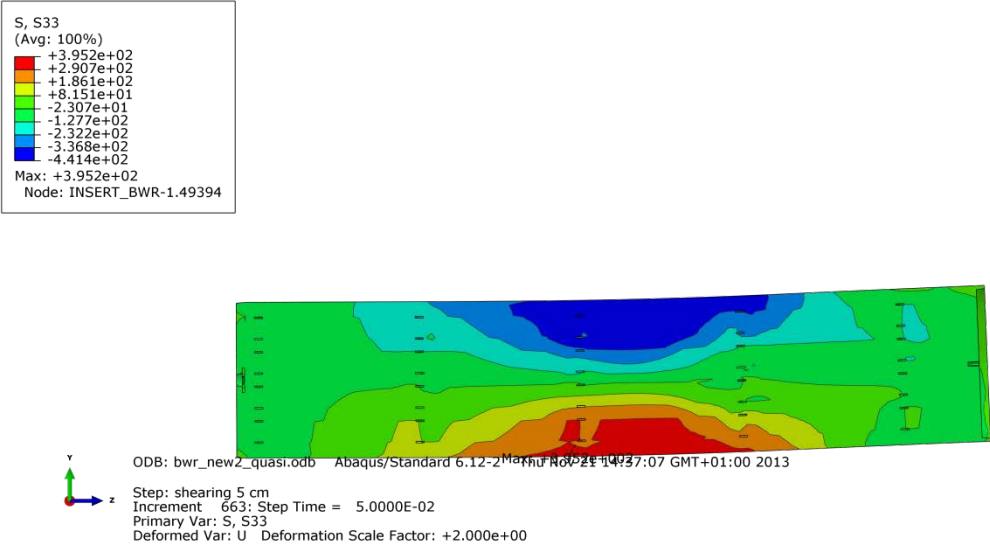


Figure A7-3 Plot showing axial stress [MPa] for the insert after 5 cm shearing.

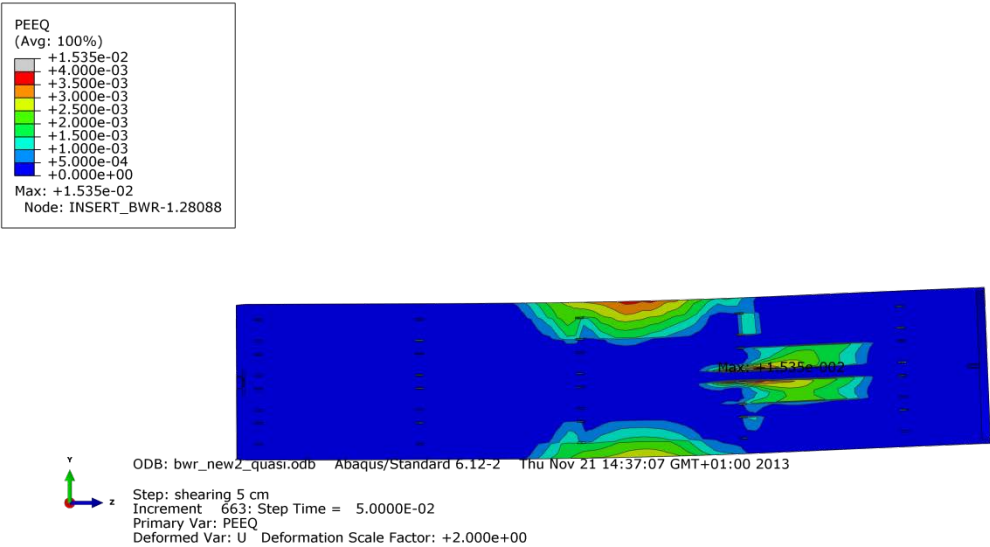


Figure A7-4 Plot showing equivalent plastic strain (PEEQ) for the insert after 5 cm shearing.

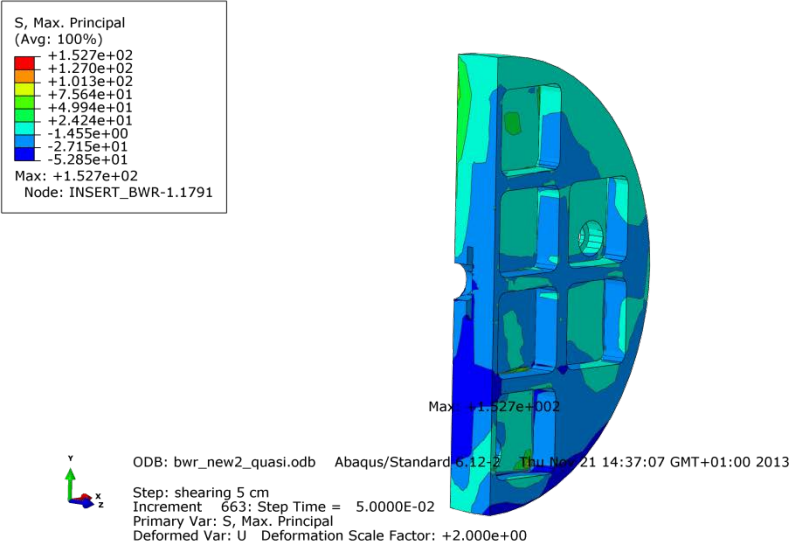


Figure A7-5 Plot showing maximum principal stress [MPa] for the insert base after 5 cm shearing.

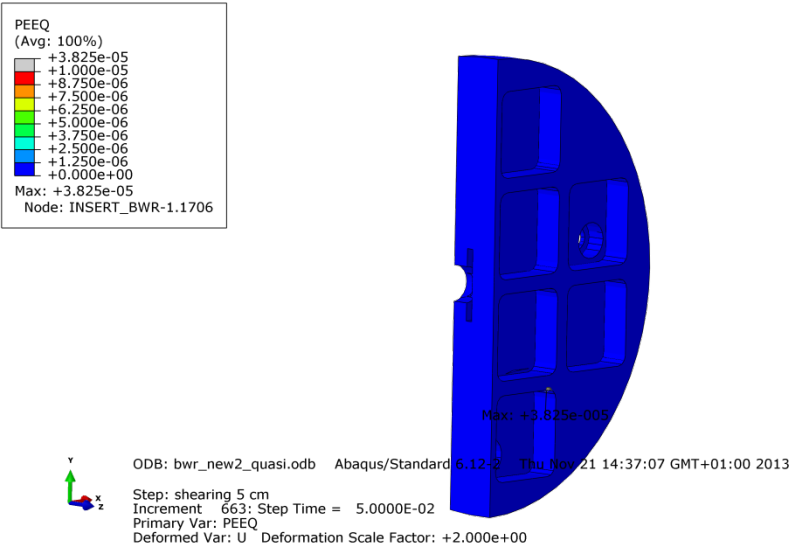


Figure A7-6 Plot showing equivalent plastic strain (PEEQ) for the insert base after 5 cm shearing.

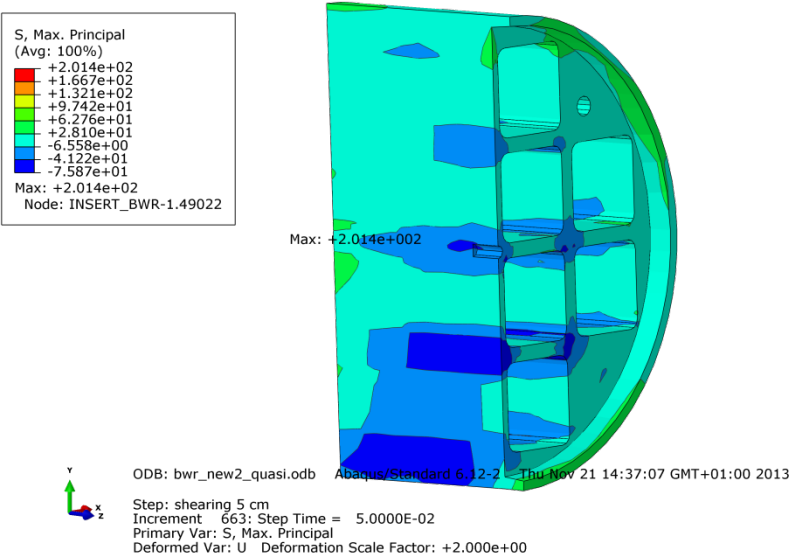


Figure A7-7 Plot showing maximum principal stress [MPa] for the insert top after 5 cm shearing.

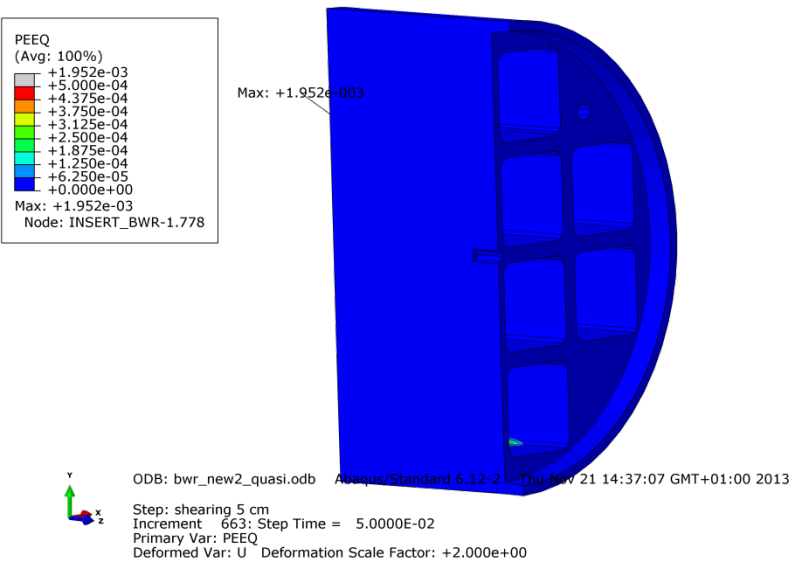


Figure A7-8 Plot showing equivalent plastic strain (PEEQ) for the insert top after 5 cm shearing.

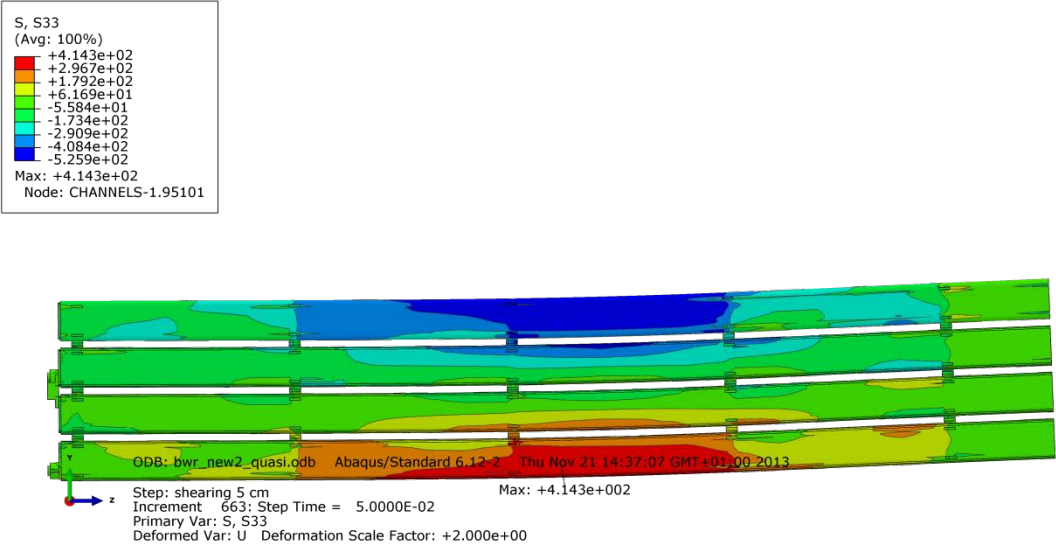


Figure A7-9 Plot showing axial stress [MPa] for the steel channel tubes after 5 cm shearing.

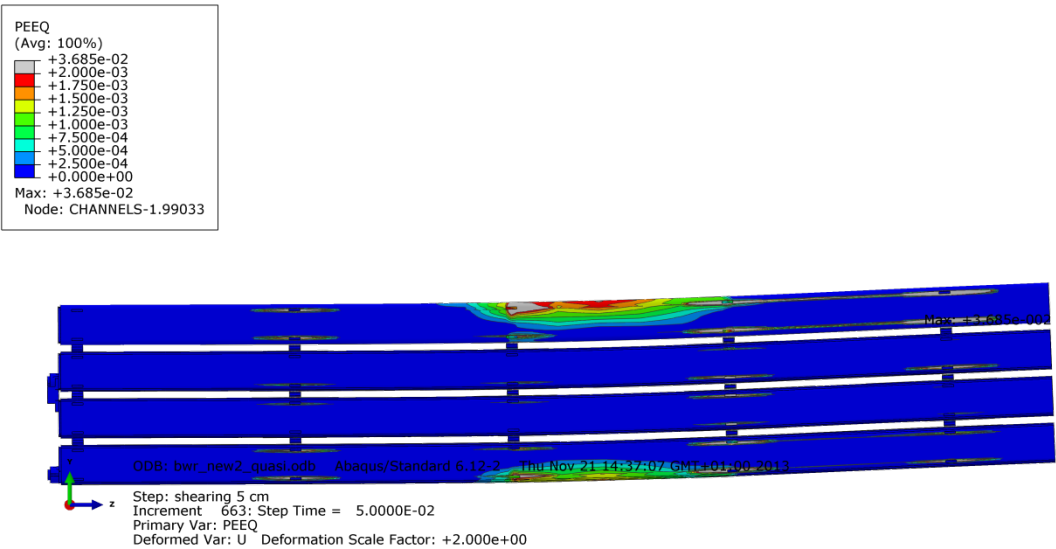


Figure A7-10 Plot showing equivalent plastic strain (PEEQ) for the steel channel tubes after 5 cm shearing.

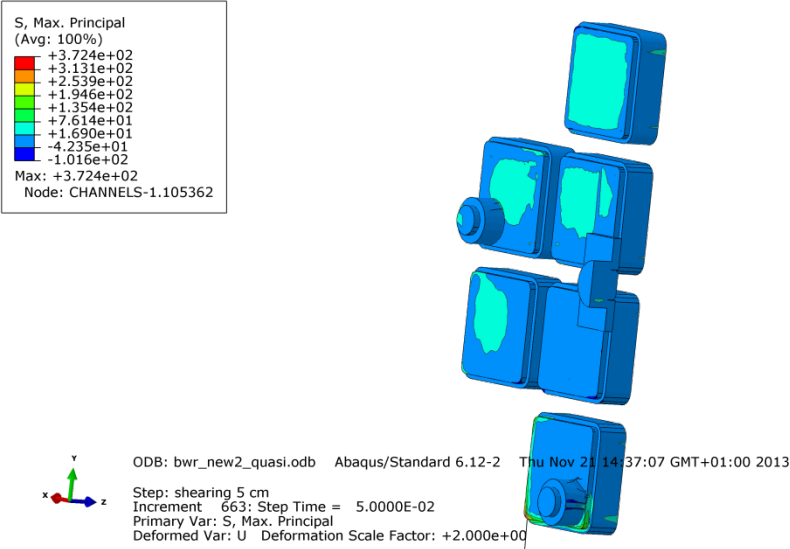


Figure A7-11 Plot showing maximum principal stress [MPa] for the steel channel tubes base plates after 5 cm shearing.

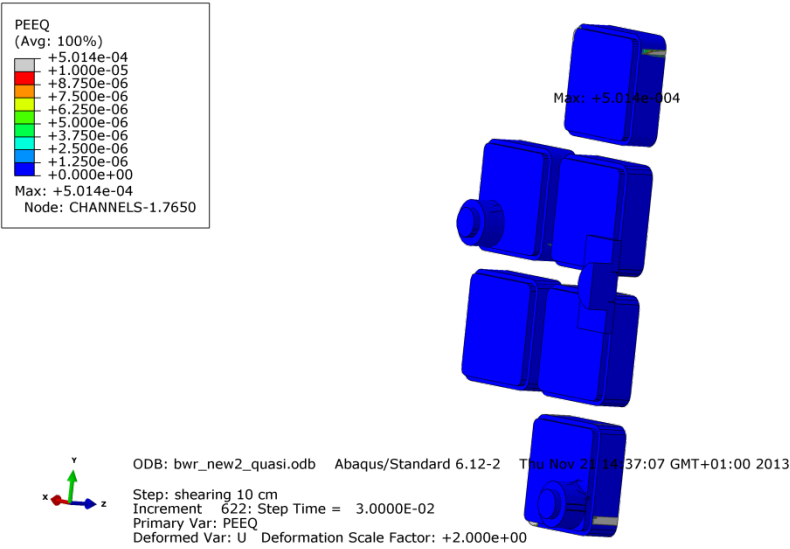


Figure A7-12 Plot showing equivalent plastic strain (PEEQ) for the steel channel tubes base plates after 5 cm shearing.

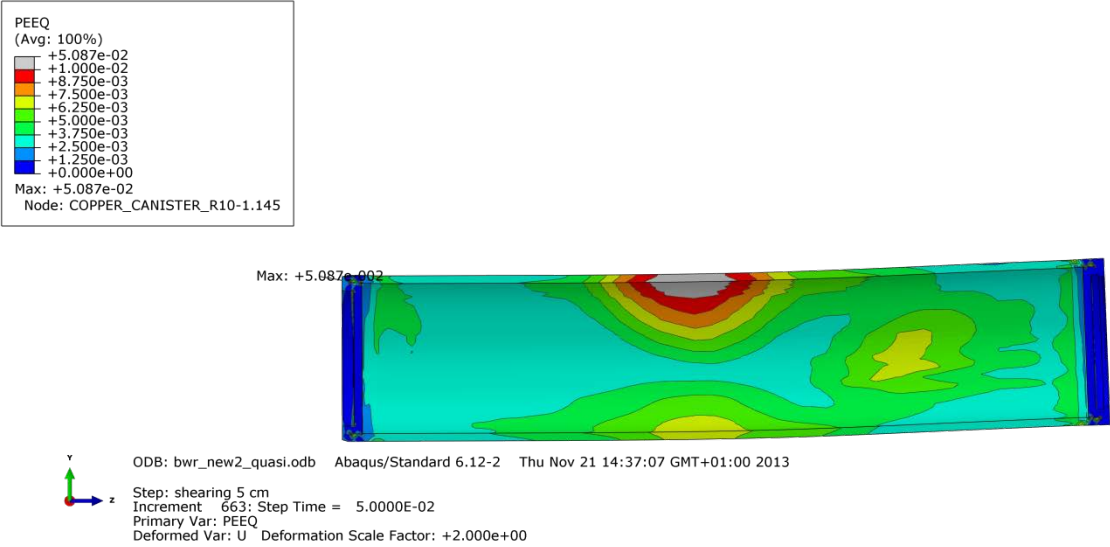


Figure A7-13 Plot showing equivalent plastic strain (PEEQ) for the copper shell after 5 cm shearing.

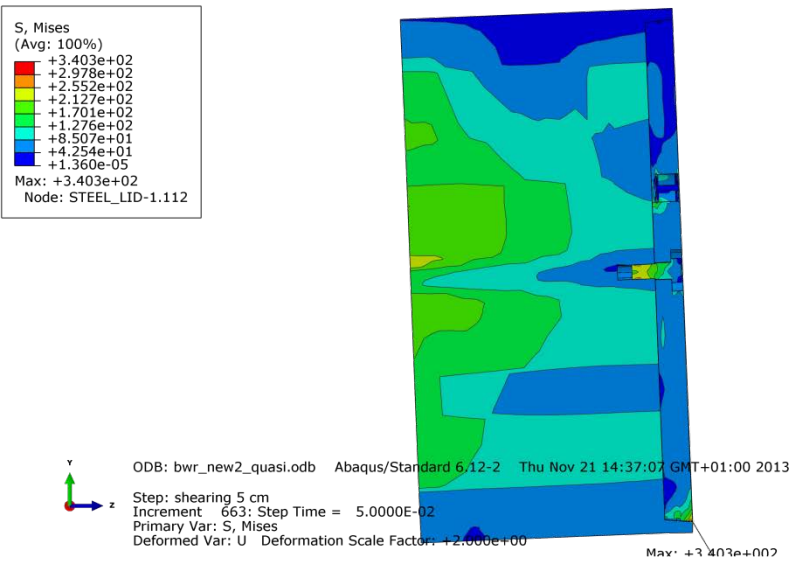


Figure A7-14 Plot showing Mises stress [MPa] close to the steel lid fixing screw after 5 cm shearing.

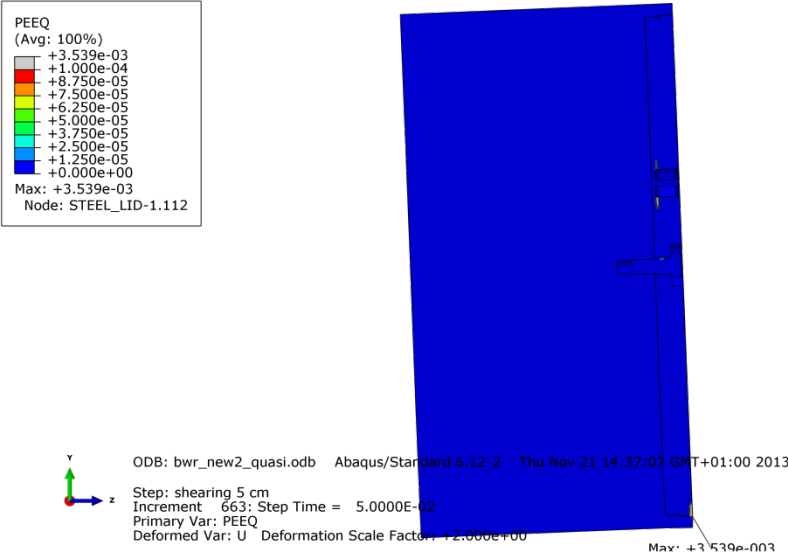


Figure A7-15 Plot showing equivalent plastic strain (PEEQ) close to the steel lid fixing screw after 5 cm shearing.

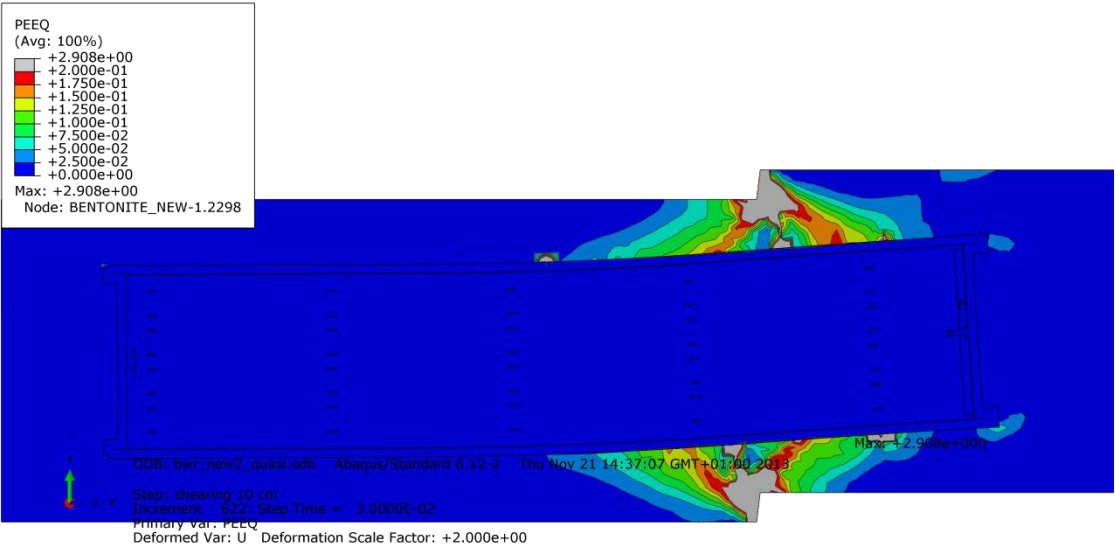


Figure A7-16 Plot showing equivalent plastic strain (PEEQ) after 8 cm shearing.

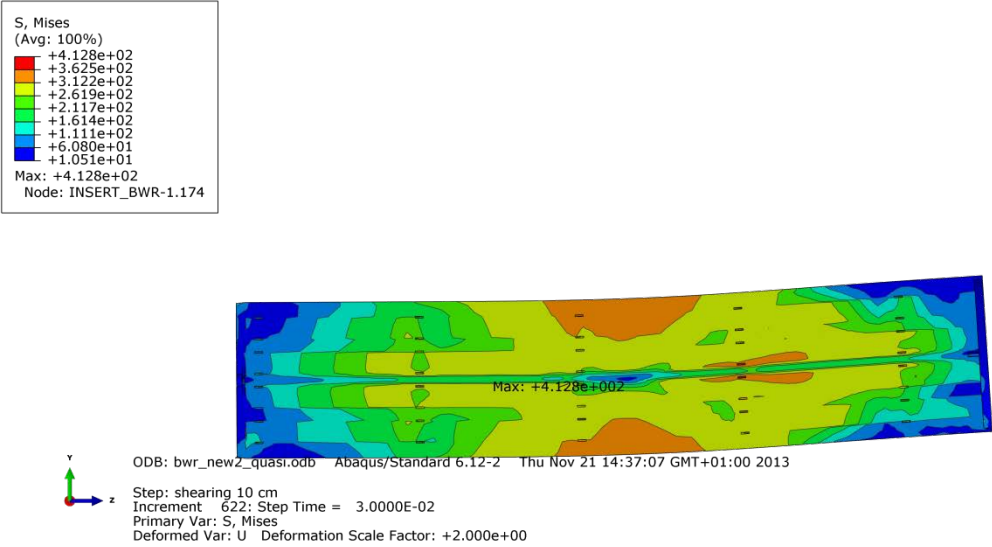


Figure A7-17 Plot showing Mises stress [MPa] for the insert after 8 cm shearing.

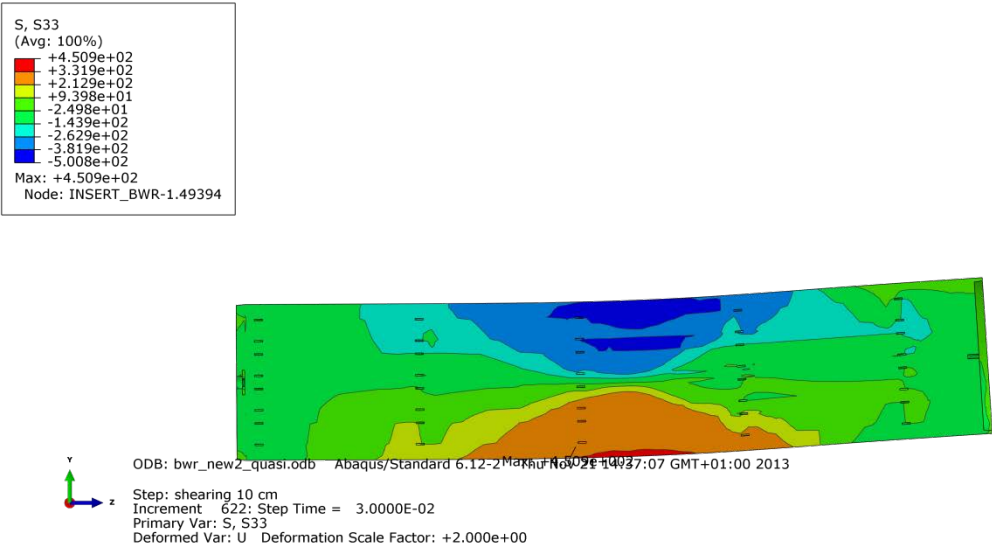


Figure A7-18 Plot showing axial stress [MPa] for the insert after 8 cm shearing.

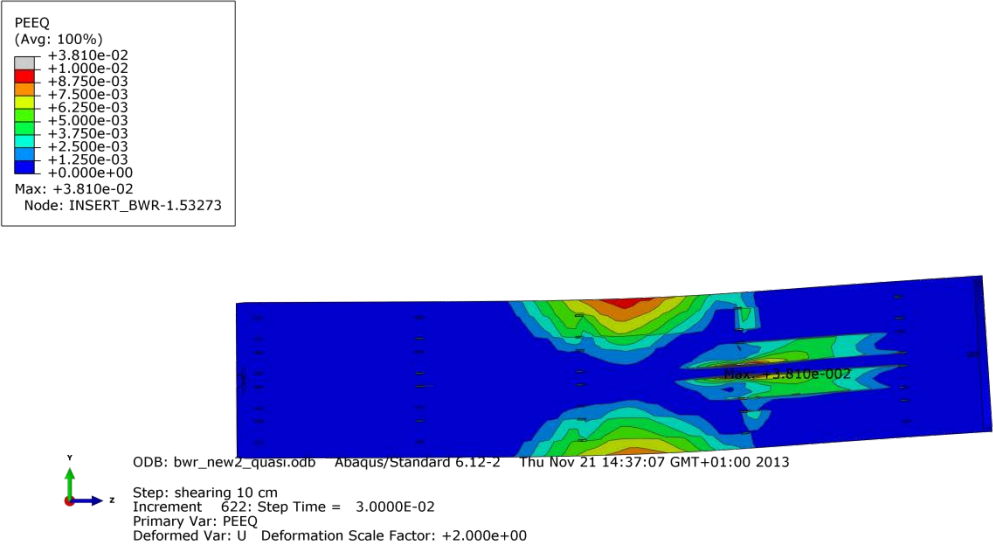


Figure A7-19 Plot showing equivalent plastic strain (PEEQ) for the insert after 8 cm shearing.

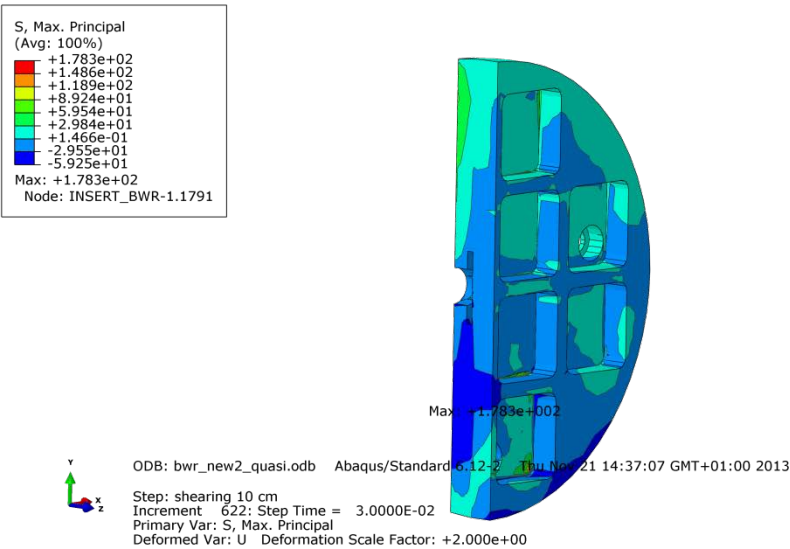


Figure A7-20 Plot showing maximum principal stress [MPa] for the insert base after 8 cm shearing.

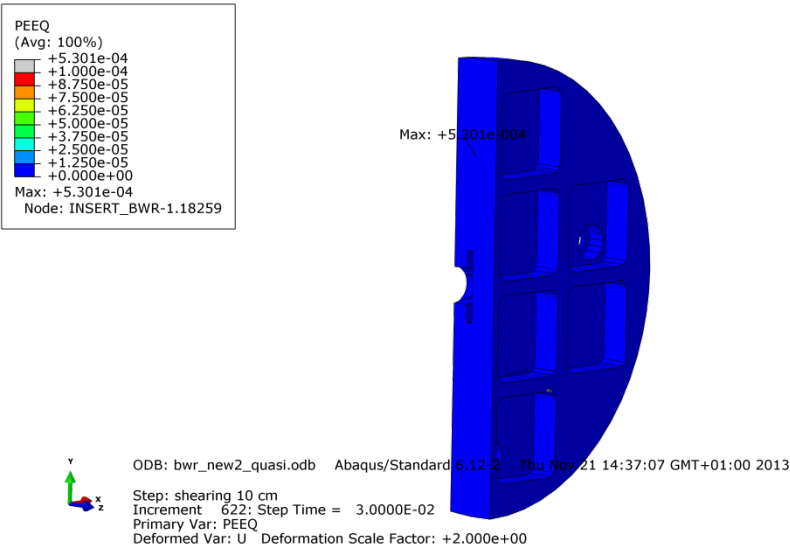


Figure A7-21 Plot showing equivalent plastic strain (PEEQ) for the insert base after 8 cm shearing.

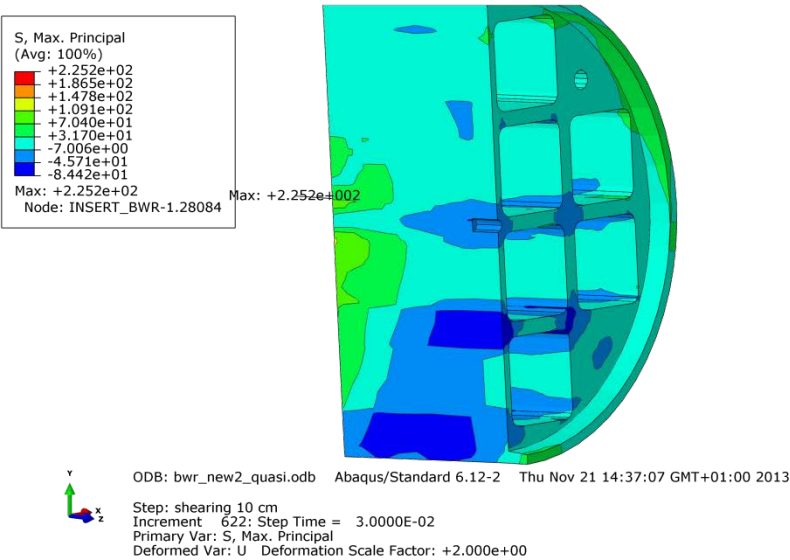


Figure A7-22 Plot showing maximum principal stress [MPa] for the insert top after 8 cm shearing.

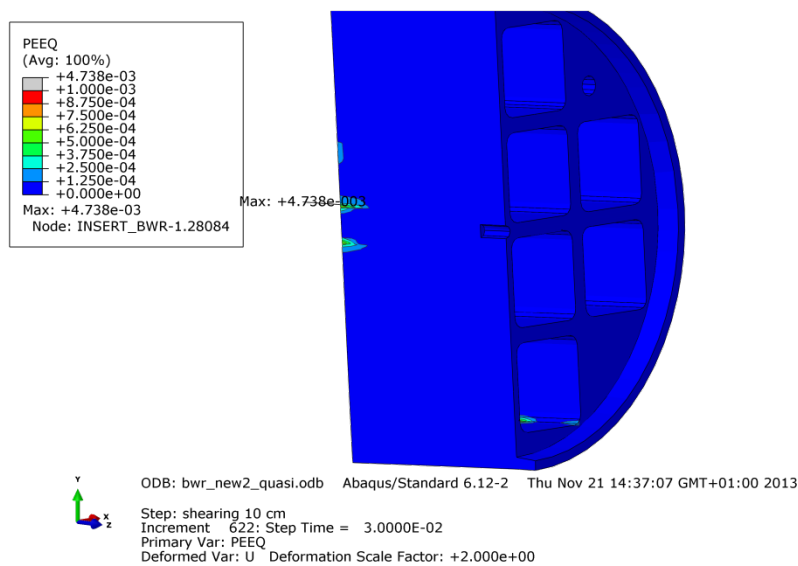


Figure A7-23 Plot showing equivalent plastic strain (PEEQ) for the insert top after 8 cm shearing.

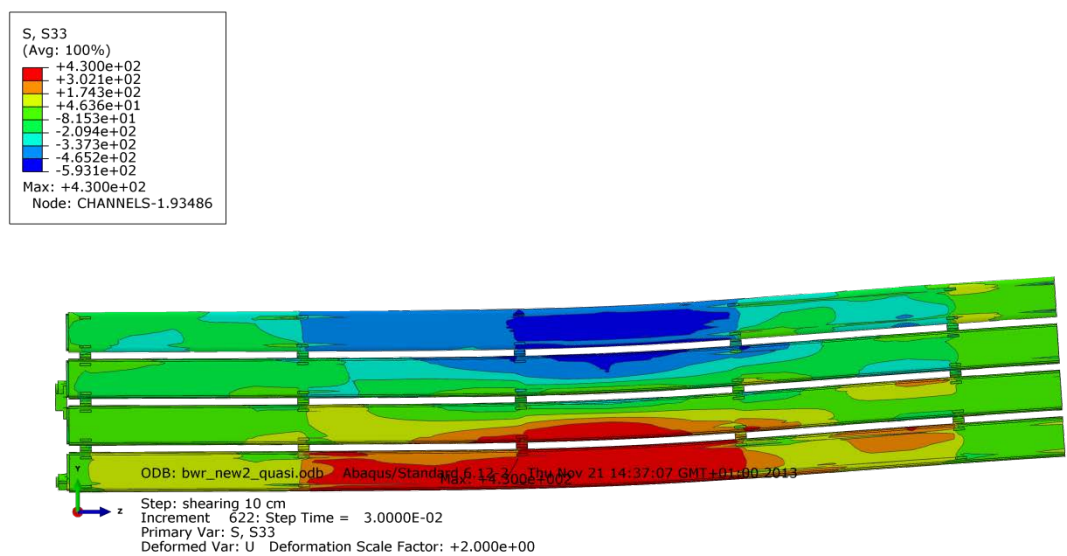


Figure A7-24 Plot showing axial stress [MPa] for the steel channel tubes after 8 cm shearing.

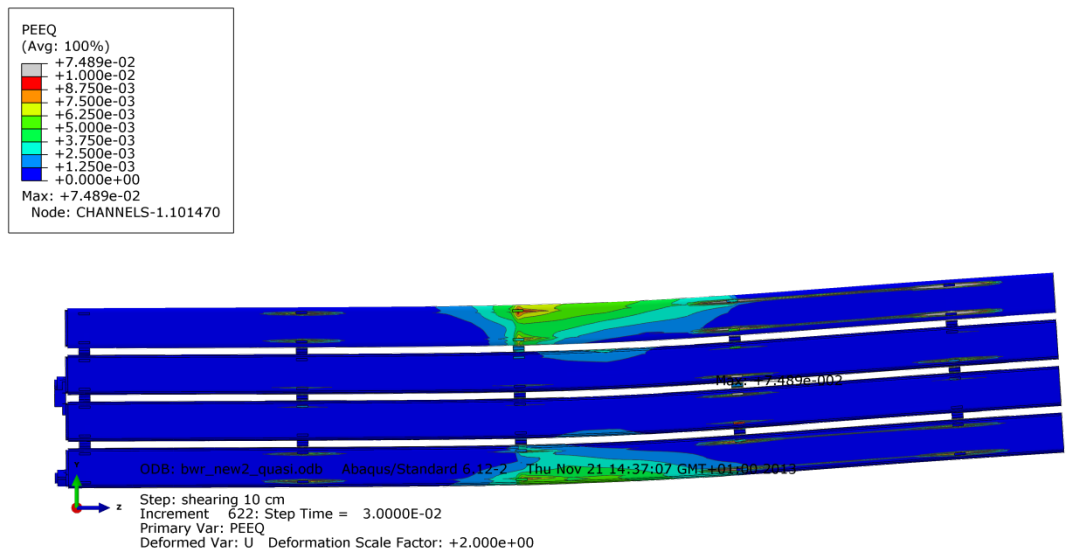


Figure A7-25 Plot showing equivalent plastic strain (PEEQ) for the steel channel tubes after 8 cm shearing.

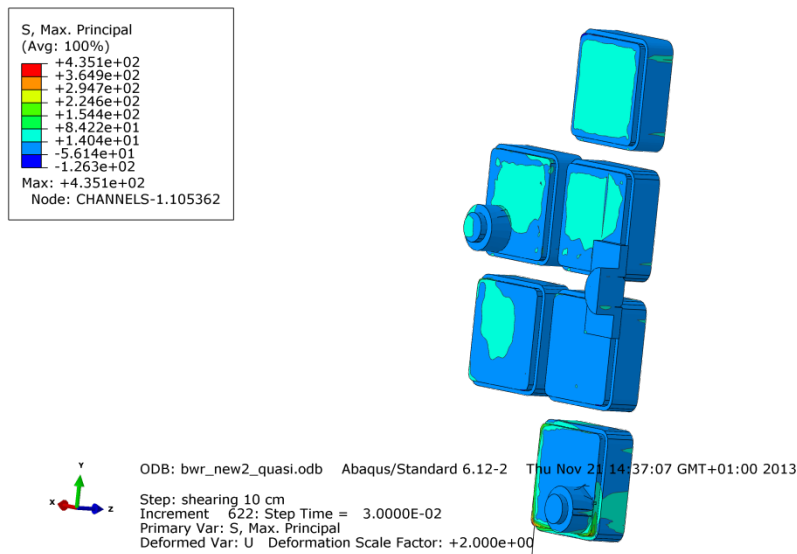


Figure A7-26 Plot showing maximum principal stress [MPa] for the steel channel tubes base plates after 8 cm shearing.

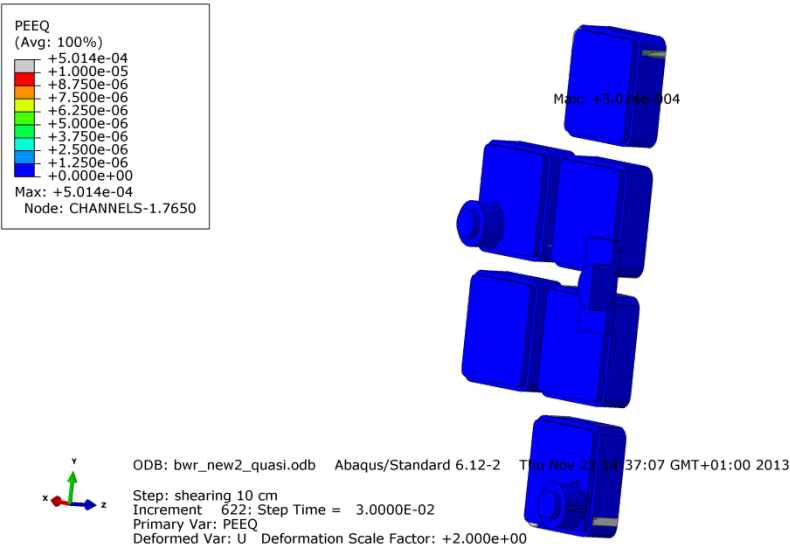


Figure A7-27 Plot showing equivalent plastic strain (PEEQ) for the steel channel tubes base plates after 8 cm shearing.

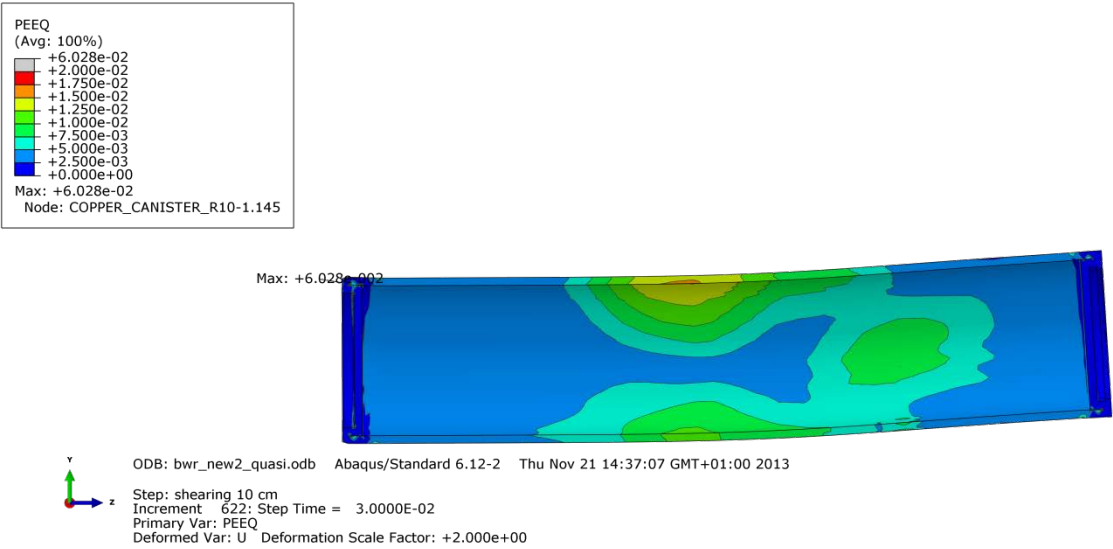


Figure A7-28 Plot showing equivalent plastic strain (PEEQ) for the copper shell after 8 cm shearing.

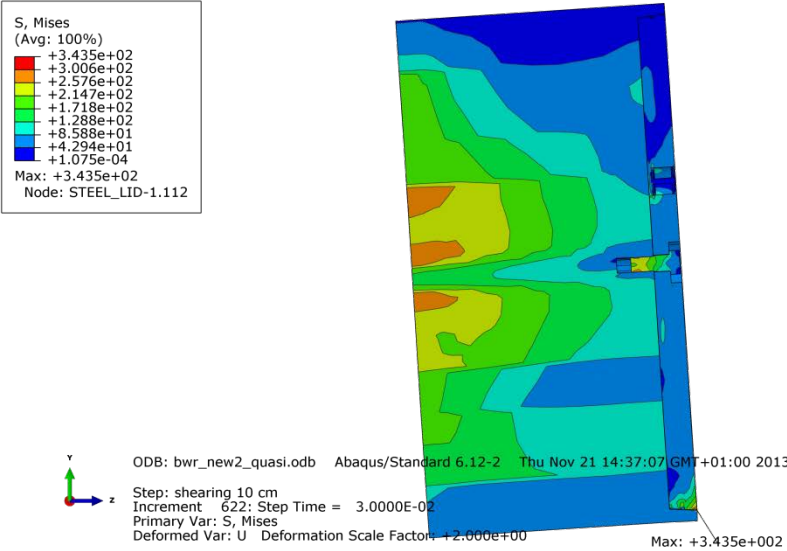


Figure A7-29 Plot showing Mises stress [MPa] close to the steel lid fixing screw after 8 cm shearing.

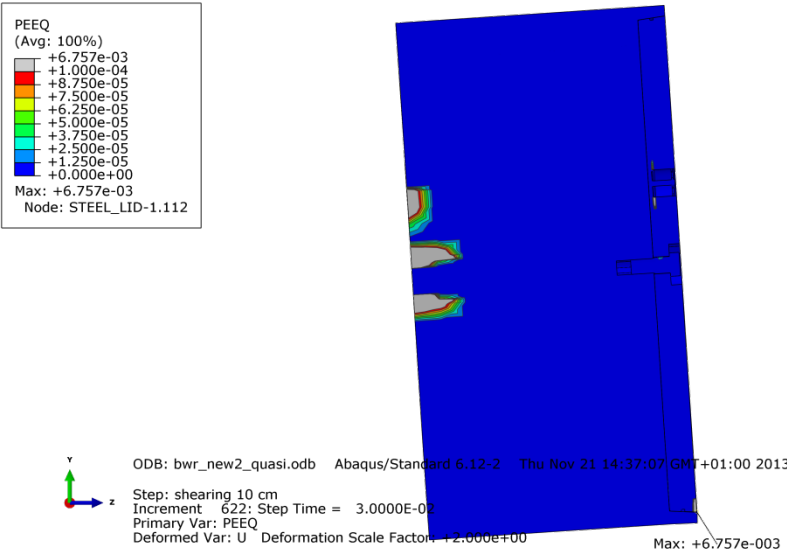


Figure A7-30 Plot showing equivalent plastic strain (PEEQ) close to the steel lid fixing screw after 8 cm shearing.

Appendix 8 – Comparison pwr_new3_quasi versus model6g_PWR_normal_quarter_2050ca3 at 5 cm shearing

Plots showing comparison between detailed modelling and the reference case at shearing magnitude 5 cm (horizontal shearing at $\frac{3}{4}$ distance from insert base). The view shows the symmetry plane and all deformations are scaled by a factor of two.

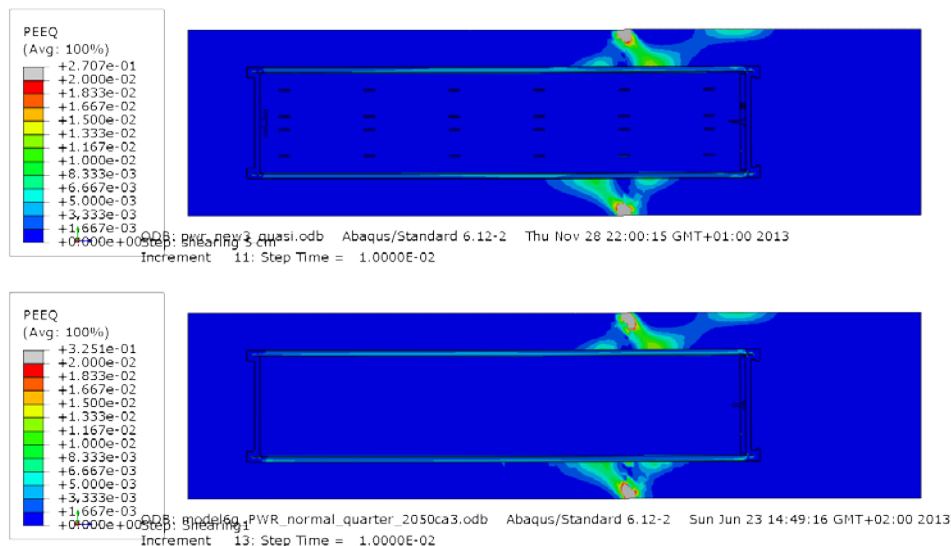


Figure A8-1 Plot showing plastic equivalent strain (PEEQ) after 5 cm shearing for detailed PWR model (top) and the reference PWR model (bottom).

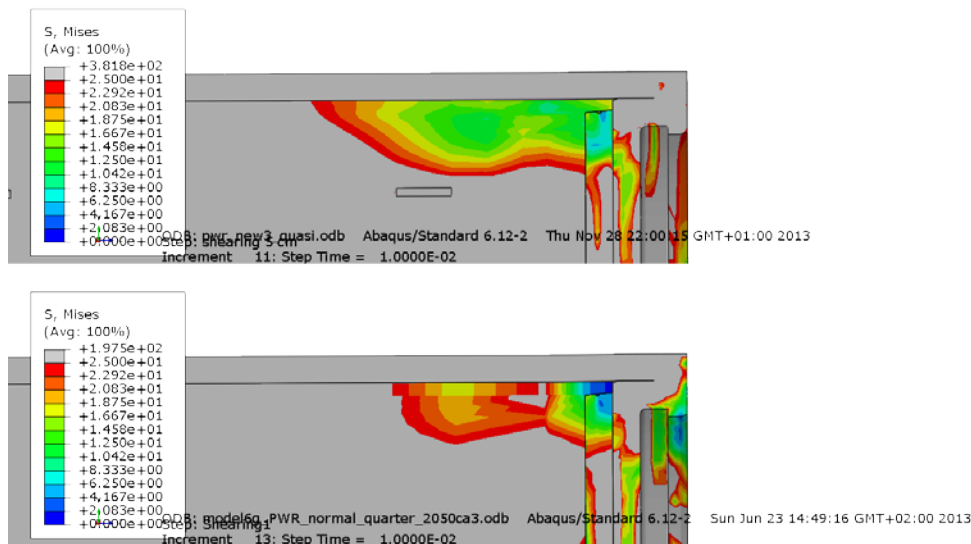


Figure A8-2 Plot showing Mises stress [MPa] at the top left corner after 5 cm shearing for detailed PWR model (top) and the reference PWR model (bottom).

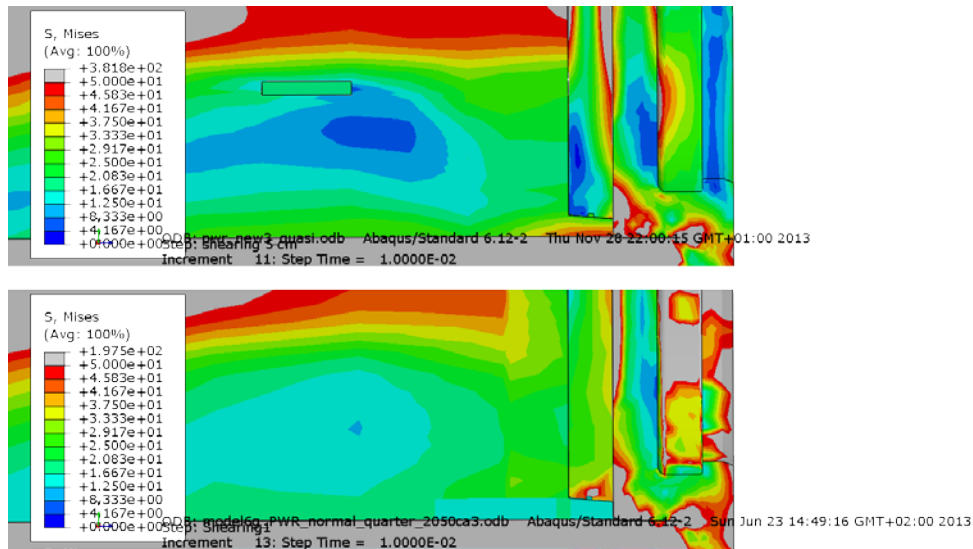


Figure A8-3 Plot showing Mises stress [MPa] at the top right corner after 5 cm shearing for detailed PWR model (top) and the reference PWR model (bottom).

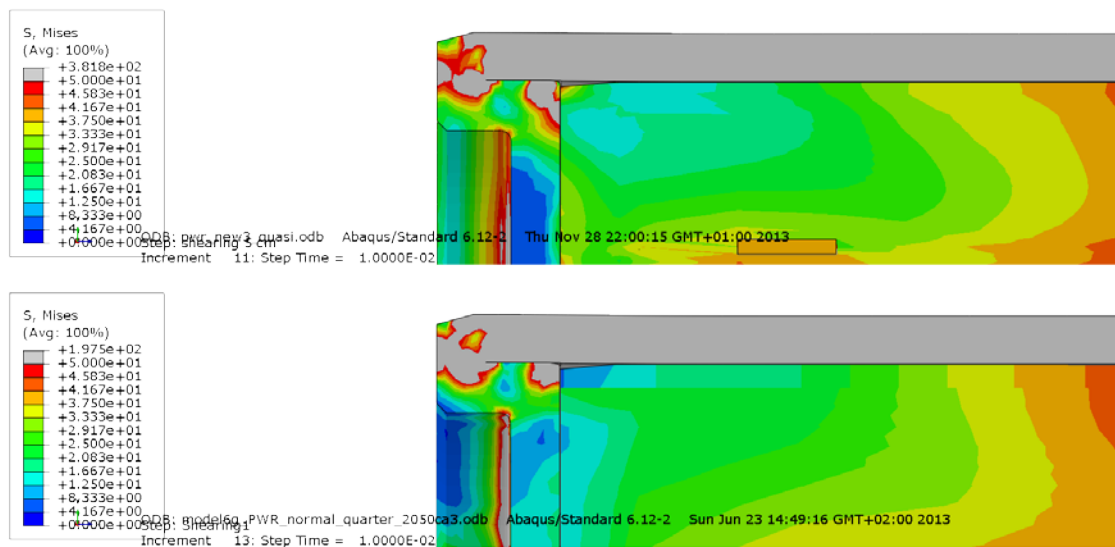


Figure A8-4 Plot showing Mises stress [MPa] at the bottom left corner after 5 cm shearing for detailed PWR model (top) and the reference PWR model (bottom).

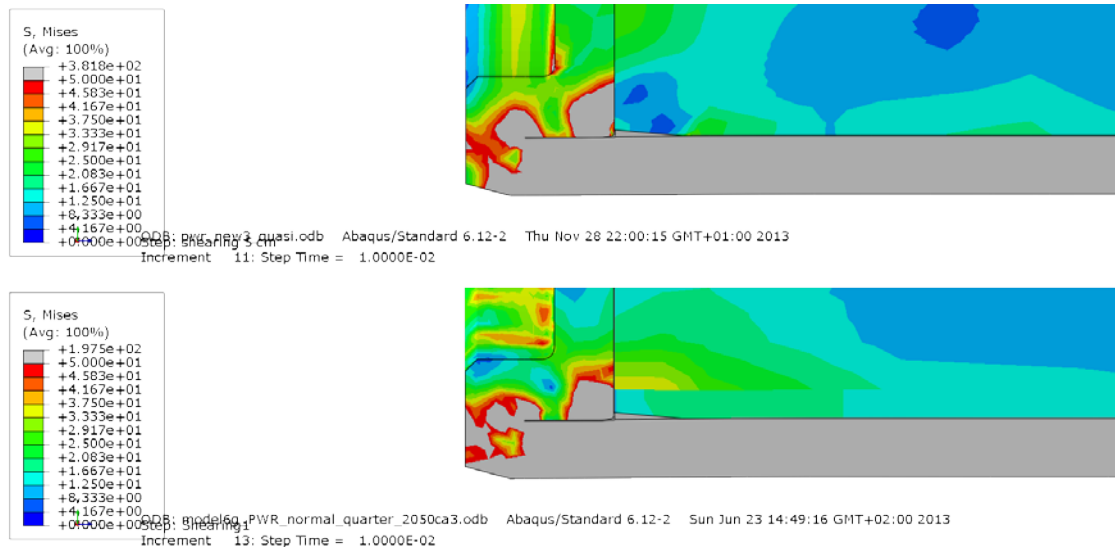


Figure A8-5 Plot showing Mises stress [MPa] at the base right corner after 5 cm shearing for detailed PWR model (top) and the reference PWR model (bottom).

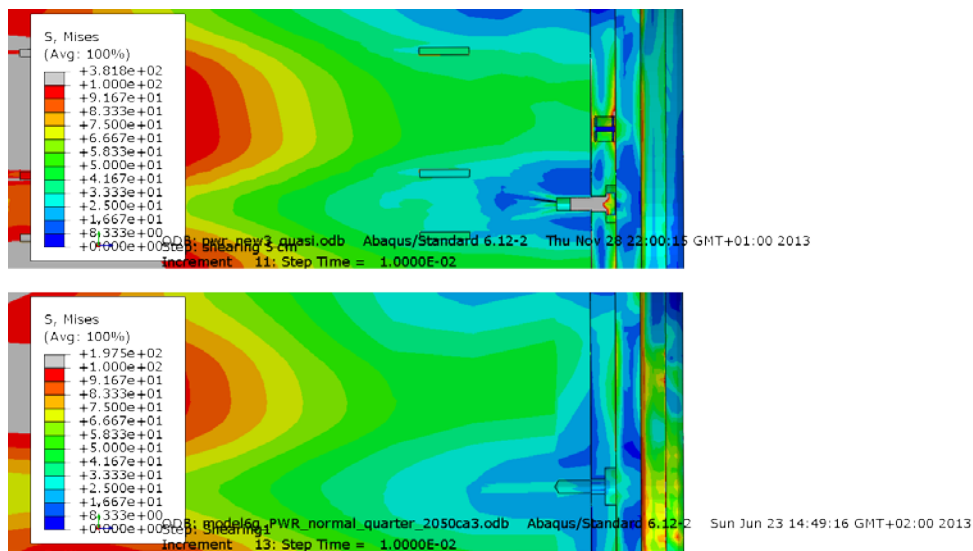


Figure A8-6 Plot showing Mises stress [MPa] at the top close to the screw after 5 cm shearing for detailed PWR model (top) and the reference PWR model (bottom).

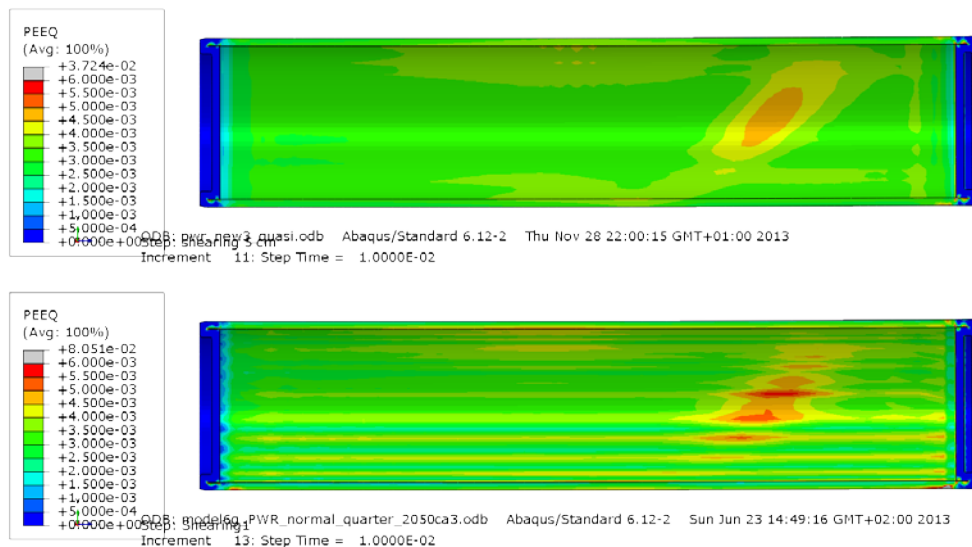


Figure A8-7 Plot showing plastic equivalent strain (PEEQ) for the copper shell after 5 cm shearing for detailed PWR model (top) and the reference PWR model (bottom).

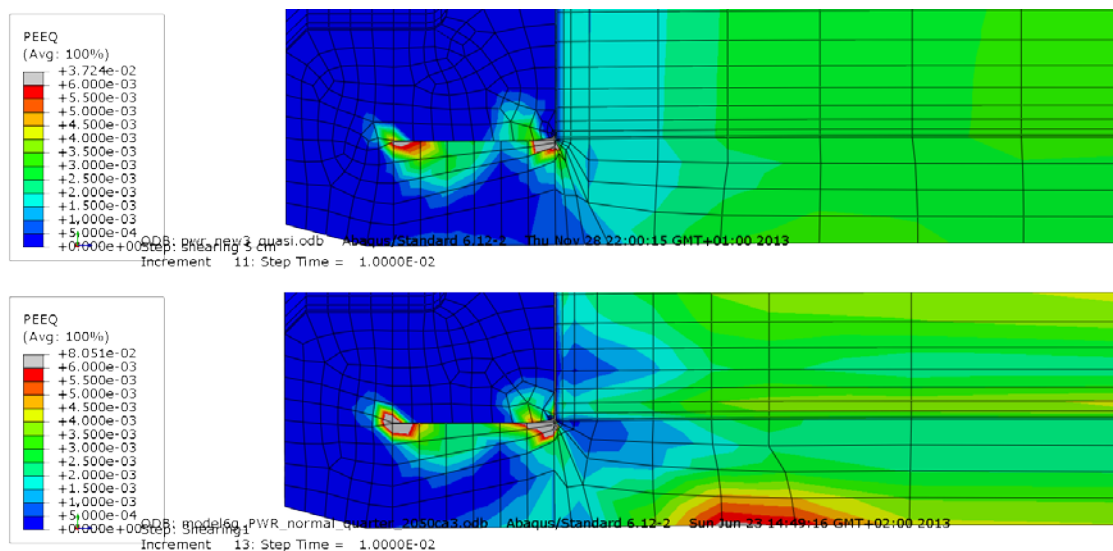


Figure A8-8 Plot showing plastic equivalent strain (PEEQ) for the copper shell after 5 cm shearing for detailed PWR model (top) and the reference PWR model (bottom).



Figure A8-9 Plot showing plastic equivalent strain (PEEQ) for the insert after 5 cm shearing for detailed PWR model (top) and the reference PWR model (bottom).

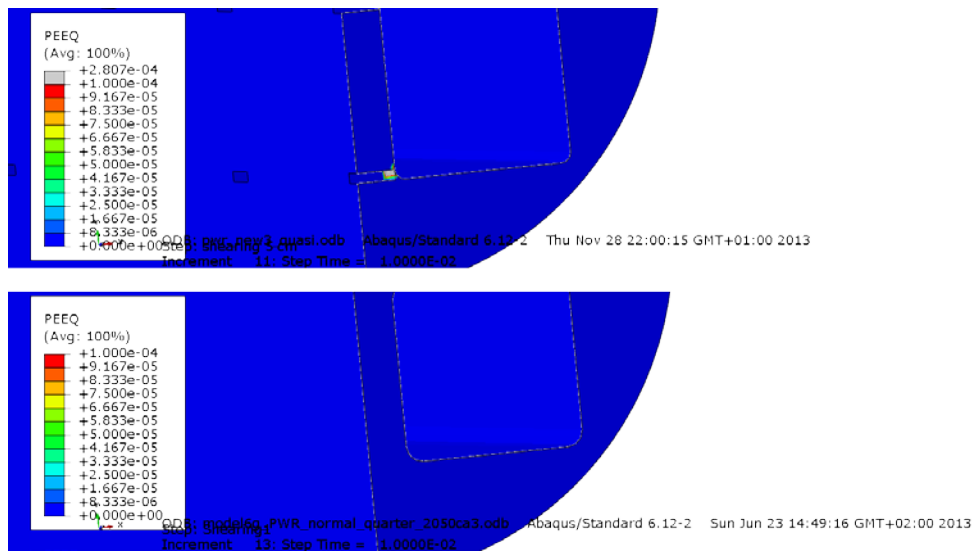


Figure A8-10 Plot showing plastic equivalent strain (PEEQ) for the insert after 5 cm shearing for detailed PWR model (top) and the reference PWR model (bottom).

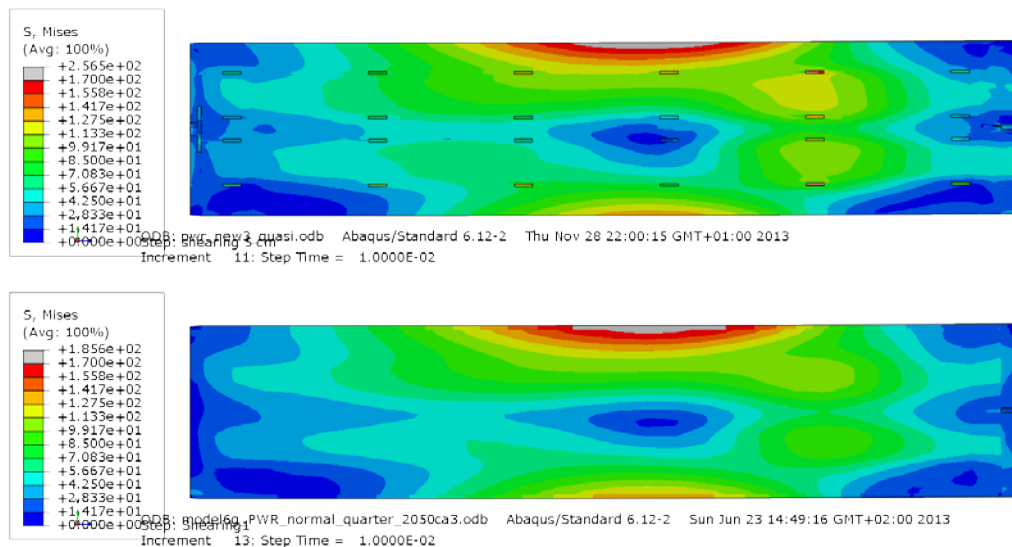


Figure A8-11 Plot showing Mises stress [MPa] for the insert after 5 cm shearing for detailed PWR model (top) and the reference PWR model (bottom).

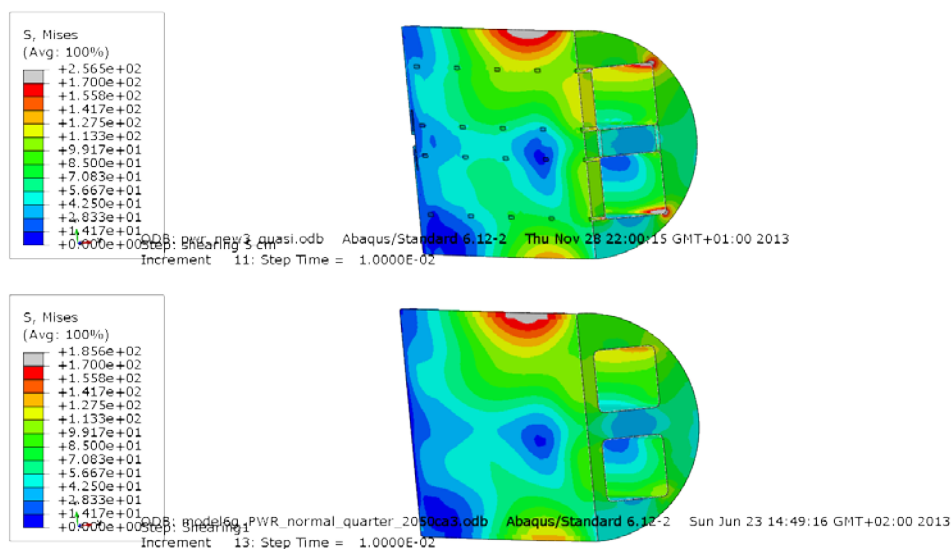


Figure A8-12 Plot showing Mises stress [MPa] for the insert after 5 cm shearing for detailed PWR model (top) and the reference PWR model (bottom).

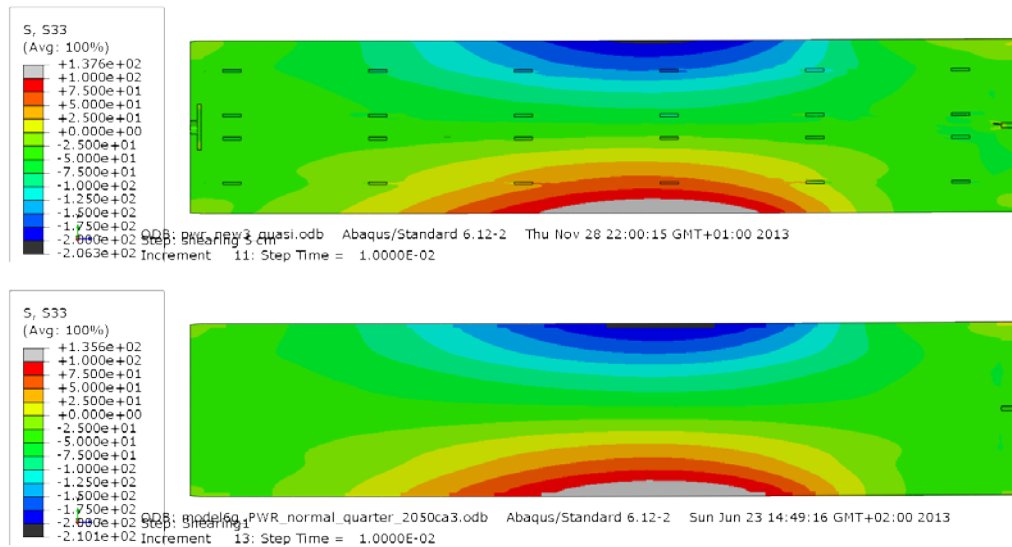


Figure A8-13 Plot showing axial stress, S_{33} , [MPa] for the insert after 5 cm shearing for detailed PWR model (top) and the reference PWR model (bottom).

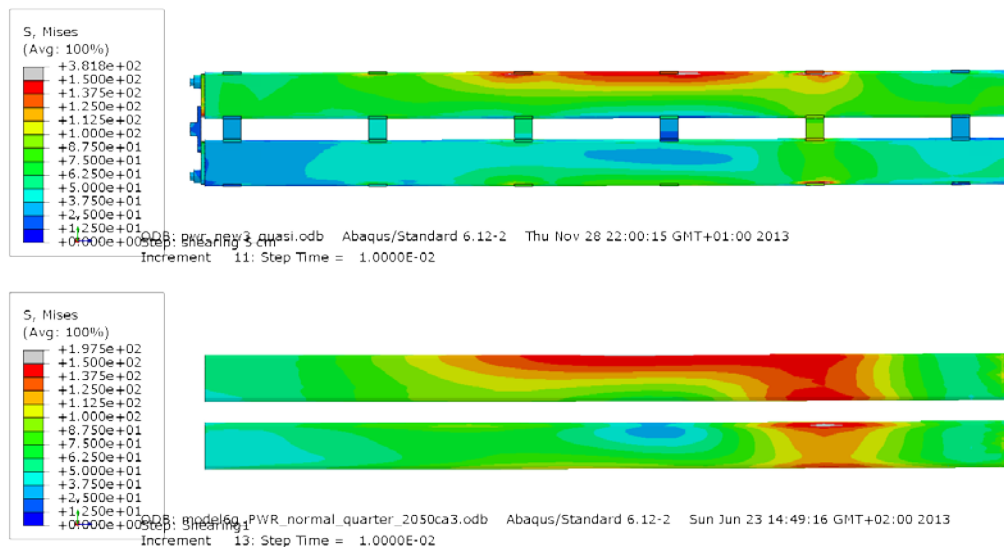


Figure A8-14 Plot showing Mises stress [MPa] for the steel channel tubes after 5 cm shearing for detailed PWR model (top) and the reference PWR model (bottom).

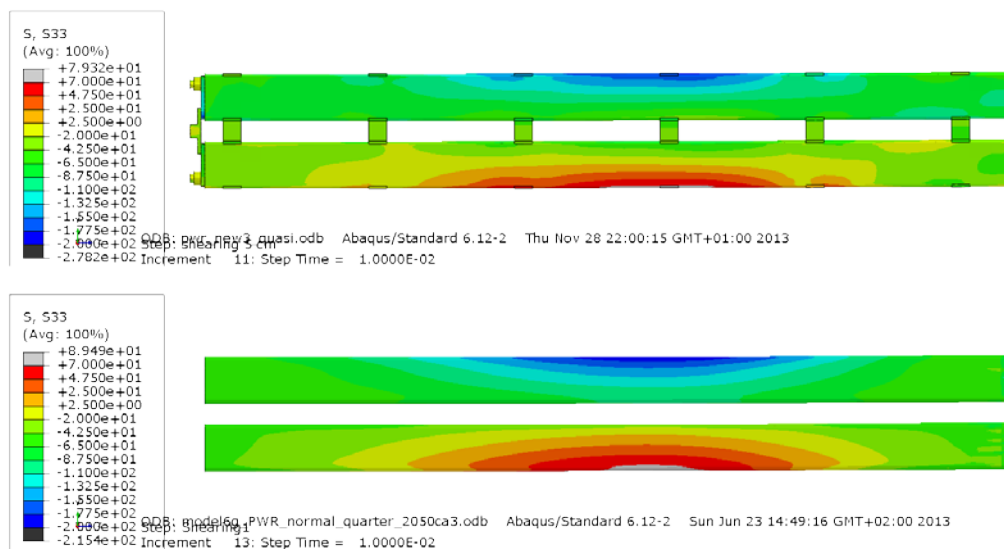


Figure A8-15 Plot showing axial stress, $S33$, [MPa] for the steel channel tubes after 5 cm shearing for detailed PWR model (top) and the reference PWR model (bottom).

Appendix 9 – Storage of files

This report is based on the results from a lot of FE-simulations using ABAQUS which is a commercial available code and is thus not stored as part of the work. Below is a short description of files used in the project and directories for storage of these. These files are also stored at SKB.

The files are stored in directories as:

Geometry Input-files Plots Detailed analyses BWR/PWR.docx - this report Scripts

1 – Plot-files used in the report

Contents in C:\Users\jhd\mappar\skb\Detailed_PWR_BWR\Plots

Geometry plots

Fig2-1-shearing_planes.png
Fig2-2-detailes.png
Fig2-3-detailes_washer.png
Fig2-4-detailes_bottom.png
Fig3-1-buffer.png
Fig3-steel_lid.png
Fig3-screw.png
Fig3-washer.png
Fig3-pwr-insert1.png
Fig3-pwr-insert2.png
Fig3-pwr-insert3.png
Fig3-pwr-insert4.png
Fig3-pwr-channels1.png
Fig3-pwr-channels2.png
Fig3-pwr-channels3.png
Fig3-bwr-insert1.png
Fig3-bwr-insert2.png
Fig3-bwr-insert3.png
Fig3-bwr-insert4.png
Fig3-bwr-insert5.png
Fig3-bwr-insert6.png
Fig3-bwr-channels1.png
Fig3-bwr-channels2.png
Fig3-bwr-channels3.png

Contents in C:\Users\jhd\mappar\skb\Detailed_PWR_BWR\Plots

Results – comparison

compare-pwr_new-model6g_detail_mid_corner_plates-mises.png
compare-pwr_new-model6g_detail_bottom-mises.png
compare-pwr_new-model6g_detail_hole-mises.png
compare-pwr_new-model6g_detail_screw-mises.png
compare-pwr_new-model6g_detail_bot_corner-mises.png
compare-pwr_new-model6g_detail_bot2_corner-mises.png
compare-pwr_new-model6g_detail_top2_corner-mises.png
compare-pwr_new-model6g_detail_top_corner-mises.png
compare-pwr_new-model6g_channels-mises.png
compare-pwr_new-model6g_channels-s33.png
compare-pwr_new-model6g_insert-s33.png
compare-pwr_new-model6g_insert-mises.png
compare-pwr_new-model6g_insert-mises2.png
compare-pwr_new-model6g_insert-pee2.png
compare-pwr_new-model6g_insert-pee.png
compare-pwr_new-model6g_copper-pee.png
compare-pwr_new-model6g_copper-pee_max.png
compare-pwr_new-model6g-pee.png
compare-pwr_new-model6g_detail_mesh3-mises.png
compare-bwr_new-model6g_detail_mid_corner_plates-mises.png
compare-bwr_new-model6g_detail_bottom-mises.png
compare-bwr_new-model6g_detail_hole-mises.png
compare-bwr_new-model6g_detail_screw-mises.png
compare-bwr_new-model6g_detail_bot_corner-mises.png
compare-bwr_new-model6g_detail_bot2_corner-mises.png
compare-bwr_new-model6g_detail_top2_corner-mises.png
compare-bwr_new-model6g_detail_top_corner-mises.png
compare-bwr_new-model6g_channels-mises.png
compare-bwr_new-model6g_channels-s33.png
compare-bwr_new-model6g_insert-s33.png
compare-bwr_new-model6g_insert-mises.png
compare-bwr_new-model6g_insert-mises2.png
compare-bwr_new-model6g_insert-pee2.png
compare-bwr_new-model6g_insert-pee.png
compare-bwr_new-model6g_copper-pee.png
compare-bwr_new-model6g_copper-pee_max.png
compare-bwr_new-model6g-pee.png
compare-bwr_new-model6g_detail_mesh3-mises.png

Contents in C:\Users\jhd\mappar\skb\Detailed_PWR_BWR\Plots

Results – comparison

compare_lock_shear-top_right-mises.png
compare_lock_shear-top_right-pee.png
compare_lock_shear-top_right-s22.png
compare_lock_shear-top_left-s22.png
compare_lock_shear-top_left-pee.png
compare_gap_moved-position2.png
compare_gap_moved-position1.png
compare_gap_moved-insert_pee.png
compare_gap_moved-channels_s33.png
compare_gap_moved-channels_pee.png
compare_gap_moved-pee.png
compare_gap_moved-mises.png
compare_gap_moved-top_right-pee.png
compare_gap_moved-top_right-s22.png
compare_gap_moved-top_left-s22.png
compare_gap_moved-top_left-pee.png
compare_eccentric-insert_position.png
compare_eccentric-insert_pee.png
compare_eccentric-channels_s33.png
compare_eccentric-channels_pee.png
compare_eccentric-pee.png
compare_eccentric-mises.png
compare_eccentric-top_right-pee.png
compare_eccentric-top_right-s22.png
compare_eccentric-top_left-s22.png
compare_eccentric-top_left-pee.png
compare_pwr_screw-pee-8cm.png
compare_pwr_screw-u2-8cm.png
compare_pwr_screw-pee-5cm.png
compare_pwr_screw-s22-5cm.png
compare_pwr_screw-u2-5cm.png
compare_pwr_screw-pee-gravity.png
compare_pwr_screw-s33-gravity.png

Appendix 1

pwr_new2_quasi 10cm peeq screw.png
pwr_new2_quasi 10cm mises screw.png
pwr_new2_quasi 10cm peeq channels_bot.png
pwr_new2_quasi 10cm maxPrin channels_bot.png
pwr_new2_quasi 10cm S33 channels.png
pwr_new2_quasi 10cm peeq channels.png
pwr_new2_quasi 10cm peeq insert_bot.png
pwr_new2_quasi 10cm maxPrin insert_bot.png
pwr_new2_quasi 10cm peeq insert_top.png
pwr_new2_quasi 10cm maxPrin insert_top.png
pwr_new2_quasi 10cm peeq insert.png
pwr_new2_quasi 10cm S33 insert.png
pwr_new2_quasi 10cm mises insert.png
pwr_new2_quasi 10cm peeq.png
pwr_new2_quasi 5cm peeq screw.png
pwr_new2_quasi 5cm mises screw.png
pwr_new2_quasi 5cm peeq channels_bot.png
pwr_new2_quasi 5cm maxPrin channels_bot.png
pwr_new2_quasi 5cm S33 channels.png
pwr_new2_quasi 5cm peeq channels.png
pwr_new2_quasi 5cm peeq insert_bot.png
pwr_new2_quasi 5cm maxPrin insert_bot.png
pwr_new2_quasi 5cm peeq insert_top.png
pwr_new2_quasi 5cm maxPrin insert_top.png
pwr_new2_quasi 5cm peeq insert.png
pwr_new2_quasi 5cm S33 insert.png
pwr_new2_quasi 5cm mises insert.png
pwr_new2_quasi 5cm peeq.png

Appendix 2

pwr_eccentric3_quasi 10cm peeq channels_bot.png
pwr_eccentric3_quasi 10cm maxPrin channels_bot.png
pwr_eccentric3_quasi 10cm S33 channels.png
pwr_eccentric3_quasi 10cm peeq channels.png
pwr_eccentric3_quasi 10cm peeq insert_bot.png
pwr_eccentric3_quasi 10cm maxPrin insert_bot.png
pwr_eccentric3_quasi 10cm peeq insert_top.png
pwr_eccentric3_quasi 10cm maxPrin insert_top.png
pwr_eccentric3_quasi 10cm peeq insert.png
pwr_eccentric3_quasi 10cm S33 insert.png
pwr_eccentric3_quasi 10cm mises insert.png
pwr_eccentric3_quasi 10cm peeq.png
pwr_eccentric3_quasi 10cm peeq screw.png
pwr_eccentric3_quasi 10cm mises screw.png
pwr_eccentric3_quasi 5cm peeq channels_bot.png
pwr_eccentric3_quasi 5cm maxPrin channels_bot.png
pwr_eccentric3_quasi 5cm S33 channels.png
pwr_eccentric3_quasi 5cm peeq channels.png
pwr_eccentric3_quasi 5cm peeq insert_bot.png
pwr_eccentric3_quasi 5cm maxPrin insert_bot.png
pwr_eccentric3_quasi 5cm peeq insert_top.png
pwr_eccentric3_quasi 5cm maxPrin insert_top.png
pwr_eccentric3_quasi 5cm peeq insert.png
pwr_eccentric3_quasi 5cm S33 insert.png
pwr_eccentric3_quasi 5cm mises insert.png
pwr_eccentric3_quasi 5cm peeq.png
pwr_eccentric3_quasi 5cm peeq screw.png
pwr_eccentric3_quasi 5cm mises screw.png

Appendix 3

pwr_new_gap_moved2_quasi 10cm peeq channels_bot.png
pwr_new_gap_moved2_quasi 10cm maxPrin channels_bot.png
pwr_new_gap_moved2_quasi 10cm S33 channels.png
pwr_new_gap_moved2_quasi 10cm peeq channels.png
pwr_new_gap_moved2_quasi 10cm peeq insert_bot.png
pwr_new_gap_moved2_quasi 10cm maxPrin insert_bot.png
pwr_new_gap_moved2_quasi 10cm peeq insert_top.png
pwr_new_gap_moved2_quasi 10cm maxPrin insert_top.png
pwr_new_gap_moved2_quasi 10cm peeq insert.png
pwr_new_gap_moved2_quasi 10cm S33 insert.png
pwr_new_gap_moved2_quasi 10cm mises insert.png
pwr_new_gap_moved2_quasi 10cm peeq.png
pwr_new_gap_moved2_quasi 10cm peeq screw.png
pwr_new_gap_moved2_quasi 10cm mises screw.png
pwr_new_gap_moved2_quasi 5cm peeq channels_bot.png
pwr_new_gap_moved2_quasi 5cm maxPrin channels_bot.png
pwr_new_gap_moved2_quasi 5cm S33 channels.png
pwr_new_gap_moved2_quasi 5cm peeq channels.png
pwr_new_gap_moved2_quasi 5cm peeq insert_bot.png
pwr_new_gap_moved2_quasi 5cm maxPrin insert_bot.png
pwr_new_gap_moved2_quasi 5cm peeq insert_top.png
pwr_new_gap_moved2_quasi 5cm maxPrin insert_top.png
pwr_new_gap_moved2_quasi 5cm peeq insert.png
pwr_new_gap_moved2_quasi 5cm S33 insert.png
pwr_new_gap_moved2_quasi 5cm mises insert.png
pwr_new_gap_moved2_quasi 5cm peeq.png
pwr_new_gap_moved2_quasi 5cm peeq screw.png

Appendix 4

Restart_pwr_new_lock_quasi 10cm peeq channels_bot.png
Restart_pwr_new_lock_quasi 10cm maxPrin channels_bot.png
Restart_pwr_new_lock_quasi 10cm S33 channels.png
Restart_pwr_new_lock_quasi 10cm peeq channels.png
Restart_pwr_new_lock_quasi 10cm peeq insert_bot.png
Restart_pwr_new_lock_quasi 10cm maxPrin insert_bot.png
Restart_pwr_new_lock_quasi 10cm peeq insert_top.png
Restart_pwr_new_lock_quasi 10cm maxPrin insert_top.png
Restart_pwr_new_lock_quasi 10cm peeq insert.png
Restart_pwr_new_lock_quasi 10cm S33 insert.png
Restart_pwr_new_lock_quasi 10cm mises insert.png
Restart_pwr_new_lock_quasi 10cm peeq.png
Restart_pwr_new_lock_quasi 10cm peeq screw.png
Restart_pwr_new_lock_quasi 10cm mises screw.png
Restart_pwr_new_lock_quasi 5cm peeq channels_bot.png
Restart_pwr_new_lock_quasi 5cm maxPrin channels_bot.png
Restart_pwr_new_lock_quasi 5cm S33 channels.png
Restart_pwr_new_lock_quasi 5cm peeq channels.png
Restart_pwr_new_lock_quasi 5cm peeq insert_bot.png
Restart_pwr_new_lock_quasi 5cm maxPrin insert_bot.png
Restart_pwr_new_lock_quasi 5cm peeq insert_top.png
Restart_pwr_new_lock_quasi 5cm maxPrin insert_top.png
Restart_pwr_new_lock_quasi 5cm peeq insert.png
Restart_pwr_new_lock_quasi 5cm S33 insert.png
Restart_pwr_new_lock_quasi 5cm mises insert.png
Restart_pwr_new_lock_quasi 5cm peeq.png
Restart_pwr_new_lock_quasi 5cm peeq screw.png
Restart_pwr_new_lock_quasi 5cm mises screw.png

Appendix 5

pwr_new_lock_half_quasi 5cm peeq channels_bot.png
pwr_new_lock_half_quasi 5cm maxPrin channels_bot.png
pwr_new_lock_half_quasi 5cm S33 channels.png
pwr_new_lock_half_quasi 5cm peeq channels.png
pwr_new_lock_half_quasi 5cm peeq insert_bot.png
pwr_new_lock_half_quasi 5cm maxPrin insert_bot.png
pwr_new_lock_half_quasi 5cm peeq insert_top.png
pwr_new_lock_half_quasi 5cm maxPrin insert_top.png
pwr_new_lock_half_quasi 5cm peeq insert.png
pwr_new_lock_half_quasi 5cm S33 insert.png
pwr_new_lock_half_quasi 5cm mises insert.png
pwr_new_lock_half_quasi 5cm peeq.png
pwr_new_lock_half_quasi 5cm peeq screw.png
pwr_new_lock_half_quasi 5cm mises screw.png

Appendix 6

pwr_new2_washer3_quasi 10cm peeq channels_bot.png
pwr_new2_washer3_quasi 10cm maxPrin channels_bot.png
pwr_new2_washer3_quasi 10cm S33 channels.png
pwr_new2_washer3_quasi 10cm peeq channels.png
pwr_new2_washer3_quasi 10cm peeq insert_bot.png
pwr_new2_washer3_quasi 10cm maxPrin insert_bot.png
pwr_new2_washer3_quasi 10cm peeq insert_top.png
pwr_new2_washer3_quasi 10cm maxPrin insert_top.png
pwr_new2_washer3_quasi 10cm peeq insert.png
pwr_new2_washer3_quasi 10cm S33 insert.png
pwr_new2_washer3_quasi 10cm mises insert.png
pwr_new2_washer3_quasi 10cm peeq.png
pwr_new2_washer3_quasi 10cm peeq screw.png
pwr_new2_washer3_quasi 10cm mises screw.png
pwr_new2_washer3_quasi 5cm peeq channels_bot.png
pwr_new2_washer3_quasi 5cm maxPrin channels_bot.png
pwr_new2_washer3_quasi 5cm S33 channels.png
pwr_new2_washer3_quasi 5cm peeq channels.png
pwr_new2_washer3_quasi 5cm peeq insert_bot.png
pwr_new2_washer3_quasi 5cm maxPrin insert_bot.png
pwr_new2_washer3_quasi 5cm peeq insert_top.png
pwr_new2_washer3_quasi 5cm maxPrin insert_top.png
pwr_new2_washer3_quasi 5cm peeq insert.png
pwr_new2_washer3_quasi 5cm S33 insert.png
pwr_new2_washer3_quasi 5cm mises insert.png
pwr_new2_washer3_quasi 5cm peeq.png
pwr_new2_washer3_quasi 5cm peeq screw.png
pwr_new2_washer3_quasi 5cm mises screw.png

Appendix 7

bwr_new2_quasi 5cm peeq channels_bot.png
bwr_new2_quasi 5cm maxPrin channels_bot.png
bwr_new2_quasi 5cm S33 channels.png
bwr_new2_quasi 5cm peeq channels.png
bwr_new2_quasi 5cm peeq insert_bot.png
bwr_new2_quasi 5cm maxPrin insert_bot.png
bwr_new2_quasi 5cm peeq insert_top.png
bwr_new2_quasi 5cm maxPrin insert_top.png
bwr_new2_quasi 5cm peeq insert.png
bwr_new2_quasi 5cm S33 insert.png
bwr_new2_quasi 5cm mises insert.png
bwr_new2_quasi 5cm peeq.png
bwr_new2_quasi 5cm peeq screw.png
bwr_new2_quasi 5cm mises screw.png
bwr_new2_quasi 10cm peeq screw.png
bwr_new2_quasi 10cm mises screw.png
bwr_new2_quasi 10cm peeq channels_bot.png
bwr_new2_quasi 10cm maxPrin channels_bot.png
bwr_new2_quasi 10cm S33 channels.png
bwr_new2_quasi 10cm peeq channels.png
bwr_new2_quasi 10cm peeq insert_bot.png
bwr_new2_quasi 10cm maxPrin insert_bot.png
bwr_new2_quasi 10cm peeq insert_top.png
bwr_new2_quasi 10cm maxPrin insert_top.png
bwr_new2_quasi 10cm peeq insert.png
bwr_new2_quasi 10cm S33 insert.png
bwr_new2_quasi 10cm mises insert.png
bwr_new2_quasi 10cm peeq copper.png
bwr_new2_quasi 10cm peeq.png

Appendix 8

compare_5cm-pwr_new-model6g_pwr_channels-mises.png
compare_5cm-pwr_new-model6g_pwr_channels-s33.png
compare_5cm-pwr_new-model6g_pwr_insert-s33.png
compare_5cm-pwr_new-model6g_pwr_insert-mises.png
compare_5cm-pwr_new-model6g_pwr_insert-mises2.png
compare_5cm-pwr_new-model6g_pwr_insert-peq2.png
compare_5cm-pwr_new-model6g_pwr_insert-peq.png
compare_5cm-pwr_new-model6g_pwr_copper-peq.png
compare_5cm-pwr_new-model6g_pwr_copper-peq_max.png

2 – Input files used for the simulations

Each analysis is started by abaqus job=input-file (w/o .inp).

Contents in C:\Users\jhd\mappar\skb\Detailed_PWR_BWR\Input-file

bwr_new2_quasi.inp
pwr_new2_quasi.inp
pwr_eccentric3_quasi.inp
pwr_new_gap_moved2_quasi.inp
pwr_new_lock_quasi.inp
pwr_new_lock_half_quasi.inp
pwr_new2_washer3_quasi.inp

4 – Scripts used for post-processing

Used inside ABAQUS/CAE or by abaqus cae startup=script.py after appropriate editing of job-name inside the script-file.

Contents in C:\Users\jhd\mappar\skb\Detailed_PWR_BWR\Scripts

contour2_plots_bwr.py	- script for contour plots (BWR)
contour2_plots.py	- script for contour plots (PWR)
shear_lock.py	- script for comparison
plots (PWR)	
shear_gap_moved.py	- script for comparison plots
(PWR)	
shear_eccentric.py	- script for comparison plots
(PWR)	
pictures.py	- script for geometry

5 – Geometry definitions

Contents in C:\Users\jhd\mappar\skb\Detailed_PWR_BWR\Geometry

bwr.cae bwr.jnl	- ABAQUS/CAE-database and journal files (BWR-insert)
pwr2.cae pwr2.jnl	- ABAQUS/CAE-database and journal files (PWR-insert)

CAD-geometries received from SKB:

IDE-00015.pdf
IDE-00015.stp
IDE-00015-001.pdf
IDE-00015-21.pdf
IDE-00015-211.pdf
IDE-00015-001.stp
IDE-00015-21.stp
IDE-00015-211.stp
IDE-00025-131.stp
IDE-00025-13.stp
IDE-00015-121.stp